Analysis of Mount Ruapehu Tephra Deposits From 4.3 to 6.1 ka; Within a Transitional Timeframe.

A thesis presented in partial fulfilment of the requirements for the degree of

Master of Science

in

Earth Science

Joseph Fleming

2024

This thesis is dedicated to Dave G. Young

June 8th, 1964 – January 27th, 2023

Abstract

Mount Ruapehu is the largest active volcano in New Zealand, having shown a dominant eruptive record within the last 1,800 years. However, it showed a long period of relative dormancy beyond that time frame, extending to ~12 ka. Within this period of time sits the Papakai Formation. This formation is dominated by tephra deposits from the upper reaches of the Tongariro Volcanic Centre with only eight Ruapehu sourced tephras being found within the extents of this formation dating between 11-3.5 ka.

This study aimed to analyse tephra deposits from Mount Ruapehu's eastern ring plain found within the Papakai Formation. To define their geographical extents and physical characteristics within the field as well as their componentry and geochemical composition within the laboratory. Conducting this study allowed for insight into the eruptive processes from Mount Ruapehu throughout a period of dormancy as well as any trends in ashfall deposition and geochemistry over time. Two black ash layers found beneath the Taupō Ignimbrite were sampled and collected alongside the five Papakai Formation tephras for comparison.

Four of the five layers had been previously identified by Donoghue (1991) but had not been fully analysed with field observations having only been made at a handful of locations. This study aimed to provide more information of the ashfall deposits.

The two black ash layers and three orange lapilli layers within the Papakai Formation were found to be basaltic andesite with each showing definable traits and characteristics within the field. The tephras showed a trend towards higher silica content over time with deposits younger than the Taupō Ignimbrite being dacitic in nature (Voloschina, 2020). This trend could reflect the lower eruptive frequency of Mount Ruapehu within the span of the Papakai Formation and could potentially show the point at which volcanic activity reactivated at the southern crater after a long period of dormancy. Maximum extents to the north, west and south were estimated but access into the Rangipo Desert would be required to provide a more accurate analysis on the geographical extents of each tephra layer within the eastern ring plain stratigraphy.

Acknowledgements

There are several people who, without their support, this thesis would not have been possible. From the university, I have to give a massive thank you to my supervisor Jon Procter who helped set me up with this topic and showed me the ropes. Thank you for giving me the opportunity to partake in a study well suited to my skills. There were many sharp learning curves and I appreciate you giving me the space and tools to figure it all out. I also must give a big thank you to Anja Moebis for all of the help in the lab and pushing me to get the most out of my study as possible. I would still be stuck in the lab to this day without your guidance. Thank you to Shannen Mills for checking over my thesis before the final submission. You three really helped me get the most out of this topic and I really appreciate it.

A thank you goes out to those who I undertook field work with. Thank you, Brian Perttu, for your help in the Karioi Forest with locating my site locations and teaching me how to traverse the location. Your company was valued even when you made fun of me! A thank you also goes out to Anke Zernack and Janine Krippner for your company into the Karioi Forest and letting me bounce ideas off you. Your knowledge was invaluable to helping me make sense of some thin ash layers in the ground.

Thank you to Kate Arentsen, Fiona Bardell, Tara Penketh and Judith Stepper for your help with organising my adventures into the outdoors. I know it must be a pain to trust a master's student with a vehicle for three days going offroad, but you handled it with utmost grace. I would also like to thank Ian Furkert for providing access to the muffler furnace and scales and his aid within the lab as well as Keith Wood of ERNSLAW for providing access into the Karioi Forest and for your incredible hospitality.

Being the only masters student in earth science at the time, there were times where I felt pretty isolated and the odd one out, so I give a massive thank you to all my PhD friends Dan, Rae, Anna, Juliette, Sam, Emmy, Maia and Jeff as well as the VRS crew Matt, Gabor, Gert, Georg, Ermanno, Mel and Stuart for making me feel included within the department.

Outside of the university, I am so grateful for the support network I had surrounding me throughout the work. A big thank you to my flatmates Matt, Caylee and Kelsey for giving me a family away from home and I apologise for disappearing on field work without letting you guys know. I'll be sure to remember for next time!

Thank you to the Massey University Alpine Club for giving me the chance to go on adventures and try new hobbies such as rock climbing and hiking. Big thank you to all my friends I've made throughout. Especially to Ash and Amelie for being my biggest supporters throughout this last year. You guys are the best.

Thank you to my friends Hannah, Ben, Jack, Shani and Zara for keeping me company throughout, you've all been there for me through some tough patches, and it means a great deal to me. A thank you goes out to my undergraduate friends Michelle, Caitlin, Hayden and Ruby for helping make an undergrad through COVID not all bad. Thank you to Jess for being there and supporting me during the final writing push. Your motivation kept me going during the hardest points of this thesis and I will always appreciate that.

A big thank you to my family back up in Pukekohe and overseas. You've always supported me even if my dream is to climb volcanoes and study natural hazards. Thank you for your commitment towards my future and for giving me what I needed to push myself to where I am today. I hope I keep making you proud.

Finally, I wanted to save my final thank you for Sandy Wild and Dave Young. Thank you so much to both of you for believing in me and for supporting me. To Sandy, thank you for everything you did for me and Matt and for helping us achieve our dreams. It means more than I can describe with words. To Dave, thank you for caring and for your willingness to help all those around you. You are my motivation, and this thesis is dedicated to you.

Thank you.

Table of Contents

List of Figures

List of Tables

Introduction

1.1 Introduction

Volcanic activity has resulted in some of the most devastating natural disasters throughout human history with death tolls exceeding 90,000 within the last century alone (Witham, 2005). New Zealand is not exempt from these impacts with volcanic systems occurring all across the North Island, as a result of plate subduction along the Hikurangi trench and intra-plate volcanism primarily located underneath New Zealand's largest city, Auckland. These systems have shaped the geology of New Zealand over the last five million years and will continue to do so, impacting communities and the economic stability of the country. Due to this, it is critical to understand the past activity of a volcano to better understand and identify its eruptive characteristics. Hazard models can be produced that provide valuable insight into the likelihood of future events, the extent at which hazards can reach and what actions can be taken to mitigate risk.

Mount Ruapehu is one of the most studied volcanoes in New Zealand due to its size and eruptive history. The geological record of Ruapehu's activity within the last 1,800 years has been studied in detail with this period of time being designated the Tufa Trig Formation (Voloschina et al, 2020). It is to be expected that the most recent formation is the one that is studied the most intensively as it would most closely resemble contemporary events and activity. However, piecing together records older than the Tufa Trig Formation such as the Papakai Formation is still an important process and provides insights into the volcano's behaviour. (Moebis et al, 2011).

Figure 1.1: Mount Ruapehu, captured during field work.

1.1.1 Outline of Mount Ruapehu and the Geological Setting

Mount Ruapehu represents the southernmost point of the Taupō Volcanic Zone (TVZ) (Wilson et al, 1995), a 200-kilometre-long region (not including the offshore extent which reaches a further 100 kilometres north) consisting of large calderas and active volcanic systems formed through subduction processes east of the North Island. Here the dense Pacific Plate is being subducted underneath the buoyant Australasian plate (Wilson et al, 1995). At a depth of around 65 kilometres, the oceanic plate begins to melt through intense pressure and heat. This process is aided by the inclusion of seawater which reduces the rock's melting point (Scambelluri and Philippot, 2001). Due to the melt being less dense than the surrounding rock it pushes upwards towards the surface. This process leads to the formation of a volcanic chain that runs parallel to the subduction zone (Wilson et al, 1995). In the case of the TVZ, onshore backarc extension is observed within the continental Australasian plate (Harrison and White, 2006). The region is plagued by shallow seismic activity and high heat flow that is presented through the high levels of volcanism within the region (Wilson et al, 1995).

Mount Ruapehu is located around fifteen kilometres south of Mount Tongariro, a compound volcano composed of numerous volcanic vents and craters with the most recent being Mount Ngauruhoe. Despite the close proximity of the two volcanoes, they both produce chemically distinct tephras that can often be attributed to one volcano or the other (Waight et al, 1999). It is believed that both volcanoes are formed through subduction processes but do not share a shallow magma chamber (Waight et al, 1999). This also highlights that the eruptive history of the two volcanoes is not inherently linked with an eruption at Mount Ruapehu not triggering activity at Mount Tongariro and vice-versa. It can however highlight periods of increased magma injection through subduction processes if activity at both volcanoes increase (Leonard et al, 2021). Mount Ruapehu has commonly produced multi-hazard eruptions throughout its eruptive history (Voloschina et al, 2020) with multi-phase eruptive periods being seen within the Tufa Trig Formation (Voloschina et al, 2021). Recent hazards produced from the volcano usually consist of buoyant ash fall that falls to the east of the volcano due to the prevailing winds and lahars that travel down the volcano through the Whangaehu valley. Historically the volcano is known to have produced large lava flows (Conway et al, 2016), debris avalanches (Tost et al, 2014), ballistics (Leonard et al, 2021) and pyroclastic flows (Cowlyn et al, 2020). The latter is mostly absent throughout the geological record with the only contemporary record of it occurring is in the 1943 eruption although it is still debated (Cowlyn et al, 2020).

1.1.2 Outline of the Study Area

The area being researched centres around Mount Ruapehu within the Tongariro Volcanic Centre (TgVC) with a primary focus on the ring plain formed through frequent eruptive episodes. The TgVC is a large region of the central North Island which encapsulates the volcanic centres of Ruapehu and Tongariro (figure 1.2). Contemporary volcanic activity in the region began approximately 340 ka (Tost and Cronin, 2015) but the TVZ has shown activity for the last two million years (Wilson et al, 1995). Most of the visible landscape has been shaped by eruptions from the two main volcanic systems with older deposits being buried and difficult to access.

Figure 1.2: Region of interest in comparison to the North Island of New Zealand. Ruapehu is marked by a yellow dot and Tongariro is marked by a red dot.

The time frame which is being studied is found within the Papakai Formation which occurred 11-3.5 ka. Some locations of interest are noted to the south-east of the volcano such as the Karioi forest where intensive logging is conducted. Areas that have been cleared such as forestry units and roadside cuttings will provide the greatest opportunity to scout older deposits within the stratigraphy. The area being examined for potential deposits will comprise of the south-eastern section of the Ruapehu ring plain to identify the geographical extents of the unidentified stratigraphy as well as its thickness at key points.

The extents of the search area will predominantly be located along State Highway 1 as numerous road cuttings are available that follow a transect of the volcanic plain. The furthest extents of the surveyed area are aiming to be the Mangatoetoenui Quarry to the north, State Highway 1 to the east, Rock Road to the west and State Highway 49 to the south. All of these are subject to change as parameters are adjusted in accordance with deposit distribution.

1.1.3 Objectives of the Study

The deposits being studied have been identified within other studies such as Donoghue (1991) and Moebis (2010) but have never been thoroughly analysed to determine tephra extents and origins. This study aims to provide details regarding their geographical extents within the Ruapehu ring plain and clarity for Mount Ruapehu's behaviour within a transitional period of its eruptive history. The aim of this study is to provide a comprehensive understanding of the eruptive behaviour of Mount Ruapehu within a transitional period of its history through the analysis of tephra deposits located within its eastern ring plain.

Objectives for this study include:

- Uncovering the geographical extents and chemical properties of definable deposits within Ruapehu's eastern ring plain.
- Establish the origins of deposits and the circumstances under which deposition occurred.
- Incorporate findings into the record of Mount Ruapehu's eruptive history.

1.2 Literature Review

1.2.1 The Taupō Volcanic Zone

Most of the volcanism found within New Zealand has formed through convergent plate interactions occurring to the east of the North Island (Wilson et al, 1995). Plate subduction occurring between the oceanic Pacific Plate and the continental Australasian Plate is represented by the Hikurangi Trench which in turn belongs to the south-western end of the Pacific Ring of Fire (figure 1.3, Wilson et al, 1995). The term "Ring of Fire" is commonly used to refer to the plate margins that are situated around the Pacific Plate, forming a ring of heightened volcanic activity in regions such as Japan, Russia, the United States of America, Chile, and New Zealand. The particular stretch that New Zealand's activity is associated with spans over 3,000 kilometres across the ocean floor (Ballance et al, 1999).

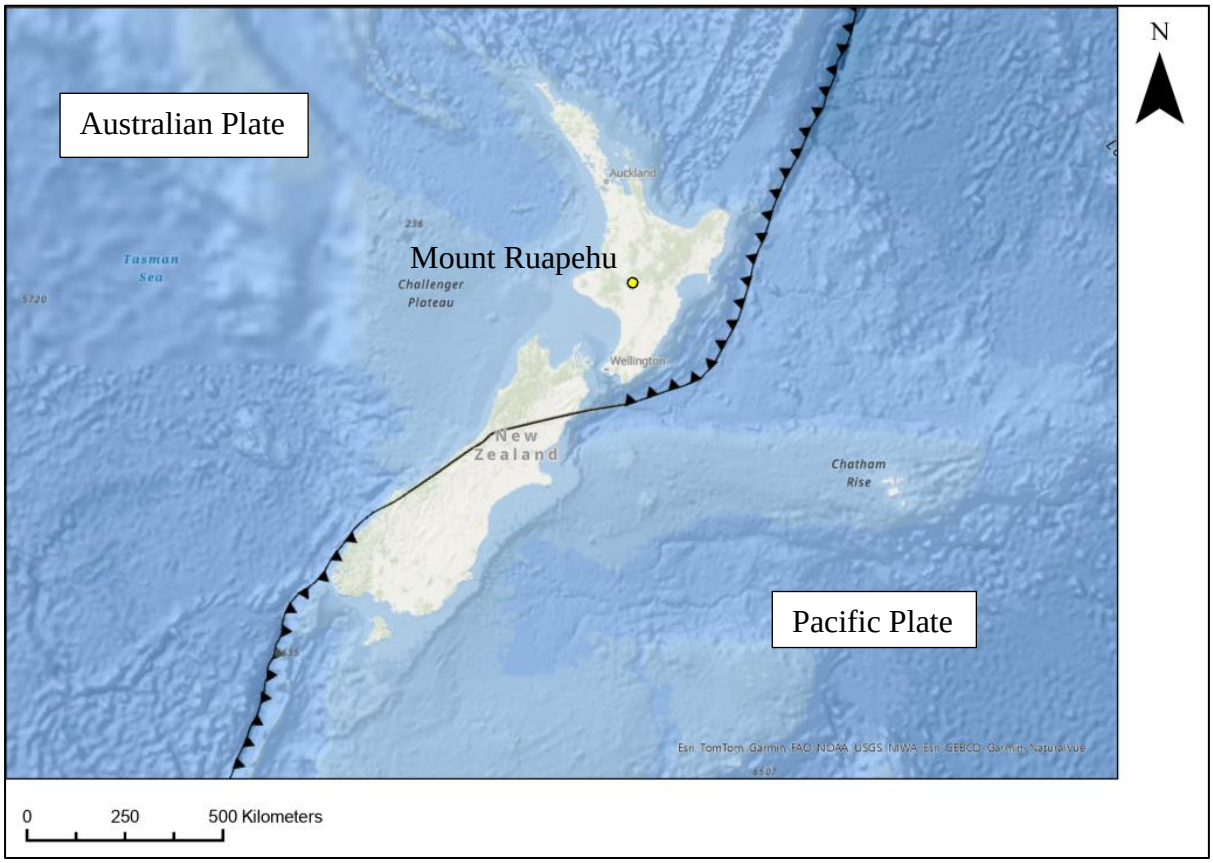

Figure 1.3: The tectonic boundary around New Zealand. Triangles indicate subduction processes and direction.

The subduction of the Pacific Plate underneath the North Island of New Zealand progresses at a rate of 42 to 50 millimetres per year (DeMets et al, 1990) with the plate having been subducted to a depth of around 65 kilometres by the time it reaches the TVZ. It is believed that the subduction processes can be seen all across the width of the North Island with Mount

Taranaki being considered a product of subduction processes occurring 600 kilometres below the surface (Moebis, 2010). The crust around the TVZ is considerably thinner than the surrounding area which can be attributed to clockwise rotation of the plate margin (Stratford and Stern, 2006) with the crust-mantle boundary beneath the TVZ ranging from 15 to 20 kilometres in depth (Stratford and Stern, 2006).

Volcanism in the TVZ began around two million years ago with the majority of activity having been rhyolitic in nature with around 80% of erupted material being rhyolitic and the remaining 20% encompassing the basaltic, andesitic and dacitic material that has been produced throughout the history of the TVZ (Wilson et al, 1995) with the most northern extent being marked by Whakaari/White Island and the southern extent reaching the town of Ohakune found on the southern border of Mount Ruapehu's ring plain.

The TgVC encompasses the two active volcanic centres of Mount Ruapehu and Mount Tongariro. Modern activity within this region began at least 300,000 years ago with activity commencing at Ruapehu around this time (Wilson et al, 1995). The complex also includes older volcanic centres that are no longer active such as Hauhungatahi to the west of Ruapehu and Pihanga and Kakaramea located at the border between the TgVC and Lake Taupō. The volcanic systems generally follow an NNE – SSW orientation which matches the orientation of the TVZ parallel to the Hikurangi Trench (Wilson et al, 1995). The area is covered in overlapping eruptive material that has accumulated over time (figure 1.4), with depths of around 800 metres recorded around the Tama Lakes between the two volcanic cones (Cassidy et al, 2009). The region is known to have three major faults running through including the Ruapehu Graben, the Karioi Fault and the Ohakune-Raetihi Fault. Expansion at the Ruapehu Graben is occurring at a rate of 2.3 ± 1.2 millimetres per year and has been growing for at least 400,000 years (Villamor and Berryman, 2006).

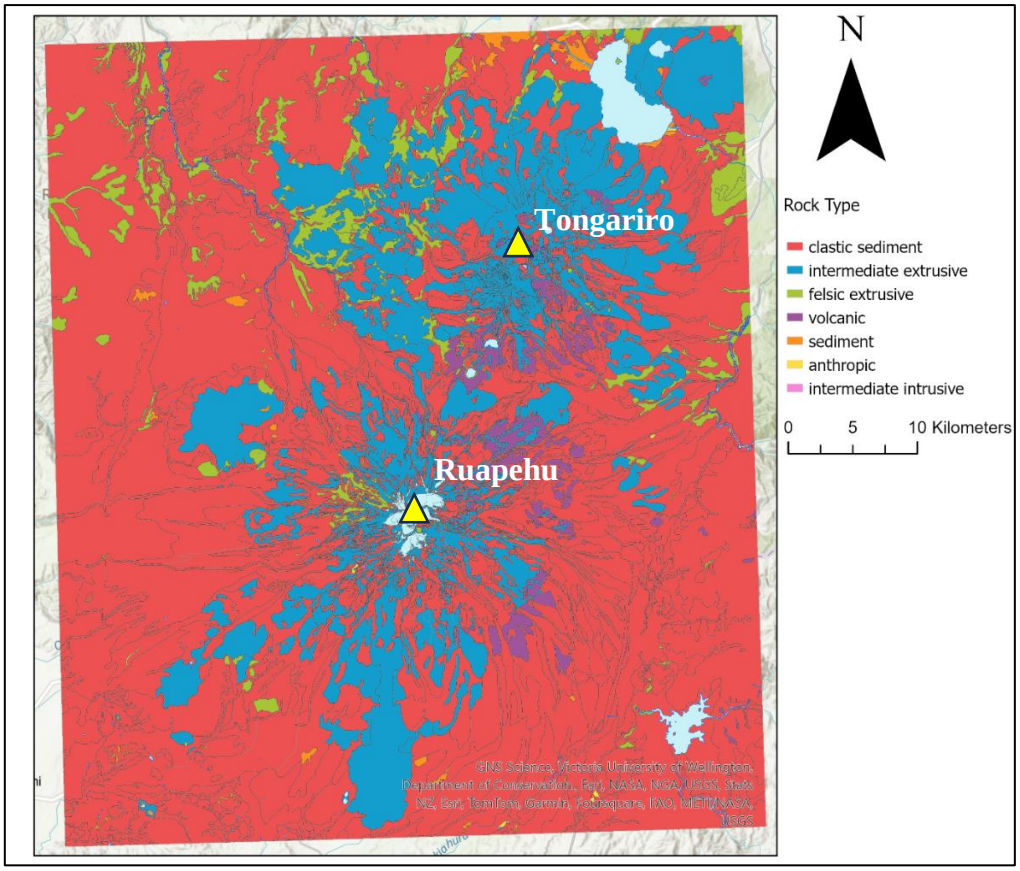

Figure 1.4: Rock types found within the TVZ. Lava flows that have not been buried or eroded away can be observed in light blue and purple (Data provided by GNS, 2024).

1.2.2 Geological Background of the Taupō Volcanic Zone

The TVZ has experienced many periods of activity stemming from its three main regions with the northern reaches characterised by andesitic-dacitic volcanism from mostly off-shore volcanoes such as Whakaari and Moutohora. The central region is dominated by rhyolitic activity and calderas with at least eight rhyolitic centres being found including Lake Taupō and Okataina. The southern reaches constitute the TgVC with volcanoes such as Mount Ruapehu and Mount Tongariro presenting historical activity (Wilson et al, 1995).

The central region is not exclusively rhyolitic with some basaltic magma being erupted at volcanoes such as the 1886 eruption at Mount Tarawera. This eruption was unique within the regions historical record as all other eruptive material from the volcano is predominantly rhyolitic with only a small fraction being considered basaltic (Walker et al, 1984). This eruption was also the last significant eruption to occur within the central region of the TVZ, producing approximately 2 cubic kilometres of material (Walker et al, 1984) killing 120 people. The largest eruption to occur in New Zealand in the last twenty thousand years was produced by the Taupō supervolcano around the year 232 ± 10 C.E. The Taupō eruption ejected over 45

cubic kilometres of tephra and blanketed an area of 30,000 square metres in volcanic material more than ten centimetres thick (Wilson and Walker, 1985). This eruption is important for stratigraphic analysis as its pumice rich deposits are highly contrasted against the surrounding tephra layers and allows for a geological marker to determine the time scales of nearby eruptive material, with layers appearing above the Taupō deposits being confidently dated to a time younger than ~1800 years. Deposits above this layer from Mount Ruapehu are designated as part of the Tufa Trig Formation (Voloschina et al, 2021).

The eruptive history of the TgVC dates back to around 300 ka based on deposits located in the Whanganui Basin from Mount Ruapehu (Parish, 1994), although volcanism in the area is known to extend as far back as 900 ka with activity at the eroded cone of Hauhungatahi commencing around this time period (Cameron et al, 2010). The volcanic system has evolved throughout its life span with volcanism occurring at a number of satellite cones such as Pukeonake and Saddle Hill as well as at older, smaller cones such as Pihanga, Hauhungatahi and Mount Kakaramea. These systems are all found within the wider TgVC region which could infer that activity within the TgVC has become more confined over time.

Activity from Mount Ruapehu has also evolved with at least five recorded eruptive, cone building pulses 15, 22, 45, 134 and 200 ka (Gamble et al, 2003). Within these pulses there has been numerous multi-phase eruptive periods that have built up the volcano to its present-day stature (Voloschina et al, 2021). Mount Tongariro is significantly more complex with activity being recorded from at least 17 craters located within the complex, all overlapping and building upon the other (Leonard et al, 2021). Forming a silhouette not commonly seen with volcanoes, this is exemplified through Mount Ngauruhoe's conical shape located on the southern edge of the complex. Activity at Tongariro can be split between younger and older periods with activity >20 ka being recorded near to the Tama Lakes located between Ruapehu and Ngauruhoe and younger deposits being found between Ngauruhoe and North Crater. The last recorded eruption from Mount Tongariro was from the Te Maari craters located on the northern face of the volcano in 2012. (Leonard et al, 2021).

Table 1.1: Tephrostratigraphical record within the Tongariro Volcanic Centre up until the end of the Papakai Formation after Moebis (2010). Updated as of Voloschina (2020). Entries in italics indicate rhyolitic deposits from outside the TgVC. Bold formations have formations originating from Mount Ruapehu present.

Formation	Member	Source	Age in Cal yrs B.P.	Reference of member and age
Tufa Trig Fm. & Ngauruhoe Tephra F. Stage 4	Tf26-Tf32	Ruapehu & Ngauruhoe	0-295 cal yrs B.P.	Voloschina (2020)
Burrell Lappilli		Taranaki	295 cal yrs B.P.	Druce (1966)
Tufa Trig Fm. & Ngauruhoe Tephra F. Stage 4	Tf14-Tf26	Ruapehu & Ngauruhoe	295-603 cal yrs B.p.	Voloschina (2020)
Tufa Trig Fm. & Ngauruhoe Tephra F. Stage 4	Tf13	Ruapehu & Ngauruhoe	603.5 ± 46.5 cal yrs B.P.	Voloschina (2020)
Tufa Trig Fm. & Ngauruhoe Tephra F. Stage 4	Tf8-Tf11	Ruapehu & Ngauruhoe	603-1337 cal yrs B.P.	Voloschina (2020)
Tufa Trig Fm.	Tf5	Ruapehu		Voloschina (2020)
Tufa Trig Fm.	Tf2	Ruapehu	1555 ± 135 cal yrs B.P.	Voloschina (2020)
Taupo Tephra	*Taupo Ignimbrite*	*TVC*	*1717 ± 13 cal yrs B.P.*	*Lowe et al. (2008)*
Mangatawai Fm.	MtF 62 (informal)	Ruapehu		Moebis (2010)
Mangatawai Fm. Stage 3	MtF 58 (informal)	Ngauruhoe	2766 ± 226 cal yrs B.P.	Moebis (2010)
Mangatawai Fm. Stage 3	Mtf 46 (informal)	Ngauruhoe	2810 ± 70 cal yrs B.P.	
Maketawa Tephra		Taranaki	3058 ± 268 cal yrs B.P.	Alloway et al. (1995)
Manganiu Tephra		Taranaki	3550 ± 145 cal yrs B.P.	Alloway et al. (1995)
Mangatawai Fm. Stage 2	MtF 9-45	Ngauruhoe	3694 ± 133 cal yrs B.P.	
Mangatawai Fm.	MtF 1-8 (informal)	Ngauruhoe	3592 ± 89 cal yrs B.P.	Moebis (2010)
Papakai Formation		TgVC		
Inglewood Tephra		Taranaki	3924 ± 224 to 4060 ± 231 cal yrs B.P.	
Mangatepopo Lapilli Stage 1	Informal	Ngauruhoe		Moebis (2010)
Stent Tephra	*Q*	*TVC*	*4323 ± 174 cal yrs B.P.*	*Alloway et al. (1995)*
Koritto Tephra		Taranaki	4647 ± 230 cal yrs B.P.	
Papakai Formation Stage 1	soil + black ash	Ruapehu & Ngauruhoe		Moebis (2010)
Papakai Formation	**Black Ash-2**	**Ruapehu**		**Donoghue (1991)**
Papakai Formation	**Black Ash-1**	**Ruapehu**	**5562 ± 268 cal yrs B.P.**	**Donoghue (1991)**
Hinemaiaia Tephra	*K*	*TVC*	*5120 ± 150 cal yrs B.P.*	*Lowe et al. (2008)*
Papakai Formation				
Tariki Tephra		Taranaki	5277 ± 305 cal yrs B.P.	Alloway et al. (1995)
Papkai Formation	**Orange Lapilli-2**	**Ruapehu**		**Donoghue (1991)**
	Orange Lapilli-1	**Ruapehu**		**Donoghue (1991)**
Whakatane Tephra Wk		*OVC*	*5530 ± 60 cal yrs B.P.*	*Lowe et al. (2008)*
Waipuku		Taranaki	6025 ± 255 cal yrs B.P.	Alloway et al. (1995)
Papakai Formation	Pp	TgVC		
Moutere Formation	*G-H*	*TVC*	*6122 ± 185 cal yrs B.P.*	*Froggatt and Lowe. (1990)*
Papakai Formation				
Rotoma		*OVC*	*9505 ± 25 cal yrs B.P.*	*Lowe et al. (2008)*
Kaponga		Taranaki	9998 ± 388 cal yrs B.P.	Alloway et al. (1995)
Opepe Tephra	*E*	*TVC*	*10075 ± 155 cal yrs B.P.*	*Lowe et al. (2008)*

1.2.3 Geological Markers

Geological markers within any stratigraphic section are critical to being able to accurately determine the correlation of the surrounding landscape and the timeframes in which events occurred. These generally consist of layers that contrast greatly to the surrounding material, allowing for it to be identified and allows for an idea of the types of deposits one can expect from that region. The most defined geological marker within the TgVC is the 232 C.E. Taupō Ignimbrite. Most tephrochronological markers within the TgVC are rhyolitic tephras as the white colouring and pumice dense layers provide high contrast to deposits that are generally black or brown, they are also fairly infrequent throughout the stratigraphy as no volcanoes south of Lake Taupō produce rhyolitic eruptions (Reid, 1983). So, all rhyolites found within Mount Ruapehu's ring plain originate from Lake Taupō or further north (Reid, 1983).

1.2.3.1 Taupō Ignimbrite

The Taupō eruption of 232 ± 10 C.E. produced the largest eruption in New Zealand within the last 20,000 years and the resulting ignimbrite deposits are located all across the TgVC (figure 1.5). Characterised by a thick, pale deposit with clasts ranging from large pumices to fine white ash. The layer was deposited fairly recently in the geologic history of the TVZ (Lowe et al, 2013). It is known that the Rangipo Desert at the time had an expansive forest that was destroyed by the eruption, leaving large volumes of charred organic material within the ignimbrite, allowing it to be confidently aged through carbon dating (Lowe et al, 2013). It is very distinctive and is found in all regions of the eastern ring plain of Mount Ruapehu and thus is a critical marker within the landscape.

Figure 1.5: Example of Taupō Ignimbrite found along State Highway 1.

1.2.3.2 Stent Tephra

The Stent Tephra was deposited around 4322 ± 112 years ago from a relatively large Plinian eruption from Lake Taupō (Lowe et al, 2013; Alloway et al, 1994). Deposits usually consist of discontinuous segments of a white very fine ash layer; it is chemically similar to Taupō's other eruptions from within this period and is commonly the next distinctive rhyolitic ash layer found beneath the Taupō ignimbrite (Lowe et al, 2013). These two events are useful for identifying eruptions and conditions within the TgVC from the last 5 ka.

1.3 Eruptive Record of Mount Ruapehu

1.3.1 Geologic Framework

Mount Ruapehu is a 2,797-metre-tall andesitic stratovolcano located in the central North Island of New Zealand. Activity commenced approximately 340 ka (Tost and Cronin al, 2015) with periods of activity and dormancy being observed throughout its stratigraphic history. Its last major eruption occurred in 1995 with minor eruptions occurring in 2007 and 1975. An eruption frequency of 20-30 years has been observed at Mount Ruapehu which can be linked to an open venting system found beneath its Crater Lake (Gamble et al, 1999).

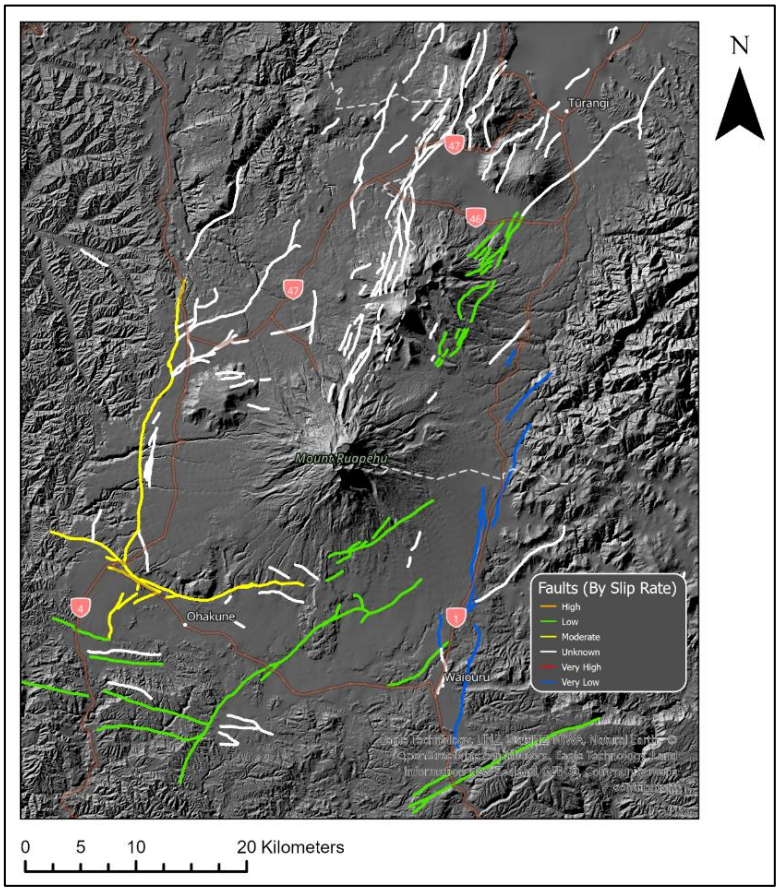

Figure 1.6: Known fault lines within the TVZ. Shown based on their slip rate (Data provided by GNS, 2024).

Mount Ruapehu is found within a significantly faulted region of the North Island (figure 1.6), specifically named the Ruapehu Graben. This forty-kilometre-wide area experiences crustal thinning brought through the clockwise rotation of the plate margin alongside magma intrusion into the upper mantle. The crust here is thicker than in other parts of the TVZ due to the point of rotation being closer to Ruapehu than regions further north such as Okataina (Villamor and Berryman, 2006). Areas in the northern extent of the TVZ have to move a greater distance to match the rotational speed of the plate motion which produces greater thinning of the crust.

The Rangipo Fault constrains the Ruapehu Graben to the east, a ≥ 32-kilometre-long fault line consisting of N-S normal faults interspersed within a 1-4-kilometre-wide system (Villamor et al, 2007). To the west, the Ruapehu Graben is bordered by the Raurimu Fault, this normal fault is a common location for seismic swarms within the TgVC to occur near with local seismicity being mostly restricted to two locations west of Ruapehu, possibly located on eastward facing branches of the Fault (Rowlands et al, 2005). Other faulting such as the Waihi Fault occurs on the north-western edge of the volcano that travels NNE towards Lake Taupō as well as the Poutu Fault which extends from the north-eastern slope of Ruapehu to Pihanga (Gómez-Vasconcelos et al, 2019).

The basement rock of Mount Ruapehu predominantly consists of greywacke and argillite originating from the Mesozoic Torlesse Terrane, this bedrock is one of two distinct terranes observed within the North Island of New Zealand, the other being the Waipapa terrane (Price et al, 2012). This terrane is located on the west of the North Island with the point of contact between terranes being found to the west of Ruapehu (figure 1.7). Price et al (2012) hypothesises that this seam may have had a significant impact on the spatial development of the Taupō Volcanic Zone. The Mesozoic bedrock is separated by the volcanic material deposited in the late Quaternary period by Cenozoic sediments such as limestone and silts derived from the Whanganui Basin (Mortimer et al, 1997)

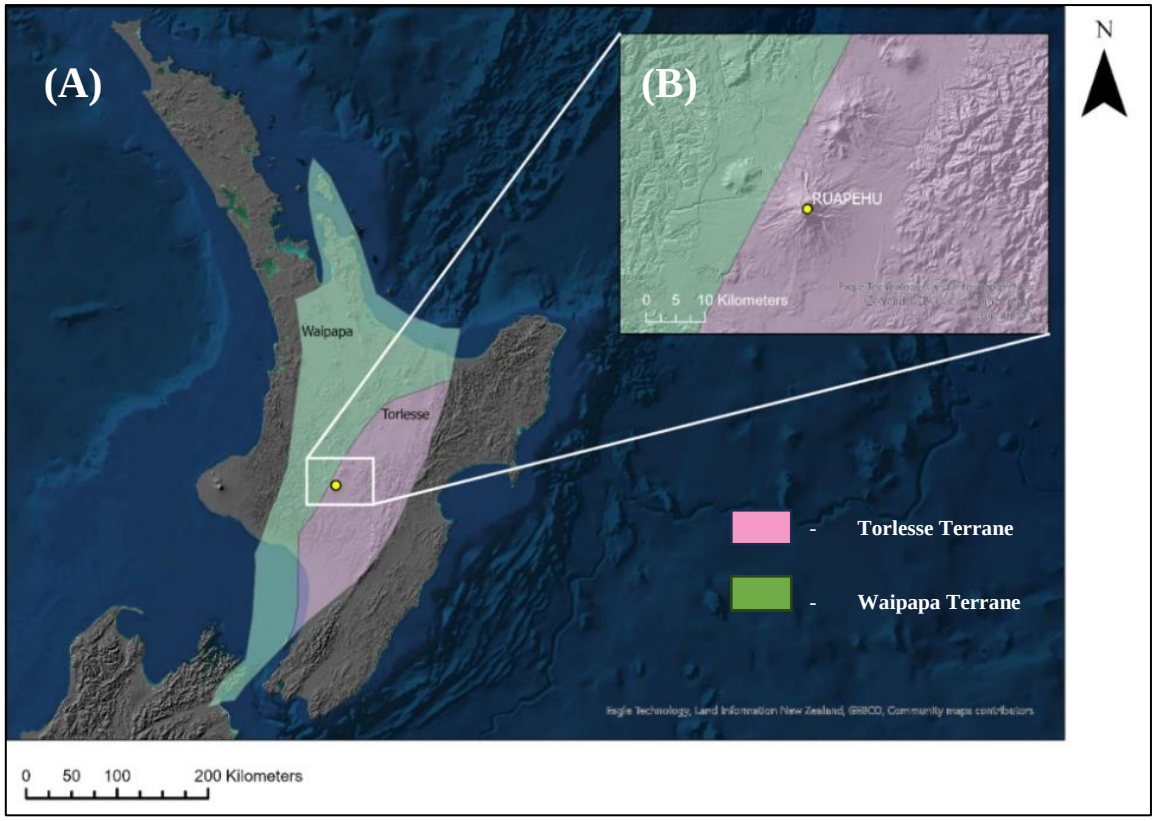

Figure 1.7: (A) Terranes that the TVZ sits upon and their geographical extent across the North Island. (B) Position of Ruapehu with it bordering the terrane transition (Data provided by LINZ, 2024).

Mount Ruapehu has had at least four major periods of activity which has constructed the present-day edifice. This activity first began around 250 ka with the Te Herenga Formation which persisted for ~ 70,000 years before a quiet period of low activity commenced. Further cone-building formations occurred from 160-115 ka (Wahianoa), 55-20 ka (Mangawhero) and 10-2 ka (Whakapapa) (figure 1.8, Price et al, 2012; Gamble et al, 2003). Activity within the last two millennia has been characterised by small but frequent phreatomagmatic eruptions from its permanent Crater Lake (Price et al, 2012; Gamble et al, 2003). Activity at Mount Ruapehu began to migrate southwards ~11.6 ka, towards its present-day location beneath the Crater Lake, the Crater Lake itself forming ~2.6 ka based on lahar deposits (Topping, 1974; Pardo et al, 2012). This movement has left the volcano with a large summit plateau with younger volcanic material being found on the southern end of the system (Pardo et al, 2012).

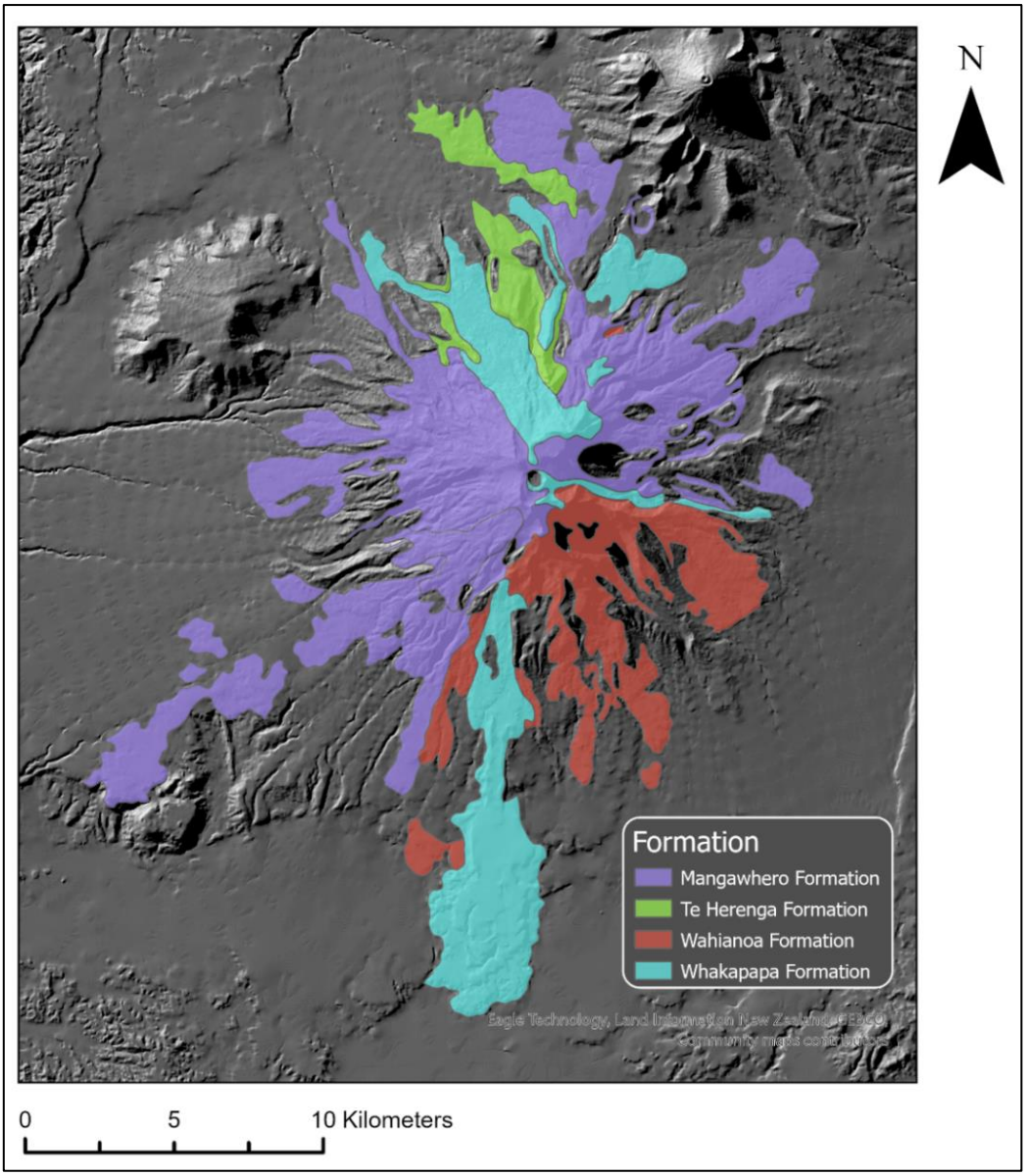

Figure 1.8: Cone building, lava flow formations of Mount Ruapehu overlaid on a hillshade basemap for visibility (data provided by GNS, 2024).

Mount Ruapehu is surrounded by a large ring plain that has been shaped since the last glacial maximum 23-13 ka with a volume similar to the Mount Ruapehu Massif itself of 110 cubic kilometres (Topping, 1974, Hackett and Houghton, 1989). Aggradation within the ring plain has been constructed through tephra deposition and reworked material from lahars or debris avalanches (Topping, 1974). Five distinct formations, representing periods of aggradation, were defined within the ring plain, ranging from >22.6-14.7 ka (Te Heuheu), 14,7-5.4 ka (Tangatu), 5.4-3.2 ka (Manutahi), 4.6 ka (Mangaio) and <1.9 ka (Onetapu) (Donoghue and Neall, 2001). These formations provide much clearer depictions of stratigraphy than what could be achieved proximally to the vent as erosion processes are much greater at higher elevations with greater exposure.

1.3.2 Tufa Trig Formation

The Tufa Trig Formation (TTF) is a term used to describe all tephra deposits originating from Mount Ruapehu found above the Taupō pumice layer produced by Taupō in 232 ± 10 C.E. The TTF was classified by Donoghue et al (1995 B) where it was lumped together with tephra deposits from Mount Tongariro within the Ngauruhoe Formation. As of Voloschina (2020), 31 distinct tephra members have been identified within the stratigraphy, thirteen of these were newly recognised while the other eighteen had been previously identified by Donoghue et al (1997). Many of these deposits were located between 6-15 kilometres from the southern crater with vegetation allowing for the preservation of fine material. Regions <6 kilometres from source were subjected to high levels of erosion and reworking so it made it difficult to discern discrete layers (Voloschina, 2020). The furthest deposits defined by Voloschina (2020) were located ~21 kilometres away from source.

The TTF deposits are generally well sorted and presented as a consistent thickness between observed locations which infers that the deposits were produced from ashfall and not reworked via lahars or other secondary forces (Voloschina, 2020). The layers can be classified into three main deposit types: single bed ash units (SBA), multi-bed ash units (MBA) and lapilli-bearing units (L).

SBA units are generally less than 10 millimetres thick up to 15 kilometres from source. Thinning is common and makes it difficult to accurately observe separate SBA units within the stratigraphy (Voloschina, 2020). These units make up ~35 % of the observed record. They could either represent single eruption phases or poorly preserved multi-phase eruptions that were smaller than what is observed within the MBA units (Voloschina, 2020).

MBA units are defined by multiple beds with clear contact lines. Changes between these beds are very subtle in regard to grain size, colour, or texture. Individual beds within the MBA units can be further refined into subunits that can be observed between locations. MBA units compose ~55 % of the known units with ~63 % of those containing 2-3 phases (Voloschina, 2020).

L units display a lack of ash sized tephra and show lapilli sized pyroclasts interspersed within soils. These layers represent the final ~10 % of the eruptive record within the last 1800 years. Much like the SBA units, these represent single eruption phases with the critical difference being the duration and explosivity of the eruption. L units would be produced from higher energy events that cause more fragmentation to occur (Voloschina, 2020).

The TTF deposits represent a period of low to moderate intensity eruptions from Mount Ruapehu, with a varying frequency of phreatomagmatic and phreatic eruptions. Based on the deposits discovered by Voloschina (2020) there appear to be three periods of varying eruption frequency within the TTF. The first ~1000 years saw an eruption approximately every 100 years, the following 300 years showed an eruption frequency of one every 20 years and the final ~400 years show an eruption every 60-70 years (Voloschina, 2020).

1.3.3 Papakai and Mangatawai Formation

The Papakai Formation (PPF) and Mangatawai Formation (MTF) range from 10-3.5 ka and 3.5-1.8 ka respectively. Both formations contain eruptions from the TgVC as a whole and are not constricted to deposits originating solely from Mount Ruapehu (Moebis, 2010). This period of time displays a duration of reduced volcanic activity from Mount Ruapehu with activity from Mount Tongariro being prominent within the stratigraphy (Donoghue et al, 1995 B). The tephra is poorly constrained due to the thin deposits and the erosion dominated environment the distal deposits are found within.

The MTF is predominantly Ngauruhoe derived deposits with this period of time considered the height of activity from the cone (Moebis, 2010). However, some Ruapehu deposits have also been observed within this time frame within the Mangatepopo Valley. 18 Ruapehu deposits were observed in the work conducted by Moebis (2010) within the timeframe of the MTF. This formation is marked harshly by the 232 C.E. Taupō Ignimbrite and provides a useful marker to recognise where ash layers may appear. Ruapehu tephra layers found within this formation range from fine to very fine ash and appear white, grey, or black. The deposits are thinly dispersed and cannot be formed into distinct marker beds (Moebis, 2010).

The PPF consists of any tephra stratigraphy from the TgVC found between the Mangamate and Mangatawai Formation, the Poutu Lapilli is the youngest tephra member of the Mangamate Formation and is observed directly underneath the PPF (Moebis, 2010). The PPF shows evidence of rhyolitic activity occurring from the Taupō Volcanic Centre within this time period with three rhyolitic tephra layers observed, the youngest assumed to be the Stent tephra occurring ~ 4323 ± 174 years B.P (Moebis, 2010). Andesitic ash layers that bear a resemblance to formations found within the TTF are found within the PPF and are assumed to originate from Mount Ruapehu. The Ruapehu deposits are defined as being orange or black in colour with the orange layers being defined by lapilli up to ~ 20 millimetres in size encased in fine

ash of the same colour and the black layers consisting of fine ash (Moebis, 2010). Around 8 Ruapehu tephra layers have been found within the PPF (Moebis, 2010).

1.3.4 Bullot Formation

The Bullot Formation (BF) extends beyond the PPF with deposits ranging from 10 ka to ~22.6 ka (Donoghue et al, 1999). This period of activity originated from the northern vent with it being typically considered Ruapehu's most active period with at least 50 sub Plinian eruptions recorded in the eastern ring plain (**Pardo et al, 2011**). Six periods of activity have been recorded within the BF with the final activity from this formation occurring at the southern crater (Pardo et al, 2011). Ever since the BF, tephra eruptions from Mount Ruapehu have been ~1-10% the scale of the BF events with a greater number of smaller vulcanian or strombolian eruptions taking place (Moebis, 2010, Pardo et al, 2012). The TTF and BF are two significant Ruapehu formations found within the ring plain.

1.3.5 Historical Events

Since reports of Mount Ruapehu's activity began in 1830, 603 days of activity have been observed and described (Scott, 2013). The largest eruptive periods from Mount Ruapehu within the time frame of European settlement has occurred in 1945, 1969, 1971, 1975, 1977, 1978, 1995/96 and 2007 (Scott, 2013). All historical activity has been produced by the open vent beneath the permanent Crater Lake with the total expulsion of the Crater Lake only being observed within the 1945 and 1995/96 eruptions (figure 1.9, Scott, 2013). The interaction of water with magma leads to frequent phreatic and phreatomagmatic eruptions with less frequent instances of prolonged magmatic eruptions taking place.

Based on work conducted by Gamble et al (1999), an historic eruption periodicity of ~ 20-30 years can be estimated when looking at major events. This shows a higher rate of larger eruptions occurring in recent times when compared to the last ~400 years of the TTF which show an eruption frequency of ~60-70 years (Voloschina, 2020).

Figure 1.9: Ruapehu's historical eruptions dating from 1945 (left) and 1996 (right) (Images provided by the National Library of New Zealand. Photographed by Davis, B.V and Reid, P respectively).

1.4 Eruptive Characteristics

1.4.1 Geochemical Properties of Mount Ruapehu's Tephra

Mount Ruapehu has predominantly produced magmas that are andesitic/dacitic in nature with a ~57 – 64 wt% of SiO_2 found within erupted products (Kilgour et al, 2013). Interestingly, throughout all historical records there has been no dramatic change to the isotopic composition of the ejected material, possibly referring to a genetic link among all of Ruapehu's magmas (Kilgour et al, 2013). The magmas are also rich in carbon dioxide (≤1,000 ppm) but water poor (<2 wt%) when compared to standard andesites produced through arc volcanism (Kilgour et al, 2013).

Being able to provide a geochemical fingerprint to tephra is critical in being able to distinguish specific stratigraphical layers, tephra origins and the history of eruptive periods within the TgVC. The BF is distinct in that it can be reliably sourced from a single volcano. In this case tephra produced by Mount Ruapehu 25 – 12 ka (Moebis, 2010). However, the PPF consists of eruptive products from both Ruapehu and the Tongariro Massif. Producing a geochemical fingerprint of Ruapehu's products within this formation will allow for a stronger insight into its eruptive frequency and spatial extent.

Tephra collected in three separate locations by Moebis (2010) showed distinct groupings based on K_2O and FeO wt%. With all Ruapehu tephra generally showing higher percentages of K_2O (1.4- 4 wt%) and lower percentages of FeO (3.7 – 8.3 wt%) than any tephra produced by the Tongariro Massif within the same time frame. These tephras ranged in age up to at least 10 ka and thus provide a reliable and simple means to identify volcanic origins of tephra found within the TgVC. It has been noted that there is a potentially linear trend between K_2O and FeO wt%

over time with prehistoric deposits showing lower K_2O, SiO_2 and higher Fe_2O_3 (Gamble et al, 1999).

Within the Tufa Trig and Bullot Formations from Mount Ruapehu, plagioclase is the dominant phenocryst (3-15 modal%), characterised by clear to white crystals (Gamble et al, 1999; Moebis, 2010; Voloschina, 2010). These minerals are typically up to 4 millimetres across and found to be in equilibrium with proximal groundmass microphenocrysts (Gamble et al, 1999; Pardo et al, 2011). Pyroxenes are also common within tephra with an average width of 1-2 millimetres and are sometimes observed being coated in black or dark brown glass (Gamble et al, 1999; Moebis, 2010). Other phenocrysts are observed such as hornblende, clinopyroxene, orthopyroxene and olivine (Gamble et al, 1999).

1.4.2 Eruption Styles of Mount Ruapehu

Mount Ruapehu has displayed a wide variety of eruption styles throughout its history. With cyclic periods of heightened activity dispersed between lulls surrounding major events (Pardo et al, 2012; Price et al, 2012; Voloschina, 2020). Ruapehu's timeline features small but frequent explosive eruptions commonly associated with phreatomagmatic or phreatic eruptions. The emplacement of the Crater Lake above the main venting system means frequent magma-water interaction and deep hydrothermal alteration occurs at Mount Ruapehu, primarily through the Whangaehu Valley where the Crater Lake drains into. Eruptions large enough to fully displace the Crater Lake are considered "Strombolian" (Gamble et al, 1999).

While phreatomagmatic and phreatic eruptions are the most common eruptive stiles at Mount Ruapehu, the volcano has also historically produced magmatic events as was seen in the 1995/96 eruption phase where sustained activity culminated into a singular large eruption plume up to 12 kilometres in height (Cronin et al, 2003). The volcano has frequently generated multi-phase eruptions with only a very small number of single-phase eruptions having been recorded within its stratigraphy, many previously named deposits within the TTF have recently been split into multi-phase events through work conducted by Voloschina (2020).

1.4.3 Volcanic Hazards of Mount Ruapehu

Mount Ruapehu poses a wide risk to communities proximal to the TgVC, with a complex topography and its disposition towards frequent, explosive eruptions. It is important to recognise potential hazards the volcano can produce not only to incorporate into risk management processes, but to also aid in identifying deposition origins and deposition correlation. The volcano is capable of producing most hazards associated with volcanic

eruptions with lahars, debris avalanches and ashfall making up the majority of ring plain deposits.

The volcano is notorious for its ability to produce devastating lahars even outside of eruptive periods such as what occurred during the 1953 Tangiwai disaster. Lahars can be defined as mudflows originating from volcanic slopes with common instigators including Crater Lake dam failure or remobilisation of material through heavy rainfall (Procter et al, 2021). At least 13 periods of lahar generation have occurred since 1945 with most of them occurring outside of eruption windows (Keys, 2007). Historically, lahars have all been contained to the Whangaehu Valley as the Crater Lake drains through this system. Lahar deposits through this region have shown differing concentrations of flow sediments with debris-flow deposits and hyperconcentrated flow deposits being observed in the ring plain (Procter et al, 2021). Debris flows are characterised by angular sands and gravels deposited with poor sorting to the point of multiple events being indistinguishable within the stratigraphy (Procter et al, 2021). Hyperconcentrated flows are characterised by rounded clasts with faint bedding being visible within stratigraphy (Procter et al, 2021). Lahars from Ruapehu are very common and almost always occur in the event of an eruption due to the presence of the Crater Lake. For catastrophic events with a lahar volume greater than 1.5×10^7 cubic metres, only six have been recorded within the last 2,000 years at a frequency of 1 every 315 years. The frequency is not spaced evenly within the time period (LeCointre et al, 2004).

Debris avalanches from Mount Ruapehu are also prevalent within the ring plain's stratigraphy, with notable examples occurring within the ring plain. The volcano has been capable of producing debris avalanches capable of depositing material up to 80 kilometres away from source with most recorded instances occurring from the southern extent of the complex, mostly stemming from the high levels of hydrothermal alteration occurring with the incorporation of an active Crater Lake (Tost et al, 2014). At least five flank collapses have occurred on Mount Ruapehu due to weakened hydrothermally altered material failing in a highly erosive environment (Tost et al, 2014). Deposition is generally characterised by megaclasts too large to be transported through conventional fluvial methods encased within a matrix of gravels and rounded material (Tost et al, 2014). The largest debris avalanches to be produced from Ruapehu occurred between 70-200 ka with a climatic shift towards warmer climates (Tost et al, 2014).

Ashfall is the most common natural hazard produced by Mount Ruapehu. Deposits identified as ashfall are generally water saturated due to interference with the Crater Lake. Paired with

the tendency towards explosive eruptions, ashfall from Ruapehu is highly fragmented and has been recorded travelling 300 kilometres from source (Cronin et al, 2003; Pardo et al, 2012). Ashfall deposits from Mount Ruapehu are highly variable in terms of colour and composition, ranging from fine ash particles to matrix supported lapilli (figure 1.10, Voloschina, 2020).

Figure 1.10: Ashfall beds within Ruapehu's eastern ring plain, displaying the wide variety of colours, structure, and grain size visible within each band.

Other hazards produced by Mount Ruapehu such as lava flows, and pyroclastic flows are rarely seen within distal, ring plain stratigraphy as they do not travel far from source. Pyroclastic flows in particular are poorly preserved within the geological depiction of Mount Ruapehu with a small number of discrete layers having been located (Cowlyn et al, 2020)

1.4.4 Deposition Characteristics

Deposits located within Mount Ruapehu's ring plain vary depending on the age and explosivity of the event that generated it. The most complex depositional units comprise multiple bed ash units with the most detailed units containing at least 4 subunits (Voloschina, 2020). These multi-bed layers are also significantly larger in volume than other deposits found with tephra dispersal displayed as lobes oriented in different directions surrounding the volcano (Voloschina, 2020). Many of the ashfall deposits that are composed of finer grained material are more susceptible to erosion with the surrounding area having a high effect on the preservation of layers through dense vegetation cover or flat topography (figure 1.11, Cutler et al, 2018). Due to this it can be hard to differentiate between small and moderate sized MBA units with clear edges between layers being less defined (Voloschina, 2020). Deposits from

Mount Ruapehu have migrated southwards with the evolution of the active venting system over the last 12,000 years, with more lahar flows being visible in contemporary deposits (Leonard et al, 2021). Deposits from the volcano outside of the ring plain can be observed to the southwest of the volcano primarily through remobilisation via river systems such as the Whangaehu River. Ashfall deposits commonly extend eastwards due to the prevailing winds (Cronin et al, 2003). Within the observed time period most intact deposits should be found within the south-eastern reaches of the ring plain but the horizontal extent of these deposits may disperse widely across the Rangipo Desert.

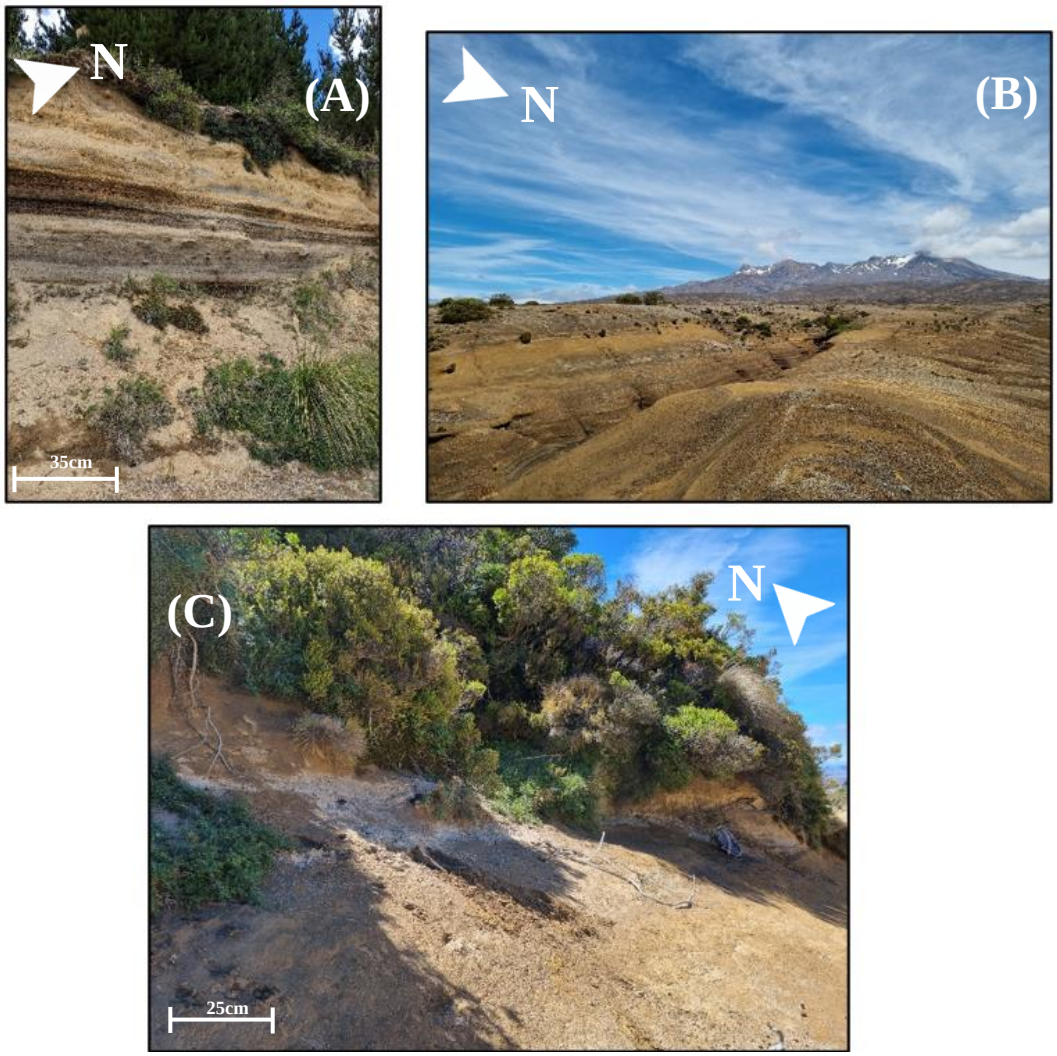

Figure 1.11: Stratigraphic sections across Mount Ruapehu's eastern ring plain. (A) An outcrop with thick ashfall bands ranging from black to a light orange. (B) Rolling hills common within the ring plain. Open channels allow for views of underlying stratigraphy. (C) Deposit within Ruapehu's ring plain with the Taupō Ignimbrite visible.

Methodology

2.1 Field Work

Field work consisted of visiting 25 sites within the eastern ring plain of Mount Ruapehu (figure 2.1) to quantify the dispersal and characteristics of two separate periods within the stratigraphy: (1) Black ash layers found below the 232 C.E. Taupō pumice layer and above the Stent Tephra (~4 ka), (2) Black ash/ orange lapilli layers found between the Stent Tephra and the Moturere Tephra (~7 ka). These visits were used to observe deposits in the field as well as collect samples to perform geochemistry and grain size analysis.

From these 25 locations, 45 deposits were analysed with 26 of them being collected for analysis (appendix 1). These 25 samples were retrieved from 14 of the visited locations.

Site D (figure 2.1) was used as the type locality for this study.

Tephras were identified and correlated based off:

- Location (latitude/longitude).
- Distance from Crater Lake (kilometres).
- Elevation and depth (metres).
- Deposit thickness and grain size (millimetres).
- Colour and texture.
- Bedding, contact between units and lithology.
- Clast shape and roundness.
- Environmental conditions.

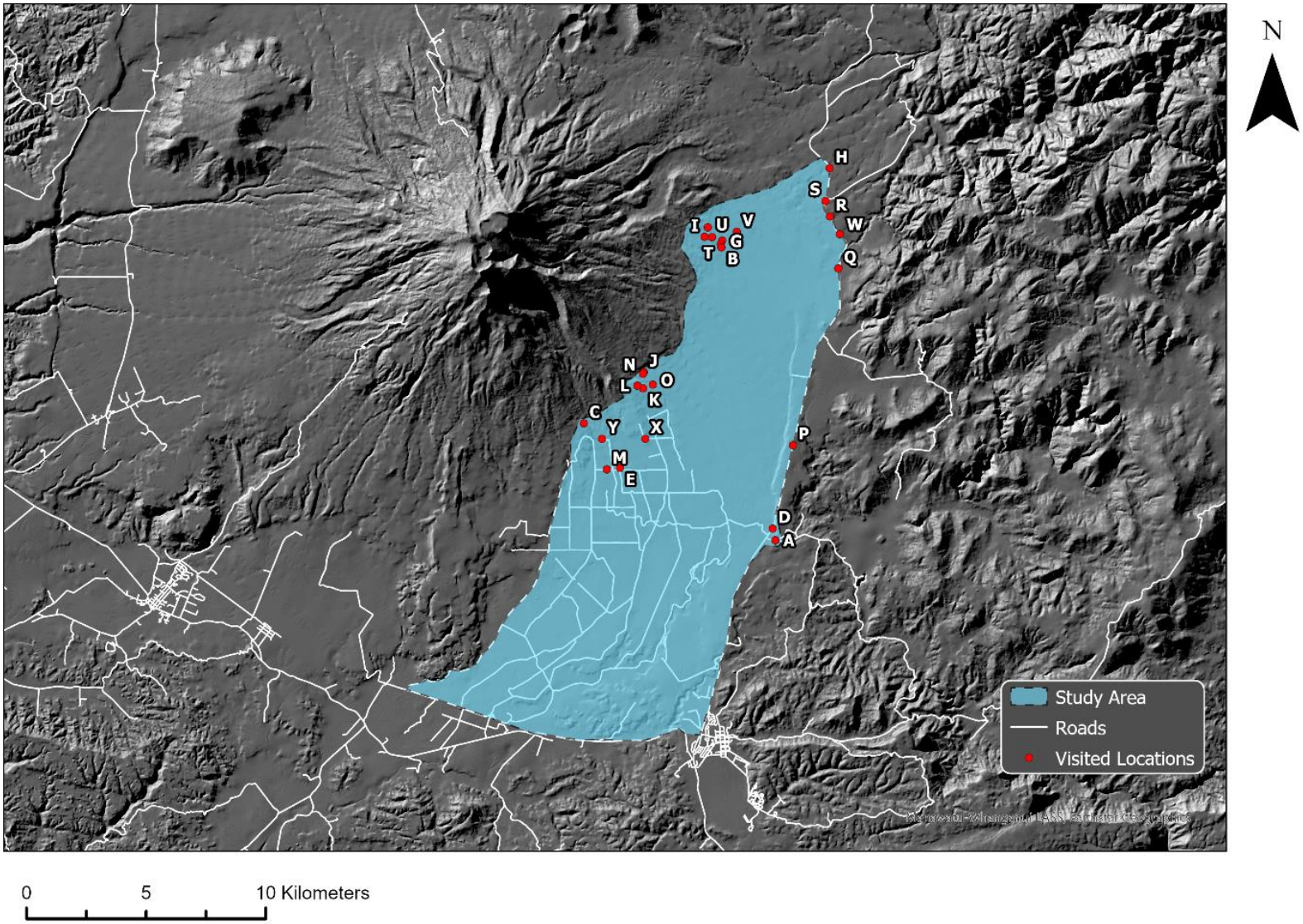

Figure 2.1: Studied region overlaid on a hillshade basemap for visibility. Red points show the visited sites with their corresponding letter. Site D is the study type locality

2.2 Tephra Characterisation

2.2.1 Grain Size Analysis

Samples collected in the field were brought back to the laboratory at Massey University to begin grain size analysis. Samples were dried out at 50°C overnight to remove moisture. They were then wet sieved to prevent fine particles from exiting the sample. Sieving for this study was conducted using the Wentworth scale which allocates grain sizes based on a measurement of phi (ϕ) with 0 ϕ equating to a grain size of 1 millimetre. Grain size doubles with a sequential decrease in phi and halves with a sequential increase in phi. Wet sieving occurred at 1 ϕ and 3 ϕ for a distinct view of coarse, medium, and fine ash within each sample. Samples were then placed back in the 50°C oven for up to a week before dry sieving. Dry sieving was done between -3 ϕ and 3 ϕ at 1 ϕ intervals to further distinguish between clast sizes. Size classes were weighed for each sample after dry sieving and weights were compared to the total weight of the sample to provide grain size weight ratios.

For all samples, the size fraction >3 ϕ was analysed using a LA-950V2 Laser Scattering Particle Size Distribution Analyser from Horiba. Using two separate wavelengths of light it is able to differentiate different particle sizes within any given sample. Normally this would require identifying the refractive index of each sample prior to use. However, a measuring routine using the Fraunhofer approximation was applied to the LPA which does not require the refractive index of the material and ignores particles smaller than 2 microns. This provides a good observation of larger particles which is more important than having a full overview of every particle which requires the refractive index which can be difficult to obtain. Each sample was run until three sequential measurements were overlapping and then merged.

Results from the LPA were combined with measurements obtained from manual hand sieving to provide full grain size distributions of each sample obtained within the field. These were then input into GRADISTAT V8 (Blott and Pye, 2001). This software is capable of providing in depth statistics of grain size distribution through in built excel macros, these provide charts and tables of grain size data for each sample. Single sample data input was used to provide detailed information on each sample.

2.2.2 Componentry

Characterising the clasts found within each tephra is an important factor to distinguishing eruptive conditions and deposit similarities. The ratio of lithics, pumiceous material, glass and minerals provides context to how tephras were produced and the mechanisms that initiated fragmentation. To avoid bias within samples, point counting was conducted prior to any other analysis that required the removal of clasts from the original sample.

2.2.2.1 Point Counting

To maintain statistical significance and to provide an overview that is representative, samples were split and at least 300 clasts were individually counted. Out of the 26 samples collected, 10 were used in point counting as all rhyolitic and unreliable material were excluded. The 1 ϕ size fraction was used as all samples had grains within that fraction and allowed for ash based and lapilli-based beds to be compared.

The clasts from each of the 14 samples were categorised into six classes based on visible characteristics. These being lithics, pumiceous material, smooth glass, vesicular glass, feldspars, and pyroxenes. Once all grains were classed, the results were normalised to the total number of grains and calculated as ratios of the total sample. Lithics incorporated all clasts that were either accidental, cognate, or difficult to allocate to any of the other more concise classes. Accidental and cognate clasts being ones that did not match the rest of the sample or were recycled material from previous eruptions respectively. These typically showed signs of hydrothermal alteration or rounding.

2.2.3 Tephra Dispersal and Volume Calculations

2.2.3.1 Isopach and Isopleth Construction

Isopach construction is the basis for calculating volume estimates for target deposits within the ring plain. They were constructed based on deposit thickness at different locations as measured in the field. A shaded basemap of New Zealand's central North Island from GNS (https://data.gns.cri.nz/server/rest/services) was used as a template to manually draw isopachs onto through ArcGIS.

Isopleths are constructed in a similar way as the isopachs but will be based on the average grain size found at each location for each tephra layer based on summaries produced through GRADISTAT (Blott and Pye, 2001).

2.2.3.2 Volume Calculations

Calculating the volume of each tephra layer is a critical step to analysing the distances and thicknesses each tephra deposit reaches. There are a number of different calculations used to estimate volumes of tephra dispersal with each having their own benefits and drawbacks. Methods posed by Fierstein et al (1992) and Pyle (1989) have both been used extensively within the field but ignore distal deposits and could potentially underestimate the total volume for each deposit. The Weibull method proposed by Bonadonna et al (2012) uses the basis that tephras do not typically thin exponentially but instead through straight line segments (Bonadonna et al, 1998).

The method for volume calculation being used for the tephras being analysed was coined by Legros (2000) which estimates a minimum tephra volume based on the average isopach thickness and the total area that is encapsulated within. Tephra volume is calculated as:

$$V = 3.69 * T * A$$

Where:

T = average thickness of the tephra layer
A = total area found within the largest tephra isopach.

The Legros method is utilised as it is simple and can be applied to all datasets that had been collected in the field.

2.3 Geochemistry

2.3.1 X-Ray Fluorescence

X-Ray Fluorescence (XRF) is a method of using the interaction between X-rays and the material to determine the composition. It occurs through the process of knocking an electron out of orbit around a nucleus producing a hole in the orbital. This unstable configuration is quickly restored to equilibrium through a higher energy electron from an outer orbital falling into the gap (Brouwer, 2006). Through this action, the energy difference is ejected as fluorescent X-rays. The energy difference is unique to each atom and thus can be measured to

determine the composition of the material at an atomic level (Brouwer, 2006). There are two methods of XRF, each with their own benefits. These being Energy Dispersive (ED) and Wavelength Dispersive (WD). ED directly measures the energies emitted from the sample whereas WD splits the X-rays by their wavelength, allowing for lighter materials to be spotted and a higher spectral resolution to be achieved. The instrument used was a Bruker S8 TIGER at Massey University in Palmerston North, New Zealand. The Bruker S8 TIGER utilises WDXRF for a higher resolution to be achieved.

All 26 samples were analysed using this method. Grain sizes of 2 ϕ were used as 25 of the samples had ≥2 grams of material while one outlier had to use 1 ϕ, the differences were deemed to be minimal. One sample each of Oreas 24-B and 24-C were also included as standard reference material to check if the final results could be deemed reliable. Once 2 grams of each sample and reference material had been measured out to 4d.p. and the weight of each crucible was also accounted for, they were placed in a 105°C oven overnight to remove all moisture. Once sufficiently dried they were each reweighed to find their dry weight and kept in desiccators until they could be moved into a muffle furnace. Samples were mapped out and left for 7-8 hours at 1200°C before being left to cool to above 100°C. Samples were once again reweighed to find their combusted weight.

From here, loss on ignition (LOI) was calculated through this calculation:

$$\text{L.O.I. (weight \%)} = 100 \times ((n_2 - n_3) / (n_2 - n_1))$$

Where:

n_1 = weight of the crucible
n_2 = weight of the crucible plus oven dried sample
n_3 = weight of the crucible plus combusted sample

0.8 grams of each sample are weighed out (4.d.p.) and mixed with 8 grams of 57:43 flux (57% Lithium Tetraborate and 43% Lithium Metaborate. 4.d.p.). Once sufficiently mixed, each sample was placed within a platinum crucible and inserted into an XRFuse2 to be melted into a glass bead under the long fusion program. Crucibles were cleaned in diluted citric acid between each batch. Beads were then inserted into a Bruker S8 TIGER to begin WDXRF.

Field Observations

3.1 Overview of Study Area

The study area consisted of four major zones with one of them being inaccessible for the duration of the field work. The three accessible regions were chosen for their proximity to Mount Ruapehu and their abundance of exposed outcrops through human alteration or natural formations. Within these three accessible zones, 25 locations were visited (table 3.1).

The eastern region of Mount Ruapehu's ring plain consists entirely of the Rangipo Desert, this region is heavily altered by volcanic activity from a number of sources including Ruapehu, Tongariro and Lake Taupō. Due to the dynamic nature of the region, there are many instances of overlapping deposits ranging from extremely thin ashfall to large ignimbrite deposits that blanket the region. Due to this, geological markers within the stratigraphy are imperative to be able to reliably correlate and measure distal deposits.

For this study, the two main geological markers used to investigate deposits were the 232 C.E. Taupō Ignimbrite and the 4322 ± 112 ka Stent Tephra. When these markers were not visible, the appearance of other studied tephras aided in correlating tephra layers in the field.

Table 3.1: Site identifiers including their latitude/longitude coordinates, distance from source (Ruapehu Crater Lake) and the elevation (metres)

Site ID	Marker location (lat/long)	Marker DFS (km)	Elevation (m)
A	-39.39303, 175.70899	17.60	945.00
B	-39.27998, 175.68236	10.20	1180.00
C	-39.34788, 175.61387	8.60	1135.00
D	-39.38848, 175.70776	17.20	930.00
E	-39.36498, 175.63183	11.00	1010.00
F	-39.27228, 175.67563	9.70	1220.00
G	-39.27732, 175.68273	10.30	1195.00
H	-39.24948, 175.73616	15.30	1010.00
I	-39.27594, 175.67395	9.50	1235.00
J	-39.32808, 175.64374	8.60	1180.00
K	-39.33409, 175.64352	9.00	1160.00
L	-39.33329, 175.64049	8.80	1215.00
M	-39.36551, 175.62486	10.80	1050.00
N	-39.32865, 175.64339	8.70	1195.00
O	-39.33287, 175.64821	9.30	1150.00
P	-39.35633, 175.71778	15.70	1040.00
Q	-39.28816, 175.74045	15.30	1065.00
R	-39.26805, 175.73622	14.90	1065.00
S	-39.26203, 175.73415	14.80	1055.00
T	-39.27864, 175.68189	10.20	1200.00
U	-39.27607, 175.67775	9.80	1215.00
V	-39.27405, 175.69000	10.90	1165.00
W	-39.27489, 175.74116	15.30	1055.00
X	-39.35378, 175.64436	10.60	1085.00
Y	-39.35377, 175.62298	9.50	1075.00

3.2 Overview of Major Zones

3.2.1 Karioi Forest

Preservation of primary Papakai deposits across the eastern ring plain within the Karioi Forest allowed for accessibility to 10 sites (figure 3.1). This was due to its abundance of outcrops and its proximity to Mount Ruapehu allowed for clearer stratigraphy especially within its northern reaches. 17 tephra layers were observed with the clearest outcrop appearing at a large metal pit within the northern end of the forest (Site E). Out of the 17 observations, 9 tephra layers from sites C, E, J, K and L were sampled for further analysis. A few of these were obtained north of the forest itself but are still considered to be from within the Karioi Forest Zone (figure 3.2 B and C).

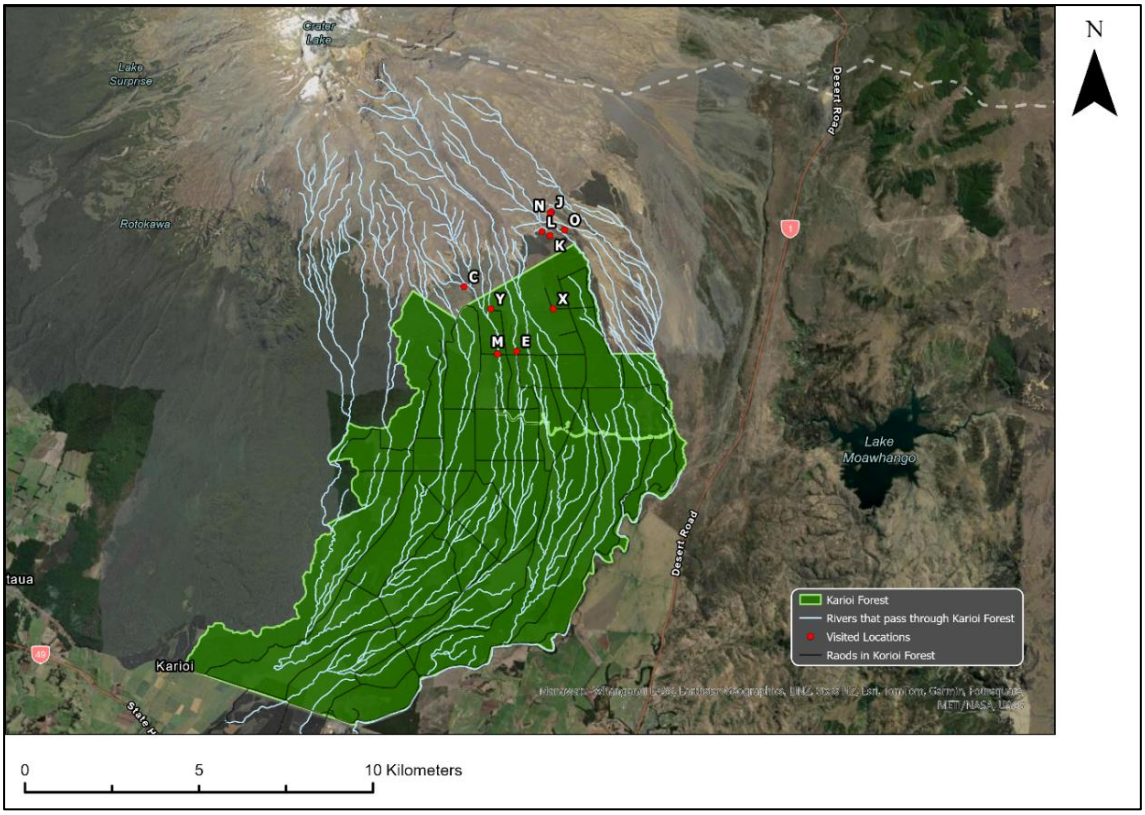

Figure 3.1: Geographical extent of the Karioi Forest. Sample sites in and around the zone are labelled.

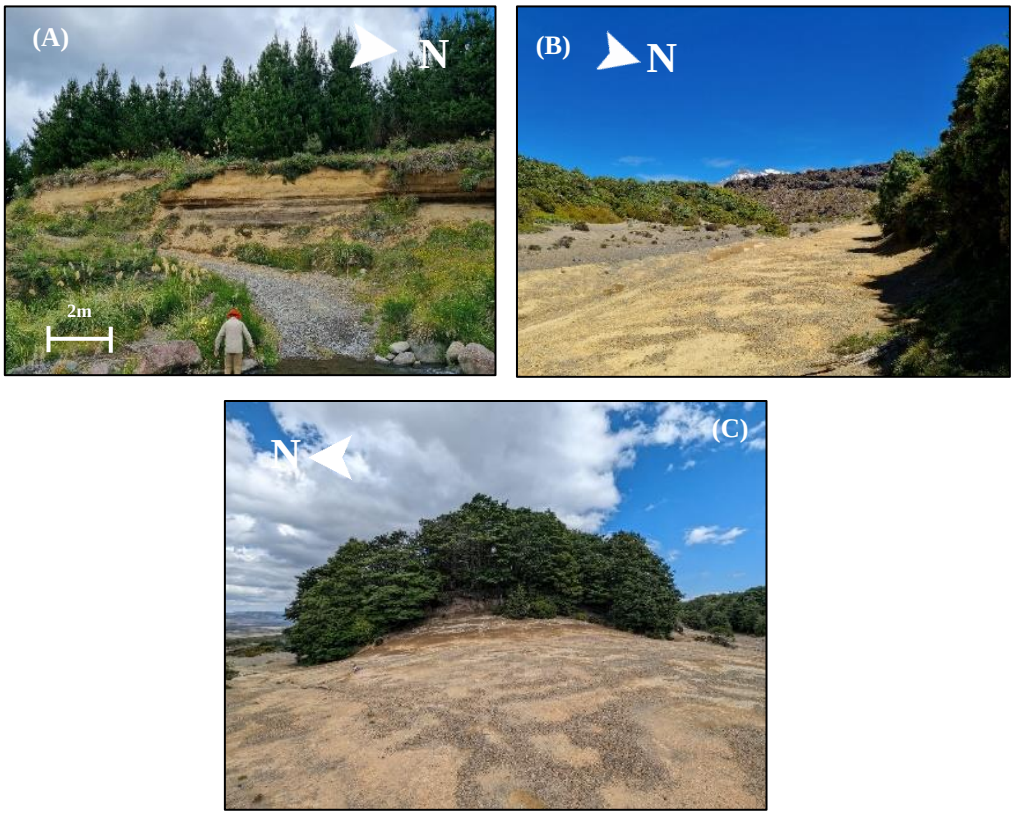

Figure 3.2: Outcrops within the Karioi Forest Zone. (A) Large outcrop found along Extreme Road within the Karioi Forest (Site M). (B) Mount Ruapehu with an old river plain in the foreground. (C) One of the northern points of the zone facing south with the Tufa Trig type locality visible (Site K).

3.2.2 State Highway 1 (Desert Road)

The Desert Road was a very useful zone to examine variation in deposits over large distances due to its predominantly straight layout and abundance of road-side outcroppings. These deposits were usually the furthest from source and the most distal deposits available as any further east was operated by the military. Despite this, the most northern, eastern, and southern observations were taken through this zone (Sites H, Q and A respectively). 8 sites were visited with 17 units observed and 9 samples collected from sites A, D and H (figure 3.3).

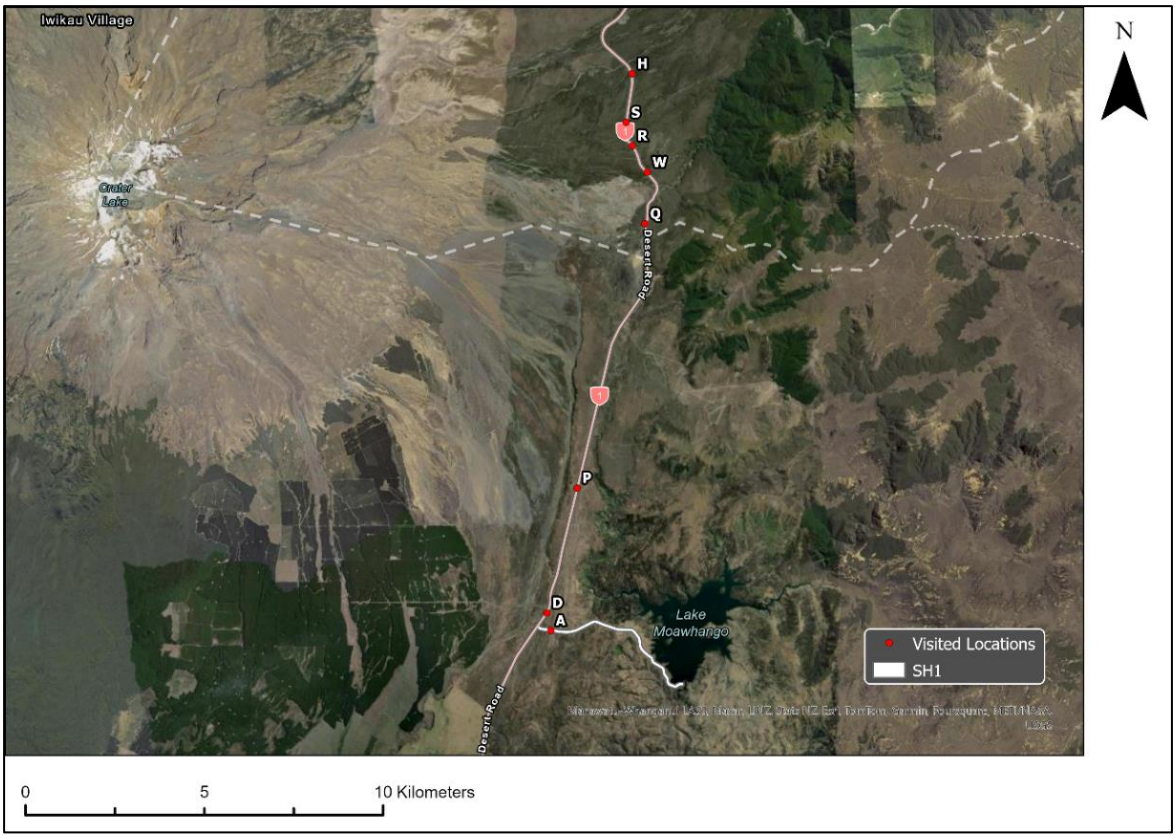

Figure 3.3: Location map of State Highway 1. This zone includes Access Road 17 (Site A) to the southeast of the surveyed area. Site D in the south of the zone is the type locality

Due to the distal and exposed nature of the Desert Road, many sites were poorly preserved with intact tephra being observed at the northern and southern ends of the zone, usually on large outcrops (figure 3.4A). The type locality for this study was found within this zone at site D. All tephra layers being studied were observed and sampled from this site.

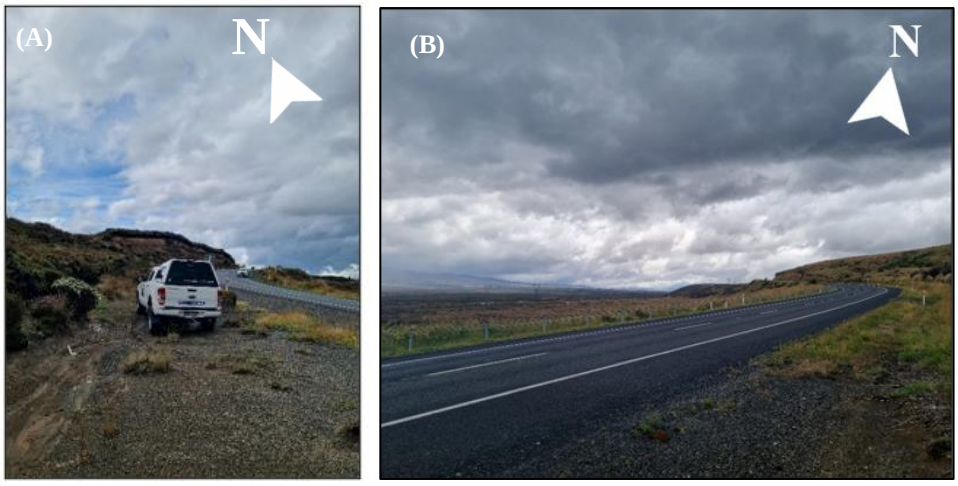

Figure 3.4: Locations along State Highway 1. (A) Site Q presented in the background, facing away from Mount Ruapehu. (B) An image facing north from the type locality.

3.2.3 Tukino Access Road

7 sites were visited with 11 tephra layers having been observed along the Tukino Access Road with 4 samples collected from sites G and I (figure 3.5). This zone was used as the northernmost border for tephra observations and aimed to check if PPF deposits were found north of the crater lake in any capacity. Deposits along this zone become visible ~5 kilometres west of State Highway 1. (figure 3.6). Stratigraphy within this zone was very weathered with very little being observed.

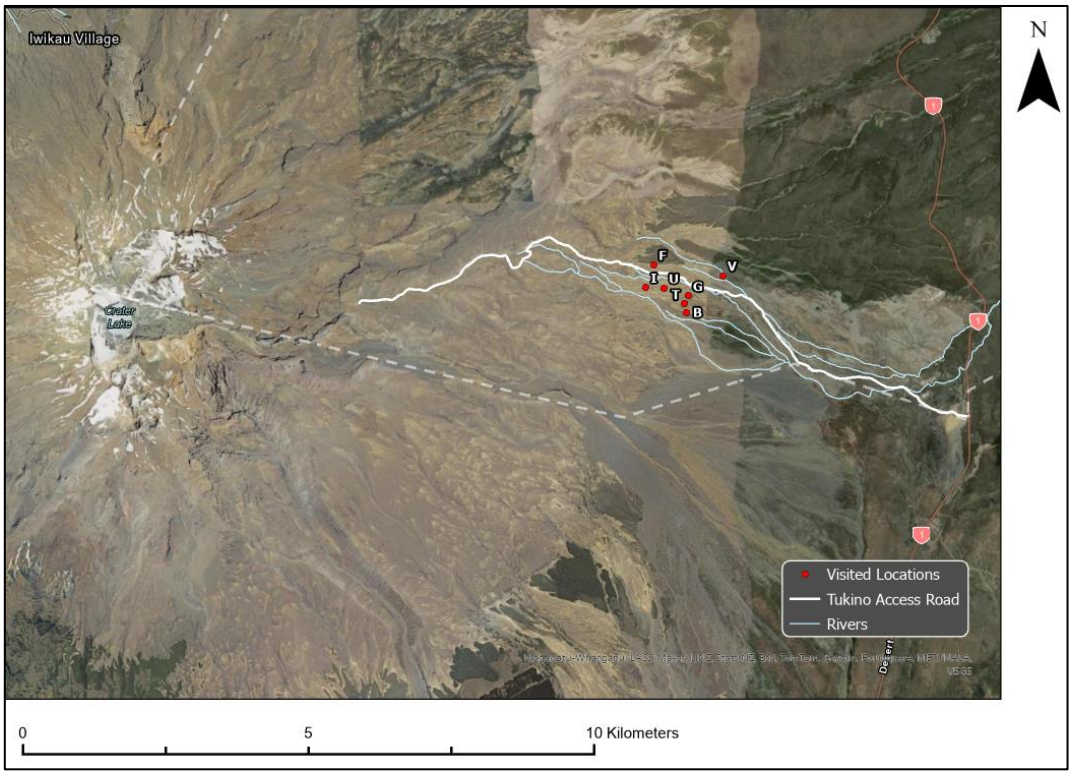

Figure 3.5: The Tukino Access Road Zone. Sites visited are shown as red dots

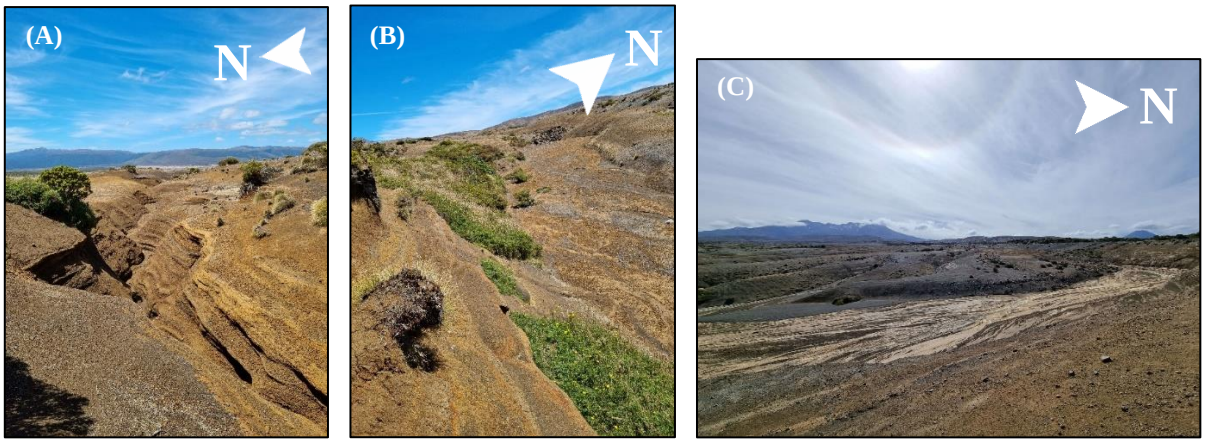

Figure 3.6: The Tukino Access Road Zone. (A) Typical topography found within the zone. (B) A near vertical wall with Layers observed at the peak (site T). (C) A relatively young riverbed to the north of the study area is framed with Mount Ruapehu in the background (Site V).

3.2.4 Military Grounds

The military controlled region in the central section of Ruapehu's eastern ring plain was the most expansive zone that was intended to be surveyed for deposits. As this zone was situated in the middle of the other areas it was a key region that held significance for advancing the aim of this study. For research based within this region work from Donoghue (1991) will be used as a substitute.

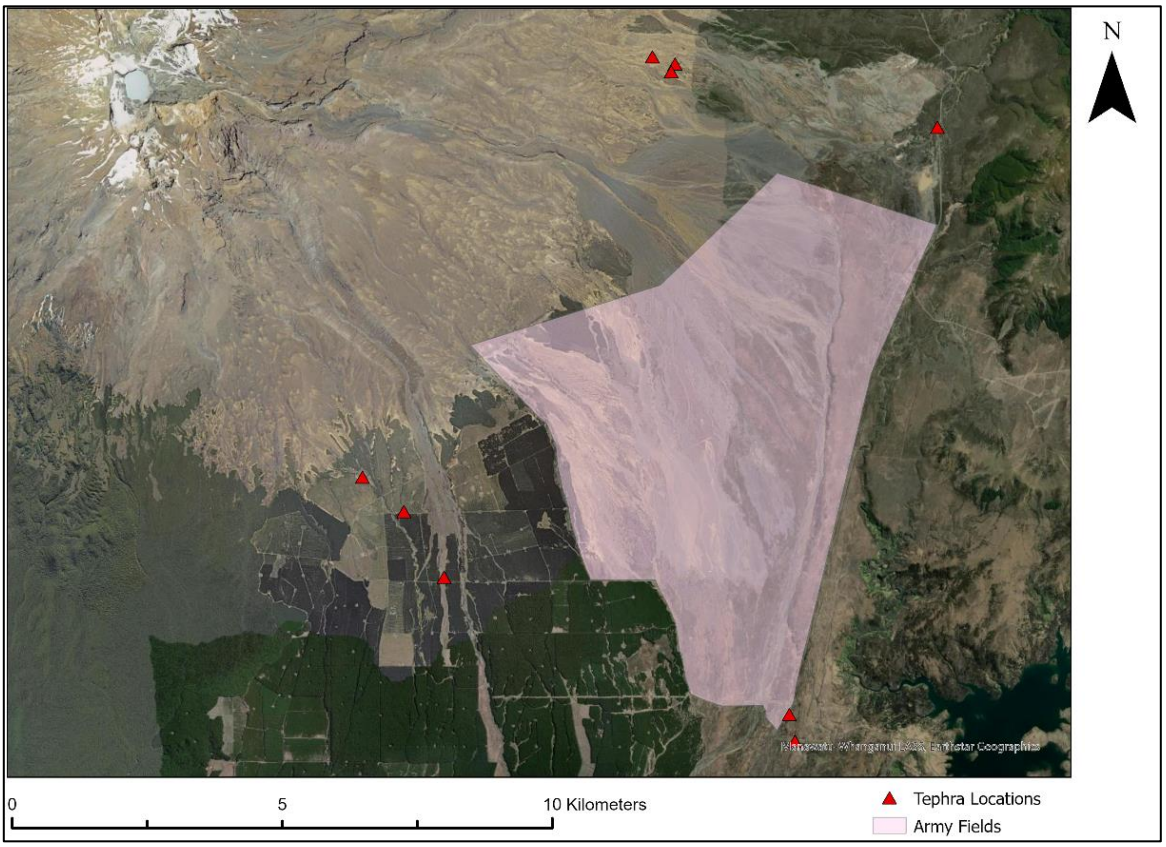

Figure 3.7: Military Ground search zone based on Donoghue (1991) Locations where PPF deposits were found are shown.

The zone utilised by Donoghue (1991; figure 3.7) constituted primarily of regions within what is deemed The Badlands, Death Valley, Scorpion Gully, and The Chute. It was through here where the majority of their depictions for the tephra layers were found. These areas fall within the western portion of the Rangipo Desert and are aptly named due to their extreme conditions through exposure to wind, sun, and snow. Extensive sampling and mapping would have been conducted through this region had access been permitted. Particularly through Death Valley where black ash deposits were noted by Donoghue (1991).

3.3 Field Characterisation of Deposits

The deposits specific to this study fall under two designations: black ash or orange lapilli. These were defined under Moebis (2010 – Table 1.1). Four layers had been previously defined and stated to appear beneath the Stent Tephra by Donoghue (1991).

Being able to create a detailed characterisation of the studied tephra layers based on their stratigraphy and physical appearance is critical in being able to accurately identify them. It also allows for the creation of isopachs to be generated based on section thicknesses. Location data as well as bedding are also useful observations to predict dispersion patterns and deposition characteristics. A number of observations were made for each layer observed in the field. Samples were collected and further analysed for grain size and geochemistry.

The black ash layers were the most frequently observed out of the four primary layers being investigated. This would be due to their contrast to the surrounding soils but also their depth having a greater chance of not being too buried to observe. However, these two layers were still poorly preserved within the stratigraphy with only a few locations being reasonably considered to have those layers.

The orange lapilli layers were the least defined within the stratigraphy with very little deposits observed. This will be mostly due to accessibility to the tephra layers at visited sites. When the layers were visible, they were very recognisable as they stood out directly from the surrounding material due to clast size and colour.

An orange lapilli layer was found in some locations sitting directly above the deeper black ash layer. It does not appear in previous works and is very discernible within the outcrops it appears in. Samples were taken to provide further information on its geochemical composition and relation to the main deposits being studied.

3.3.1 Black Ash Layers

3.3.1.1 Black Ash T 1

Black Ash T 1 (BAT-1) is a commonly occurring ashfall layer found within the eastern ring plain with observations having been made at sites C, D, G, K, M, P and X. Samples were collected from sites D, G and K.

Observations of BAT-1 occurred between 930 metres to 1195 metres above sea level and was found between 9 kilometres and 17.2 kilometres. Its physical appearance was a very fine ash that was partially cemented with a blocky appearance. It was black/gunmetal grey. The thickness of the layer ranged from 15 millimetres to 74 millimetres. A mix of orange and brown soils surrounded the visible deposits with soils getting more pumiceous further up from the tephra layer. All observed tephra layers showed fine-grained ashfall. The tephra layer was never found to be in contact with the other black ash T layer (BAT-2).

BAT-1 deposits followed similar trends to BAT-2 deposits with them being found beneath the Taupō pumice layer. Tephra layers were generally thicker than BAT-2 deposits but also showed a higher degree of cementing across most observed deposits. There were also more deposits within the grey colour range. Both of these factors could imply greater susceptibility to erosion and weathering. The tephra layer was found between 9 centimetres to 30 centimetres beneath the Taupō pumice layer and was generally quite pocketed in appearance. Orange and brown soils surround much like BAT-2. BAT-1 had little lateral variation at all observed deposits.

3.3.1.2 Black Ash T 2

Black Ash T 2 (BAT-2) was the most commonly noted deposit in the field, most likely due to its proximity to the Taupō Ignimbrite. The tephra layer was found at sites D, G, H, I, J, K, L, N, O, R, S and V with samples being collected at sites G, H, I, J, K and L.

Observations for it ranged from an elevation of 1010 metres to 1230 metres above sea level. Its proximity to source ranged from 8.6 kilometres to 17.1 kilometres. In the field it was usually found in a blocky, almost cemented state and mostly conformed to the shape and nature of the Taupō Ignimbrite that was always found above it.

Usually surrounded by orange or brown soils with dark ash layers observable beneath it. The BAT-2 tephra thickness varied between 13 millimetres to 41 millimetres. Grading was fairly homogenous with all observed units of this tephra layer showing a fine-grained ashfall. This

layer was never found to be in contact with BAT-1 with fine grained soils observed between them.

For BAT-2, all observed layers were a defined black to dark grey colouring with a thickness appearing to slightly increase to the northern extents of the surveyed area but staying generally consistent. Texture ranged from very fine, homogeneous ashfall layers that had very little cohesion to cemented blocks that appeared distinctly in contrast to the orange/brown soils that surrounded it. Lateral variation of the deposit across the sites it was located at varied from conforming to the Taupō pumice layer above to an erratic, non-conforming layer. Despite this, it was generally an easy tephra layer to identify and observe within the local stratigraphy. Its depth beneath the Taupō pumice generally ranged between 1 centimetre to 30 centimetres with the more proximal layers showing less cementing. All visible grain sizes were too small to define with no larger clasts being observed in any deposit.

3.3.1.3 Black Ash 1

Black Ash 1 (BA-1) was unique in that it was usually found in direct contact with an orange lapilli layer directly above it (Orange Lapilli 3). BA-1 was found at sites A, C, D, E and Q with samples being collected at all sites except Q.

BA-1 was observed between 930 and 1135 metres above sea level and was 8.6 to 17.6 kilometres away from source (its distal deposit being the furthest from source recorded in the study). Deposits had larger grain sizes than other black ash deposits with the largest grains being ~8 millimetres in diameter.

BA-1 deposits appeared less weathered than Black Ash 2 layers (BA-2). The contact between units was fairly homogeneous with one observed layer having a grey top layer with the grading becoming darker with depth. Orange soils are found surrounding the layer. This layer is a dependable geological marker for other tephras as its surrounding bedding is quite defined and easy to spot within the stratigraphy. The tephra layer was black in colour with weathered sections appearing grey. The observable grain size ranged from fine to medium ashfall. The only layer BA-1 was in contact with was Orange Lapilli 3. When both layers were visible in the stratigraphy they were always in contact.

BA-1 was easy to observe simply due to its association with Orange Lapilli 3. That greatly improved its chance of being observed and correlated within the field but nevertheless it was still poorly preserved within the ring plain. Alongside this, it showed lesser degrees of cementing in comparison to BA-2 but still showed signs of weathering. All observations

deemed it to be a consistent black/metal grey ash layer with one layer showing grains that could be measured by hand. Tephra layers were generally found between 100 to 160 centimetres beneath the Taupō ignimbrite with fairly concise lateral variation although some layers were hard to track laterally and appeared infrequently within its outcrop.

3.3.1.4 Black Ash 2

Black Ash 2 (BA-2) was the youngest out of the studied PPF tephras. The deposit was very difficult to locate with observations made at sites D, E and G with samples being collected at all three sites.

The BA-2 tephra ranged in thickness between 4.3 millimetres to 7 millimetres with one exception being 50 millimetres. BA-2 was found between an altitude of 930 metres to 1195 metres and between 10.3 kilometres and 17.2 kilometres from source. The largest grain size found was smaller than 4 millimetres. The tephra layer was found to be black in less eroded states such as at site E but when cemented such as at site D it took on a more metal-grey appearance. Dark orange soils were typically found surrounding it with a gradual transition towards a lighter orange the closer they got to Orange Lapilli 3. The observable grain size for BA-2 ranged from fine to medium-grained ashfall. This layer was also never in contact with other tephra layers with soils always surrounding it. All three layers that were found were cemented to some degree with little matrix found. It was mostly found in pockets with minor lateral variation. Tephra layers were found between 89 centimetres to 119 centimetres beneath the Taupō Ignimbrite layer.

3.3.2 Orange Lapilli Layers

3.3.2.1 Orange Lapilli 1

Orange Lapilli 1 (OL-1) was the most observed lapilli layer within the PPF due to its striking orange colour and the large clasts it comprised of. The tephra layer was observed at sites C, D and E with samples being collected at all sites. The largest grain sizes observed were <34 millimetres with angular, irregular grains. OL-1 grains were also vesicular and could be broken apart by hand. Orange soils surrounded the tephra with the observed layer at site C showing high amounts of weathering had occurred with a pale-yellow colour and a thick, fused matrix that made sampling difficult.

OL-1 deposits were found at elevations between 930 metres and 1135 metres and 8.6 to 17.2 kilometres from source. The OL-1 tephra deposits ranged between 53 millimetres to 130 millimetres in thickness. Deposits were quite visible within the stratigraphy. This layer was used as the base of the stratigraphy and the oldest Ruapehu derived tephra within the PPF described in this study. Orange Lapilli 2 was sometimes in contact with this layer, but the two tephra layers often had coarse orange soils between them and orange soils that transitioned to fine, brown soils beneath OL-1. OL-1 deposits were always seen as a medium to coarse grained lapilli layer.

OL-1 was easily observable when not buried which was a likely scenario as it was usually found between 125 centimetres to 170 centimetres beneath the Taupō Ignimbrite. In the deposits there was a wide variety of clast sizes with very little matrix being visible with clasts being in full contact. The lithology of the non-welded clasts was generally quite pumiceous although less vesicles than what was found in Orange Lapilli 2. These clasts were also rather regular in shape just with a variety of clast sizes. They were also found to be between sub-angular to rounded in shape. The welded clasts were solid with very little vesicles and were jagged and irregular in shape. This layer saw orange soils sitting above with brown soils sitting below. At site E, large boulders could be observed beneath which had potentially been deposited during a lahar event in the area.

3.3.2.2 Orange Lapilli 2

Orange Lapilli 2 (OL-2) was found to consist of fine to medium-grained lapilli with grains usually around 8 millimetres in diameter with the largest measured clasts being ~20 millimetres. These grains were more rounded than what was observed in OL-1 tephra layers and were irregular in shape. They were quite pumiceous and appeared in non-homogenous clumps within the stratigraphy. OL-2 was observed at sites C, D and T with a sample being collected at site D.

The deposits were found 930 metres to 1200 metres above sea level and 9.5 kilometres to 17.2 kilometres from source. Deposits showed a consistent thickness with a range between 53 millimetres and 80 millimetres. It appeared to be poorly preserved within the ring plain stratigraphy and sometimes bordered OL-1 in field sites. Orange soils were usually seen between these layers and darker orange-brown soils sat above OL-2.

OL-2 was the least observed layer in the field with only one site where observations were reliable enough to warrant sampling. Tephra layers were found between 90 centimetres to 140

centimetres beneath the Taupō pumice and all layers consisted of a bright orange layer with clasts suspended in a matrix. Contact between units was generally poorly defined as the clasts were sporadic within the matrix. Clast shapes were considered sub angular to sub rounded with a greater leaning towards rounded clasts with an irregular shape. The clasts themselves could crumble under little pressure and had distinct vesicles. The surrounding matrix was also orange in colour which could show that the ashfall that suspended the matrix was comprised of the same material as the clasts just at a much smaller grain size.

3.3.2.3 Orange Lapilli 3

Orange Lapilli 3 (OL-3) was unique in that it was always found in contact with BA-1 and was observed between BA-1 and BA-2. It was observed at sites D, E and U with samples collected at sites D and E. The grain size was comparable to OL-1 with the largest clasts being around 25 millimetres. The tephra layer had a thickness ranging from 2 millimetres to 25 millimetres. The largest clasts occupying the entire vertical portion of the deposit at site D. OL-3 layers were a bright orange colour with sub-angular, irregular clasts suspended in a thin, orange matrix with orange, medium grained soils found above it and BA-1 found directly in contact beneath it.

OL-3 was found between 930 metres to 1215 metres above sea level with observations being made 9.8 to 17.2 kilometres from the Crater Lake. The tephra layer was observed as a medium to coarse lapilli layer within the stratigraphy. It never came into contact with BA-2.

Irregularly shaped clasts taking on a sub angular/rounded appearance were observed. These clasts sat within a thin orange matrix with the clasts showing small vesicles. One layer was found elsewhere that appeared to be relatively ashy with little to no clasts (Site U). Due to the abrupt change in composition and the location, a sample was not collected but observations were still made.

3.4 Stratigraphy

Understanding and representing the field stratigraphy for future use is critical in being able to sort data and tie analytical information back to physical observations. The tephras in question were difficult to find with only a few locations showing signs of potential deposits with even less being in a condition to observe, note and collect samples. One location provided an in-depth view of the entire sequence being examined with other locations providing geographical context and comparative data.

3.4.1 SH1 Lookout – Site D (Type Locality)

The most important site visited during the field work was labelled site D. This site was found just south of a lookout point along State Highway 1 at the bottom of a ridgeline (figure 2.1). This section showed a detailed stratigraphy and the PPF tephras were found at the very lowest point of the observable stratigraphy. It provided the most complete record of the sequence being investigated and was the only location where all PPF tephras were sampled for analysis (figure 3.8; Table 3.2).

Site D was also one of the furthest locations from source being 17.2 kilometres away from Mount Ruapehu's Crater Lake. Site D was found at an elevation of 930 metres above sea level and was found to be the furthest extent observed for all but one deposit. The tephras themselves were well preserved and did not appear too weathered or disrupted despite facing strong westerly winds.

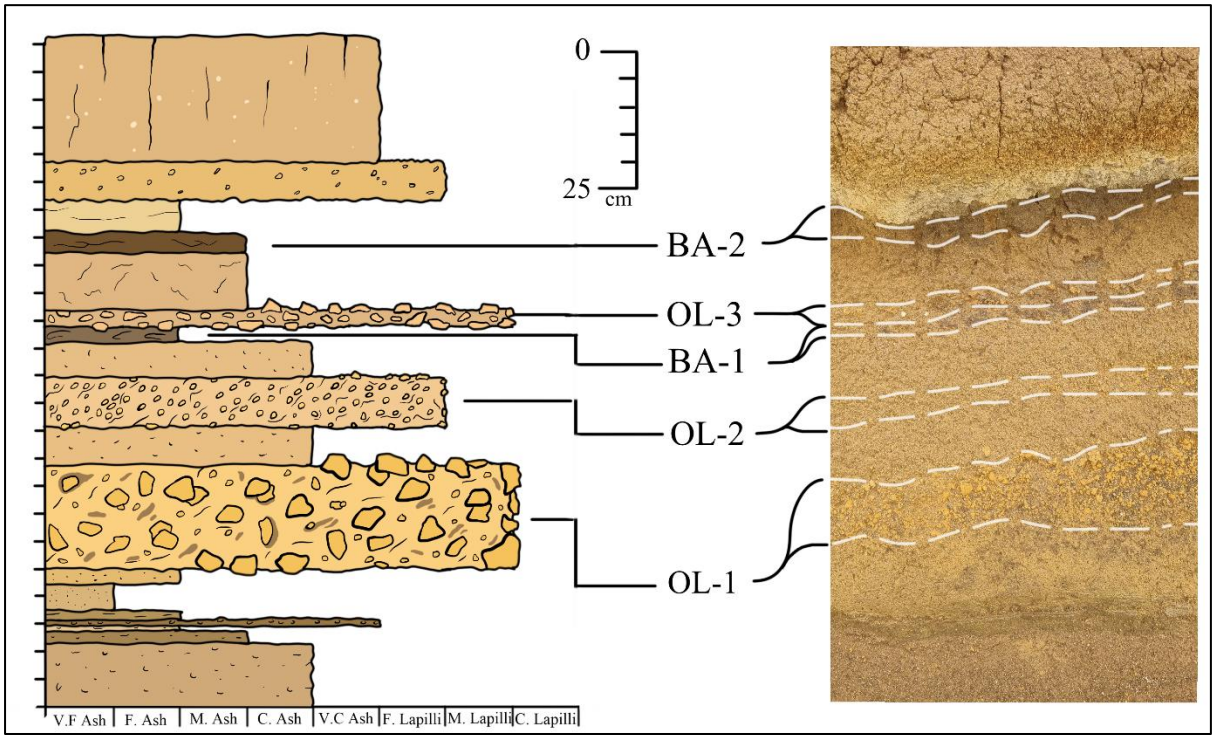

Figure 3.8: Stratigraphic log of the type locality – Site D.

Table 3.2: Field observations at Site D

Sample ID	Layer ID	Depth (m)	Layer Thickness (mm)	Grain Size (mm)	Colour	Texture	Depth Below Taupō (cm)	Contact Between Units	Clast Lithology	Clast Shape	Clast Roundness	Bedding	Lateral Variation
10D	BAT-1	1.5	15	<1	Grey	Fine ash	16	Non cohesive, small clumps				Surrounded by orange/brown soils.	No discernible variation. small pockets
16D	BAT-1	1	35	<1	Black	Partly cemented, blocky	13	Not cohesive, blocky				Orange soils surrounding. varying colours of Taupō sit above	Minimal, quite straight
2D	BA-2	1.69	7	<1	Metal grey	Very cemented	119	Complete contact, no matrix				Soils change colour above it	Appears in patches
25D	OL-3	1.8	2	<25	Orange	Large blocks	130	Blocky		Irregular	Sub angular	Sits directly on top of BA-1	Consistent with BA-1
7D	BA-1	1.8	24	<5	Black	Cemented but can break apart	130	Fairly homogeneous				Orange tephra sits right above, embedded in orange soils	Minimal. fairly cohesive
18D	OL-2	1.9	70	<10	Orange	Same as OL-1 but much smaller grain sizes	135	BLOCKY, not homogeneous	Almost pumiceous, crumbly	Irregular	Sub angular/ sub rounded	Sits between BA-1 and OL-1	Dispersed pockets
22D	OL-1	2	130	<25	Orange	Coarse chunks	140	Defined chunks in a matrix	Coarse, almost pumiceous.	Blocky, large variation	Sub-angular	Surrounded by darker orange soils	Minimal

3.4.2 Karioi Forest Metal Pit – Site E

Site E was the most prominent location within the Karioi Forest. Found within a large, excavated metal pit. The deposits were well preserved with all but one PPF layer identified (figure 3.9; table 3.3). This location was found 6.2 kilometres closer to source than site D at an elevation of 1010 metres. This was exemplified with some layers displaying larger clasts such as OL-3.

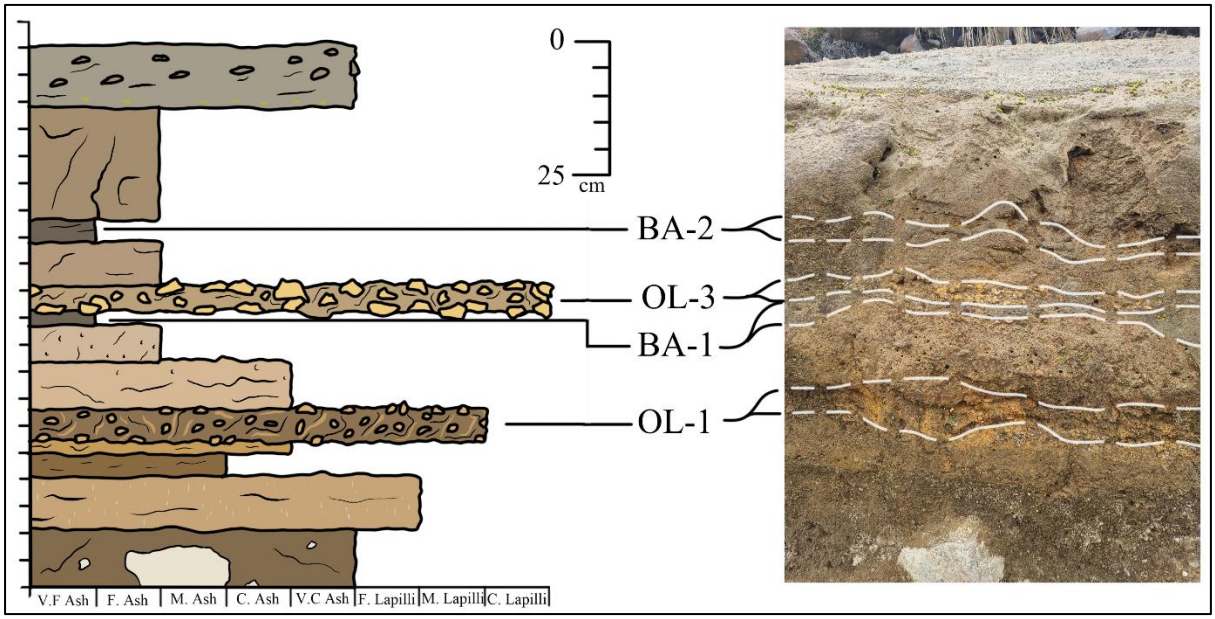

Figure 3.9: Stratigraphic log of Site E.

The stratigraphy of the outcrop was very linear allowing for identification of the tephra layers across the entire length of the outcrop with some patches having a greater degree of access than others. This site and site D provided the bounds of deposition at which most if not all PPF deposits should be found within Mount Ruapehu's eastern ring plain.

Table 3.3: Field observations at Site E.

Sample ID	Layer ID	Depth (m)	Thickness (mm)	Grain Size (mm)	Colour	Texture	Depth Beneath Taupō (cm)	Contact Between Units	Clast Lithology	Clast Shape	Clast Roundness	Bedding	Lateral Variation
3E	BA-2	2.38	50.00	<1	Black	Fine, nearly cemented	83.00	Non homogenous, chunks				Dark orange soils above, orange soils below	Minimal
26E	OL-3	2.60	25.00	<20	Orange	Fine textured, small vesicles	105.00	In a matrix	Pumiceous	Irregular	Sub-rounded	Directly above BA-1. orange soils above	Minimal
8E	BA-1	2.60	16.00	<1	Black	Fine, almost cemented	105.00	Blocky, semi homogenous				OL-3 sits above, orange soils surround	Minimal
23E	OL-1	3.00	53.00	<16	Orange	Pumiceous	145.00	Lapilli, no matrix	Pumiceous, light	Regular	Rounded	Orange soils above, brown soil beneath	Very consistent

3.4.3 Comparisons of Physical Attributes between Site D and E

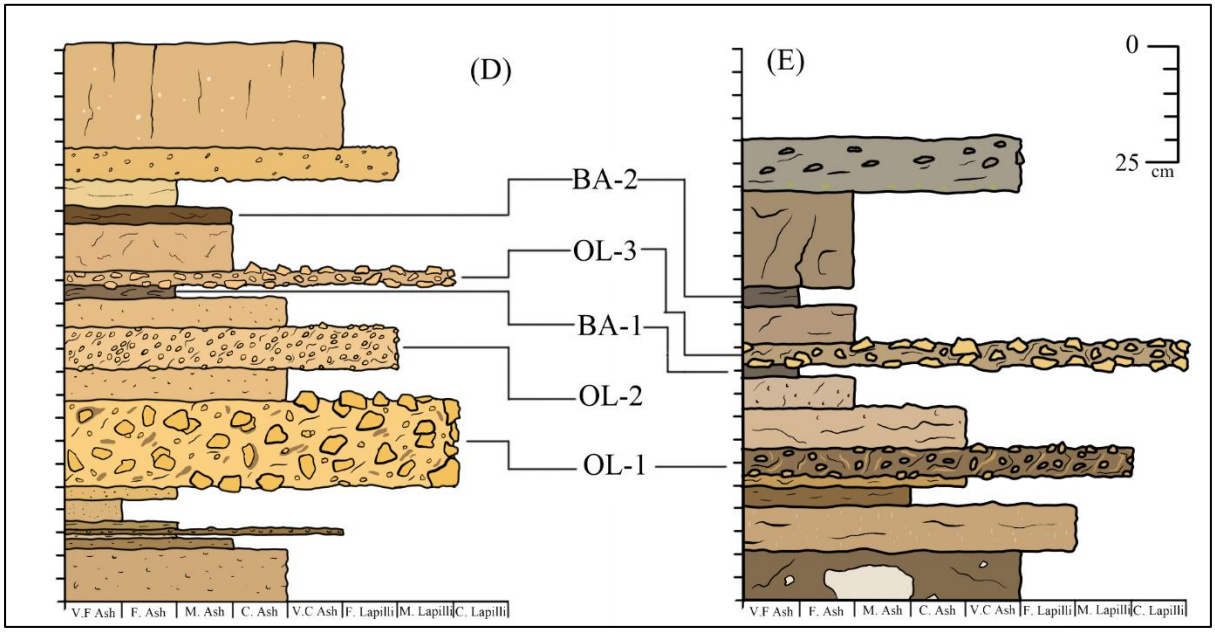

Figure 3.10: Fence diagram comparing Site D and E.

Sites D and E are the two sites within the field with the clearest view of the investigated tephras. However, they both present different characteristics of the tephra layers which can be explained due to differences in proximity and surrounding environment (figure 3.10).

Thinner black ash layers with thicker orange lapilli layers were observed at Site D. This could be due to the directionality of deposition. OL-2 is present at Site D while it was unobserved at Site E.

Site E could represent the thinning of deposition towards the south with the primary depositional axis trending towards Site D. OL-1 has major characteristic differences between the locations (table 3.2 and 3.3) with Site D showing large orange clasts within an orange matrix whereas site E shows smaller orange clasts within a brown matrix. The black ash layers appear similar, and OL-3 appeared similar between sites too.

3.4.4 Comparative Observations Made at Other Locations.

3.4.4.1 Access Road 17 – Site A

Site A was the most distal location 17.6 kilometres from source. Only one layer was identified within this location with it being deemed BA-1 after chemical analysis. At an elevation of 945 metres above sea level. (figure 3.11; table 3.4).

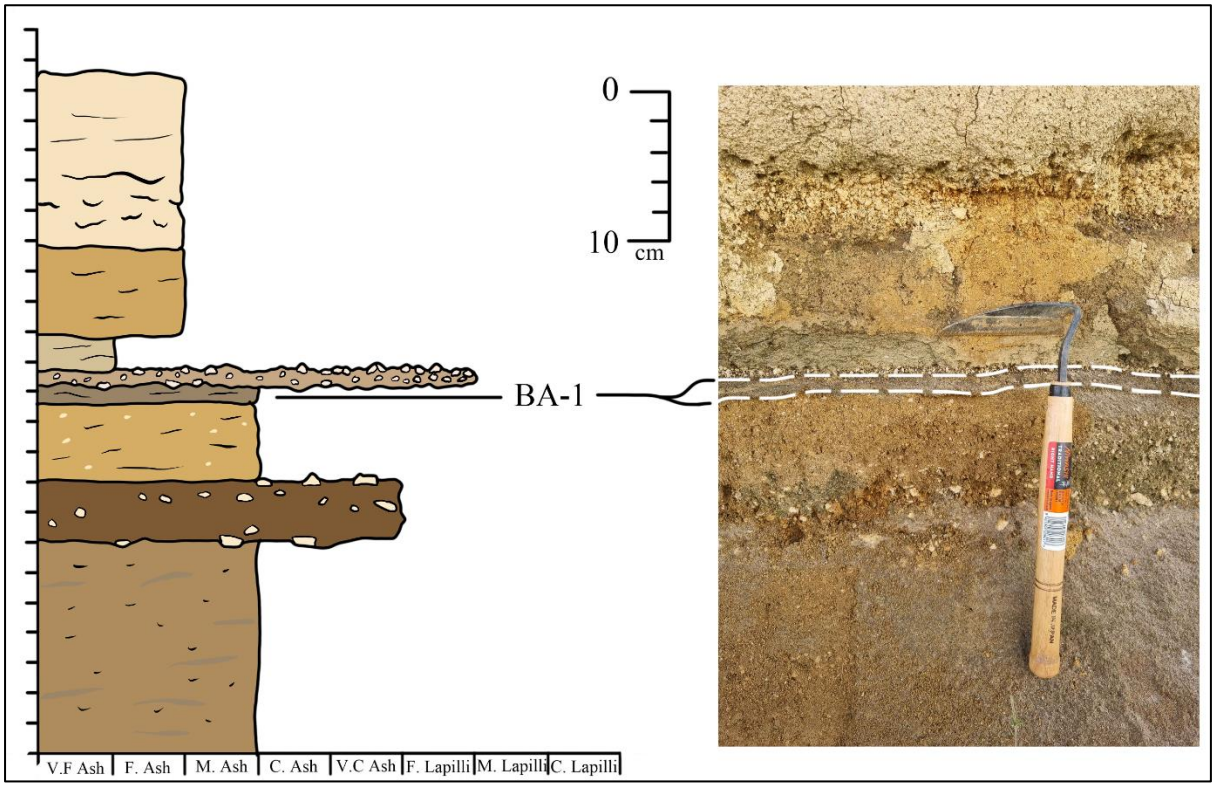

Figure 3.11: Stratigraphic log of site A (left) with the reference image (right).

Table 3.4: Field observations at Site A.

Sample ID	Layer ID	Depth (m)	Thickness (mm)	Grain Size (mm)	Colour	Texture	Depth Beneath Taupō (cm)	Contact Between Units	Bedding	Lateral Variation
1A	BA-1	1.90	8.00	<1	Metal grey	Rough, almost cemented	160.00	Homogenous	Very thin above lapilli sections, potentially OL-1and2	Appears straight

3.4.4.2 Karioi Forest Access Road 57 – Site C

Site C was found within the northern reaches of the Karioi Forest 8.6 kilometres from source. At 1135 metres above sea level, it sits within the middle range of altitudes where samples were collected. Deposits were quite clear within the stratigraphy. The site itself was also the furthest west any investigations were made during field work (figure 3.12; table 3.5).

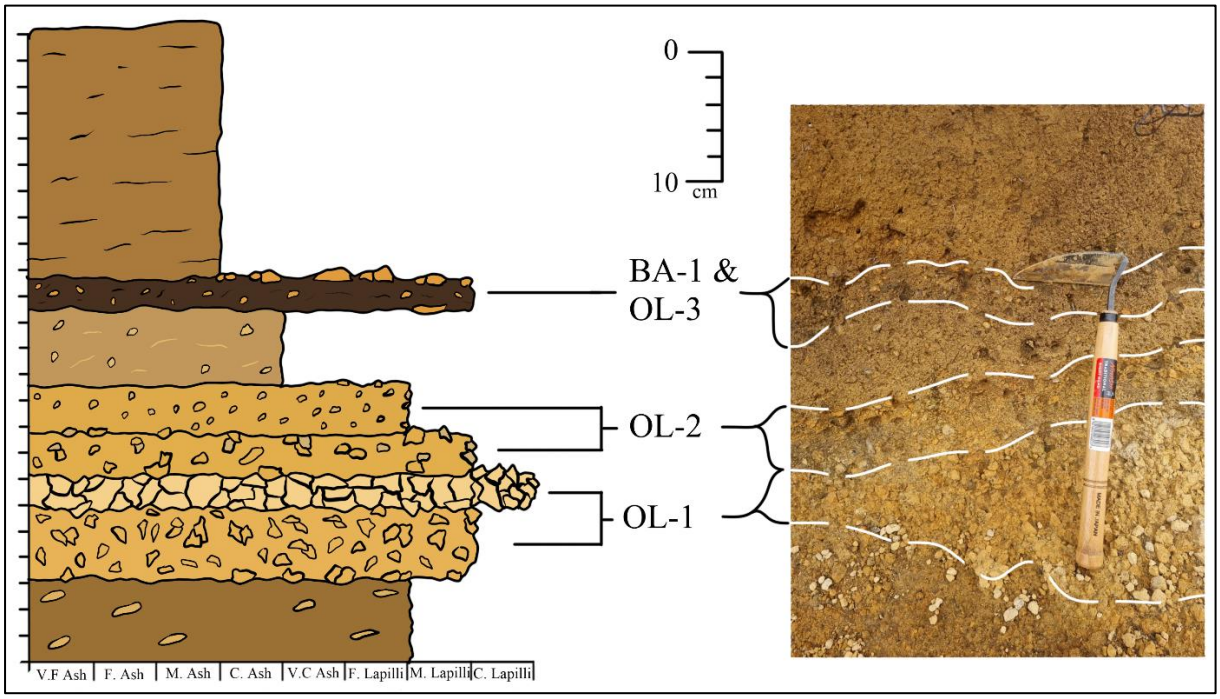

Figure 3.12: Stratigraphic log of site C (left) with the reference image (right).

Table 3.5: Field observations at Site C. OL-2 and 3 were present but not noted. BAT-1 was not sampled.

Sample ID	Layer ID	Depth (m)	Thickness (mm)	Grain Size (mm)	Colour	Texture	Depth Beneath Taupō (cm)	Contact Between Units	Clast Lithology	Clast Shape	Clast Roundness	Bedding	Lateral Variation
	BAT-1	0.30	33.00	<1	Black	Very fine,	24.00	Blocky in matrix				Brown soils surround, Taupō ash found further above	Relatively concise
6C	BA-1	1.59	42.00	<1	Black	Partially cemented ash	159.00	Irregular, patchy				OL-3 directly above, orange soils found above and below	Irregular chunks
21C	OL-1	1.70	112.00	<34	Pale yellow	Solid blocks	170.00	Almost fused chunks	Solid, not many vesicles	Jagged and irregular	Angular	Yellow and orange soils above	Minimal. very concise

3.4.4.3 Tukino Access Road 1st Stop – Site G

Site G had a few tephras visible with all layers being exceptionally thin and fine grained. The deposits were thinned out greatly to the north and were primarily distributed to the south-east of the volcano. The site was quite weathered with the layers being hard to distinguish and obtain samples of. Taupō Ignimbrite was visible at Site G which aided in sampling the BAT tephra layers. This was the furthest north where a PPF deposit was located and sampled. The orange lapilli layers were in the worst condition this far north with exceptionally fine grains visible that could not be reliably correlated as the orange lapilli in question (figure 3.13).

Table 3.6: Field observations at site G. OL-3 and BA-1 were possibly observed but not noted.

Sample ID	Layer ID	Depth (m)	Thickness (mm)	Grain Size (mm)	Colour	Texture	Depth Beneath Taupō (cm)	Contact Between Units	Bedding	Lateral Variation
9G	BAT-2	2.26	15.00	<1	Grey	Very fine ash	20.00	Mostly homogenous	Grey soils above. with orange ash found sporadically beneath	Follows stratigraphy
4G	BAT-1	2.28	15.00	<1	Black	Very fine ash	22.00	Fairly homogenous	Pale soils surround	
11G	BA-2	2.50	4.30	<1	Black	Cemented fine ash	50.00	Blocky but mostly homogenous	Surrounded by brown soils, very thick black layers found beneath	Minimal

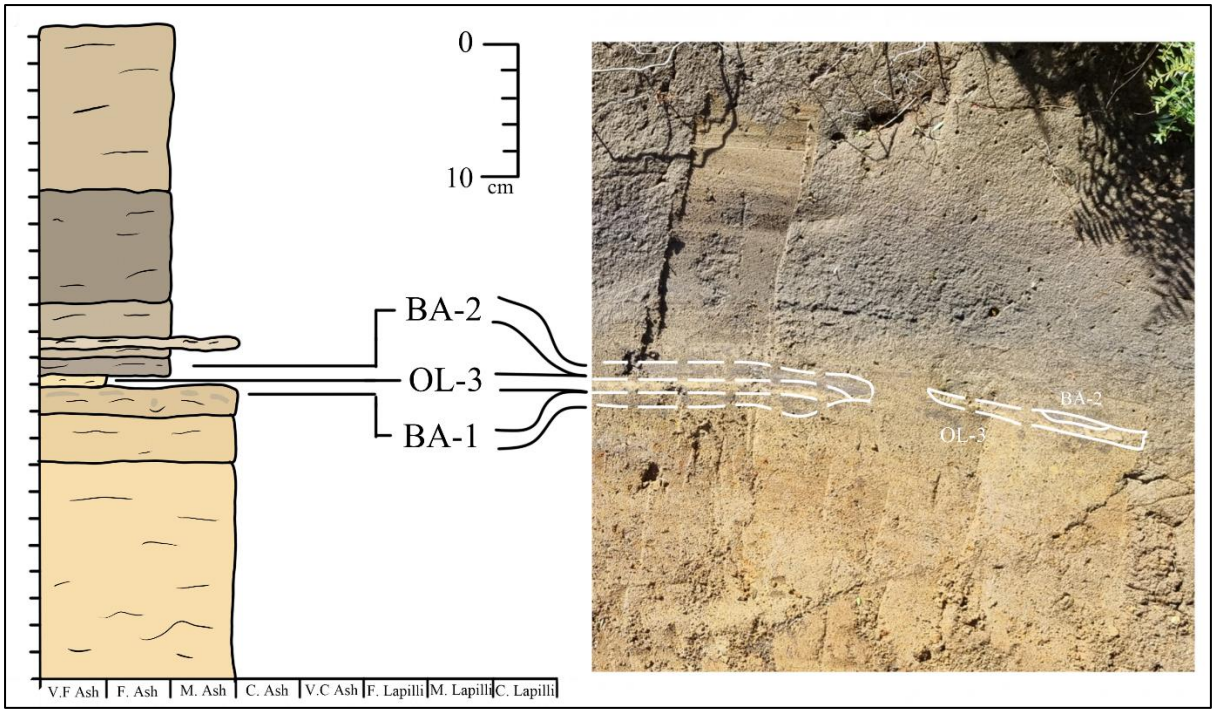

Figure 3.13: Stratigraphic log of site G (left) and reference image (right).

3.4.4.4 Other Locations

Observations were made at 25 locations in total with 12 sites having samples collected from. 14 of the 25 sites only showed evidence of the BAT tephras. These locations were spread out along the eastern ring plain and provided a solid geographical extent to provide isopach data and other insights into geographical variations between tephras such as grain size and appearance (figure 2.1; table 3.7; table 3.8).

Table 3.7: Field observations at sites where samples were collected. Samples 20B, 24F and 19H were sampled but were later deemed to not be PPF Ruapehu deposits.

Site	Sample ID	Layer ID	Depth (m)	Thickness (mm)	Grain Size (mm)	Colour	Texture	Depth Beneath Taupō (cm)	Contact Between Units	Clast Roundness	Bedding	Lateral Variation
H	**12H**	**BAT-2**	1.50	41.00	<1	Black	Cemented fine ash	12.00	Blocky in matrix		Deep brown soils surround it, many dark layers found beneath	Minimal
I	**5I**	**BAT-2**	2.30	25.00	<1	Black	Standard ash	4.30	None, chunks in matrix		Dark orange soils surround it	Minimal
J	**13J**	**BAT-2**	3.00	40.00	<1	Black	Very fine ash, non-cohesive	1.00	Continuous, homologous		Right beneath a massive Taupō section. dark orange soils beneath	Little variation. concise
K	**17K**	**BAT-1**	0.30	74.00	<1	Dark grey	Fine ash, cemented	30.00	Blocky, visible			Concise, blocky
K	**14K**	**BAT-2**	0.10	11.00	<1	Black	Very fine, homogenous ash	3.00				Minimal, quite dispersed
L	**15L**	**BAT-2**	0.30	14.00	<1	Dark grey	Fine ash	2.10	Blurry, not homogenous or cemented		Surrounded by orange soils with grey sections throughout. Taupō pumice sits above	Dispersed laterally
B	**20B**	-	3.00	70.00	<24	Orange	Lapilli coarse		Irregular	Sub rounded	Muddled up with reddish soils	
F	**24F**	-	2.00	34.00	<13	Orange	Loose lapilli, crumbly		Hard to discern	Sub angular	Found below what could be BA-1 with OL-3 above it. surrounded by orange soils	
H	**19H**	-	3.20	60.00	<20	Orange	Solid chunks, little matrix		Lapilli in a thin matrix	Sub angular/rounded		Minimal

Table 3.8: Field observations at sites where samples were not collected, Layer ID is an assumption based on observations and is not confirmed.

Site	Layer ID	Depth (m)	Thickness (mm)	Grain Size (mm)	Colour	Texture	Depth Beneath Taupō (cm)	Contact Between Units	Bedding	Lateral Variation
I	**BAT-2**	2.00	19.00	<1	Black	Fine ash, cemented exterior	4.00	Blocky, mostly homogenous	Thin Taupō layer sits above. brown soils beneath	Stays in line with Taupō layer
M	**BAT-1?**	1.50	42.00	<1	Medium grey	Very fine	60.00	Fragmented, no matrix		Relatively confined, concise across deposit
N	**BAT-1**	3.00	13.00	<1	Black	Fine ash	5.00	Defined patches. not continuous	Wide vertical variation of pumice above it. pumice line found below. light orange soil in between	Varied vertical placement, confined line but has a large drop to it
O	**BAT-2**	3.00	16.00	<1	Black	Fine ash	3.30	Blocky, almost cemented	Large Taupō section above with pumice located beneath. surrounded by dark orange soils	Minor vertical variation across. change in cluster sizes too
P	**BAT-1**	1.20	50.00	<1	Black	Very cemented ash	15.00	Continuous	Soft soils beneath, leads into Taupō above	Minimal, seems to be a second similar layer right above
Q	**BA-1**	3.00	23.00	<1	Black	Fine ash	100.00	Homogenous	Convoluted. Orange ash surrounds it sporadically.	
R	**BAT-2**	1.00	30.00	<1	Black	Cemented chunks	15.00	Chunks	Brown soils surround deposit, Taupō found above. BAT-1 observed below	Quite concise
S	**BAT-2**	1.90	24.00	<1	Black	Cemented, blocky ash	30.00	Not homogenous	Large black layer beneath it	Minimal, uniform
T	**OL-2**	2.70	80.00	<7	Orange	Finer lapilli	260.00			
U	**OL-3**	4.50	22.00	<1	Orange	Semi cemented but ashy			Sits right above a deposit of black ash. potentially BA2	
V	**BAT-2**	1.40	23.00	<1	Black	Fine ash	15.00	Blocky but mostly homogenous	Taupō pumice sits above it. dark brown soils surround it	Minimal
W	**BAT-2**	1.00	19.00	<1	Black	Fine ash	9.40	Clumps of ash, little contact	Taupō pumice sits above. brown soils surround. Thick black layer found below	
X	**BAT-1**	1.20	42.00	<1	Black/grey	Cemented, fine	9.00	Homogenous, constant	Orange soils surround, BAT-2 may be visible above	Flows in a wave pattern, stays consistent thickness
Y	**OL-2**	1.10	53.00	<8	Orange	Quite fine, chunks	90.00	Blocky	Orange soils beneath, brown soils above. BA-1 and OL-3 can be seen above	Relatively confined

3.4.5 Total Stratigraphic Column

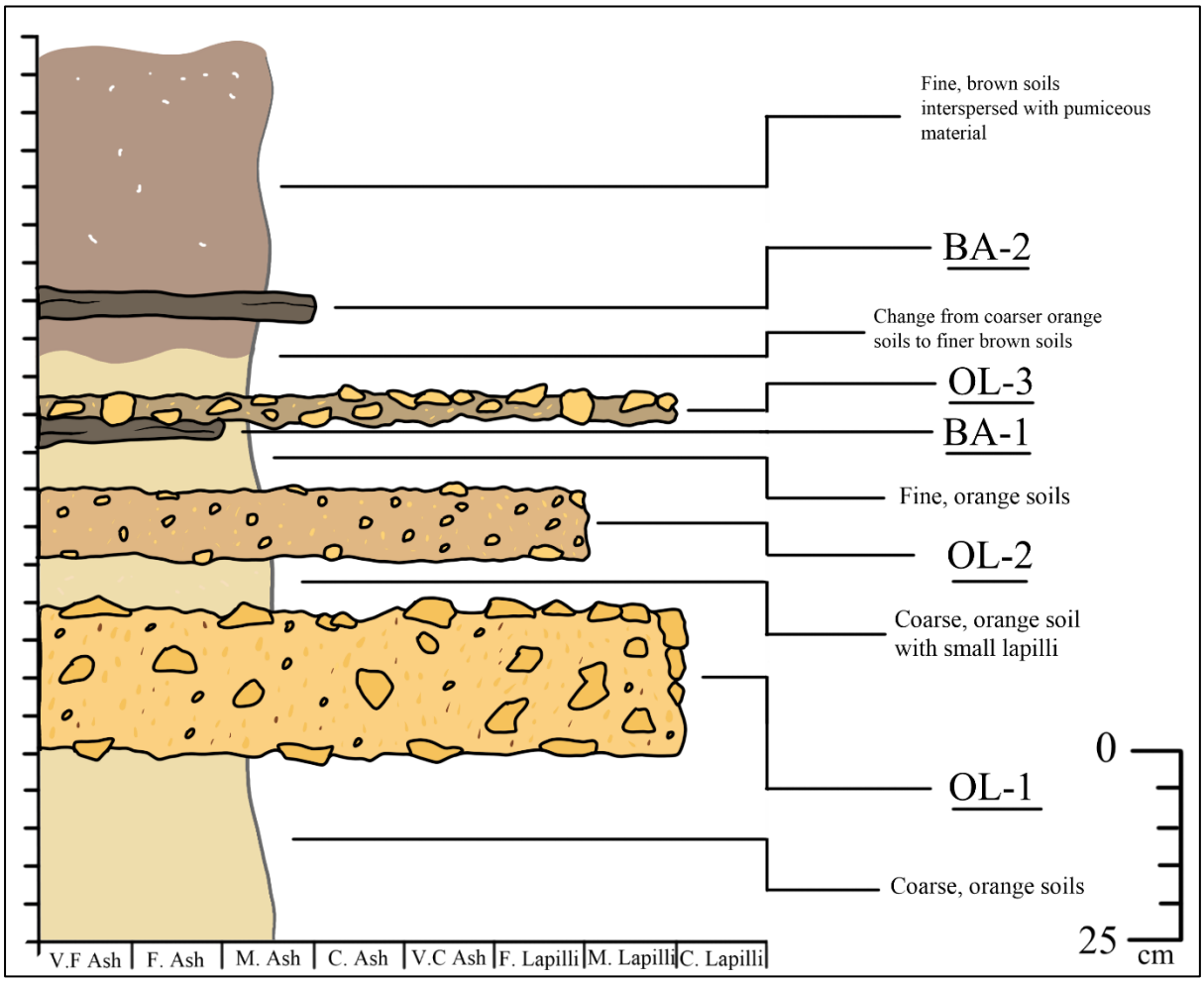

Figure 3.14: General structure of the tephra within the field. Basic details of soil structure between tephra layers are also provided.

Observations from Sites D and E were combined to generate a stratigraphic overview of the PPF deposits across the Eastern Ruapehu ring plain (figure 3.14). Pumiceous material was observed in the upper extents of the darker soils at most sites. These soils persisted until they reached BA-2, which was characterised as a fine, thin black ash layer. Below this, soils gradually changed to an orange colour before reaching OL-3 which generally showed coarse, irregular lapilli within a beige matrix. Directly below was BA-1, which was generally thinner, finer and darker than BA-2. Orange soils separated BA-1 and OL-2 with the latter showing fine, vesicular lapilli grains within an orange matrix. Coarse, orange soils with interspersed lapilli separated this layer from OL-1 which contained large, coarse-grained lapilli within a light orange matrix. Orange soils were generally found beneath this layer.

Most sites only displayed one or two poorly preserved layers that could only be reliably identified through geochemical analysis (figure 3.15).

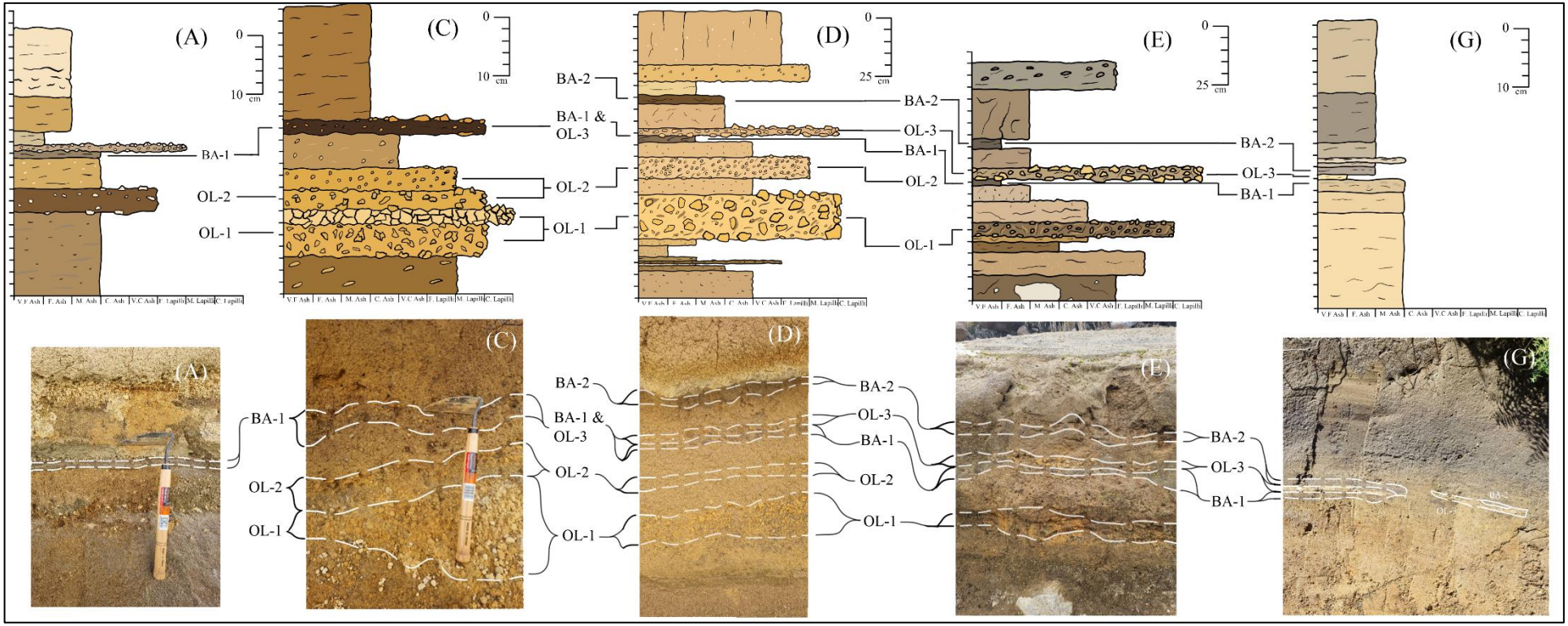

Figure 3.15: Fence diagram showing the relation between the five clearest sites (labelled) where at least one tephra layer was visible (top). Reference images for each location is shown below.

3.5 Isopachs and Isopleths

3.5.1 BA-2 Isopach and Isopleth

The geographical extents reached by BA-2 as shown through its isopach (figure 3.16) and isopleth (figure 3.17) represent a reasonably wide, elliptical zone of deposition from the Crater Lake with a southeast direction while the grain sizes were the largest at the most distal location which could infer a focused directionality of deposition for larger clasts with finer material fanning away.

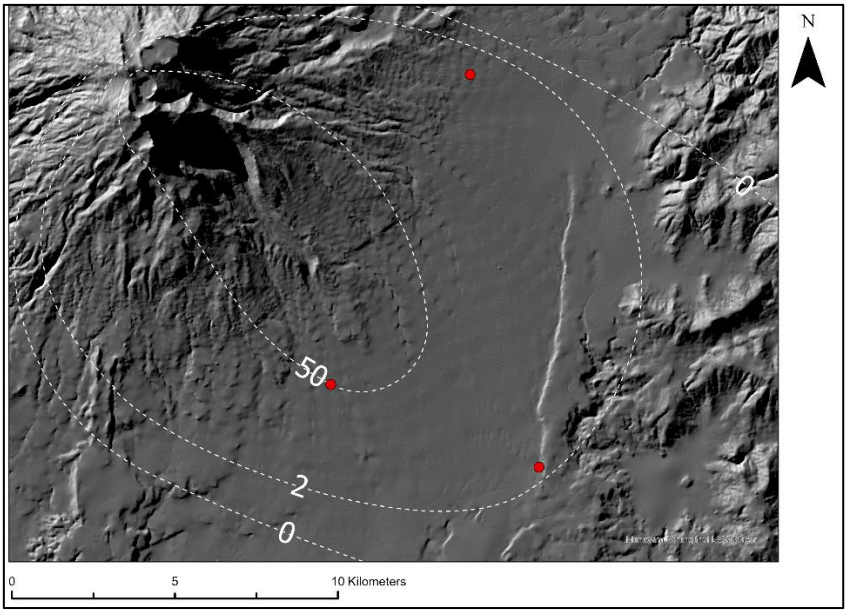

Figure 3.16: Isopach map of BA-2 thickness (mm).

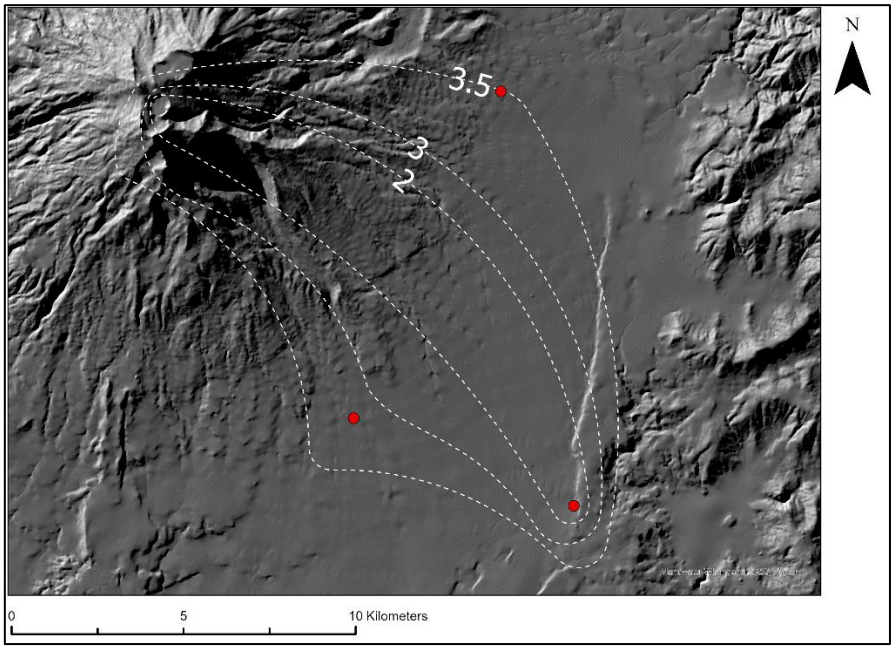

Figure 3.17: Isopleth map of BA-2 grain size (ϕ).

3.5.2 BA-1 Isopach and Isopleth

The maps presented for BA-1 show a wide depositional range (figure 3.18). The BA-1 isopleth (figure 3.19) shows similarities to the BA-2 isopleth (figure 3.17) with a non-symmetrical 3 ϕ contour due to land topography in the more proximal southern reaches.

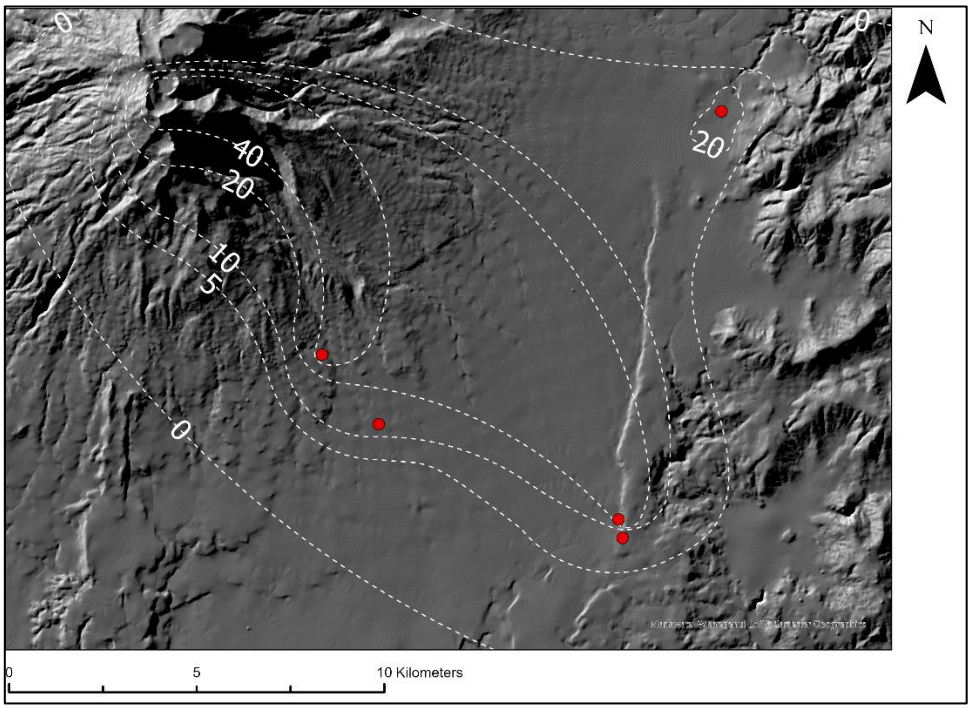

Figure 3.18: Isopach map of BA-1 thickness (mm).

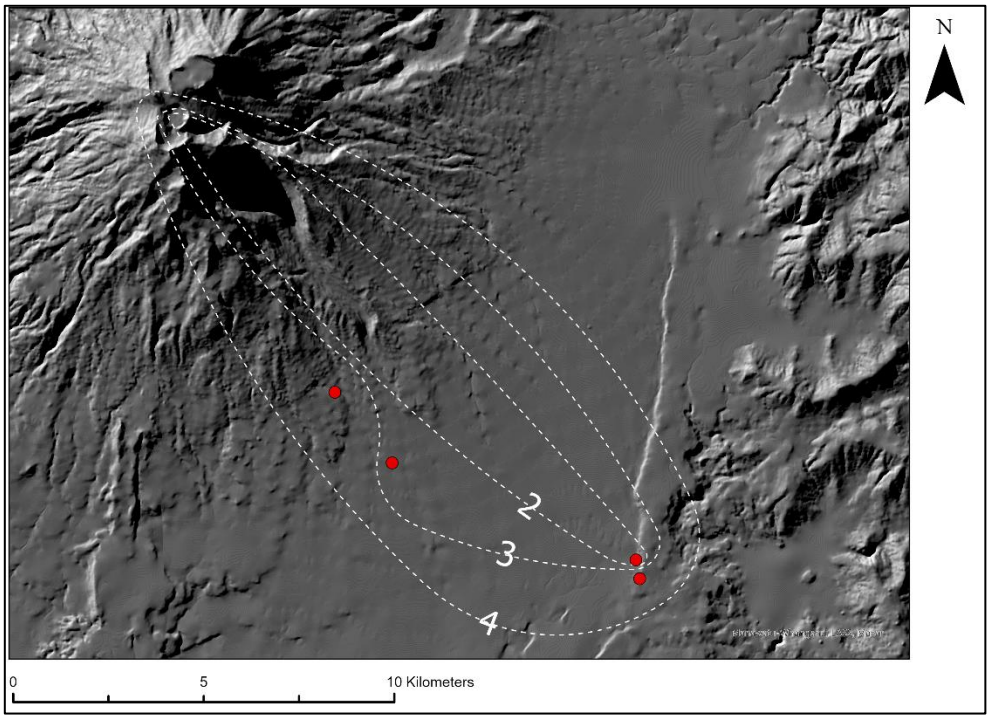

Figure 3.19: Isopleth map of BA-1 grain size (ϕ).

3.5.3 OL-2 Isopach and Isopleth

The isopach for OL-2 (figure 3.20) shows a rotation southward with the thinnest OL-2 deposits being found to the south and the thickest being found to the east. The OL-2 isopleth (figure 3.21) shows the only grain size sample collected at site D.

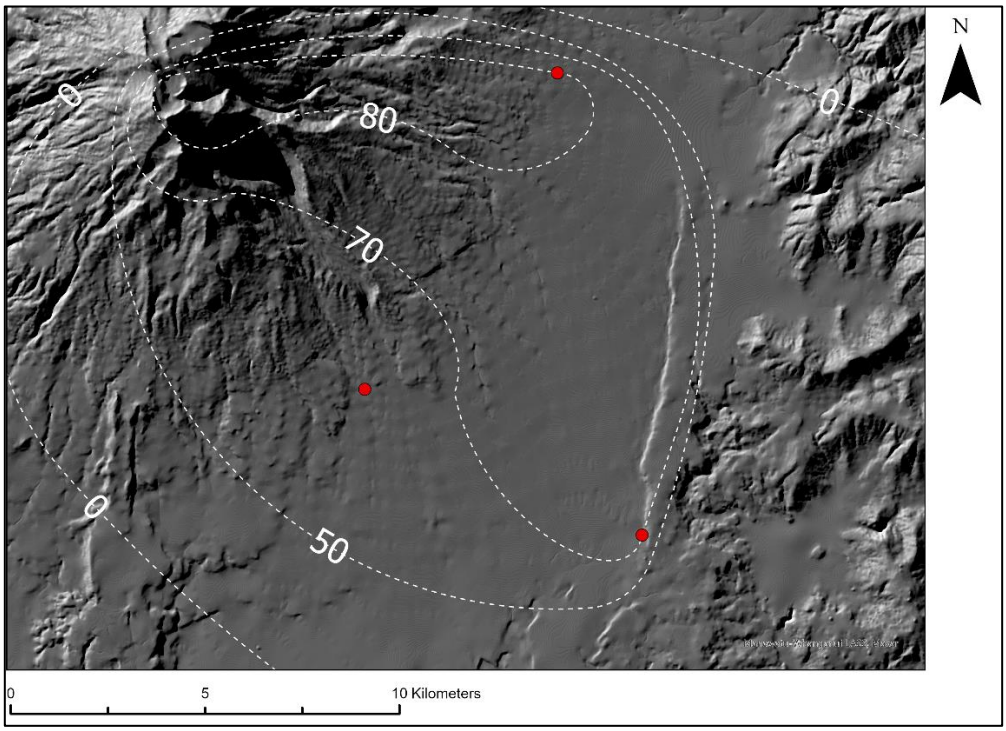

Figure 3.20: Isopach map of OL-2 thickness (mm).

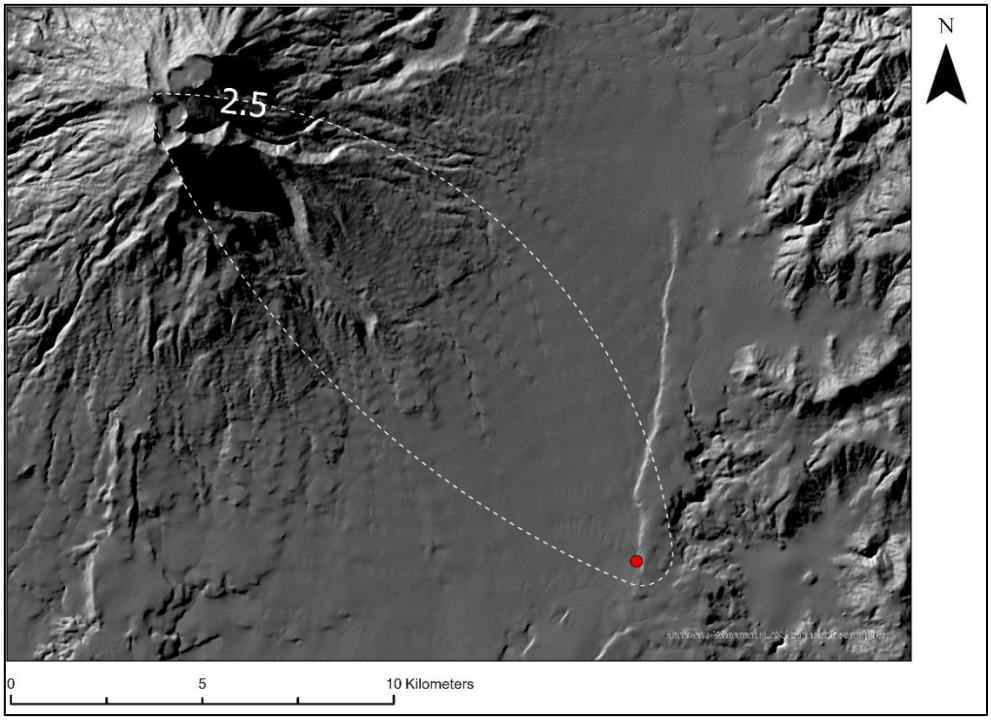

Figure 3.21: Isopleth map of OL-2 grain size (ϕ).

3.5.4 OL-1 Isopach and Isopleth

OL-1 shows a strong southeast trend in deposition (figure 3.22) The isopleth (figure 3.23) shows a more elliptical trend from the Crater Lake with the largest grain sizes being found more proximal to the vent.

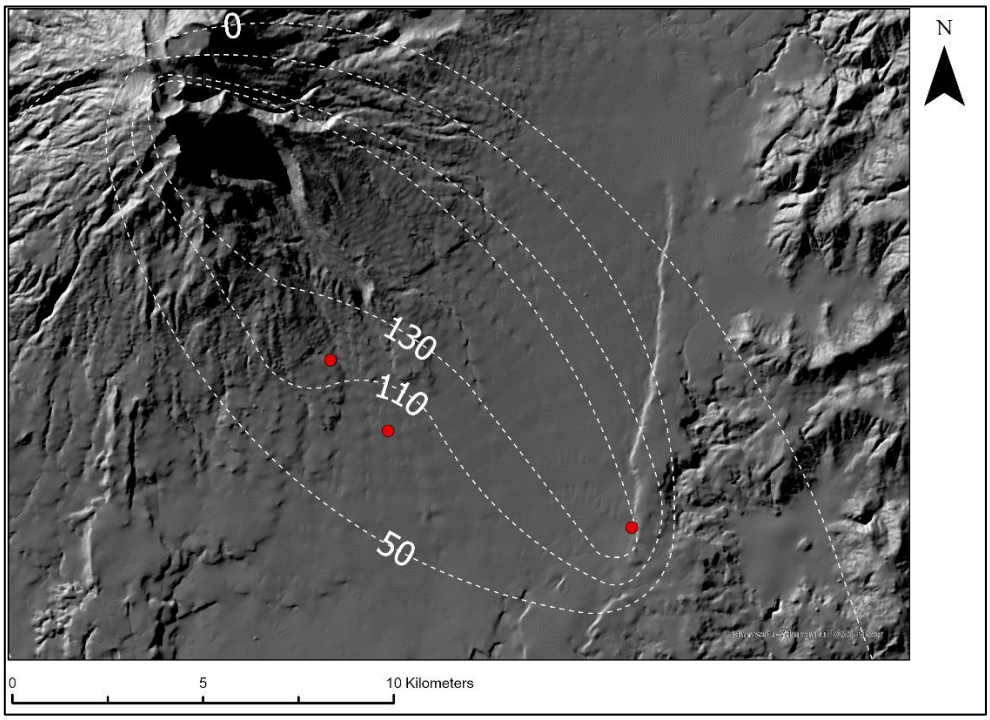

Figure 3.22: Isopach map of OL-1 thickness (mm).

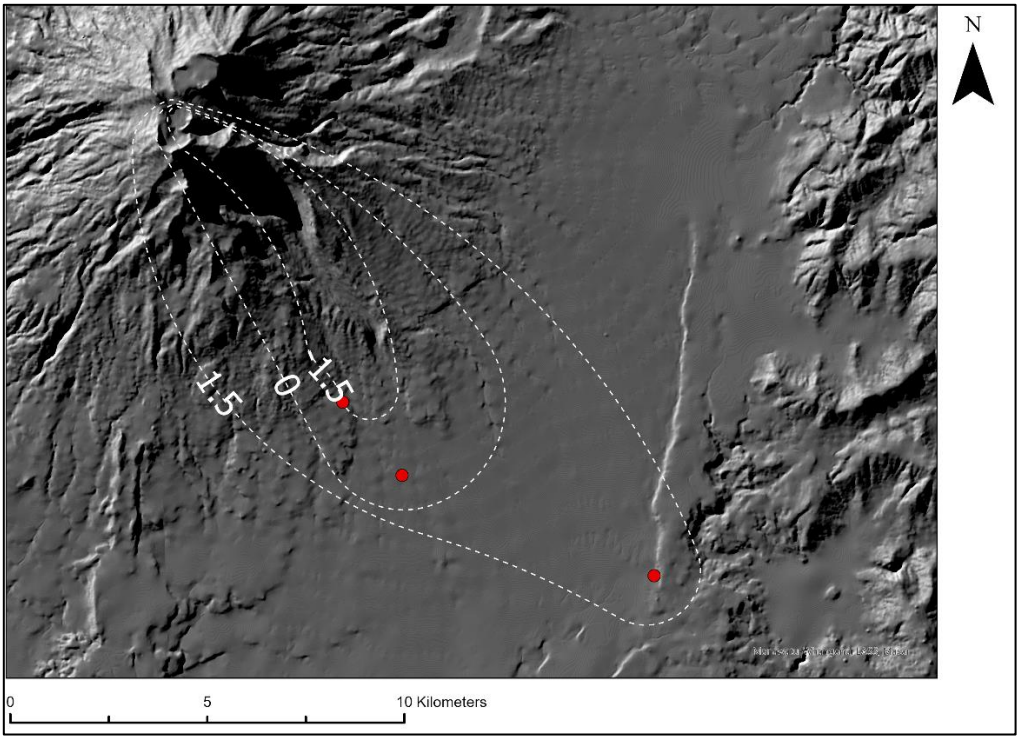

Figure 3.23: Isopleth map of OL-1 grain size (ϕ).

3.5.5 OL-3 Isopach and Isopleth

Isopach trends with OL-3 (figure 3.24) are similar to what was seen with BA-1 which matches observations in the field. The isopleth for OL-3 (figure 3.25) shows a more focused directionality towards the southeast with the largest grains being observed at the most distal site.

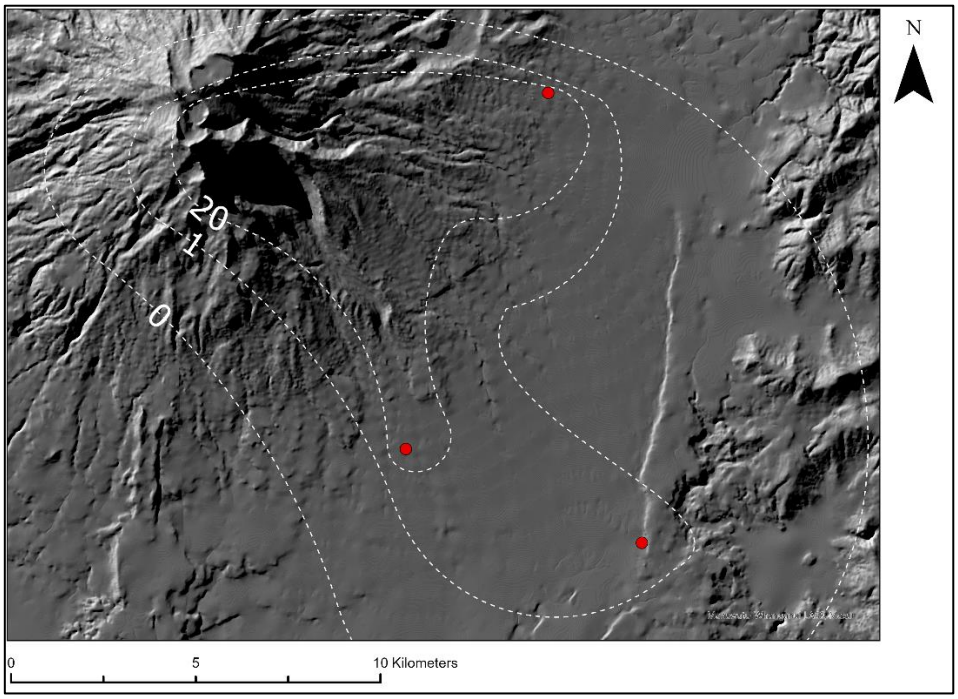

Figure 3.24: Isopach map of OL-3 thickness (mm).

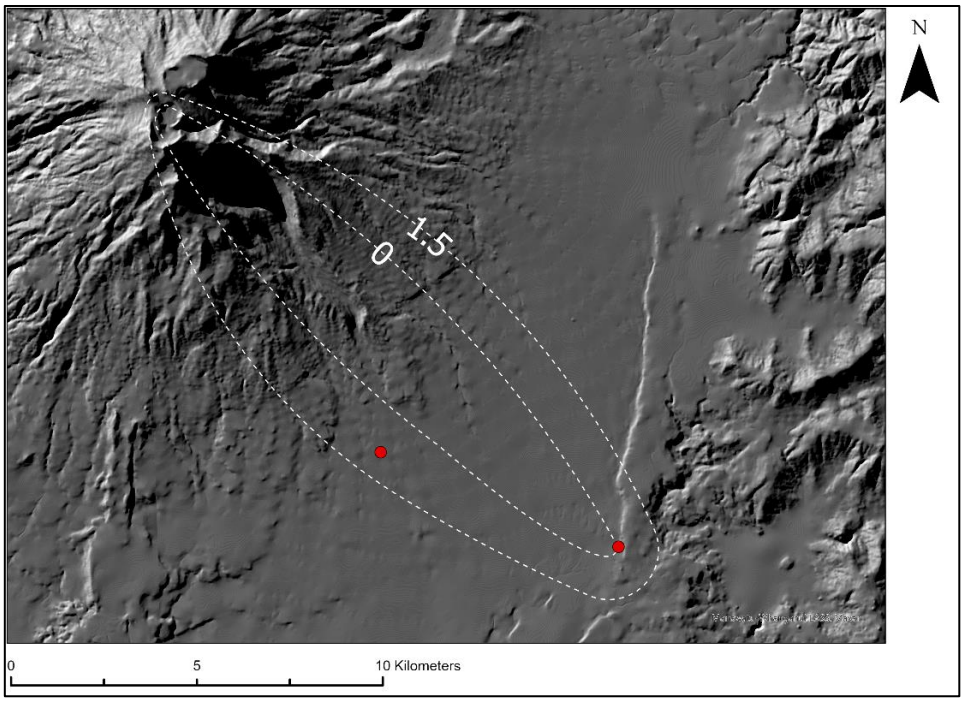

Figure 3.25: Isopleth map of OL-3 grain size (ϕ).

3.6 Volume Estimates

Table 3.9: Total volume estimates for each Ruapehu PPF tephra layer using the Legros Method.

Tephra Layer	Isopach area (square meters)	Thickness (m)	Volume (cubic metres)
BA-2			
	219094609.6	0.0055	4446525.102
BA-1			
	183046136	0.008	5403521.935
OL-2			
	188938880.7	0.053	36950776.89
OL-1			
	142779681	0.053	27923422.22
OL-3			
	125247857.3	0.002	924329.1869

Based off of the Legros Method and isopach areas produced through field observations, the minimum volumes of each Ruapehu derived, PPF deposit has been calculated:

- BA-2 volume = 4.45 x 10^6 cubic metres
- OL-3 volume = 9.24 x 10^5 cubic metres
- BA-1 volume = 5.40 x 10^6 cubic metres
- OL-2 volume = 3.70 x 10^7 cubic metres
- OL-1 volume = 2.79 x 10^7 cubic metres (rounded to 3 s.f.)

OL-1 and OL-2 are significantly larger in volume than the other deposits with the largest minimum volume being OL-2. OL-3 has the smallest minimum volume of the sampled deposits and the black ash deposits sit within the middle range between. All of these are based on the smallest tephra layers observed in the field with most of OL-1 showing a wider variety in clast size than OL-2 but more often having larger clasts and thicker sections. So, while its minimum volume estimate is smaller than OL-2, it is most likely larger considering its predominantly thicker field sections.

Componentry

4.1 Tephra Physical Componentry

Point counts are useful in determining the eruptive environmental conditions of each tephra layer being studied. The material found within each tephra provides insights into eruptive processes, potential deposition circumstances and the overall composition of the layer (table 4.1; figure 4.1).

Table 4.1: Point counting results for each sample. Other data represents point counts that were removed from the final overview.

	Sample ID	Pumice	Smooth Glass	Vesicular Glass	Lithics	Feldspars	Pyroxenes	Total
BAT-2								
	12H	32	19	340	0	12	52	455
BAT-1								
	16D	119	99	11	51	15	11	306
BA-2								
	2D	11	53	64	380	10	4	522
	11G	70	18	356	213	17	22	696
BA-1								
	7D	48	31	57	136	29	16	317
	8E	59	103	27	115	23	17	344
OL-2								
	18D	183	288	7	9	260	39	786
OL-1								
	21C	158	29	13	86	21	38	345
	22D	158	18	48	11	49	40	324
	23E	159	5	47	6	38	73	328
Other Data								
	20B	136	38	19	30	45	35	303
	19H	18	102	2	25	257	5	409
	24F	126	45	9	99	38	6	323
	10D	9	155	14	105	38	16	337

4.1.1 Pumice

Pumice is a juvenile, vesicular material produced through fragmentation during a highly explosive eruption. Pumice was generally defined as white/cream coloured vesicular material within the point counts.

Sample 12H for BAT-2 showed 7% pumiceous material with 32/455 of the clasts. This appeared to be a relatively low number when compared to other samples with the only other layer within that range being BA-2 with 2.1% and 10.1% pumice. BAT-1 showed a high volume of pumice with 38.9% of the clasts from sample 16D being light coloured and highly vesicular, this was also the greatest material percentage within the sample.

From BA-2 and below, there was a general trend towards greater volumes of pumice with BA-1 showing 15.1% and 17.2% pumice. The orange lapilli layers show a high percentage of pumice which coincides with their highly vesicular clasts and general composition with sample 18D for OL-2 showing 23.3% composition and OL-1 showing 45.8%, 48.8% and 48.5%. Interestingly, despite the similarities OL-2 and OL-1 have, pumice is not the highest percentage material within OL-2 which is instead smooth glass. OL-1 has the highest percentages of pumice out of the point counted deposits which would account for its bright orange colour and highly vesicular nature that was identified within the field.

4.1.2 Glass

Glasses are usually found non-weathered, and their appearance can point to eruption characteristics. For this point count, glasses were split into two categories based on whether the glass was smooth or vesicular. Splitting this group allows for more insight into the mechanisms behind the deposit.

4.1.2.1 Smooth Glass

BAT-2 showed a small amount of smooth glass with 4.2% of its contents whilst BAT-1 showed a much higher amount with 32.4% of its point counted sample being smooth glass. BA-2 deposits showed 10.2% and 2.6% smooth glass content, sitting between the BAT tephra layers. BA-1 showed 9.8% and 29.9% smooth glass content. This difference could be due to subtle differences with the vesicularity of the glass between locations.

The orange lapilli layers showed differences to the black ash layers especially through OL-2 which had the highest value of smooth glass in the point counted samples at 36.6% of the

sample being smooth glass. OL-1 had a smooth glass content of 8.4%, 5.6% and 1.5%. So, a much lower range than OL-2 and even sat within the BA-2 content.

4.1.2.2 Vesicular Glass

BAT-2 showed a very large percentage of vesicular glass within its point count with it consisting of 74.7% of that material. Conversely, BAT-1 only had a vesicular glass content of 3.6% which is significantly smaller.

BA-2 had a vesicular glass content of 12.3% and 51.1% which could be related to location with the further north location having a much higher vesicular glass count. This also ties in with the point count results from BAT-2 which is also significantly far north within the studied region. BA-1 had vesicular glass percentages of 18% and 7.8% which is a narrower range and within the lower limits of vesicular glass for the black ash deposits.

OL-2 had a vesicular glass content of 0.9% which is the lowest amount observed within the point counts. This alongside its high smooth glass content could be an implication towards the eruptive processes that generated the material. OL-1 had percentages of 3.8%, 14.8% and 14.3%. The one sample that is significantly lower (21C) could be due to its more welded nature in the field.

4.1.3 Lithics

Lithics within the tephras would be predominantly andesites ejected from the volcano as pre-existing material. These clasts generally show evidence of hydrothermal alteration through nonstandard colours or rounding of the clasts which would not be visible in fresh materials such as glasses.

BAT-2 was unique in that it showed no visible signs of containing lithics within its count of 455 grains. This could be due to the eruptive processes not causing too much damage to the existing conduit on the volcano. BAT-1 showed 16.7% lithic material as a contrast showing that whatever occurred to BAT-2 to display so little, if any, lithic material is unique to its own event and not shared with other black ash deposits from its period of time, this could also be due to its location so far north of the volcano as is observed with BA-2 with a reduction in lithic material to the north of the study area, being further away from the deposition axis.

BA-2 shows the highest volume of lithics out of the point counted deposits with 72.8% and 30.6% lithic material observe. The difference between these percentages could be attributed to location as site D and G were 12.5 kilometres away from each other with the higher lithic count

being found to the south at site D. BA-1 also had a high percentage of lithics present with the two samples showing 42.9% and 33.4% lithic content. Lithics being the highest percentage material within BA-1.

The orange lapilli layers show a relatively small percentage of lithics with OL-2 showing 1.1% lithic content while OL-1 shows 24.9%, 3.4% and 1.8%. The spike with OL-1 could be related to the location of the sample site in relation to ejected material and deposition direction. This result for OL-1 is more focused on the two similar results with the orange lapilli layers generally showing much lower lithic percentages than the black ash deposits.

4.1.4 Pyroxenes

Pyroxenes are a group of rock-forming minerals predominantly found within igneous or metamorphic rock. They play a critical role in looking for Ruapehu andesites as they are a major part of the rock structure with 10-20% of Ruapehu andesites typically consisting of clino or ortho pyroxenes (Price et al, 2012). They typically form as brown/green monoclinic crystals within the rock and can be distinguished by their smooth, columnar shape. The pyroxenes mainly visible within the samples were clinopyroxenes and were free crystals.

BAT-2 showed a pyroxene content of 11.4% which falls within the typical range found for Ruapehu andesites. BAT-1 showed 3.6%. In a similar tone, BA-2 showed a pyroxene content of 0.8% and 3.2%. BA-1 had pyroxene contents of 5% and 4.9%. Higher values than BA-2 but still relatively low. This result can however be explained through geochemical analysis with the older material being basaltic andesites and thus a lower pyroxene content would be reasonable.

OL-2 had a pyroxene content of 5% which could be attributed to the same reasons as BA-1. OL-1 had higher point count percentages of 11%, 12.3% and 22.3%. These could show chronological trends with material from Ruapehu having varying pyroxene componentry over time.

4.1.5 Plagioclase Feldspar

Plagioclase is another dominant crystal found within Ruapehu andesites. Commonly found at greater volumes than pyroxenes, especially to the east of the volcano within the Wahianoa Formation (Price et al, 2012). These crystals are commonly white or clear compared to green/brown pyroxenes. They are usually some of the first minerals to be formed in the cooling of mafic magma and are a key component to tephra composition.

BAT-2 showed a plagioclase content of 2.6% which was one of three-point counts that showed lower values of plagioclase than pyroxenes. This could be due to it being to the far north of the study area and away from the axis of deposition. BAT-1 showed a content of 4.9% which is still low compared to other samples but higher than BAT-2. BA-2 showed the lowest plagioclase content of 1.9% and 2.4%. BA-1 showed an increase in plagioclase with contents of 9.1% and 6.7%.

The orange lapilli layers also showed an increase in plagioclase with OL-2 having a content of 33.1% which is significantly higher than other mineral values. OL-1 has values ranging from 6.1%, 11.6% and 15.1%. The OL-1 layer that was anomalous for almost all ranges could be based on its location due to it being the furthest west sample location and the most proximal site to the Crater Lake.

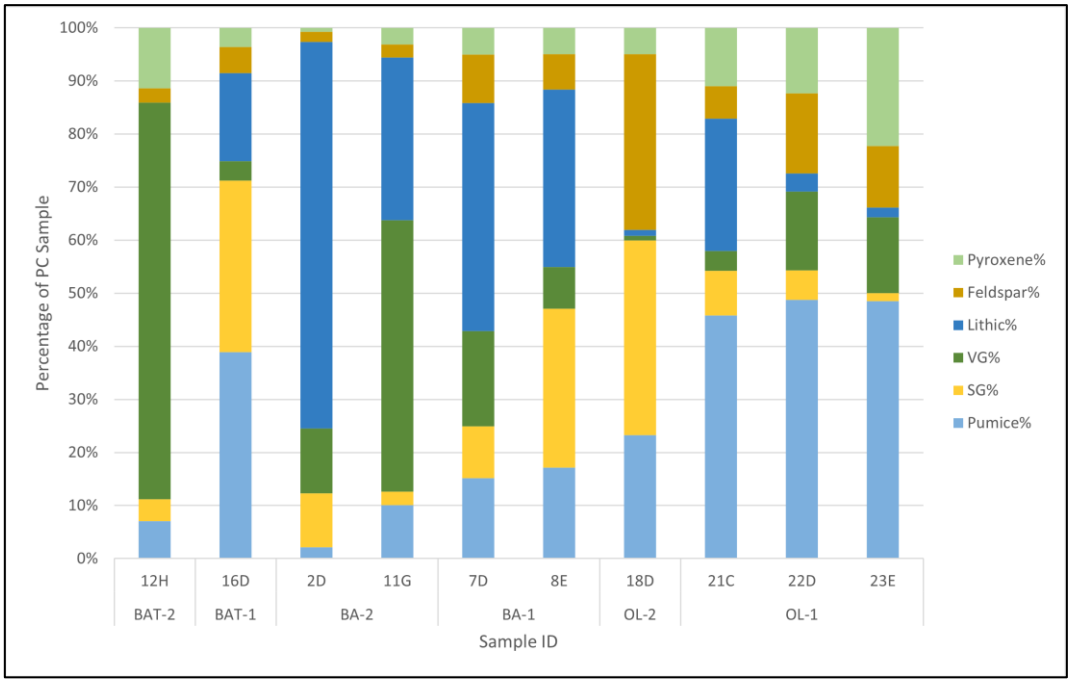

Figure 4.1: Point count percentages of samples normalised to 100%

4.2 Grain Size Distribution

Grain size distribution is a very important measure to accurately define the physical composition of a tephra layer. Through wet and dry sieving, an accurate depiction of grain size percentages within samples was uncovered which can then be compared to guideline values for ashfall and lapilli. The use of LPA for grain sizes smaller than 3 ϕ allowed for visuals on the tail end of grains too small to sieve by hand and allowed for distribution curves and grain summaries to be created through GRADISTAT (Blott and Pye, 2001). Some samples showed

a dip within their distribution curves which is through the combining of hand sieved analysis and LPA (appendix 6, figure 4.2).

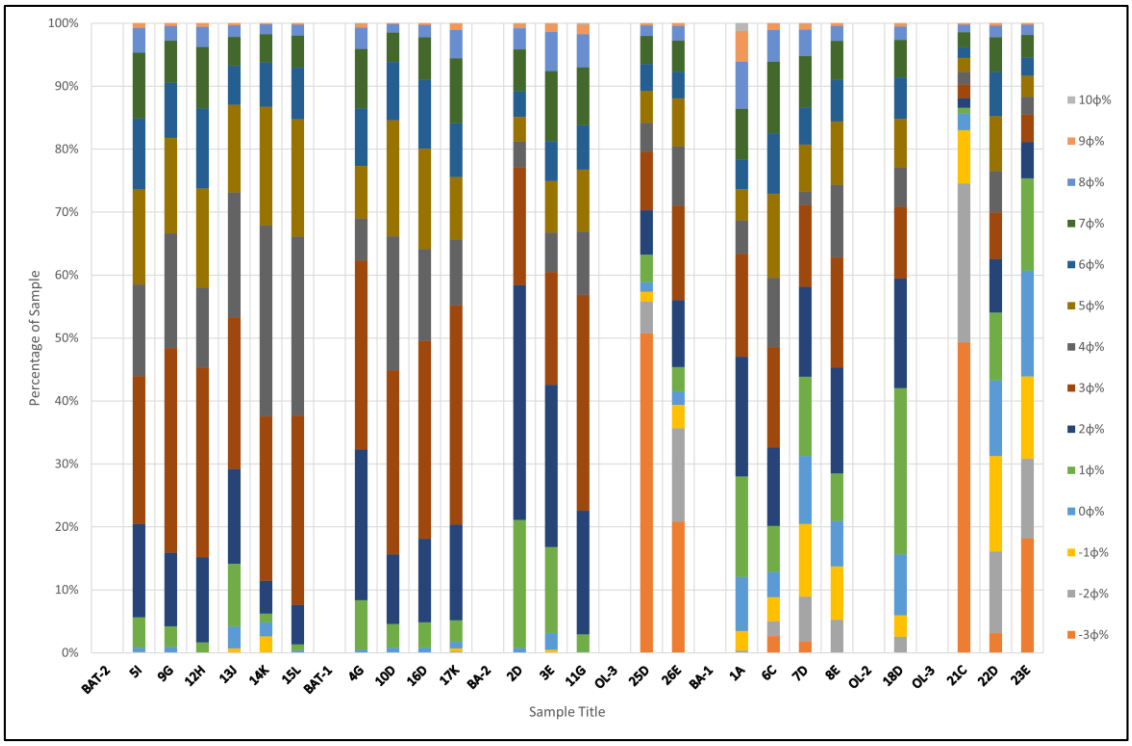

Figure 4.2: Grain size percentages of each sample normalised to 100%.

4.2.1 Black Ash Taupō Grain Size

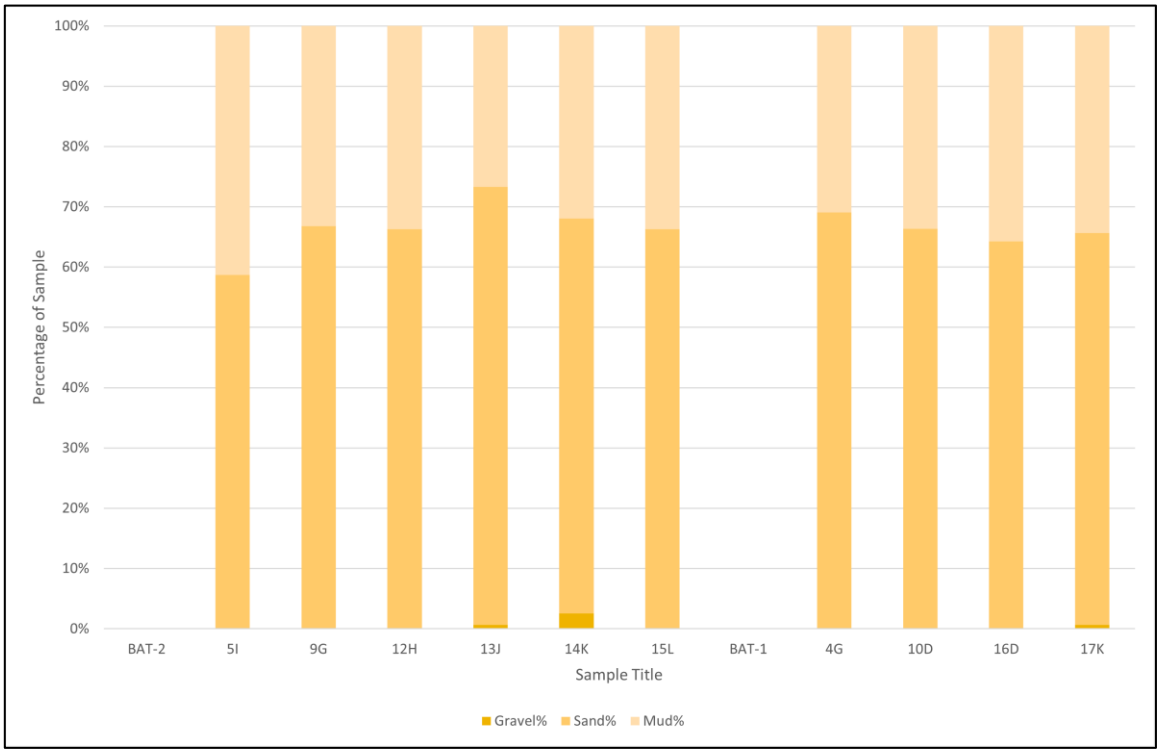

Figure 4.3: Grain size percentage of BAT samples.

The BAT layers showed minimal variation between their different samples regarding grain sizes. Both layers showed very minimal evidence of larger clasts being present but were all poorly sorted (appendix 5; figure 4.3).

BAT-2 showed an interesting range of grain sizes as it was the only tephra collected that did not have a grain size that reached -2 ϕ or 10 ϕ (appendix 4), instead sitting within the middle ranges of the studied values. The mean phi for this layer sat between 2.92 ϕ and 3.72 ϕ indicating a very fine layer. Most of the samples had a fine skew to them. One sample (14K) showing a higher observation of outliers through its kurtosis. Two samples were considered platykurtic and three samples were deemed mesokurtic showing that majority of the samples showed a reasonably low number of outliers. Both 13J and 14K were seen to have a symmetrical skew to their samples (Appendix 5). All samples were poorly sorted and composed of fine to very fine sand. All but one sample had their highest percentage composition found within 3 ϕ with 14K having its highest grain percentage found in 4 ϕ (appendix 2). Two layers showed no grains beyond 0 ϕ (12H and 15L) with the other four samples having a maximum grain size within the 1 ϕ range.

BAT-1 showed differences to BAT-2 layers with half of the layers observed reaching a grain size of 10 ϕ although these only constituted for 0.04% and 0.06% sample weight percentage. It also had two samples have a maximum grain size beyond 0 ϕ with one reaching 1 ϕ and the other having grain sizes within 2 ϕ (appendix 4). Grains at this size made up a very small percentage of the overall weight. All four samples for BAT-1 were considered very fine sands with an average mean phi between 3.21 ϕ and 3.5 ϕ. Showing very little grain size variation occurring between samples. Samples were split with two being considered platykurtic and two being considered mesokurtic although all kurtosis values were within 0.09 of each other. The two platykurtic samples (4G and 17K) both showed a very fine skewness to their distribution graphs with the other two samples still showing fine skewness but to a lesser extent. Sample 4G was the only BAT sample considered very poorly sorted with the rest being poorly sorted. The highest weight percentage for BAT-1 was all found within 3 ϕ with it ranging from 29.28% to 34.86% (appendix 2). The mean grain size is very similar to what was observed with BAT-2.

4.2.2 Black Ash Grain Size

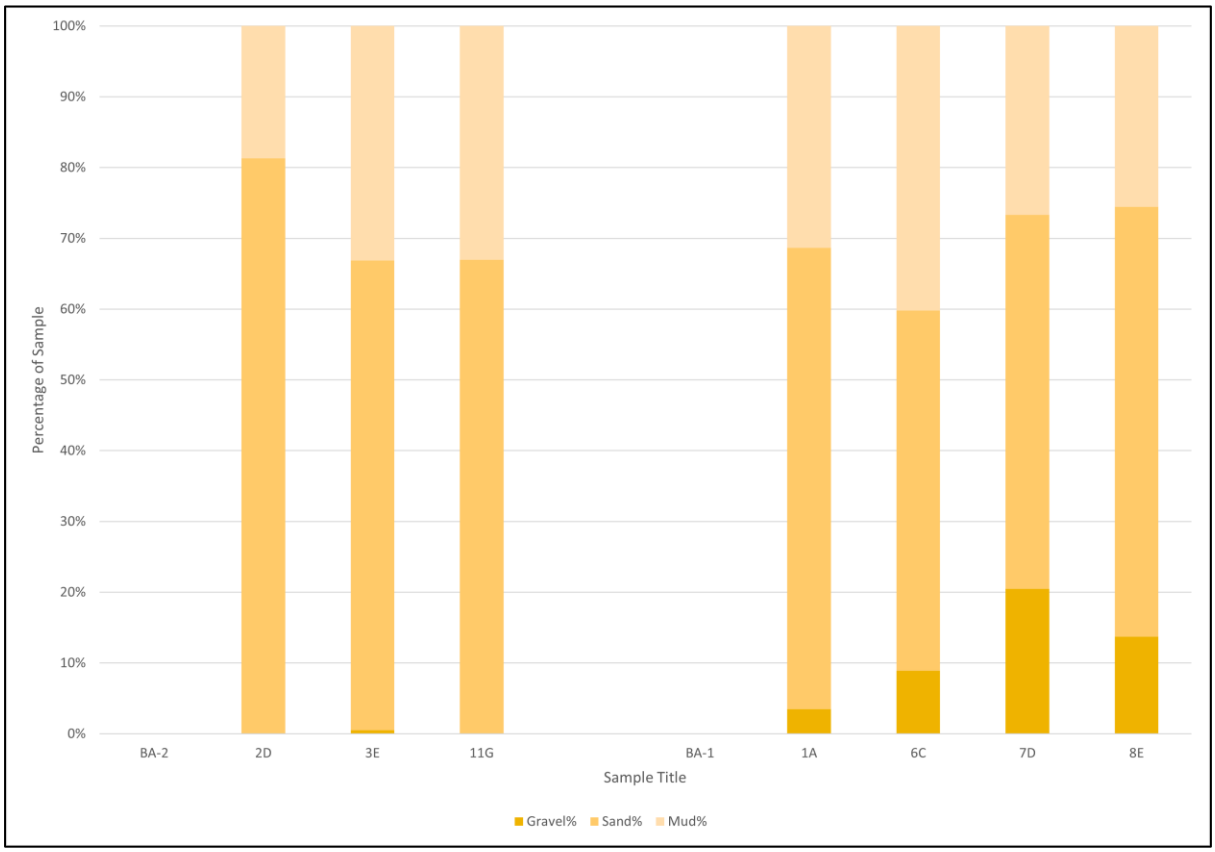

Figure 4.4: Grain size percentage of BA samples.

The BA samples had a variety of data produced but trends can be followed within each sample. Both samples were very different from one another with the only major similarity being their poor sorting (appendix 5; figure 4.4).

BA-2 samples had a mean ϕ ranging from 2.41 ϕ to 3.48 ϕ showing that the samples were ashfall deposits that were slightly coarser than BAT deposits. All three samples showed very fine skewing with them being defined as fine to very fine sands. All three samples had some percentage of their weight composition be found around 10 ϕ with percentages of 0.07%, 0.11% and 0.24% (appendix 2). Two of the samples reached -1 ϕ with one reaching a max grain size of 0 ϕ (appendix 4). There was a range of kurtosis values with sample 2D being deemed very leptokurtic indicating a high range of outliers. This could be attributed to the tephra's thin, cemented appearance as sample 3E was not very cemented and presented a platykurtic kurtosis. The final sample (11G) presented a mesokurtic kurtosis. The highest weight percentage for BA-2 was found within 2 ϕ for samples 2D and 3E with sample 11G having the highest weight percentage found within 3 ϕ which further supports its ashier appearance in the field.

BA-1 samples were unique in that two of them were the only ones to display a negative value for skewness with samples 6C and 8E showing values of -0.03 and -0.02. While these are minimal and are considered symmetrical. The four samples for BA-1 were all very poorly sorted and were split evenly between being mesokurtic and platykurtic indicating a low number of outliers present in the data. Samples 1A and 6C were deemed very fine sand, 8E was deemed fine sand and sample 7D was deemed medium sand. The mean values for these layers ranged from 3.22 ϕ to 1.86 ϕ which is a very wide margin for grain sizes for the same tephra layer. The two layers that were not considered symmetrical had a fine to very fine skew. Samples 1A and 7D showed a highest weight percentage at 2 ϕ while samples 6C and 8E presented it at 3 ϕ. Alongside this, sample 1A had the highest sample percentage composed of grains within 10 ϕ at 1.19% (appendix 2) and still showed a small number of grains appearing -2 ϕ. Sample 8E also reached a maximum grain size of -2 ϕ while the other two samples reached a maximum grain size of -3 ϕ. All samples had grains within 10 ϕ except for sample 8E which reached a minimum grain size of 9 ϕ (appendix 4).

4.2.3 Orange Lapilli Grain Size

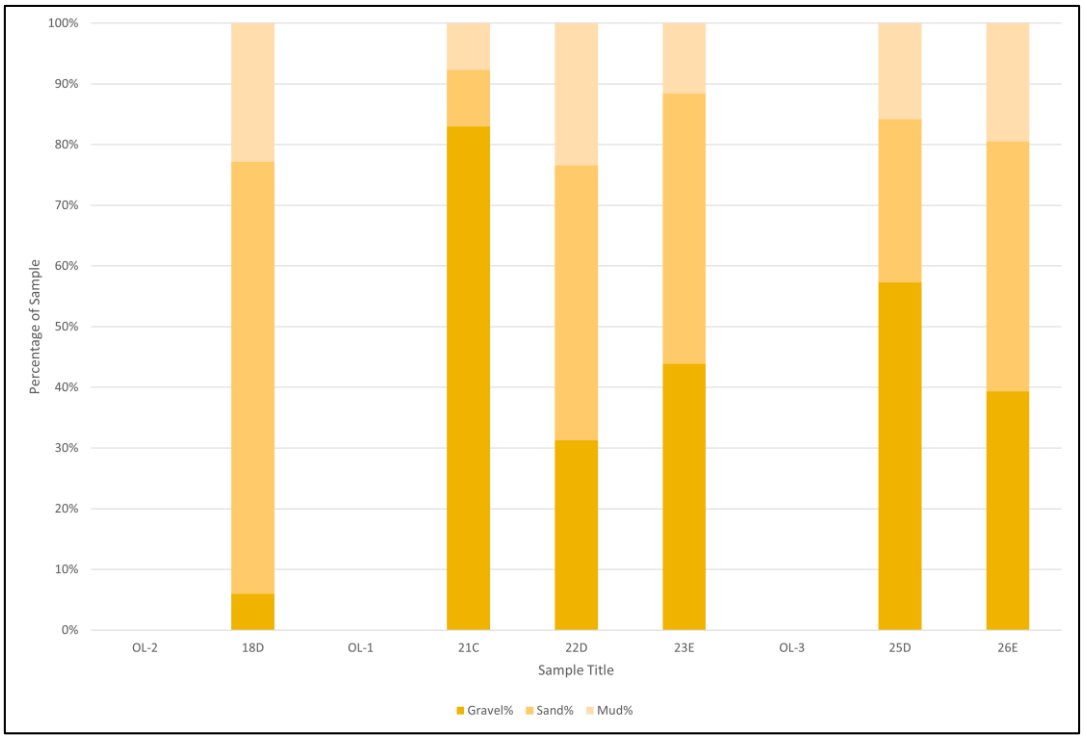

Figure 4.5: Grain size percentage of OL samples.

The OL layers are interesting to compare against each other with consistent details within tephra layers, but differences seen between them. None of the OL layers are leptokurtic showing minimal outliers within the grain size data (appendix 5; figure 4.5).

The single OL-2 layer that was put through grain size analysis was found to have a mean grain size of 2.12 ϕ which is relatively fine for a layer containing visible clasts. This is exemplified through its very fine skew and being deemed fine sand. This would be attributed to vesicularity of the clasts reducing the weight percentages. The lapilli within this layer were not very large to begin with, with the largest grain sizes found being within the 2 ϕ range. The surrounding matrix holding the larger grains together would also play a contributing factor in the samples being more skewed towards finer grains. The sample was very poorly sorted which coincides with the wide range of grain sizes within the layer and it was deemed to have a mesokurtic kurtosis. The layer had 0.03% of its weight found within the 10 ϕ layer (appendix 2) with its largest grain sizes found within -2 ϕ (appendix 4).

OL-1 layers were significantly different to the single OL-2 layer observed, The layer had an average grain size between -1.53 ϕ to 1.16 ϕ which shows much larger clasts than any other layer observed. The layer that had an average grain size of -1.53 ϕ (21C) was unique in that it was the only sample deemed to be very fine gravel, moderately sorted and very platykurtic. All of these indicating that the tephra was primarily large clasts with little to no matrix supporting it. This was supported by observations made in the field at the sample site (figure 3.12). This layer was however the only OL-1 tephra layer that showed any percentage of weight being within 10 ϕ at 0.01% (appendix 2). All three samples reached -3 ϕ with clasts potentially reaching a larger greater size than what was recorded (appendix 4). Two samples also had their highest weight percentage found at -3 ϕ (21C and 23E) with the other sample (22D) showing the highest weight percentage at -1 ϕ. Sample 22D was classified as medium sand and presented a fine skew while sample 23E was deemed very coarse sand with a very fine skew. Both samples were very poorly sorted and platykurtic.

OL-3 was found to sit directly between OL-2 and OL-1 in terms of average grain size with the two samples showing a mean of 0.02 ϕ and 1.2 ϕ indicating fairly large clasts. Both samples were very poorly sorted with sample 25D being classified as coarse sand whilst also being very fine skewed and platykurtic in nature. Sample 26E was classified as medium sand and was fine skewed but very platykurtic, which indicates a very low value of outliers within the data. Both samples had their highest weight percentage occur within the -3 ϕ value showing that a large portion of their composition was larger clasts much like OL-1. Sample 25D also reached a grain size of 10 ϕ having 0.02% of its sample weight (appendix 2). These findings matched field observations of OL-3 usually consisting of large clasts suspended in a thin matrix directly above BA-1.

Geochemistry

5.1 Tephra Composition

Table 5.1: Whole Rock major element composition (wt. %) of sampled tephra determined by XRF analysis.

	Sample ID	Zone	Calibration Method	Preparation name	SiO2 (%)	Al2O3 (%)	TiO2 (%)	MnO (%)	Fe2O3 (%)	MgO (%)	CaO (%)	Na2O (%)	K2O (%)	P2O5 (%)	SO3 (%)	LOI (%)	Sum (%)	Ignited mass	Additive mass		Rock Type
BAT-2																					
	5I	T	Geomajors2	57-43 Bead	58.87	14.38	0.64	0.16	8.42	7.55	6.94	2.91	1.35	0.10	0.01	0.02	101.32	0.7938	7.9949		Andesite
	9G	T	Geomajors2	57-43 Bead	59.77	16.19	0.66	0.13	7.63	6.23	7.14	3.12	1.32	0.11	0.01	0.02	102.32	0.8002	8.0617		Andesite
	12H	D	Geomajors2	57-43 Bead	59.39	16.73	0.71	0.17	9.63	8.38	9.02	2.74	0.98	0.12	0.00	0.01	107.88	0.8215	8.0302		Andesite
	13J	K	Geomajors2	57-43 Bead	59.34	16.13	0.63	0.15	8.31	6.63	6.89	3.05	1.25	0.10	0.01	0.03	102.52	0.7996	8.0289		Andesite
	14K	K	Geomajors2	57-43 Bead	59.53	15.41	0.67	0.14	7.65	6.63	6.86	3.02	1.39	0.10	0.01	0.01	101.41	0.8021	8.0375		Andesite
	15L	K	Geomajors2	57-43 Bead	59.07	16.24	0.65	0.14	7.74	6.45	7.31	3.13	1.28	0.11	0.00	0.01	102.11	0.8015	7.9927		Andesite
avg					**59.33**	**15.85**	**0.66**	**0.15**	**8.23**	**6.98**	**7.36**	**2.99**	**1.26**	**0.10**	**0.01**	**0.02**	**102.93**	**0.80**	**8.02**		
BAT-1																					
	4G	T	Geomajors2	57-43 Bead	57.58	14.65	0.62	0.16	8.74	8.11	8.13	2.56	1.09	0.10	0.01	0.01	101.73	0.7981	7.9961		Andesite
	10D	D	Geomajors2	57-43 Bead	57.98	14.71	0.60	0.15	8.63	8.14	7.86	2.56	1.10	0.08	0.01	0.02	101.84	0.7968	7.9856		Andesite
	16D	D	Geomajors2	57-43 Bead	57.93	16.05	0.64	0.14	8.20	7.04	8.00	2.70	1.14	0.10	0.01	0.03	101.98	0.7932	7.9621		Andesite
	17K	K	Geomajors2	57-43 Bead	58.50	15.98	0.68	0.13	8.05	6.44	7.39	2.67	1.27	0.11	0.01	0.02	101.24	0.8092	8.0247		Andesite
avg					**58.00**	**15.35**	**0.64**	**0.15**	**8.40**	**7.43**	**7.84**	**2.62**	**1.15**	**0.10**	**0.01**	**0.02**	**101.70**	**0.80**	**7.99**		
BA-2																					
	2D	D	Geomajors2	57-43 Bead	54.71	18.12	0.75	0.16	9.76	5.99	8.06	2.67	0.79	0.12	0.00	0.04	101.16	0.8086	8.0152		Basaltic Andesite
	3E	K	Geomajors2	57-43 Bead	55.66	16.80	0.79	0.17	10.79	7.20	6.83	2.51	0.83	0.09	0.00	0.06	101.73	0.8059	7.9796		Basaltic Andesite
	11G	T	Geomajors2	57-43 Bead	55.92	17.28	0.73	0.15	8.73	6.43	8.66	2.75	1.00	0.13	0.00	0.02	101.78	0.8029	8.0024		Basaltic Andesite
avg					**55.43**	**17.40**	**0.76**	**0.16**	**9.76**	**6.54**	**7.85**	**2.64**	**0.87**	**0.11**	**0.00**	**0.04**	**101.56**	**0.81**	**8.00**		
OL-3																					
	25D	D	Geomajors2	57-43 Bead	56.97	15.65	0.71	0.19	10.58	8.39	8.37	2.53	0.82	0.10	0.00	0.01	104.33	0.8077	8.0492		Basaltic Andesite
	26E	K	Geomajors2	57-43 Bead	55.42	16.28	0.73	0.19	10.46	8.07	7.48	2.36	0.86	0.08	0.00	0.05	101.98	0.8050	7.9794		Basaltic Andesite
avg					**56.20**	**15.97**	**0.72**	**0.19**	**10.52**	**8.23**	**7.92**	**2.44**	**0.84**	**0.09**	**0.00**	**0.03**	**103.16**	**0.81**	**8.01**		
BA-1																					
	1A	D	Geomajors2	57-43 Bead	56.76	17.38	0.63	0.15	8.37	6.27	8.07	2.80	1.09	0.11	0.00	0.02	101.66	0.7992	7.9995		Basaltic Andesite
	6C	K	Geomajors2	57-43 Bead	56.57	14.98	0.77	0.19	10.56	8.14	6.93	2.34	1.05	0.08	0.00	0.04	101.65	0.8103	8.0164		Basaltic Andesite
	7D	D	Geomajors2	57-43 Bead	56.15	15.68	0.70	0.18	9.87	7.67	8.14	2.57	0.94	0.09	0.01	0.02	102.01	0.7938	7.9964		Basaltic Andesite
	8E	K	Geomajors2	57-43 Bead	56.77	17.06	0.73	0.17	9.41	6.83	7.35	2.54	1.10	0.09	0.00	0.04	102.08	0.7913	7.9913		Basaltic Andesite
avg					**56.56**	**16.28**	**0.71**	**0.17**	**9.55**	**7.23**	**7.62**	**2.57**	**1.05**	**0.09**	**0.00**	**0.03**	**101.85**	**0.80**	**8.00**		
OL-2																					
	18D	D	Geomajors2	57-43 Bead	54.97	15.30	0.69	0.20	10.70	8.70	8.16	2.37	0.79	0.08	0.01	0.02	101.99	0.8025	8.0065		Basaltic Andesite
OL-1																					
	21C	K	Geomajors2	57-43 Bead	53.00	18.88	0.76	0.43	10.74	7.37	7.05	2.22	0.63	0.09	0.01	0.08	101.26	0.8136	8.0113		Basaltic Andesite
	22D	D	Geomajors2	57-43 Bead	53.89	17.03	0.60	0.18	9.83	7.99	8.62	2.49	0.69	0.08	0.01	0.02	101.43	0.8039	8.0191		Basaltic Andesite
	23E	K	Geomajors2	57-43 Bead	52.97	16.02	0.72	0.22	11.76	9.42	7.83	2.01	0.58	0.09	0.01	0.03	101.65	0.8004	8.0900		Basaltic Andesite
avg					**53.29**	**17.31**	**0.69**	**0.28**	**10.78**	**8.26**	**7.84**	**2.24**	**0.63**	**0.09**	**0.01**	**0.04**	**101.45**	**0.81**	**8.04**		

5.1.1 Black Ash Classification

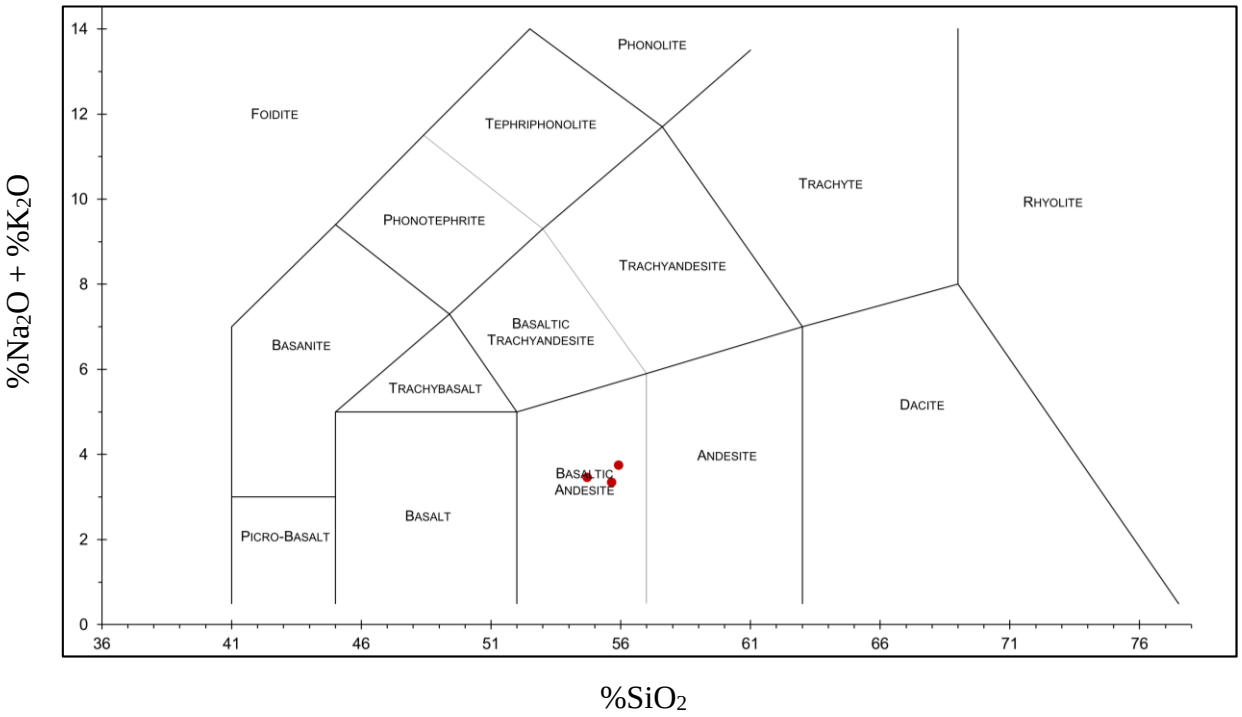

Figure 5.1: TAS Diagram for BA-2 (Le Maitre et al, 2002; Template Excel sheet provided by Iacovino, and Gouard, 2021)

The three BA-2 samples ranged in SiO_2% from 54.71%, 55.66% and 55.92% with a range of 1.21% (figure 5.1). This puts the tephra layer within the middle ranges of basaltic andesite. Na_2O and K_2O values are fairly concise with sample 11G showing slightly higher values.

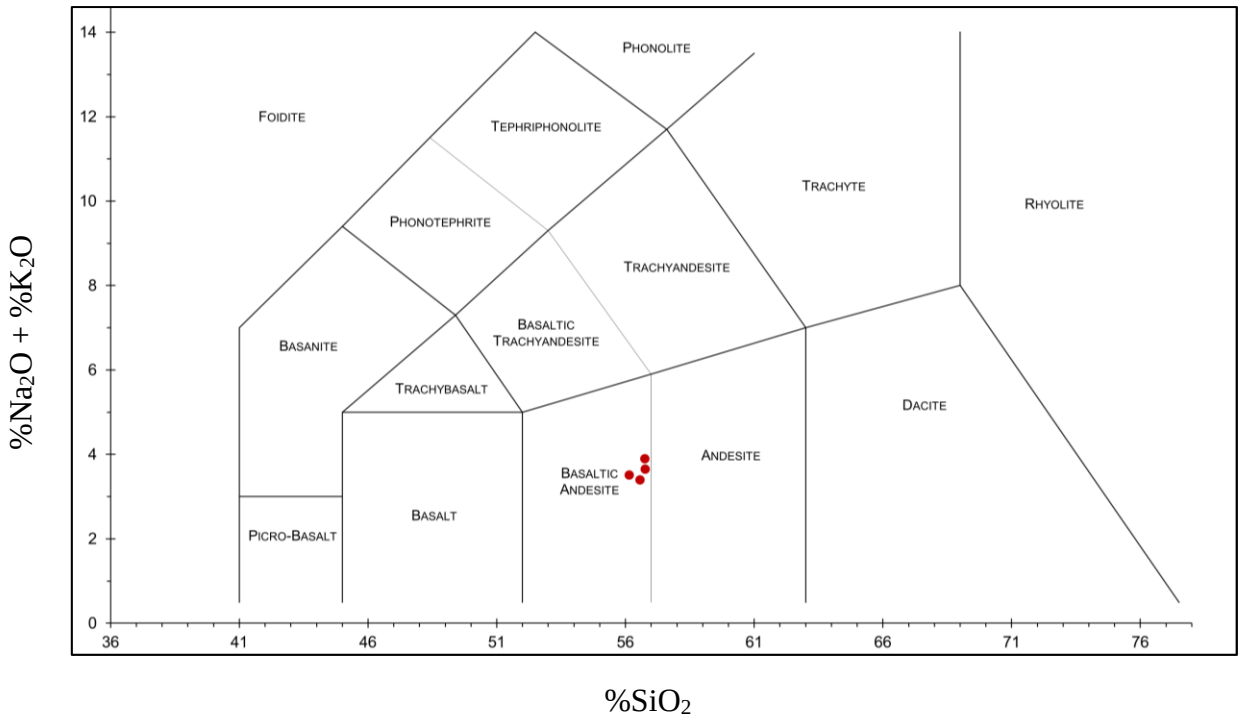

Figure 5.2: TAS Diagram for BA-1. (Le Maitre et al, 2002; Template Excel sheet provided by Iacovino, and Gouard, 2021).

The four BA-1 samples showed a higher percentage of SiO_2 than BA-2 with values of 56.76%, 56.57%, 56.15% and 56.77% with a range of 0.62%. These samples were also much more precise with little variation across Na_2O and K_2O. These samples fell within the borders of basaltic andesite (figure 5.2) but sit much closer to the border with andesite.

5.1.1.1 Comparison Between BAT and BA Deposits

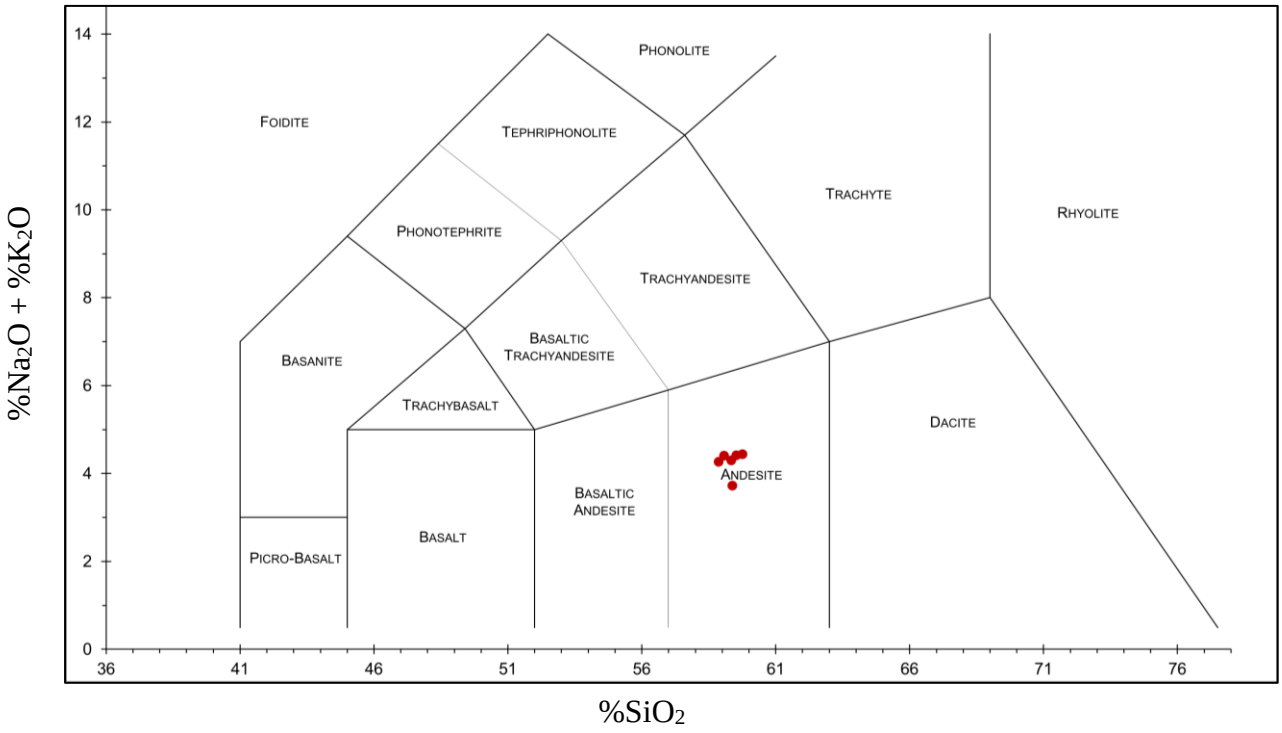

Figure 5.3: TAS Diagram for BAT-2. (Le Maitre et al, 2002; Template Excel sheet provided by Iacovino, and Gouard, 2021).

An interesting discovery regarding the difference between the BAT samples and BA samples were that they belonged to entirely different rock types despite appearances and physical componentry being so similar (figure 5.3). BAT-2 samples were very precise in their geochemical fingerprint with only one outlier point being sample 12H. The other five points were very precise within the andesite zone. The SiO_2 percentages for each of the six samples were 58.87%, 59.77%, 59.39%, 59.34%, 59.53% and 59.07% with a range of 0.9%.

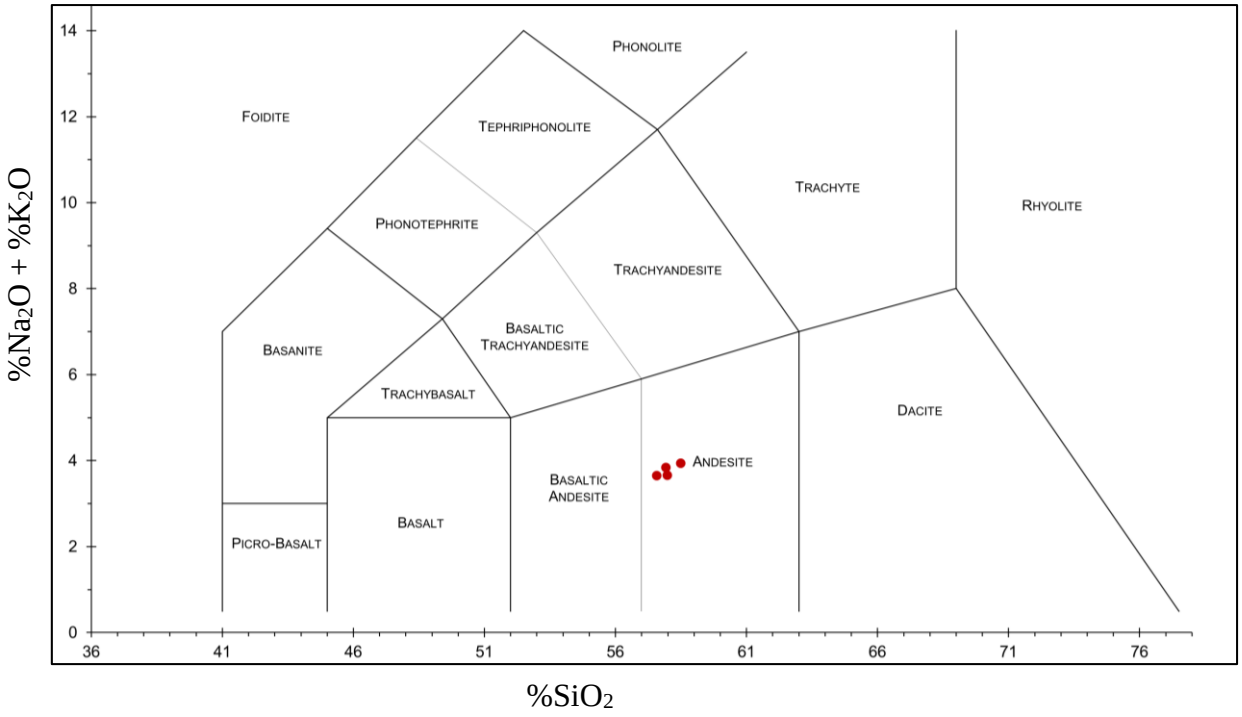

Figure 5.4: TAS Diagram for BAT-1. (Le Maitre et al, 2002; Template Excel sheet provided by Iacovino, and Gouard, 2021).

Much like BAT-2, the four BAT-1 layers were also found to belong to the andesite zone (figure 5.4) with a slight leaning closer towards basaltic andesite. The four samples had SiO_2 percentages of 57.58%, 57.98%, 57.93% and 58.5% with a range of 0.92%. Three of the samples fall very closely together with one found at a slightly higher SiO_2 level, this sample being 17K. Both BAT-2 and BAT-1 appear to belong to the andesites whilst BA-2 and BA-1 belong to the basaltic andesites. It appears that there was a general trend towards higher silica content within Ruapehu ashfall tephra over this period of time with the newer layers having a minimum SiO_2 increase of 0.81% from sample 8E to sample 4G. This increase is not chronological but more a reflection of the gap between the black ash layers found within the basaltic andesites and the black ash layers found within the andesites.

5.1.2 Orange Lapilli Classification

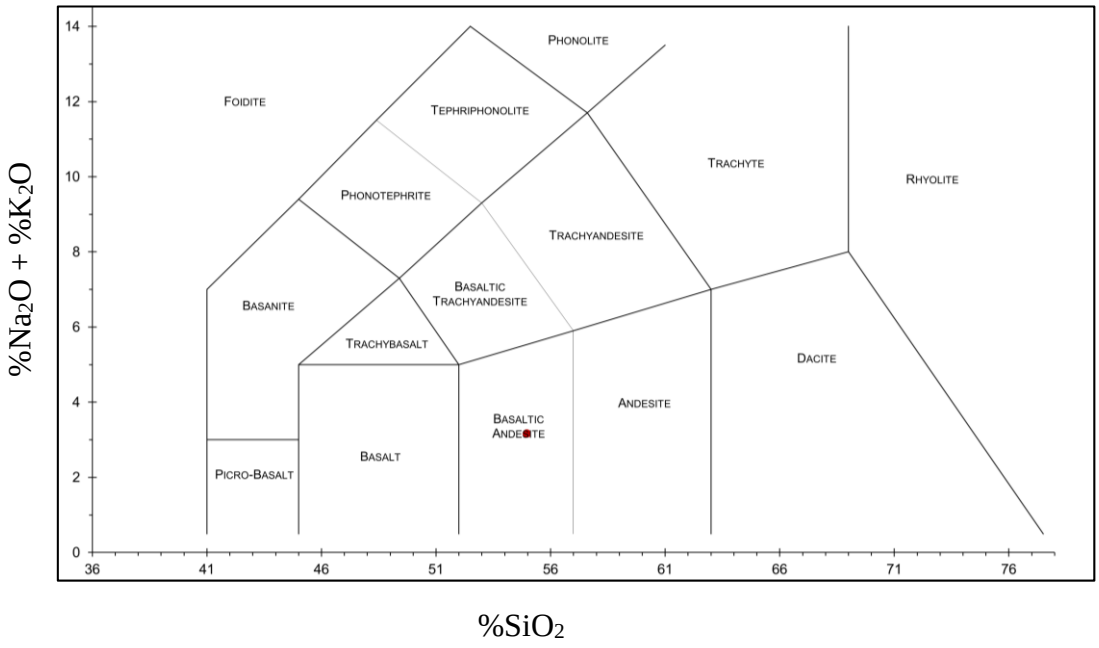

Figure 5.5: TAS Diagram for OL-2 (Le Maitre et al, 2002; Template Excel sheet provided by Iacovino, and Gouard, 2021).

The orange lapilli layers, despite contrasting appearances to the black ash layers still show a chronological change in silica content at Mount Ruapehu. Sample 18D (OL-2) had a silica content of 54.97%. This sample however sits barely within the confines of BA-2 samples (figure 5.1) with an overlap of 0.26%. It does sit within the confines of basaltic andesite (figure 5.5).

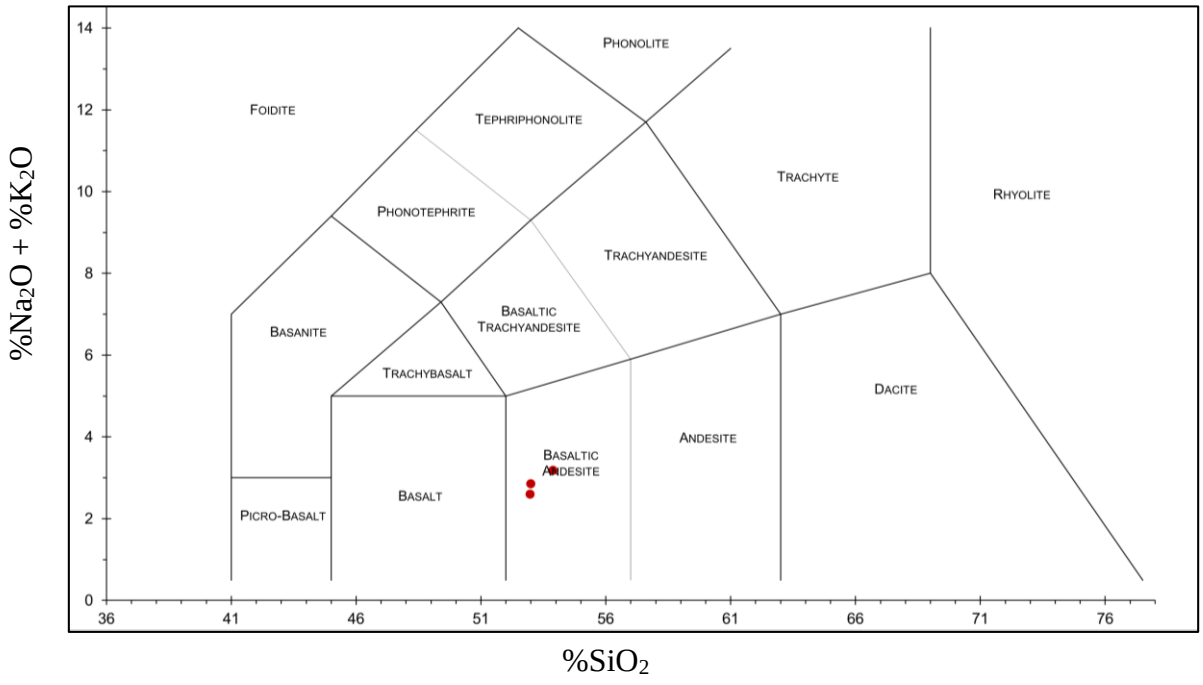

Figure 5.6: TAS Diagram for OL-1 (Le Maitre et al, 2002; Template Excel sheet provided by Iacovino, and Gouard, 2021).

OL-1 layers show a more dramatic shift in SiO_2 values with three samples showing silica contents of 53%, 53.89% and 52.97% with a range of 0.92%. These also fall within the basaltic andesite perimeter (figure 5.6) but are noticeably closer to the basalt zone. Sample 22D is a partial outlier within the data with slightly higher Na_2O and K_2O values. This sample was collected much further east than the other two which could be a potential reason for differences with geochemical composition. These samples were the lowest silica content recorded from field deposits.

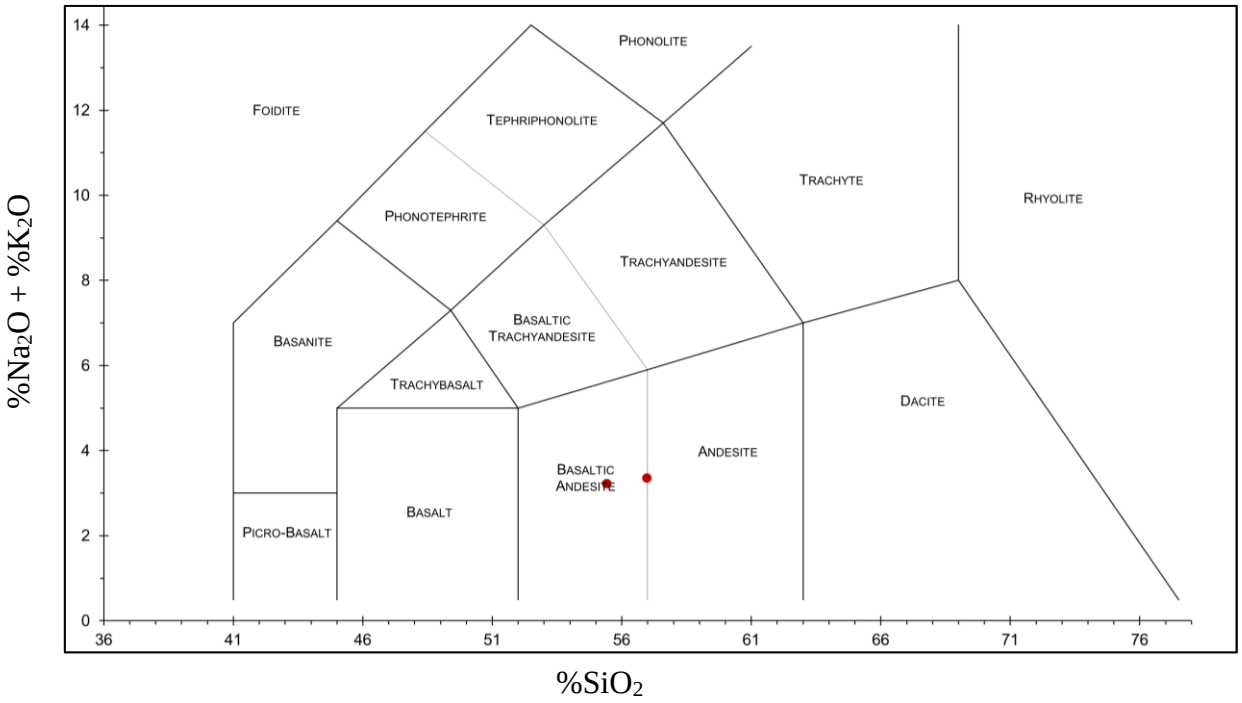

Figure 5.7: TAS Diagram for OL-3 (Le Maitre et al, 2002; Template Excel sheet provided by Iacovino, and Gouard, 2021).

OL-3 samples showed the widest range of silica content. These samples being 25D and 26E with silica contents of 56.97% and 55.42% respectively with a range of 1.55%. While these two samples show a wide silica range their Na_2O and K_2O values are very similar (figure 5.7). Both samples sit within the basaltic andesite perimeter with 26E sitting within the centre and 25D sitting on the border between andesite and basaltic andesite.

5.2 Black Ash Element Trends

5.2.1 BA Major Elements

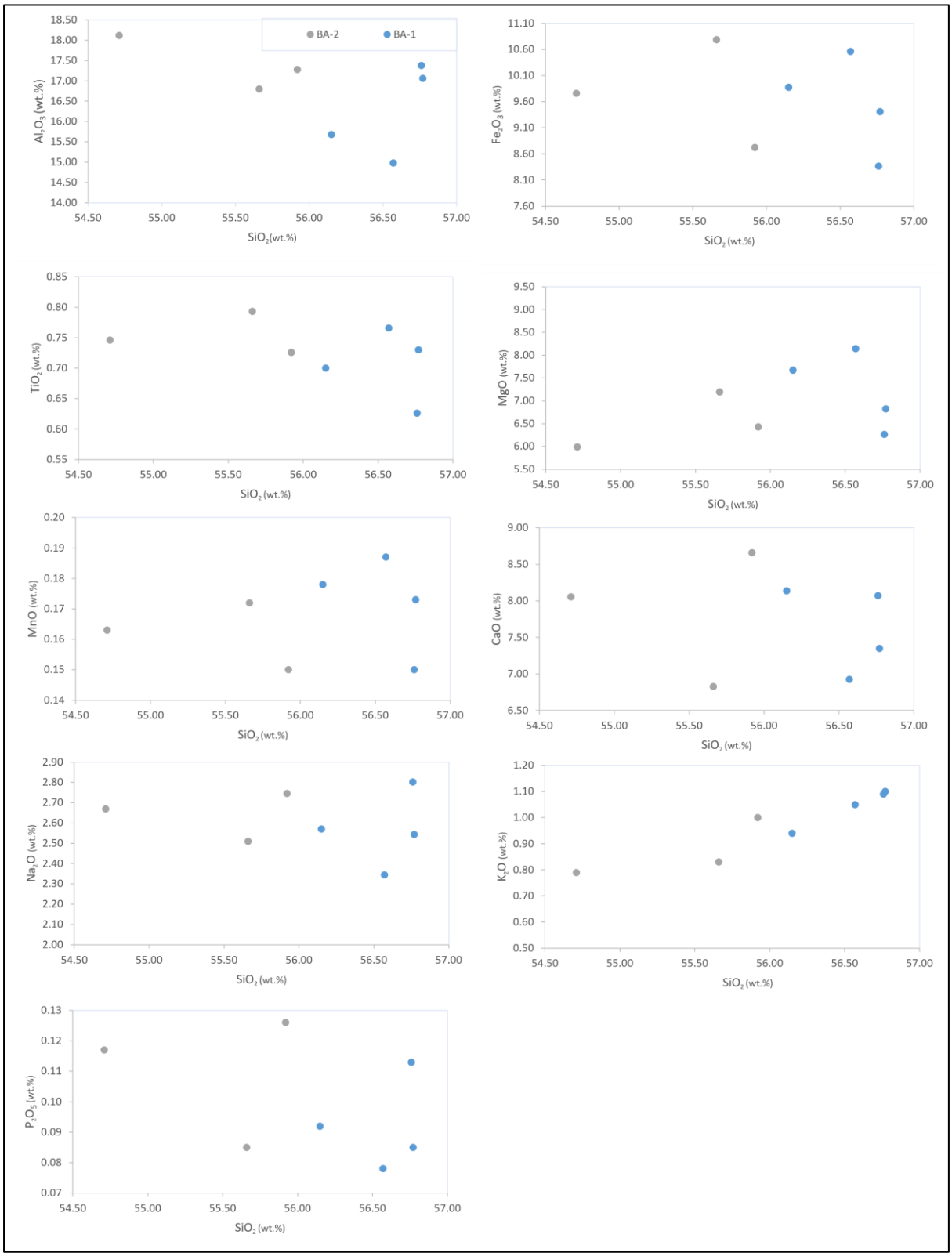

Figure 5.8: Harker variation graphs showing major element trends plotted against SiO_2 for BA-2 and BA-1 samples. All Fe is expressed as Fe_eO_3.

Looking into the major element trends for the black ash layers (figure 5.8) trends can be observed between BA-2 and BA-1. BA-2 shows greater Al_2O_3 content with a noticeable decrease with BA-1 samples. TiO_2 levels are generally the same with one BA-1 outlier showing a lower TiO_2 level (sample 1A). It generally shows a very small negative trend in TiO_2 between layers. MnO levels between BA-2 and BA-1 shows a slight increase in content with increasing SiO_2, but it is still a mostly linear trend. Na_2O does not show a visible trend with BA-1 showing the highest and lowest value within the range. P_2O_5 shows a negative trend with increasing silica content for these two tephra layers although the actual composition percentage for the tephras is very low.

The iron content (presented as Fe_2O_3) stays relatively similar across the two samples with no discernible trend being shown. MgO shows a positive increase with SiO_2 content with BA-1 showing a generally higher percentage than BA-2, CaO does not show much of a trend with BA-2 presenting the highest and lowest values. Perhaps the strongest relationship seen is between SiO_2 and K_2O with a very positive trend as BA-1 shows greater K_2O contents than BA-2.

5.2.2 BAT and BA Trend Comparison

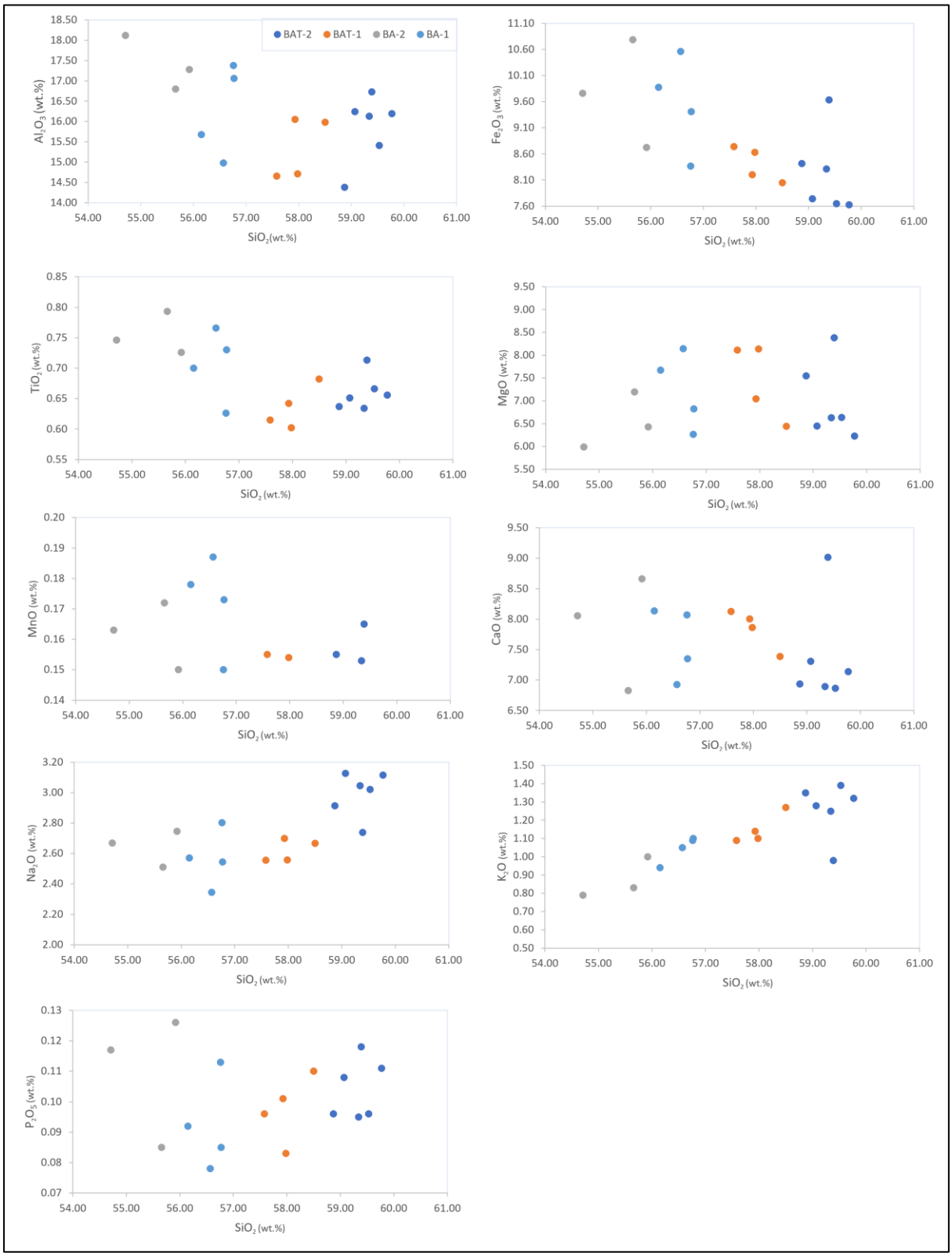

Figure 5.9: Harker variation graphs showing major element trends plotted against SiO_2 for BAT-2, BAT-1, BA-2 and BA-1 samples. All Fe is expressed as Fe_eO_3.

The differences between the BAT layers and the BA layers are quite distinct (figure 5.9). In terms of Al_2O_3. The BAT layers show the same negative trend as was seen between BA-2 and BA-1 with the lowest content being seen in sample 5I. The same can be shown with TiO_2 although it appears to have a partial dip with BAT-1 showing the lowest contents in general and not BAT-2 (which has the highest observed silica content). MnO overall shows a negative trend which goes against what was observed with BA-2 and BA-1 as the BAT layers have a slightly lower MnO content on average with their contents remaining very similar between the two layers. Na_2O content spikes with the introduction of the BAT layers with BAT-1 having a consistent content to the BA layers but BAT-2 has significantly higher Na_2O content than the other three layers. P_2O_5 maintains the same characteristics across the four layers with minimal variation.

A sharp decrease in iron is observed between the BA layers and the BAT layers with all samples showing below 8.8% Fe_2O_3 content with only one outlier showing a content of 9.63% (sample 12H - BAT-2). MgO levels with the inclusion of the BAT layers with the samples staying mostly within the range BA-1 displays, a large decline in CaO can be seen except for one result within the BAT-2 range which has the highest content of CaO of 9.02% (sample 12H). Beside that one major outlier the rest of the results fall in line with a negative CaO and SiO_2 trend. The inverse can be seen with K_2O where much like with BA-2 and BA-1, the BAT layers show a very strong positive relationship with silica content except for one BAT-2 outlier which is also sample 12H. In terms of P_2O_5, most of the BAT samples showed 0.01% with only one of the BA samples showing 0.01%.

The differences between BAT and BA samples are shown through their major element compositions with trends being observed that further compliment the alterations to Mount Ruapehu’s ashfall deposits over time.

5.3 Orange Lapilli Major Elements

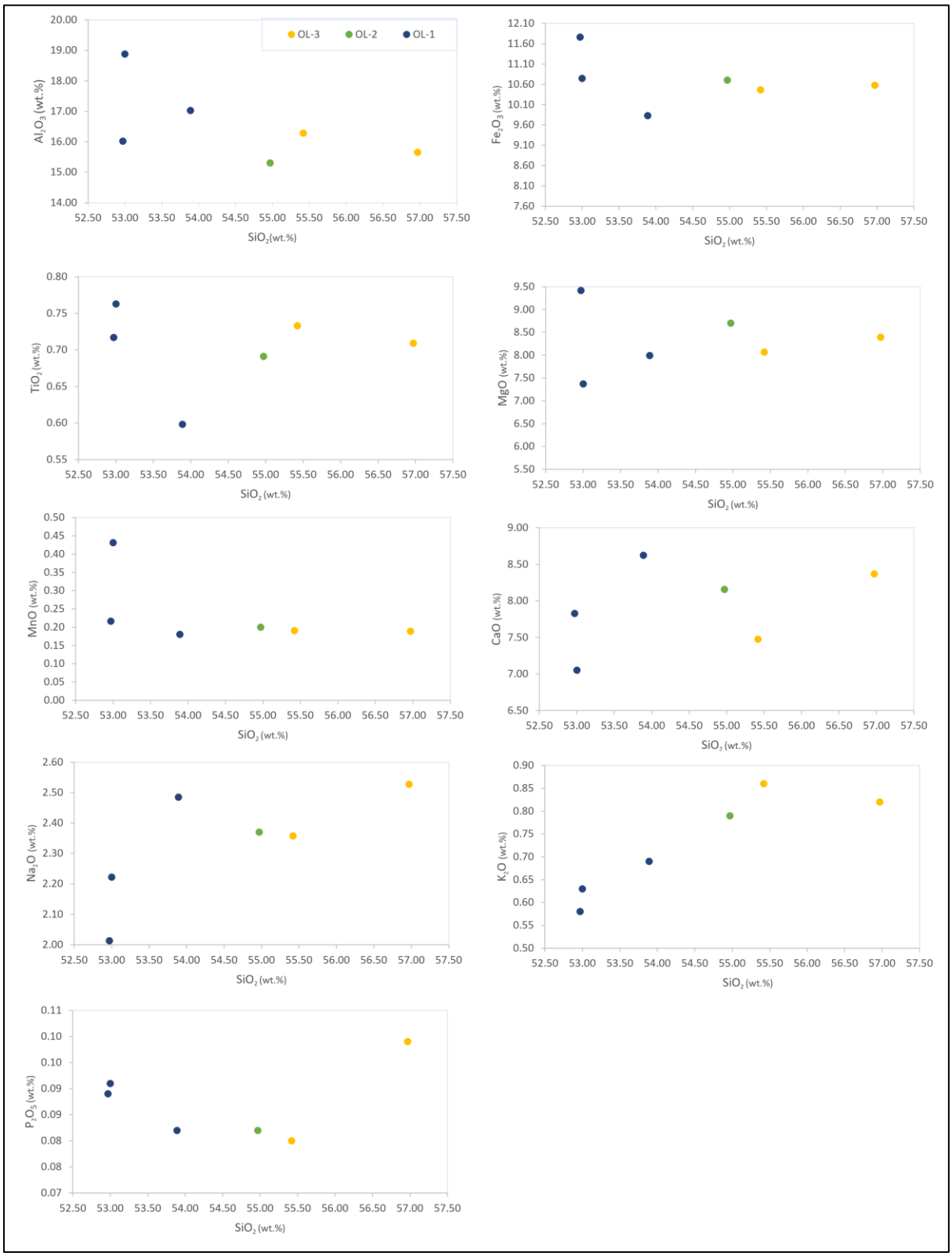

Figure 5.10: Harker variation graphs showing major element trends plotted against SiO_2 for OL-2 and OL-1 samples. All Fe is expressed as Fe_eO_3.

Trends for the orange lapilli layers (figure 5.10) do appear to match what was observed with the black ash layers such as a negative trend being seen with Al_2O_3 with OL-1 having the greatest content percentage seen out of all samples with a value of 18.88% (sample 21C). A trend cannot be properly observed regarding TiO_2 with all values staying relatively concise beside one outlier (sample 22D). The same can be shown for MnO where all the samples are concise except for one massive outlier being seen with the content percentage doubling with sample 21C. Na_2O shows similar observations except there are two outliers for OL-1 (21C and 23E) not following a linear appearing trend across the silica range. P_2O_5 shows a general negative trend except for one OL-3 sample which shows a large spike (sample 25D).

The iron content for the samples is noticeably larger than what is seen in the black ash deposits which coincides with its unique colouration. A lack of trend is observed however with OL-1 showing the highest and lowest Fe_2O_3 content out of the orange lapilli. The same trends can be seen with MgO and CaO where OL-1 marks the range for orange lapilli samples. For K_2O, the positive trend seen in the black ash deposits is reflected here with the OL-1 deposits showing the lowest percentage of K_2O out of all samples.

5.4 Geochemical Trends Across Zones

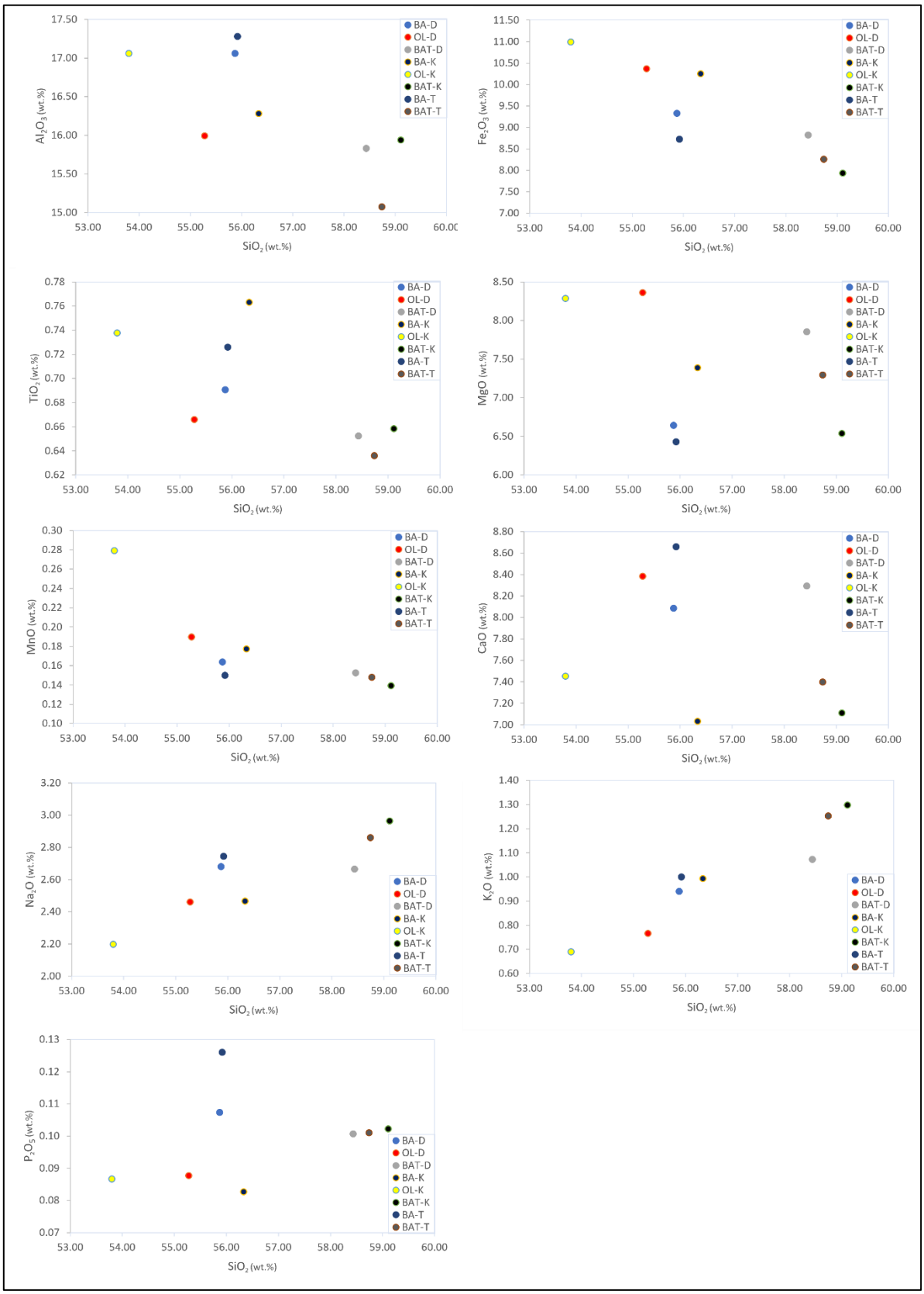

Figure 5.11: Harker Variation Graphs showing the major oxide trends across zones, samples are averaged within each zone with D referencing Desert Road, K referencing Karioi Forest and T referencing the Tukino Access Road.

Analysing tephras based on the zone they were discovered in allows for geochemical trends to be seen between layers and between regions (figure 5.11). Tephra compositions were averaged into their overarching ashfall type (BAT, BA and OL) and then averaged based on the three zones where samples were collected. Zone D being Desert Road, Zone K being the Karioi Forest and Zone T being the Tukino Access Road.

It can be seen that there are differences between the same tephras at different locations such as with the black ash from the Karioi Forest generally contrasting to BA layers from other locations with the D and T layers staying relatively similar. Compared to the orange lapilli layers where the K tephras have the lowest average silica content with an average of 53.8%. The D tephras show an average silica content of 55.28%. There is a discernible difference in silica content for each tephra zone with both BA and BAT showing their lowest silica contents within zone D, the most distal zone. Their highest silica contents are seen within zone K, the southernmost region. The BAT layers seem to show similar percentages of each major oxide within each zone whereas there is more variability between major oxide percentages for the BA and OL layers.

5.5 Comparison to Tufa Trig Geochemistry

Comparing the geochemistry of the collected tephras to ones obtained by Voloschina (2020; figure 5.12) that represent the geochemical range of the TTF is useful for identifying trends across time. The data used was produced at the Victoria University Microprobe and contains data from seven layers from the TTF, these being T5, T13-2. T13-3, T13-4, T13-5, T13-6, T15-4, T31-1 and T31-2. T13 is the most prominent Tufa Trig Layer found in the eastern ring plain of Mount Ruapehu. displaying the range of multi-phase eruptive deposits allows for an in-depth view into the best-preserved eruptive sequence from the volcano within the last 2,000 years (Voloschina, 2020).

Layer T5 shows distinct similarities to the BAT layers (figure 5.12) in all major oxides except TiO_2 and MgO. A linear trend can be observed in almost all major oxides with the sharpest correlations appearing with the Fe_2O_3, MnO, CaO and K_2O major oxides.

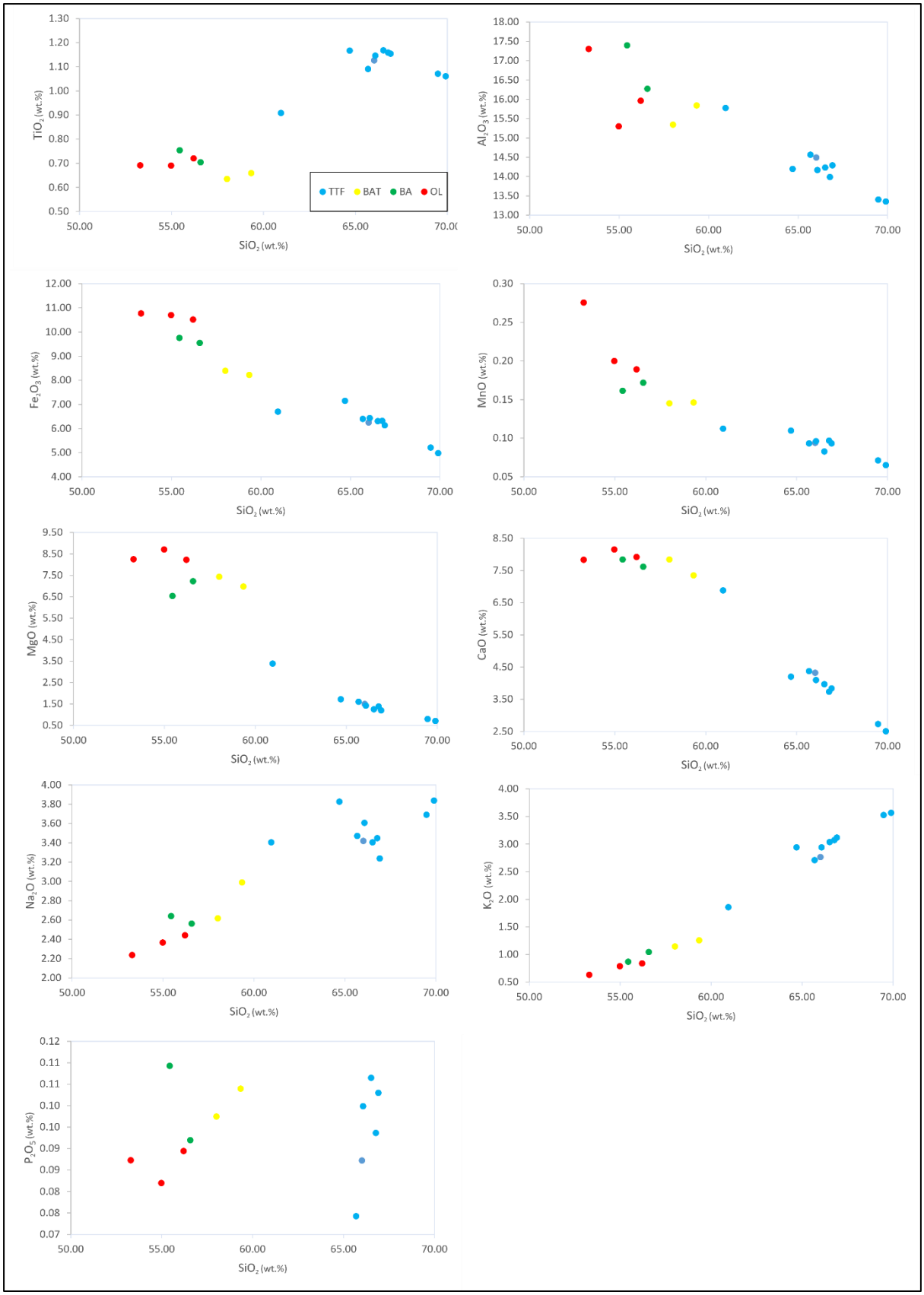

Figure 5.12: Harker Variation Graphs of the major oxide trends between the sampled data and key tephras found within the Tufa Trig Formation based on findings from Voloschina (2020).

Discussion

6.1 Physical Extents and Deposition of Tephra Deposits

The physical extents of the deposits found within the field can be loosely estimated through the isopach maps constructed (section 3.5). Due to restrictions on access to the Rangipo desert, the northern extents of the tephras are yet to be accurately defined as well as the eastern extent although this would also require military permission. The tephra layers were not observed in outcrops south of the Karioi Forest and the western-most reaches were observed to be ~ 8.5 kilometres from source with any layers found closer being buried or too weathered to be observable.

The Ruapehu derived PPF tephra deposits were deposited between 4-7 ka based on surrounding tephra, the region in which deposits are visible ends up taking on the appearance of a narrow band within the ring plain as any closer will be buried and any further out would have only deposited very thin layers which after such a time would have disappeared within the stratigraphy. This band can be defined as a region from ~8-18 kilometres from source. The distal reaches can extend much further than what was observed especially with very discernible layers visible at 17.2 kilometres from source, but it is difficult to project what the expected reach is without further field work to the east of State Highway 1; however, these deposits were not observed by Pardo (2012) or Donoghue (1991) at this range.

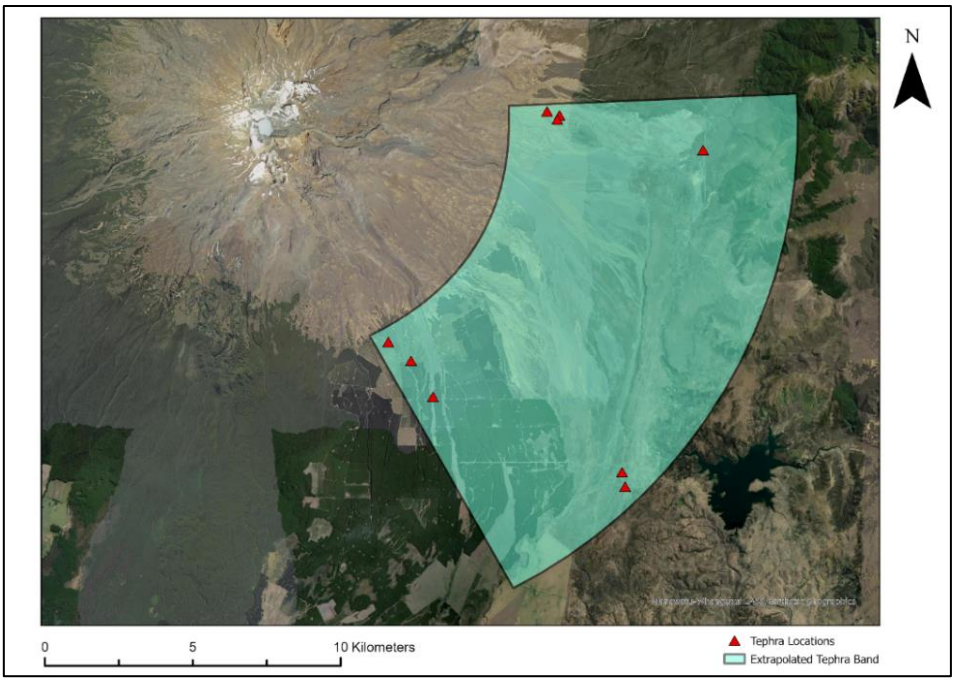

Figure 6.1: Extrapolated region of the PPF tephra layers based on an observed radius between 8 and 18 kilometres away from source.

The potential extents of the tephra being studied were based on findings within the field (figure 6.1). Tephras were not observed any further north or west than what was observed. To the east and south the findings may certainly extend beyond what was observed but further research would have to be conducted. Through mapping, it is evident that a south-easterly depositional axis was occurring during the eruptive phase throughout the Papakai Formation as all four primary tephras were found to match this trend.

The BAT tephras appear within the same reach and further north which implies a larger deposition/eruptive phase or at the very least a wider deposition area of ashfall from the eruptive events. This could however be exaggerated through the more recent nature of the deposits as they have not had enough time to degrade to the same extent as the older PPF tephras. It is unlikely that the original deposition characteristics can be defined from the current state of the tephras unless they are assumed to have not changed since deposition. The layers themselves are poorly preserved within the stratigraphy despite having recognisable characteristics which highlights their susceptibility to erosive processes.

The black ash layers appear to have a wider region of deposition based on field observations. This can be explained due to the finer grain size allowing for greater dispersal. BA-2 was found the furthest north out of the PPF tephra layers, being observed at least once in each major study region. BA-1 was not confirmed along the Tukino Access Road. The tephra was however the most observed out of the PPF tephra layers with four confirmed sightings and one potential deposit. Sampling of the deposit at site Q would be required to confirm its presence. If confirmed, then it can be assumed that its deposition area is at least comparable to BA-2.

The orange lapilli layers showed a much more confined deposition extent than what was observed with the black ash layers. OL-2 was potentially seen at site T with observations matching what was seen to the south, but sampling could not be achieved to verify it. The same can be said about the OL-3 layer at site U along the Tukino Access Road, it was measured but geochemical analysis would be required to verify the authenticity of the tephra. The inclusion of these sites increases the range at which the tephras are observed but would need to be sampled to confirm. OL-1 was the most characteristically striking out of the PPF deposits. OL-1 tephras were focused to the southern extents of the eastern ring plain and work within the Badlands or Scorpion Gully would be necessary to uncover the northern extents of the layer. However, due to it not appearing along Tukino Access road it can be assumed that it had the

most southern deposition out of the primary tephras being studied with it being the only deposit not to be observed that far north.

When the orange lapilli were observed in the field, they were striking within the stratigraphy and aided in the identification of the black ash layers. The inclusion of data from within the military zone would be necessary to accurately portray the orange lapilli layers through isopachs and isopleths. The only reliable samples could be collected in the southern extents of the study region which does not provide adequate information in terms of the geographical extents of the tephra. The depth at which these layers are found provide further uncertainty when aiming to successfully map the deposit as it is usually buried. Much like the black ash layers, a northern and southern extent would need to be ascertained.

The likelihood of the PPF tephra layers surviving within observable stratigraphy any further north than the Tukino Access road would be exceedingly low as observations were minimal and the landscape becomes crowded with tephras from other volcanic centres such as Mount Tongariro appearing more frequently. In this sense, the Tukino Access road could be deemed the furthest north where investigations should take place with the true geographical extents being within the central Rangipo Desert and still to be uncovered.

No deposits were observed at outcrops along State Highway 49 which sits outside of the expected region of deposition (figure 6.1). This would imply that deposition was not concentrated southwards despite a south-easterly deposition. It can be assumed that PPF tephras are highly unlikely to be found closer than ~8 kilometres from source due to the overlap of newer material and the higher erosion rates found at higher elevations on the cone. Through all of these factors, geographical extents for the Ruapehu derived PPF ashfall deposits can be assumed to the borders of State Highway 49 to the south, Tukino Access road to the north and to within eight kilometres of the Crater Lake on Mount Ruapehu to the west. A suitable location to narrow down an eastern deposition extent would be near Waiouru as it is south-easterly from Mount Ruapehu.

Investigation of the potential deposition area comes an increase in potential observations as well as opportunities for the tephra layers to be described in greater detail. The area outlined can also be interpreted as the hazard zone associated with these eruptive events.

6.2 Eruptive Processes

The characteristics of the erupted products is based on the geochemical composition of the magma it originated from and the eruptive scenario that ejected the material into the surrounding area. The Crater Lake that is currently above the active vent on Mount Ruapehu has been emplaced for the last 2.6 ka based on evidence from lahar deposits found to the east of Mount Ruapehu (Pardo et al, 2012). With the PPF tephra layers having been deposited earlier than ~4.3 ka, a Crater Lake was not present at the time of deposition.

The oldest Ruapehu derived PPF tephras were the two orange lapilli layers. These showed the lowest silica weight percentages out of all samples taken with an SiO_2 range of 52.97% to 54.97%. Whilst still being considered basaltic andesite, they both show lower silica content on average with greater mafic characterisations being observed such as higher iron contents (9.83-11.76%) which provides the distinct orange colouration of the material within the stratigraphy. The third and youngest lapilli layer above BA-1 is also high in iron but shows a higher silica content ranging from 55.42-56.97%. These orange lapilli layers would have been produced in less violent eruptions from the volcano with less fragmentation occurring and lower gas content. The lower fragmentation resulted in larger clasts that travelled less distance from the volcano with clasts being 0.46 ϕ on average. These layers could potentially show the point of least volatility from the volcano with trends towards re-activation and increasing volatility from Mount Ruapehu.

The black ash layers were the youngest PPF tephra deposits with a much finer composition and darker colouration than what was found with the older material. This is shown through higher silica contents ranging from 54.71 – 56.77% and lower iron contents ranging from 8.37 to 10.79%. While overlap does occur with the OL-3 and BA-1, the physical differences are striking with overlap occurring due to the material originating from the same source around the same period of eruptive activity. Clasts from the two black ash layers were found to be 2.77 ϕ on average showing a much finer composition than the older lapilli layers. An increase in silica content alongside a decrease in clast size points towards a more explosive, gas driven eruptive period generating these ashfall deposits that spread further across the eastern ring plain.

The black ash layers obtained from beneath the Taupō Ignimbrite (potentially Mangatawai deposits or TTF deposits that are not included due to their position beneath the Taupō Ignimbrite) were even finer grained with an average grain size of 3.43 ϕ and also showed a much greater content of SiO_2 ranging from 57.58 – 59.77%. With even lower iron contents of

7.63 to 8.74% (with one outlier showing an iron content of 9.63%). The trend towards more explosive eruptions is shown with the transition from a basaltic andesitic composition within the PPF to andesitic from the ash layers found beneath the Taupō ignimbrite. It indicates increased activity from Mount Ruapehu with greater gas content producing more violent eruptions.

The eruptive processes that occurred at Mount Ruapehu within the time frame being detailed were infrequent and low activity based on the basaltic andesite composition of deposits and the more mafic, coarse nature of samples that were obtained. The eruptions that produced the black ash layers may have had phreatic components due to the high counts of lithics within the samples as older material would have been ejected from the volcano. The orange lapilli layers showed generally very little lithic contents with the more recent black ash layers showing very little lithic counts too. We can assume each eruption was magmatic based on composition and the lack of a permanent Crater Lake at the time. Mount Ruapehu is strongly influenced by hydrothermal alteration indicating large volumes of groundwater which would contribute to phreatic events.

6.3 Tephra Comparisons to Donoghue (1991)

Much of the preliminary data for the PPF tephras in terms of location and appearance were based off of work conducted by Susan Leigh Donoghue in 1991. Donoghue looked into the late quaternary stratigraphy of Mount Ruapehu's south-eastern ring plain. It was through Donoghue's work that the tephras were allocated to the Papakai Formation.

The Papakai Type Locality Donoghue used was not observed during field work. Site Q was the closest site visited to the 1991 Type Locality. Alterations to the terrain could have occurred within the last 33 years such as vegetation growth which reduced visibility of deposits. Also, this type locality was for the entirety of the PPF, from all sources whereas the type locality defined in this study (Site D) was for Mount Ruapehu derived PPF tephras. The tephra layers were observed at the type locality, but the most in-depth observations were taken at Site TT2. As these layers were observed within the southern portion of the eastern ring plain it can be considered appropriate that the current type locality was found at a south-east bearing from Mount Ruapehu along its potential deposition axis. Site TT2 follows this deposition axis as well. Donoghue's Papakai Type Locality was located at site DR15 (figure 6.2), to the east of Mount Ruapehu. The PPF in its entirety appears to be more dominant to the northeastern reaches of the TgVC with tephra from Mount Tongariro, Mount Ngauruhoe and the Tama

Lakes being the predominant deposits with a smaller component from Mount Ruapehu being the primary tephras of this study (Topping, 1973).

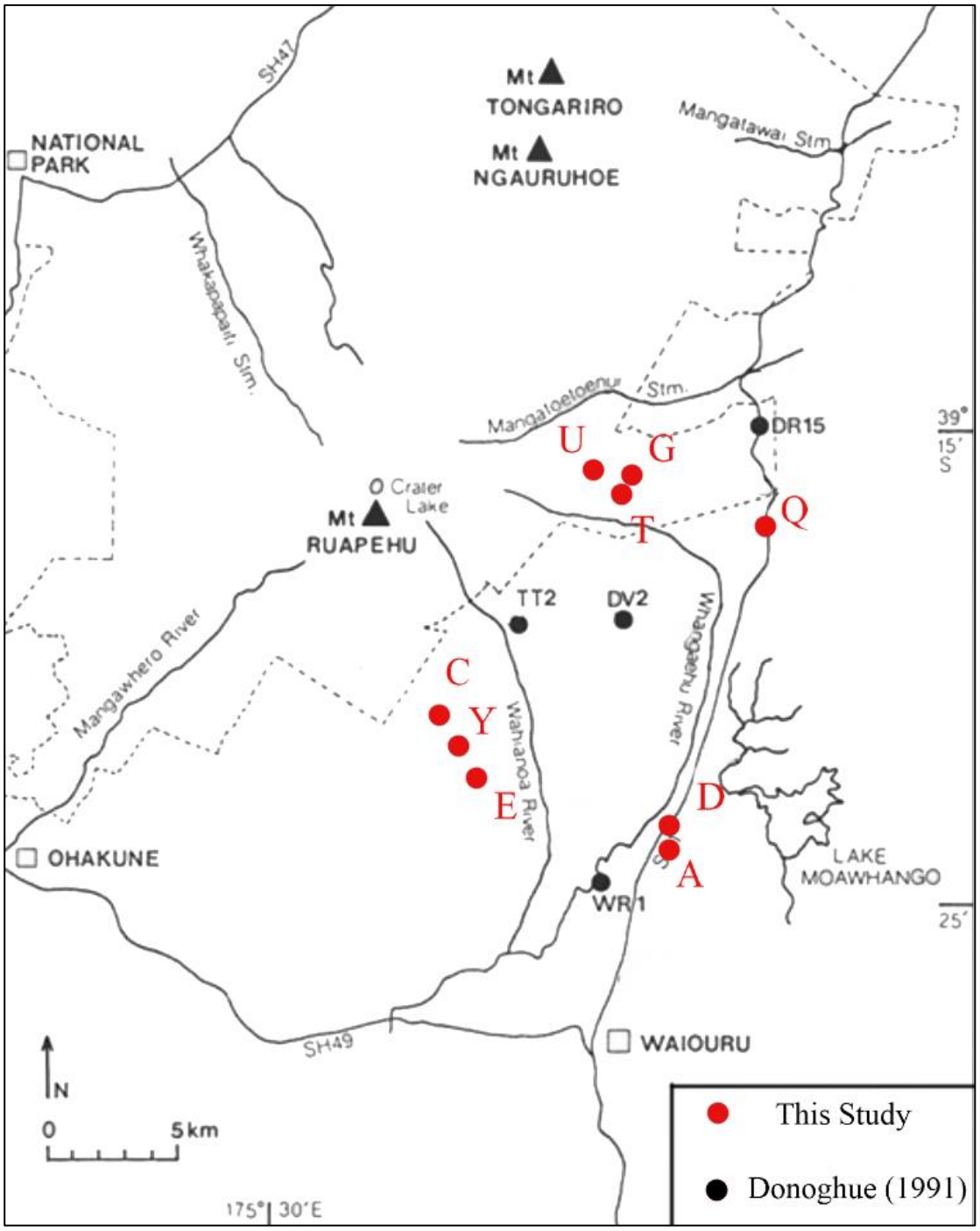

Figure 6.2: Ruapehu PPF locations repurposed from Donoghue (1991).

Four of the five PPF deposits were observed by Donoghue. These being BA-1, BA-2, OL-1 and OL-2. These were found at three sites with two of them being reference sections. These being TT2, WR1 and DV2 (figure 6.2). Interestingly, observations made at sites J, K, L, N and O were all proximal to Donoghue's TT2 site (figure 2.1) but no PPF tephras were observed in

this area. Donoghue's site could have been overgrown by vegetation or is now too weathered. Both are likely with Donoghue's observations being made over 33 years before this study took place. Overgrowth would be visible at WR1 as well with the ever-changing environment of the Karioi Forest with different logging regimes altering the visibility and accessibility of outcrops. WR1 was found relatively far south within the Karioi Forest which was being extensively logged at the time of this study and thus only the northern reaches were ideal for analysis. DV2 was found within Death Valley which was inaccessible. Tephras were also noted by Donoghue within Scorpion Gully, The Badlands and The Chute which were also inaccessible. Due to this, comparisons could not be made based on the specific sites visited as all sites used by Donoghue (1991) were either inaccessible or not observed. The tephra layers themselves can still be compared based on field observations.

For BA-2 (ba-2 in Donoghue (1991)), the tephra was described as "prominent black pocketing coarse ash". At site TT2, the tephra layer was measured at a 10-millimetre thickness and interbedded within yellow brown to olive brown ashfall layers. It was here that BA-2 was concluded to have been deposited before the Stent Tephra. BA-2 layers found within Death Valley were sampled and shown to comprise of ferromagnesian minerals alongside plagioclase and pyroclasts. Pumice was visible within the samples too. Lapilli was absent and clasts that were observed had glassy coatings with similarities being mentioned with the TTF. The observations taken by Donoghue match closely with what was found during this study with black, non-homogenous ashfall, surrounded by olive brown soils. Point counts showed similar assemblages present within the structures.

For BA-1 (ba-1 in Donoghue (1991)), the tephra was described as pocketed, black, coarse ash at a thickness of 10 millimetres at site TT2. It was surrounded by yellow brown ash. Samples were not collected of this layer by Donoghue (1991). For this study, BA-1 was found to match those descriptions with the appearance of black ash surrounded by darker soils and separated by BA-2 by brown ashfall layers and soils. Both layers are said to appear very similar in appearance to Tufa Trig members with the defining feature being their depth within the stratigraphy. The locations of these tephra layers through Donoghue (1991) suggest that the likely source is Mount Ruapehu which this study suggests also.

For OL-2 and OL-1 (or-2 and or-1 respectively in Donoghue (1991)), both layers are depicted as "strong brown fine and medium lapilli" with OL-2 also being described as pumiceous. Both were detailed at the same site (TT2) with OL-2 showing a thickness of 80 millimetres and OL-

1 showing a thickness of 300 millimetres which is significantly larger than any that were found in the field during this study. At that proximity to Mount Ruapehu though it is likely that thick deposits could be observed at the right locations. Both tephras were stated to be very similar in appearance with the deeper layer being significantly thicker. Both tephras were also found at site WR1 where their appearance takes on a more scattered, loose appearance being surrounded in a brown ash matrix. The recognised distribution was said to appear south-easterly in nature which coincides with findings from this study. Samples were not collected by Donoghue, but observations were made across the Rangipo Desert in regions such as Death Valley and The Chute. From this study, the depictions match very closely with what was found by Donoghue (1991) with two orange lapilli layers appearing distinctly within the stratigraphy with the top layer being noticeably thinner than the lower layer as well as the top layer (OL-2) showing a higher vesicularity than the lower layer (OL-1).

OL-3 found conforming to BA-1 (ba-1 in Donoghue (1991) does not appear to be mentioned within the paper. Further research into the reference sites Donoghue used would be required to investigate its appearance and lack of observation during the 1991 study. It may not have achieved an "informal member" status within the PPF due to its infrequent appearance or could have potentially not been observed at those sights.

Overall, the sightings of these tephra layers based on this study and work conducted by Donoghue (1991) convey the difficulty in acquiring observations of these tephra layers and the lack of appearances within the stratigraphy of the Ruapehu ring plain. The clearest views of the deposits that Donoghue achieved were within the Rangipo Desert which is a necessary region to access should further research into the tephra layers take place.

6.4 Comparison to Other Eruptive Periods

The Ruapehu derived PPF tephra deposits analysed through this study were deemed to be basaltic andesites. These layers would have had to of been produced between 4.3-6.1 ka based on the ages of overlying and underlying tephras. To compare these deposits to ones from other periods of Mount Ruapehu's eruptive history is important to integrate the findings into the eruptive timeline of the TgVC. Comparisons were made throughout the study with the inclusion of the BAT tephra layers.

The BAT tephra layers (BAT-2 and BAT-1) were deposited ~2 ka based on their proximity to the 232 C.E Taupō Ignimbrite. These layers were found to be andesitic in composition with silica contents ranging from 57.58% to 59.77% while the black ash layers being studied were

found to range from 54.71% to 56.77% SiO_2 content and the orange lapilli layers ranged from 52.97% to 54.97%. The comparison shows a trend towards higher silica content being produced from Mount Ruapehu over time. This is supported by Gamble et al (1999) who hypothesised that there is a linear trend towards higher silica content from Mount Ruapehu over time (Gamble et al, 1999). The BAT layers were also distinct from each other with BAT-2 showing no signs of lithics whilst being dominated by vesicular glass and BAT-1 showing high counts of pumice and smooth glass (Table 4.1). Compared to the BA layers which both showed generally high counts of lithics as well as low pyroxene counts. BAT layers were also generally finer in composition through grain size analysis when compared to BA-2 and BA-1. Within the field, the four black ash layers were visibly very similar but under a microscope and after geochemical analysis it is clear they were produced under very different conditions during Mount Ruapehu's eruptive history. The incorporation of the BAT layers into the field work and subsequent analysis allowed for similarities and differences to be quantified.

Leading on from the BAT layers, comparisons to the Tufa Trig Formation can be made based on findings from Voloschina (2020). Comparisons to this formation is useful in that it provides comparable data to the most recent eruptive period from Mount Ruapehu. Through research conducted by Voloschina (2020), the majority of Tufa Trug deposits were found between 6-15 kilometres from source which is a more proximal and narrower range than what was recorded for the primary tephras in question although the furthest sampling was conducted ~21 kilometres away from source. Having deposits be visible within such a wide range and so proximal to source would be likely attributed to the age of the material which has had less time to erode than deposits within the Papakai Formation ~2.5 thousand years older than the oldest Tufa Trig deposits.

The Tufa Trig Formation also shows significantly more Ruapehu sourced deposits than what is observed in the PPF with thirty-one tephra members being found compared to Mount Ruapehu's eight in the PPF (Moebis, 2010). It shows that activity from Mount Ruapehu has increased considerably within recent history with a rather docile period of eruptive activity being noted between 12 to 1.8 ka (Leonard et al, 2021). The single bed ash units found within the TTF are usually seen to range from 1.6 to 3.8 ϕ while the ash units in the PPF were found to range between 1.86 to 3.48 ϕ showing similar grain sizes between the two formations. The single bed ash units were however usually found beyond 15 kilometres from source whereas the PPF tephras were usually found at a more proximal distance to source. This could be attributed to the newer deposits having had less erosion occur, so their single bed ash units still

exist at such distances while the thicker multi bed ash units have not been weathered down to the point of appearing as single bed units (Voloschina, 2020). Lapilli units within the TTF were defined as tephras with a median grain size greater than -1 ϕ.

The Tufa Trig samples collected by Voloschina (2020) were found to be primarily dacitic in nature with an SiO_2 content ranging from 62.34% to 69.61% (figure 5.12). This shows a slight jump in between silica content between the BAT layers (57.58% to 59.77%; table 5.1) which are only divided by the Taupō Ignimbrite. The material found within the TTF show a much higher SiO_2 content than the PPF Ruapehu deposits which range from 52.97% to 56.77% (table 5.1). These results continue to coincide with the hypothesis that eruptive products from Mount Ruapehu have shown a linear increase in silica content over time.

Deposits within the TTF ranged in colouration between light grey to brown with some orange layers appearing. Most characterised as fine ashfall with one apparent lapilli layer (Layer T5; Voloschina, 2020). The higher concentration of finer ashfall layers compared to lapilli could be an indication of increasing volatility within eruptions with higher gas contents generating a great volume of fragmentation.

Comparing the PPF tephra compositions to previously collected data (figure 6.3) shows that the recorded data tends to sit within regions where little data had previously been identified. This could be attributed to geochemical alterations between lava flows and ashfall deposits. Geochemically it cannot be determined if the deposits belong to Mount Ruapehu or Mount Tongariro. The geographical extents of the deposits as well as the south-east depositional axis make it highly unlikely for these tephra deposits to of originated from Mount Tongariro. Comparisons to Tongariro derived ashfall deposits within the PPF would be valuable in building upon the known history of the TgVC during the PPF.

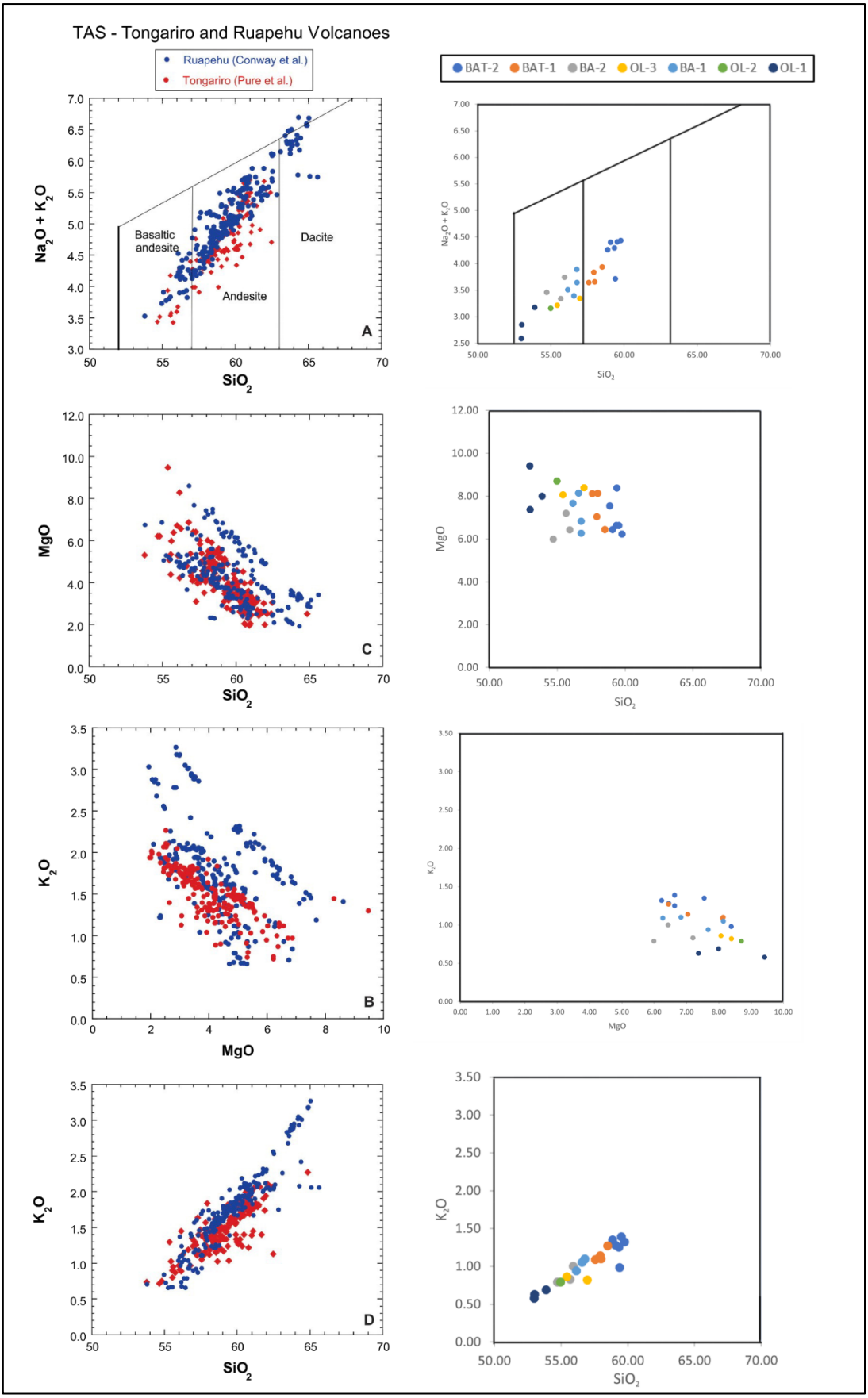

Figure 6.3: PPF tephra comparison to mapped lava deposits from Mount Ruapehu and Mount Tongariro. Repurposed from Leonard et al (2021).

6.5 Inclusion into Mount Ruapehu's Eruptive Record

Eruptions from Mount Ruapehu within the PPF were infrequent with the period of time being heavily dominated by eruptions from Mount Tongariro and other vents from the northern TgVC. This cyclical nature of volcanic activity can be observed beyond this formation with the BF being almost entirely Ruapehu derived deposits (Pardo et al, 2012). Going from a high rate of deposition with the BF to a low rate with the PPF and back to a moderate-high rate with the TTF. This could also be reflected with the composition of the erupted material within these time periods with a clear trend towards higher silica content (Voloschina, 2020). This trend is further defined by the physical characteristics of each tephra deposit. Eruptions of material with greater silica contents are known to produce finer ash layers with a connection being seen with silicic eruptions and fine ash tephra deposits (Rose and Durant, 2009). This connection is based on vesicle size within the pre-erupted magma of felsic material such as dacites being smaller than what is commonly found in mafic material such as basalts (Rose and Durant, 2009). Based on this, it should be expected to see increasing frequencies of fine grained ashfall being produced from Mount Ruapehu which is what is observed within the stratigraphy.

Both BA-1 and BA-2 showed higher silica contents than the OL-1 and OL-2 found below them. The exception being OL-3. This trend over time towards higher silica contents reflects on the activity of Mount Ruapehu within this time frame and beyond with trends being observed through the BAT tephra layers and the TTF.

The Bullot Formation tephras show high counts of pumiceous material and were deemed to of originated from sub-Plinian, magmatic eruptions (Pardo et al, 2011). Based on this, it can be assumed that deposits from this period showed a much higher silica content than what was found within the PPF, furthering the hypothesis of a cyclical eruptive nature at Mount Ruapehu.

The tephras that have been analysed through this study could potentially show the first signs of reactivated volcanic activity at the southern vent on Mount Ruapehu. BF eruptions all took place from the northern vent except its last eruption which is known to have occurred at the southern vent (Pardo et al, 2011). Activity at the northern vent ceased around the time the Whakapapa lava flows occurred around 10 ka. Activity from Mount Ruapehu ceased from the final BF eruption and showed very little activity up until the OL layers found within the PPF. These PPF tephras could represent the initial reactivation of volcanic activity from Mount Ruapehu at the southern vent before the Crater Lake was emplaced. OL-1 and OL-2 are some of the largest eruptions from Mount Ruapehu within the last 10,000 years with deposition

characteristics similar to early BF deposits (Moebis, 2010). This could be due to excess pressure due to a long period of inactivity. Which would coincide with the two orange lapilli layers contrasting physically and compositionally to other Ruapehu derived tephras within the last 10,000 years.

Based on findings from this study and Voloschina (2020). It can be assumed based on Mount Ruapehu's eruptive cycle lasting ~10,000 years that we are still within the early stages of the TTF with more silicic eruptions to be expected in the future. It is currently impossible to predict what the peak of activity will look like before activity begins to recede again but comparisons to activity within the BF could be used to make a reliable hypothesis. The only significant differences being the northern vent that produced the BF and the recent inclusion of a permanent Crater Lake. So future events will have a greater association with water with phreatic and phreatomagmatic events being more common.

Should the events that generated these ashfall deposits occur again, regions to the south-east of Mount Ruapehu would be most at risk with the only major settlement within the depositional axis being Waiouru. It is unknown the extents at which deposition would occur, but the tephra thicknesses found in the field suggest a potentially large area of inundation. It is also unknown the duration of these eruptions which would play a significant role in the risk should these events take place again. Eruptions like these however would be very unlikely to occur again in the near future based on the frequency and products of contemporary eruptive periods from Mount Ruapehu with trends pointing towards episodes of even greater volatility.

Conclusion

7.1 Conclusion

The Papakai Formation is a unique period within Mount Ruapehu's eruptive history. Showing a largely dormant period with eruptions from Ngauruhoe, Tongariro and the Tama Lakes dominating the TgVC within that time period. Understanding what the volcano was doing within this timeframe is critical to gaining a better idea of its activity and eruptive characteristics. These five observed layers within the stratigraphy allow for insights to be made into Mount Ruapehu's behaviour after a long period of dormancy.

The five deposits found within the field were generally weathered but still distinctive and can be found if the environment shows deep enough stratigraphy. The layers themselves have characteristics that physically separate themselves, especially the orange lapilli layers. The transition over time from lapilli layers to fine ashfall layers could indicate a transitional period from more iron rich mafic eruptive products to more felsic, silica rich products. Despite physical differences between ashfall deposits, all five layers found to originate from Mount Ruapehu within this time frame are basaltic andesites. These tephras coming from a volcano known to produce andesitic/dacitic material follows through with the trend hypothesised by Gamble et al (1999) of Mount Ruapehu's erupted material showing increasing levels of SiO_2 over its eruptive time.

The incorporation of the BAT layers within the analysis was incredibly useful in comparing geochemical variations over time as well as noting geographical extents and physical similarities. It was clear throughout the study that the more recent ashfall layers were much better preserved within the eastern ring plain.

The geographical extents to which these PPF tephras belong have been refined through this study but can be narrowed down further. Following the south-east depositional axis would be important to improve deposition estimates. The maximum extents to the north, west and south can be defined based on field observations. The geochemical compositions of the layers are now defined as well as the physical componentry. Utilising this knowledge to amplify further research on the activity from Mount Ruapehu within the Papakai Formation is an important step to building upon the eruptive record of Mount Ruapehu.

7.2 Further Research

Future work based on this research would require access into the central and southern reaches of the Rangipo Desert, with the primary purpose of locating the northern extents of each tephra layer described in this study. Investigating the sites used by Donoghue (1991) would be useful to cross reference visible sites for differences and similarities and to also look for the appearance of OL-3 within the stratigraphy. Investigating areas to the east of State Highway 1 would be useful to build upon the knowledge with more detailed isopachs and isopleths.

The PPF is overwhelmed by deposits from the northern TgVC, looking into deposits from Mount Tongariro within this time period and comparing them to Mount Ruapehu deposits at a geochemical level would allow for distinct similarities or differences to be defined between the two volcanoes within the time frame. Conclusions from this could aid in defining the behaviour of the volcanoes over the last ~10 ka.

Finding a method to reliably date the tephra layers instead of using age constraints would be a valuable contribution to the eruptive record so eruptive frequency from Mount Ruapehu within the PPF can be defined.

Utilising more point count data from more samples would be useful to provide greater details in regard to componentry trends.

References

Balance, P.F., Ablaev, A.G., Pushchin, I.K., Pletnev, S.P., Birylina, M.G., Itaya, T., Follas, H.A. and Gibson, G.W. (1999) Morphology and History of the Kermadec Trench-arc-backarc Basin-remnant Arc System at 30 to 32 Degrees S: Geophysical Profile, Microfossil and K-Ar Data. *Marine Geology*, 159(1-4): 35-62

Blott, S. J., and Pye, K. (2001). GRADISTAT: a grain size distribution and statistics package for the analysis of unconsolidated sediments. Earth Surface Processes and Landforms, 26(11), 1237-1248.

Bonadonna, C., and Costa, A. (2012). Estimating the volume of tephra deposits: A new simple strategy. Geology, 40(5), 415-418.

Bonadonna, C., Ernst, G., and Sparks, R. (1998). Thickness variations and volume estimates of tephra fall deposits: the importance of particle Reynolds number. Journal of Volcanology and Geothermal Research, 81(3), 173-187

Brouwer, P. (2006). Theory of XRF. Almelo, Netherlands: PANalytical BV.

Cameron, E., Gamble, J., Price, R., Smith, I., McIntosh, W., and Gardner, M. (2010). The petrology, geochronology, and geochemistry of Hauhungatahi volcano, SW Taupō Volcanic Zone. *Journal of Volcanology and Geothermal Research*, *190*(1-2), 179-191.

Cassidy, J., Ingham, M., Locke, C. A., and Bibby, H. (2009). Subsurface structure across the axis of the Tongariro Volcanic Centre, New Zealand. *Journal of Volcanology and Geothermal Research*, *179*(3-4), 233-240.

Cowlyn, J., Kennedy, B. M., Gravley, D. M., and Cronin, S. J. (2020). A Confidence-Based Assessment Method for Distinguishing Pyroclastic Density Current Deposits From Other Volcaniclastic Units. *Frontiers in Earth Science*, 8

Conway, C. E., Leonard, G. S., Townsend, D. B., Calvert, A. T., Wilson, C. J., Gamble, J. A., and Eaves, S. R. (2016). A high-resolution 40Ar/39Ar lava chronology and edifice construction history for Ruapehu volcano, New Zealand. *Journal of Volcanology and Geothermal Research*, 327, 152-179.

Cronin, S. J., Neall, V. E., Lecointre, J. A., Hedley, M. J., and Loganathan, P. (2003). Environmental hazards of fluoride in volcanic ash: a case study from Ruapehu volcano, New Zealand. *Journal of Volcanology and Geothermal Research, 121*(3-4), 271-291.

Cutler, N. A., Streeter, R. T., Marple, J., Shotter, L. R., Yeoh, J. S., and Dugmore, A. J. (2018). Tephra transformations: variable preservation of tephra layers from two well-studied eruptions. *Bulletin of Volcanology*, 80 (11), 77

DeMets, C., Gordon, R. G., Argus, D. F., Stein, S. (1990). Current plate motions. *Geophysical Journal International.* 101 (2): 425–478

Donoghue, S. L., Gamble, J. A., Palmer, A. S., and Stewart, R. B. (1995A). Magma mingling in an andesite pyroclastic flow of the Pourahu Member, Ruapehu volcano, New Zealand. *Journal of Volcanology and Geothermal Research, 68*(1-3), 177-191.

Donoghue, S. L., Neall, V. E., and Palmer, A. S. (1995B). Stratigraphy and chronology of late Quaternary andesitic tephra deposits, Tongariro Volcanic Centre, New Zealand. *Journal of the Royal Society of New Zealand*, *25*(2), 115-206.

Donoghue, S. L., Neall, V. E., Palmer, A. S., and Stewart, R. B. (1997). The volcanic history of Ruapehu during the past 2 millennia based on the record of Tufa Trig tephras. *Bulletin of Volcanology*, *59*, 136-146.

Donoghue, S. L., Palmer, A. S., McClelland, E., Hobson, K., Stewart, R. B., Neall, V. E., ... and Price, R. (1999). The Taurewa eruptive episode: evidence for climactic eruptions at Ruapehu volcano, New Zealand. *Bulletin of Volcanology*, *61*, 223-240.

Donoghue, S. L., and Neall, V. E. (2001). Late Quaternary constructional history of the southeastern Ruapehu ring plain, New Zealand. *New Zealand Journal of Geology and Geophysics*, 44(3), 439-466

Eaves, S (2015). The glacial history of Tongariro and Ruapehu volcanoes, New Zealand. Open Access Te Herenga Waka-Victoria University of Wellington. Thesis. https://doi.org/10.26686/wgtn.17012306

Fierstein, J., and Nathenson, M. (1992). Another look at the calculation of fallout tephra volumes. Bulletin of Volcanology, 54(2), 156-167.

Gamble, J. A., Wood, C. P., Price, R. C., Smith, I. E. M., Stewart, R. B., and Waight, T. (1999). A fifty-year perspective of magmatic evolution on Ruapehu Volcano, New Zealand: verification of open system behaviour in an arc volcano. *Earth and Planetary Science Letters*, 170(3), 301-314

Gamble, J., Price, R., Smith, I., McIntosh, W., and Dunbar, N. (2003) 40Ar/39Ar geochronology of magmatic activity, magma flux and hazards at Ruapehu volcano, Taupō Volcanic Zone, New Zealand. *Journal of Volcanology and Geothermal Research*, 120(3-4) 271-287

Gómez-Vasconcelos, M. G., Villamor, P., Procter, J., Palmer, A., Cronin, S., Wallace, C., ... and Leonard, G. (2019). Characterisation of faults as earthquake sources from geomorphic data in the Tongariro Volcanic Complex, New Zealand. *New Zealand Journal of Geology and Geophysics*, *62*(1), 131-142.

Hackett, W.R. and Houghton, B.F. (1989). A facies model for a Quaternary andesitic composite volcano: Ruapehu, New Zealand. *Bulletin of Volcanology*, 51, 51--68

Harrison, A., and White, R. S. (2006). Lithospheric structure of an active backarc basin: the Taupō Volcanic Zone, New Zealand. *Geophysical Journal International*, *167*(2), 968-990.

Iacovino, K, and Gouard, C (2021). TAS Diagram Plotter (3.0). Zenodo. https://doi.org/10.5281/zenodo.5907859

Keys, H (2007) Lahars of Ruapehu Volcano, New Zealand: risk mitigation. *Annals of Glaciology*. 45. 155-162

Kilgour, G., Blundy, J., Cashman, K., and Mader, H. M. (2013). Small volume andesite magmas and melt–mush interactions at Ruapehu, New Zealand: evidence from melt inclusions. *Contributions to Mineralogy and Petrology*, *166*, 371-392.

Kilgour, G. N., Saunders, K. E., Blundy, J. D., Cashman, K. V., Scott, B. J., and Miller, C. A. (2014). Timescales of magmatic processes at Ruapehu volcano from diffusion chronometry and their comparison to monitoring data. *Journal of Volcanology and Geothermal Research*, *288*, 62-75.

Lecointre, J., Hodgson, K., Neall, V., and Cronin, S. (2004). Lahar-triggering mechanisms and hazard at Ruapehu volcano, New Zealand. *Natural hazards*, *31*, 85-109.

Legros, F. (2000). Minimum volume of a tephra fallout deposit estimated from a single isopach. Journal of Volcanology and Geothermal Research, 96(1-2), 25-32

Le Maitre, R. W., Streckeisen, A., Zanettin, B., Le Bas, M., Bonin, B., and Bateman, P. (2002). Igneous rocks: a classification and glossary of terms: recommendations of the International Union of Geological Sciences Subcommission on the Systematics of Igneous Rocks. Cambridge University Press.

Leonard, G. S., Cole, R. P., Christenson, B. W., Conway, C. E., Cronin, S. J., Gamble, J. A., ... and Wilson, C. J. (2021). Ruapehu and Tongariro stratovolcanoes: a review of current understanding. New Zealand Journal of Geology and Geophysics, 64(2-3), 389-420.

Moebis, A. (2010) Understanding the Holocene explosive eruption record of the Tongariro Volcanic Centre, New Zealand; A thesis presented in partial fulfilment of the requirements for the degree of Doctor of Philosophy. Massey University

Moebis, A., Cronin, S. J., Neall, V. E., and Smith, I. E. (2011). Unravelling a complex volcanic history from fine-grained, intricate Holocene ash sequences at the Tongariro Volcanic Centre, New Zealand. *Quaternary International*, 246(1-2), 352-363.

Mortimer N, Tulloch A J, Ireland T R. (1997) Basement geology of Taranaki and Wanganui Basins, New Zealand, *New Zealand Journal of Geology and Geophysics*, 40, 223-236

Pardo, N., Cronin, S. J., Palmer, A. S., and Németh, K. (2012). Reconstructing the largest explosive eruptions of Mt. Ruapehu, New Zealand: lithostratigraphic tools to understand subplinian–plinian eruptions at andesitic volcanoes. *Bulletin of Volcanology*, *74*, 617-640.

Pardo, N., Cronin, S., Palmer, A., Procter, J., and Smith, I. (2012). Andesitic Plinian eruptions at Mt. Ruapehu: quantifying the uppermost limits of eruptive parameters. *Bulletin of Volcanology*, 74, 1161-1185.

Parish, A. (1994). Petrology and provenance of the O'Leary conglomerate, Northeast Wanganui, New Zealand. *B. Sc (Hons) thesis, Victoria University of Wellington, New Zealand*, 146.

Price, R. C., Gamble, J. A., Smith, I. E., Maas, R., Waight, T., Stewart, R. B., and Woodhead, J. (2012). The anatomy of an andesite volcano: a time–stratigraphic study of andesite petrogenesis and crustal evolution at Ruapehu Volcano, New Zealand. *Journal of Petrology*, *53*(10), 2139-2189.

Procter, J., Zernack, A., Mead, S., Morgan, M., and Cronin, S. (2021). A review of lahars; past deposits, historic events and present-day simulations from Mt. Ruapehu and Mt. Taranaki, New Zealand. *New Zealand Journal of Geology and Geophysics*, 64(2-3), 479-503.

Pyle, D. M. (1989). The thickness, volume and grainsize of tephra fall deposits. Bulletin of Volcanology, 51(1), 1-15.

Reid, F. (1983). Origin of the rhyolitic rocks of the Taupō Volcanic Zone, New Zealand. Journal of Volcanology and Geothermal Research, 15(4), 315-338.

Rose, W. I., and Durant, A. J. (2009). Fine ash content of explosive eruptions. Journal of Volcanology and Geothermal Research, 186(1-2), 32-39.

Rowlands, D. P., White, R. S., and Haines, A. J. (2005). Seismic tomography of the Tongariro volcanic centre, New Zealand. *Geophysical Journal International*, *163*(3), 1180-1194.

Scambelluri, M., and Philippot, P. (2001). Deep fluids in subduction zones. *Lithos*, *55*(1-4), 213-227.

Scott, B. J. (2013). A revised catalogue of Ruapehu volcano eruptive activity: 1830-2012. *GNS Science Report*, 2013/45

Stratford, W. R., and Stern, T. A. (2006). Crust and upper mantle structure of a continental backarc: central North Island, New Zealand. *Geophysical Journal International*, *166*(1), 469-484.Tost, M., Cronin, S., and Procter, J. (2014). Transport and emplacement mechanisms of channelised long-runout debris avalanches, Ruapehu volcano, New Zealand. *Bulletin of Volcanology*, 76(12), 1-14

Topping, W (1973). Tephrostratigraphy and chronology of late Quaternary eruptives from the Tongariro Volcanic Centre. N.Z. Journal of Geology and Geophysics 16(3) 397-423.

Topping, W (1974). Some aspects of Quaternary history of Tongariro Volcanic Centre. Unpublished PhD thesis, Victoria University of Wellington, Wellington, New Zealand

Tost, M., Cronin, S. J., and Procter, J. N. (2014). Transport and emplacement mechanisms of channelised long-runout debris avalanches, Ruapehu volcano, New Zealand. *Bulletin of Volcanology*, *76*, 1-14.

Tost, M., and Cronin, S. J. (2015). Linking distal volcaniclastic sedimentation and stratigraphy with the development of Ruapehu volcano, New Zealand. *Bulletin of Volcanology*, 77(11).

Waight, T. E., Price, R. C., Stewart, R. B., Smith, I. E. M., and Gamble, J. (1999). Stratigraphy and geochemistry of the Turoa area, with implications for andesite petrogenesis at Mt Ruapehu, Taupō Volcanic Zone, New Zealand. *New Zealand Journal of Geology and Geophysics*, *42*(4), 513-532.

Walker, G. P., Self, S., and Wilson, L. (1984). Tarawera 1886, New Zealand—a basaltic Plinian fissure eruption. *Journal of volcanology and geothermal research*, *21*(1-2), 61-78.

Wilson, C. J. N., Houghton, B. F., McWilliams, M. O., Lanphere, M. A., Weaver, S. D., and Briggs, R. M. (1995). Volcanic and structural evolution of Taupō Volcanic Zone, New Zealand: a review. *Journal of volcanology and geothermal research*, 68(1-3), 1-28.

Wilson, C. J. N., and Walker, G. P. L. (1985). The Taupō eruption, New Zealand I. General aspects. *Philosophical Transactions of the Royal Society of London. Series A, Mathematical and Physical Sciences*, *314*(1529), 199-228.

Witham, C. S. (2005). Volcanic disasters and incidents: A new database. *Journal of Volcanology and Geothermal Research*, *148*(3-4), 191-233.

Villamor, P., and Berryman, K. R. (2006). Evolution of the southern termination of the Taupō Rift, New Zealand. *New Zealand Journal of Geology and Geophysics*, *49*(1), 23-37.

Villamor, P., Van Dissen, R., Alloway, B. V., Palmer, A. S., and Litchfield, N. (2007). The Rangipo fault, Taupō rift, New Zealand: An example of temporal slip-rate and single-event displacement variability in a volcanic environment. *Geological Society of America Bulletin*, *119*(5-6), 529-547.

Voloschina, M. (2020) Eruption dynamics and frequency magnitude relationships of explosive eruptions at Mt. Ruapehu, New Zealand over the past 1800 years, A thesis presented in partial fulfilment of the requirements for the degree of Doctor of Philosophy in Earth Science. Massey University

Voloschina, M., Lube, G., Procter, J., Moebis, A., and Timm, C. (2020). Lithosedimentological and tephrostratigraphical characterisation of small-volume, low-intensity eruptions: The 1800 years Tufa Trig Formation, Mt. Ruapehu (New Zealand). *Journal of Volcanology and Geothermal Research, 402*, 106987.

Voloschina, M., Bebbington, M., Lube, G., and Procter, J. (2021). Probabilistic modelling of multi-phase eruptions found in geological records: An example from Mt. Ruapehu, New Zealand. *Journal of Volcanology and Geothermal Research,* 416

Appendix

Appendix 1 - Sample analysis checklist:

	Sample ID	GSA?	XRF?	PC?
BAT-2				
	5I	✓	✓	
	9G	✓	✓	
	12H	✓	✓	✓
	13J	✓	✓	
	14K	✓	✓	
	15L	✓	✓	
BAT-1				
	4G	✓	✓	
	10D	✓	✓	✓
	16D	✓	✓	✓
	17K	✓	✓	
BA-2				
	2D	✓	✓	✓
	3E	✓	✓	
	11G	✓	✓	✓
OL-3				
	25D	✓	✓	
	26E	✓	✓	
BA-1				
	1A	✓	✓	
	6C	✓	✓	
	7D	✓	✓	✓
	8E	✓	✓	✓
OL-2				
	18D	✓	✓	✓
OL-1				
	21C	✓	✓	✓
	22D	✓	✓	✓
	23E	✓	✓	✓
Other Data				
	20B	✓	✓	✓
	19H	✓	✓	✓
	24F	✓	✓	✓

Appendix 2 – Total GSA weight percentages

	Sample ID	-3ϕ%	-2ϕ%	-1ϕ%	0ϕ%	1ϕ%	2ϕ%	3ϕ%	4ϕ%	5ϕ%	6ϕ%	7ϕ%	8ϕ%	9ϕ%	10ϕ%
BAT-2															
	5I	0	0	0.12	0.69	4.83	14.85	23.49	14.53	15.11	11.24	10.50	3.91	0.73	0
	9G	0	0	0.06	0.88	3.28	11.67	32.52	18.24	15.12	8.80	6.65	2.32	0.45	0
	12H	0	0	0	0.06	1.61	13.56	30.10	12.68	15.74	12.68	9.79	3.18	0.58	0
	13J	0	0	0.69	3.55	9.92	15.05	24.11	19.81	13.92	6.21	4.62	1.77	0.36	0
	14K	0	0	2.60	2.27	1.36	5.19	26.15	30.34	18.81	7.10	4.44	1.54	0.21	0
	15L	0	0	0	0.41	0.94	6.28	30.09	28.40	18.63	8.23	5.11	1.68	0.24	0
BAT-1															
	4G	0	0	0	0.50	7.84	23.99	30.02	6.64	8.33	9.14	9.46	3.39	0.65	0.04
	10D	0	0	0	0.83	3.77	11.02	29.28	21.28	18.43	9.21	4.71	1.30	0.16	0
	16D	0	0	0.04	0.82	4.00	13.28	31.42	14.58	15.94	10.99	6.76	1.90	0.29	0
	17K	0	0.25	0.45	1.04	3.42	15.19	34.86	10.43	9.94	8.57	10.31	4.51	0.97	0.06
BA-2															
	2D	0	0	0	0.76	20.37	37.30	18.68	4.12	3.94	4.00	6.74	3.35	0.68	0.07
	3E	0	0	0.49	2.68	13.62	25.77	17.95	6.25	8.18	6.33	11.14	6.25	1.23	0.11
	11G	0	0	0.04	0.06	2.86	19.65	34.25	10.06	9.82	7.10	9.18	5.23	1.50	0.24
OL-3															
	25D	50.74	5.08	1.52	1.57	4.36	7.04	9.32	4.55	5.07	4.30	4.43	1.67	0.33	0.02
	26E	20.84	14.86	3.67	2.19	3.82	10.62	15.05	9.39	7.60	4.26	4.96	2.29	0.44	0
BA-1															
	1A	0	0.37	3.12	8.60	15.91	19.02	16.37	5.24	4.98	4.75	8.00	7.48	4.90	1.19
	6C	2.65	2.37	3.83	4.04	7.25	12.50	15.95	11.00	13.31	9.64	11.35	5.06	0.98	0.05
	7D	1.82	7.14	11.50	10.78	12.62	14.31	12.99	2.11	7.47	5.90	8.19	4.19	0.90	0.09
	8E	0	5.27	8.48	7.18	7.56	16.87	17.47	11.53	10.05	6.66	6.13	2.35	0.45	0
OL-2															
	18D	0	2.58	3.41	9.65	26.41	17.43	11.39	6.24	7.72	6.57	5.95	2.15	0.47	0.03
OL-1															
	21C	49.34	25.25	8.44	2.66	0.90	1.51	2.18	2.00	2.20	1.69	2.39	1.19	0.24	0.01
	22D	3.17	12.97	15.14	11.97	10.81	8.51	7.38	6.55	8.73	7.03	5.51	1.84	0.38	0
	23E	18.18	12.64	13.09	16.80	14.65	5.80	4.37	2.80	3.37	2.86	3.62	1.55	0.27	0

Appendix 3 - Tephra Location Checklist:

Site ID	A	B	C	D	E	F	G	H	I	J	K	L	M	N	O	P	Q	R	S	T	U	V	W	X	Y
BAT-2																									
Sample Appears?			✓	✓	✓		✓	✓	✓	✓	✓	✓		✓	✓	✓		✓	✓			✓	✓		
Sample Collected?							✓	✓	✓	✓	✓	✓													
Thickness (mm)				15			15	41	25	40	11	14		13	16			30	24			23	19		
BAT-1																									
Sample Appears?			✓	✓	✓		✓				✓	✓		✓	✓	✓		✓	✓				✓	✓	
Sample Collected?				✓							✓														
Thickness (mm)			33	35			15				74			42		50								42	
BA-2																									
Sample Appears?				✓	✓		✓																		
Sample Collected?				✓	✓		✓																		
Thickness (mm)				7	50		4																		
OL-3																									
Sample Appears?			✓	✓	✓																✓				
Sample Collected?				✓	✓																				
Thickness (mm)				2	25																22				
BA-1																									
Sample Appears?	✓		✓	✓	✓		✓										✓								
Sample Collected?	✓		✓	✓	✓																				
Thickness (mm)	8		42	24	16												23								
OL-2																									
Sample Appears?		✓		✓	✓		✓													✓					✓
Sample Collected?				✓																					
Thickness (mm)				70																80					53
OL-1																									
Sample Appears?		✓	✓	✓	✓		✓													✓					
Sample Collected?			✓	✓	✓																				
Thickness (mm)			112	130	53																				

Appendix 4 – Grain Size analysis for each sample measured in phi ϕ

	Sample ID	-3ϕ	-2ϕ	-1ϕ	0ϕ	1ϕ	2ϕ	3ϕ	4ϕ	5ϕ	6ϕ	7ϕ	8ϕ	9ϕ	10ϕ	Weight
BAT-2																
	5I			0.1	0.58	4.08	12.55	19.84	12.27	12.76	9.49	8.87	3.30	0.62		84.46
	9G			0.05	0.68	2.53	8.99	25.05	14.05	11.65	6.78	5.12	1.78	0.34		77.02
	12H				0.09	2.23	18.77	41.69	17.56	21.79	17.56	13.56	4.41	0.80		138.48
	13J			1.66	8.56	23.94	36.31	58.19	47.82	33.59	14.99	11.14	4.27	0.88		241.35
	14K			1.01	0.88	0.53	2.01	10.16	11.79	7.30	2.76	1.72	0.60	0.08		38.84
	15L				0.43	0.98	6.58	31.51	29.74	19.51	8.62	5.35	1.76	0.25		104.73
BAT-1																
	4G				0.72	11.34	34.69	43.41	9.60	12.05	13.21	13.69	4.90	0.94	0.06	144.62
	10D				0.46	2.09	6.11	16.22	11.78	10.21	5.10	2.61	0.72	0.09		55.38
	16D			0.09	1.86	9.11	30.24	71.55	33.21	36.30	25.02	15.39	4.32	0.65		227.74
	17K		0.53	0.94	2.19	7.17	31.88	73.16	21.88	20.85	17.99	21.65	9.46	2.04	0.13	209.86
BA-2																
	2D				0.98	26.37	48.28	24.18	5.33	5.09	5.18	8.72	4.33	0.88	0.09	129.44
	3E			0.64	3.52	17.87	33.81	23.55	8.20	10.73	8.31	14.62	8.19	1.62	0.14	131.2
	11G			0.15	0.25	11.09	76.24	132.92	39.05	38.10	27.55	35.62	20.31	5.84	0.95	388.06
BA-1																
	1A		0.5	4.2	11.58	21.43	25.62	22.05	7.05	6.71	6.40	10.78	10.08	6.60	1.60	134.7
	6C	4.08	3.65	5.89	6.21	11.15	19.22	24.53	16.91	20.47	14.82	17.45	7.78	1.51	0.08	153.76
	7D	4.36	17.1	27.54	25.81	30.21	34.26	31.11	5.04	17.90	14.13	19.60	10.02	2.15	0.22	239.45
	8E		3.29	5.29	4.48	4.72	10.53	10.90	7.20	6.27	4.16	3.83	1.46	0.28		62.41
OL-3																
	25D	36.47	3.65	1.09	1.13	3.13	5.06	6.70	3.27	3.65	3.09	3.18	1.20	0.23	0.01	71.87
	26E	29.44	21	5.19	3.09	5.4	15.01	21.26	13.27	10.74	6.02	7.01	3.24	0.63		141.3
OL-2																
	18D		7.38	9.73	27.57	75.42	49.77	32.53	17.81	22.03	18.76	16.99	6.14	1.34	0.09	285.57
OL-1																
	21C	64.39	32.96	11.01	3.47	1.18	1.97	2.84	2.61	2.87	2.21	3.12	1.55	0.31	0.02	130.51
	22D	13.52	55.34	64.6	51.09	46.14	36.32	31.51	27.97	37.25	30.00	23.50	7.86	1.64		426.74
	23E	99.19	68.95	71.43	91.63	79.9	31.64	23.86	15.26	18.36	15.60	19.77	8.44	1.46		545.5

Appendix 5 – Sorting, skewness, and kurtosis of samples based on GSA

	Sample ID	Gravel%	Sand%	Mud%	Meanϕ		Sortingϕ		Skewnessϕ		Kurtosisϕ	
BAT-2												
	5I	0.1	58.6	41.3	3.67	Very Fine Sand	1.97	Poorly Sorted	0.17	Fine Skewed	0.85	Platykurtic
	9G	0.1	66.8	33.2	3.45	Very Fine Sand	1.66	Poorly Sorted	0.30	Very Fine Skewed	1.00	Mesokurtic
	12H	0	66.3	33.7	3.72	Very Fine Sand	1.79	Poorly Sorted	0.27	Fine Skewed	0.82	Platykurtic
	13J	0.7	72.6	26.7	2.92	Fine Sand	1.87	Poorly Sorted	0.08	Symmetrical	1.07	Mesokurtic
	14K	2.6	65.5	31.9	3.48	Very Fine Sand	1.60	Poorly Sorted	0.00	Symmetrical	1.36	Leptokurtic
	15L	0	66.3	33.7	3.56	Very Fine Sand	1.40	Poorly Sorted	0.19	Fine Skewed	1.03	Mesokurtic
BAT-1												
	4G	0	69.1	30.9	3.21	Very Fine Sand	2.05	Very Poorly Sorted	0.39	Very Fine Skewed	0.85	Platykurtic
	10D	0	66.4	33.6	3.41	Very Fine Sand	1.53	Poorly Sorted	0.16	Fine Skewed	0.98	Mesokurtic
	16D	0	64.3	35.7	3.41	Very Fine Sand	1.72	Poorly Sorted	0.30	Fine Skewed	0.92	Mesokurtic
	17K	0.7	65	34.3	3.50	Very Fine Sand	1.99	Poorly Sorted	0.42	Very Fine Skewed	0.89	Platykurtic
BA-2												
	2D	0	81.3	18.7	2.41	Fine Sand	1.99	Poorly Sorted	0.50	Very Fine Skewed	1.52	Very Leptokurtic
	3E	0.5	66.4	33.1	3.19	Very Fine Sand	2.42	Very Poorly Sorted	0.41	Very Fine Skewed	0.80	Platykurtic
	11G	0	67	33	3.48	Very Fine Sand	2.03	Very Poorly Sorted	0.47	Very Fine Skewed	0.93	Mesokurtic
BA-1												
	1A	3.5	65.2	31.3	3.03	Very Fine Sand	2.97	Very Poorly Sorted	0.37	Very Fine Skewed	0.83	Platykurtic
	6C	8.9	50.9	40.2	3.22	Very Fine Sand	2.81	Very Poorly Sorted	-0.03	Symmetrical	0.98	Mesokurtic
	7D	20.5	52.9	26.7	1.86	Medium Sand	3.18	Very Poorly Sorted	0.18	Fine Skewed	0.82	Platykurtic
	8E	13.7	60.7	25.5	2.18	Fine Sand	2.73	Very Poorly Sorted	-0.02	Symmetrical	1.01	Mesokurtic

OL-3												
	25D	57.3	26.9	15.8	0.02	Coarse Sand	2.22	Very Poorly Sorted	1.81	Very Fine Skewed	0.68	Platykurtic
	26E	39.4	41.2	19.5	1.20	Medium Sand	2.79	Very Poorly Sorted	0.15	Fine Skewed	0.48	Very Platykurtic
OL-2												
	18D	6	71.2	22.8	2.12	Fine Sand	2.41	Very Poorly Sorted	0.36	Very Fine Skewed	0.98	Mesokurtic
OL-1												
	21C	83	9.3	7.7	-1.53	Very Fine Gravel	0.93	Moderately Sorted	7.39	Very Fine Skewed	-5.33	Very Platykurtic
	22D	31.3	45.3	23.4	1.16	Medium Sand	3.13	Very Poorly Sorted	0.24	Fine Skewed	0.74	Platykurtic
	23E	43.9	44.5	11.6	-0.21	Very Coarse Sand	2.37	Very Poorly Sorted	0.59	Very Fine Skewed	0.82	Platykurtic

Appendix 6 – GRADISTAT Results:

BA-2

SAMPLE STATISTICS

SIEVING ERROR: 0.0%

SAMPLE IDENTITY: **2D**

ANALYST & DATE: J Fleming, 02/05/2024

SAMPLE TYPE: Bimodal, Poorly Sorted

TEXTURAL GROUP: Muddy Sand

SEDIMENT NAME: Medium Silty Medium Sand

	µm	ϕ
MODE 1:	375.0	1.500
MODE 2:	12.00	6.466
MODE 3:		
D_{10}:	14.68	0.454
MEDIAN or D_{50}:	292.4	1.774
D_{90}:	730.2	6.090
(D_{90} / D_{10}):	49.75	13.42
(D_{90} - D_{10}):	715.5	5.636
(D_{75} / D_{25}):	3.443	2.616
(D_{75} - D_{25}):	330.1	1.784

GRAIN SIZE DISTRIBUTION

GRAVEL:	0.0%	COARSE SAND:	20.4%
SAND:	81.3%	MEDIUM SAND:	37.3%
MUD:	18.7%	FINE SAND:	18.7%
		V FINE SAND:	4.2%
V COARSE GRAVEL:	0.0%	V COARSE SILT:	3.8%
COARSE GRAVEL:	0.0%	COARSE SILT:	4.3%
MEDIUM GRAVEL:	0.0%	MEDIUM SILT:	6.6%
FINE GRAVEL:	0.0%	FINE SILT:	3.3%
V FINE GRAVEL:	0.0%	V FINE SILT:	0.7%
V COARSE SAND:	0.8%	CLAY:	0.1%

	METHOD OF MOMENTS			FOLK & WARD METHOD		
	Arithmetic	Geometric	Logarithmic	Geometric	Logarithmic	Description
	µm	µm	ϕ	µm	ϕ	
MEAN ($\bar{x}$):	346.7	187.5	2.415	188.0	2.411	Fine Sand
SORTING (σ):	266.3	3.977	1.992	3.984	1.994	Poorly Sorted
SKEWNESS (Sk):	0.900	-1.293	1.293	-0.505	0.505	Very Fine Skewed
KURTOSIS (K):	4.222	3.731	3.731	1.522	1.522	Very Leptokurtic

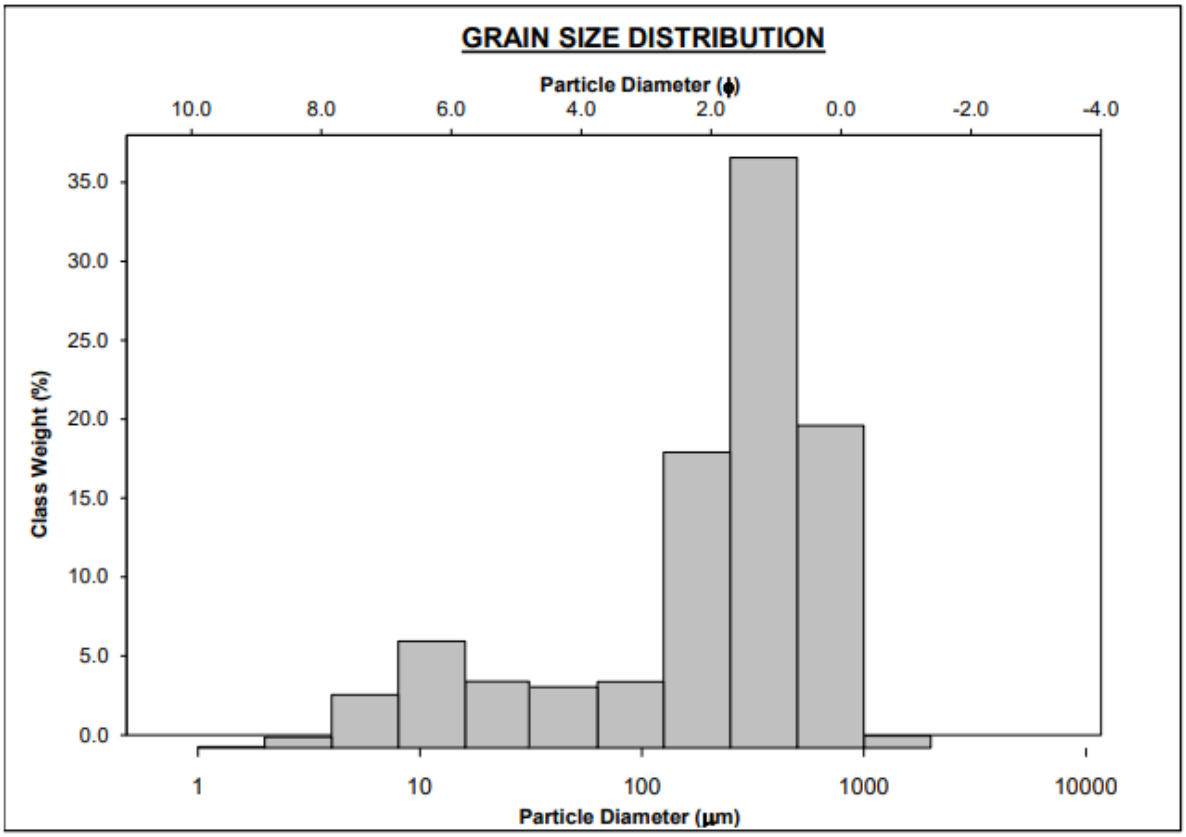

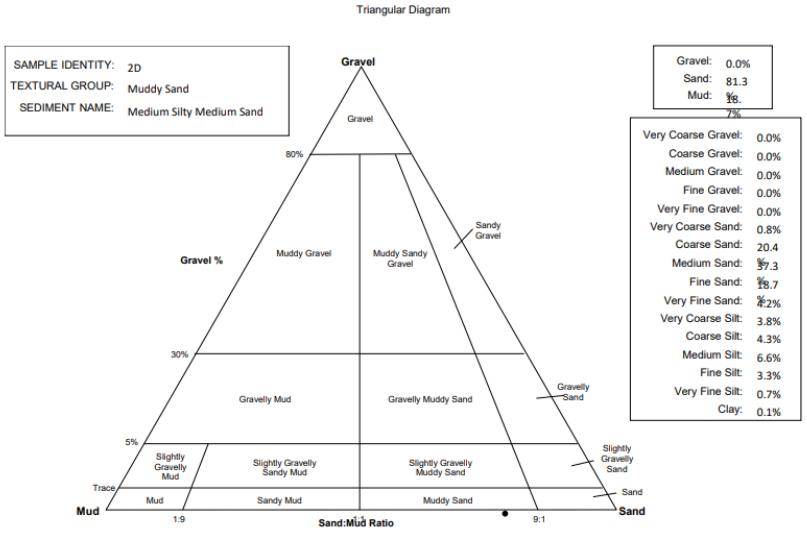
Triangular Diagram
SAMPLE IDENTITY: 2D
TEXTURAL GROUP: Muddy Sand
SEDIMENT NAME: Medium Silty Medium Sand
Gravel: 0.0%
Sand: 81.3
Mud: 18.7%
Very Coarse Gravel: 0.0%
Coarse Gravel: 0.0%
Medium Gravel: 0.0%
Fine Gravel: 0.0%
Very Fine Gravel: 0.0%
Very Coarse Sand: 0.8%
Coarse Sand: 20.4
Medium Sand: 37.3
Fine Sand: 18.7
Very Fine Sand: 4.2%
Very Coarse Silt: 3.8%
Coarse Silt: 4.3%
Medium Silt: 6.6%
Fine Silt: 3.3%
Very Fine Silt: 0.7%
Clay: 0.1%
Gravel
Gravel
80%
Gravel %
Muddy Gravel
Muddy Sandy Gravel
Sandy Gravel
30%
Gravelly Mud
Gravelly Muddy Sand
Gravelly Sand
5%
Slightly Gravelly Mud
Slightly Gravelly Sandy Mud
Slightly Gravelly Muddy Sand
Slightly Gravelly Sand
Trace
Mud
Mud
Sandy Mud
Muddy Sand
Sand
Mud
1:9
Sand:Mud Ratio
9:1
Sand

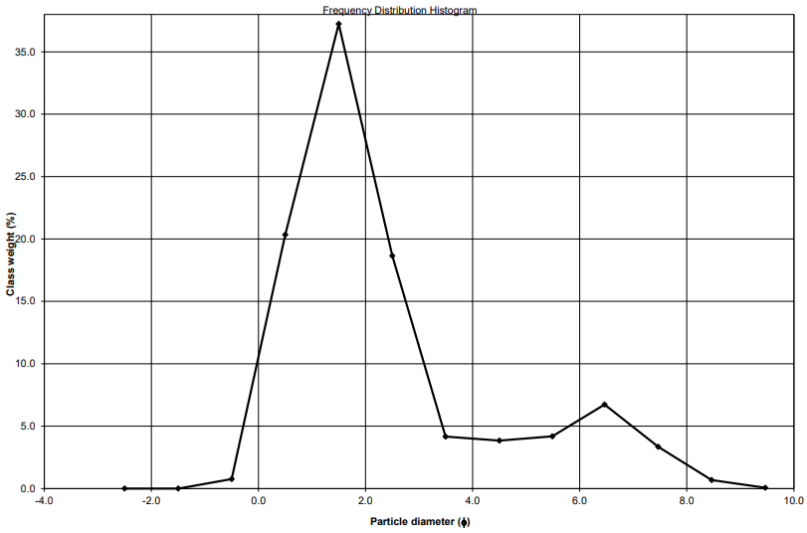
Frequency Distribution Histogram
Class weight (%)
35.0
30.0
25.0
20.0
15.0
10.0
5.0
0.0
-4.0
-2.0
0.0
2.0
4.0
6.0
8.0
10.0
Particle diameter (ϕ)

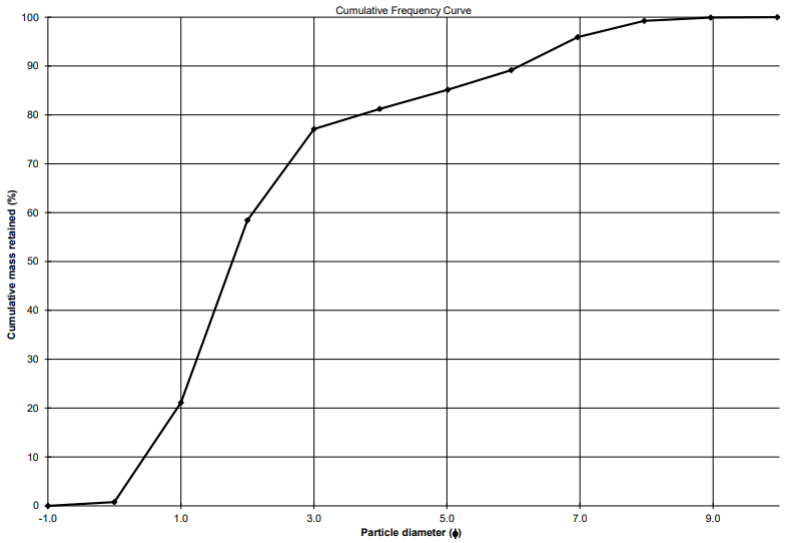
Cumulative Frequency Curve
Cumulative mass retained (%)
100
90
80
70
60
50
40
30
20
10
0
-1.0
1.0
3.0
5.0
7.0
9.0
Particle diameter (ϕ)

SAMPLE STATISTICS

SIEVING ERROR: 0.0%

SAMPLE IDENTITY: **3E**

ANALYST & DATE: J Fleming, 02/05/2024

SAMPLE TYPE: Trimodal, Very Poorly Sorted

TEXTURAL GROUP: Slightly Gravelly Muddy Sand

SEDIMENT NAME: Slightly Very Fine Gravelly Medium Silty Medium Sand

	µm	ϕ
MODE 1:	375.0	1.500
MODE 2:	12.00	6.466
MODE 3:	47.00	4.500
D_{10}:	9.296	0.501
MEDIAN or D_{50}:	187.6	2.414
D_{90}:	706.4	6.749
(D_{90} / D_{10}):	75.99	13.46
(D_{90} - D_{10}):	697.1	6.248
(D_{75} / D_{25}):	13.02	3.808
(D_{75} - D_{25}):	370.1	3.702

GRAIN SIZE DISTRIBUTION

GRAVEL:	0.5%	COARSE SAND:	13.6%
SAND:	66.4%	MEDIUM SAND:	25.8%
MUD:	33.1%	FINE SAND:	18.0%
		V FINE SAND:	6.3%
V COARSE GRAVEL:	0.0%	V COARSE SILT:	8.0%
COARSE GRAVEL:	0.0%	COARSE SILT:	6.8%
MEDIUM GRAVEL:	0.0%	MEDIUM SILT:	11.0%
FINE GRAVEL:	0.0%	FINE SILT:	6.1%
V FINE GRAVEL:	0.5%	V FINE SILT:	1.2%
V COARSE SAND:	2.7%	CLAY:	0.1%

	METHOD OF MOMENTS			FOLK & WARD METHOD		
	Arithmetic	Geometric	Logarithmic	Geometric	Logarithmic	Description
	µm	µm	ϕ	µm	ϕ	
MEAN ($\bar{x}$):	300.3	115.2	3.118	109.6	3.189	Very Fine Sand
SORTING (σ):	366.1	5.065	2.341	5.333	2.415	Very Poorly Sorted
SKEWNESS (Sk):	2.989	-0.562	0.562	-0.406	0.406	Very Fine Skewed
KURTOSIS (K):	17.95	2.181	2.181	0.802	0.802	Platykurtic

GRAIN SIZE DISTRIBUTION

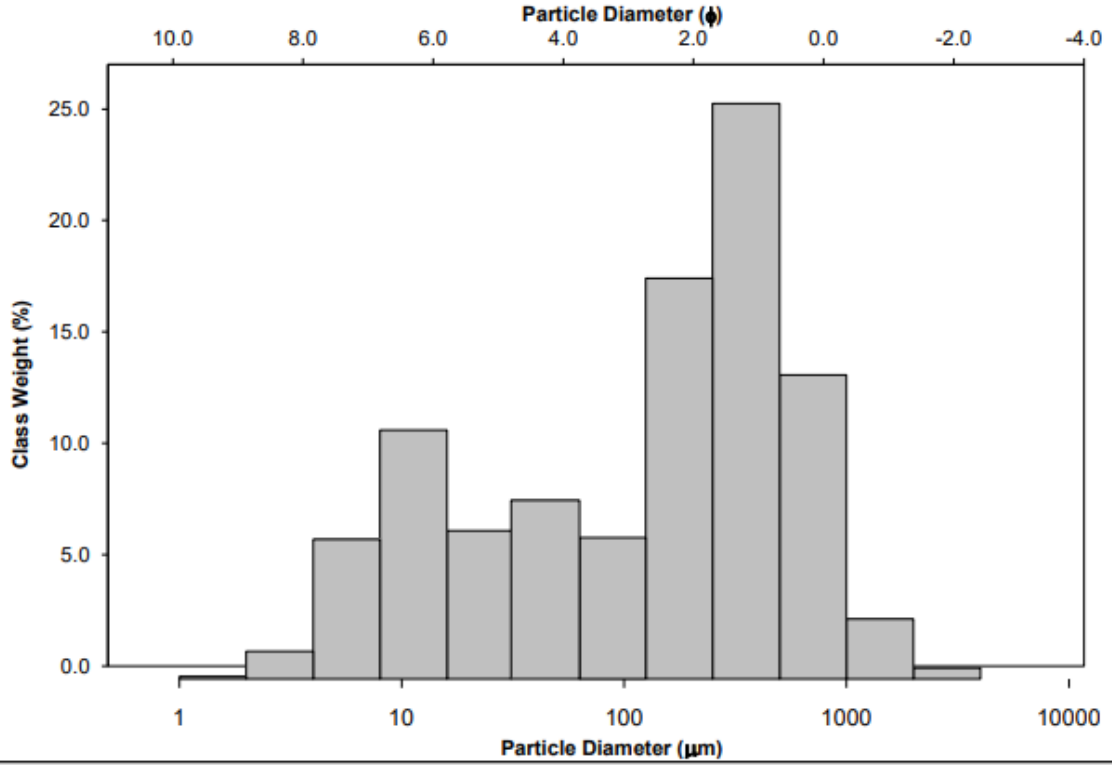

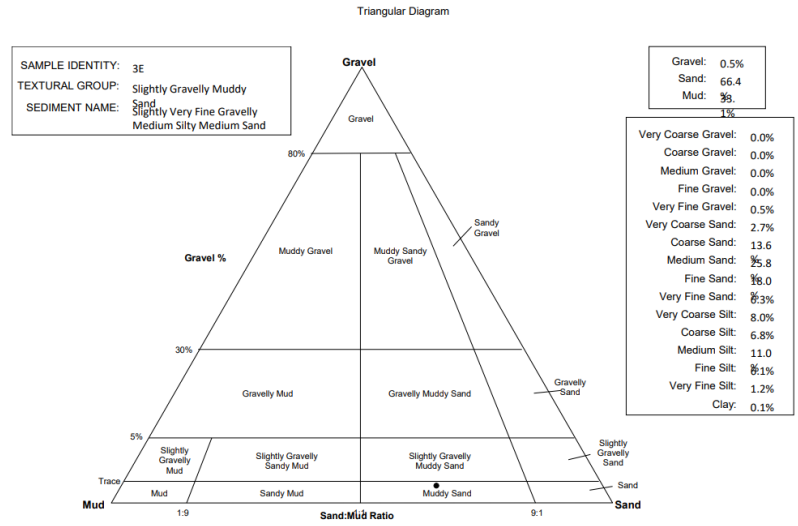
Triangular Diagram
SAMPLE IDENTITY: 3E
TEXTURAL GROUP: Slightly Gravelly Muddy Sand
SEDIMENT NAME: Slightly Very Fine Gravelly Medium Silty Medium Sand
Gravel: 0.5%
Sand: 66.4
Mud: 33.1%
Very Coarse Gravel: 0.0%
Coarse Gravel: 0.0%
Medium Gravel: 0.0%
Fine Gravel: 0.0%
Very Fine Gravel: 0.5%
Very Coarse Sand: 2.7%
Coarse Sand: 13.6
Medium Sand: 25.8
Fine Sand: 18.0
Very Fine Sand: 6.3%
Very Coarse Silt: 8.0%
Coarse Silt: 6.8%
Medium Silt: 11.0
Fine Silt: 6.1%
Very Fine Silt: 1.2%
Clay: 0.1%
Gravel
80%
30%
5%
Trace
Gravel %
Muddy Gravel
Muddy Sandy Gravel
Sandy Gravel
Gravelly Mud
Gravelly Muddy Sand
Gravelly Sand
Slightly Gravelly Mud
Slightly Gravelly Sandy Mud
Slightly Gravelly Muddy Sand
Slightly Gravelly Sand
Mud
Sandy Mud
Muddy Sand
Sand
Mud
1:9
Sand:Mud Ratio
9:1
Sand

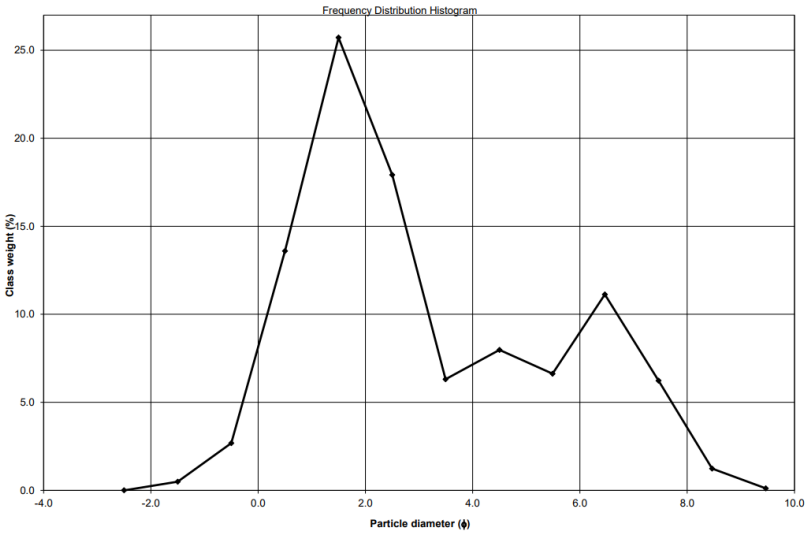
Frequency Distribution Histogram
Class weight (%)
25.0
20.0
15.0
10.0
5.0
0.0
-4.0
-2.0
0.0
2.0
4.0
6.0
8.0
10.0
Particle diameter (ϕ)

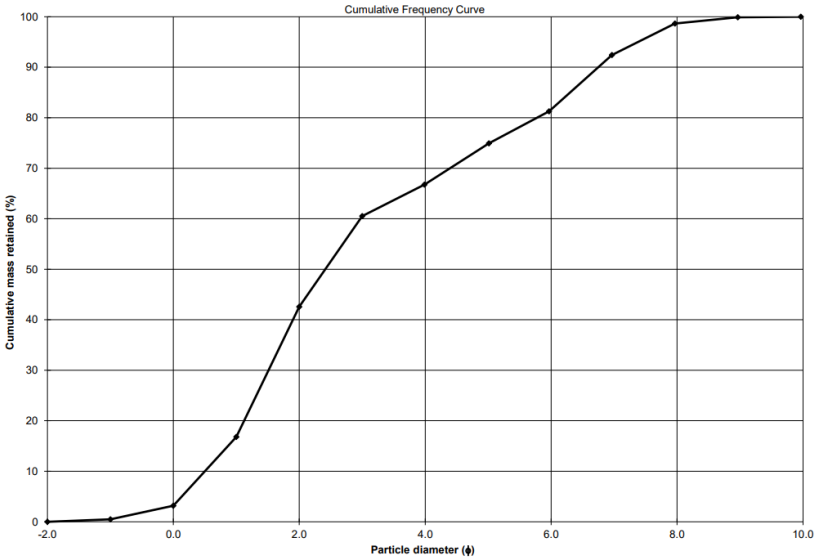
Cumulative Frequency Curve
Cumulative mass retained (%)
100
90
80
70
60
50
40
30
20
10
0
-2.0
0.0
2.0
4.0
6.0
8.0
10.0
Particle diameter (ϕ)

SAMPLE STATISTICS

SIEVING ERROR: 0.0%

SAMPLE IDENTITY: **11G**

ANALYST & DATE: J Fleming, 02/05/2024

SAMPLE TYPE: Bimodal, Very Poorly Sorted

TEXTURAL GROUP: Slightly Gravelly Muddy Sand

SEDIMENT NAME: Slightly Very Fine Gravelly Very Coarse Silty Fine Sand

	µm	ϕ
MODE 1:	187.5	2.500
MODE 2:	12.00	6.466
MODE 3:		
D_{10}:	10.05	1.358
MEDIAN or D_{50}:	143.6	2.800
D_{90}:	390.1	6.637
(D_{90} / D_{10}):	38.82	4.886
(D_{90} - D_{10}):	380.0	5.279
(D_{75} / D_{25}):	6.776	2.334
(D_{75} - D_{25}):	203.0	2.760

GRAIN SIZE DISTRIBUTION

GRAVEL:	0.0%	COARSE SAND:	2.9%
SAND:	67.0%	MEDIUM SAND:	19.6%
MUD:	33.0%	FINE SAND:	34.3%
		V FINE SAND:	10.2%
V COARSE GRAVEL:	0.0%	V COARSE SILT:	9.6%
COARSE GRAVEL:	0.0%	COARSE SILT:	7.5%
MEDIUM GRAVEL:	0.0%	MEDIUM SILT:	9.0%
FINE GRAVEL:	0.0%	FINE SILT:	5.1%
V FINE GRAVEL:	0.0%	V FINE SILT:	1.5%
V COARSE SAND:	0.1%	CLAY:	0.2%

	METHOD OF MOMENTS			FOLK & WARD METHOD		
	Arithmetic	Geometric	Logarithmic	Geometric	Logarithmic	Description
	µm	µm	ϕ	µm	ϕ	
MEAN ($\bar{x}$):	178.7	89.49	3.482	89.48	3.482	Very Fine Sand
SORTING (σ):	173.0	3.912	1.968	4.071	2.025	Very Poorly Sorted
SKEWNESS (Sk):	3.024	-0.801	0.801	-0.465	0.465	Very Fine Skewed
KURTOSIS (K):	33.53	2.676	2.676	0.927	0.927	Mesokurtic

GRAIN SIZE DISTRIBUTION

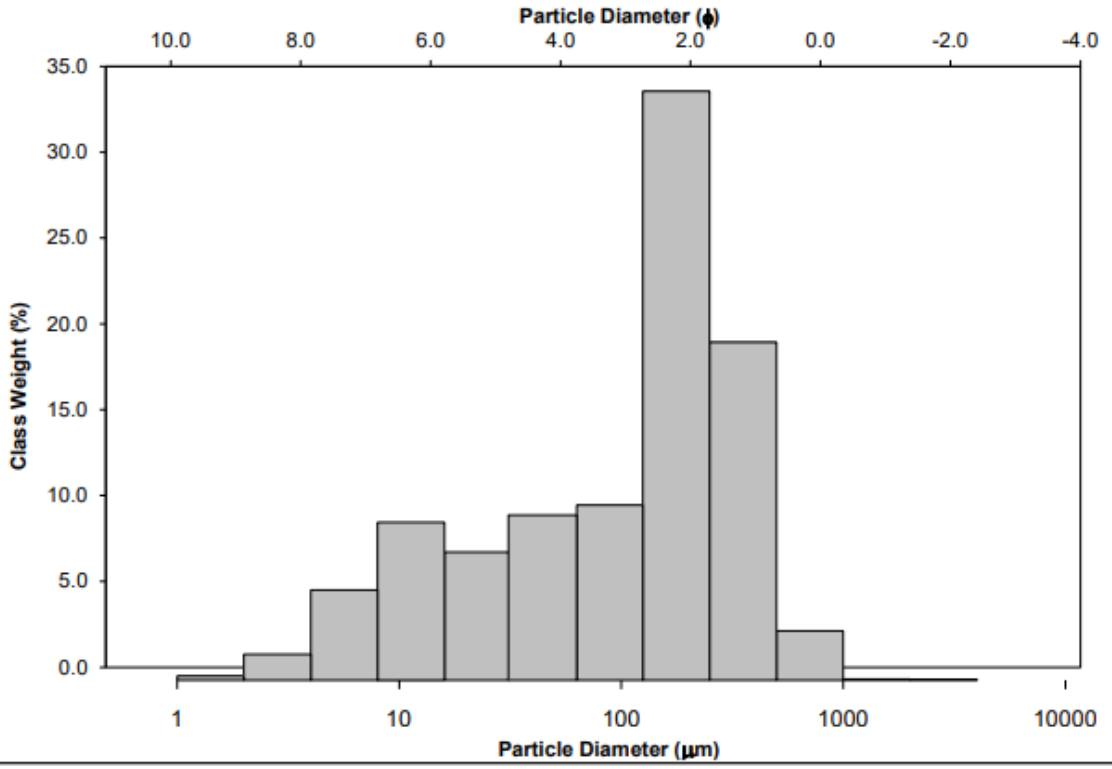

Triangular Diagram

SAMPLE IDENTITY: 11G
TEXTURAL GROUP: Slightly Gravelly Muddy Sand
SEDIMENT NAME: Slightly Very Fine Gravelly Very Coarse Silty Fine Sand

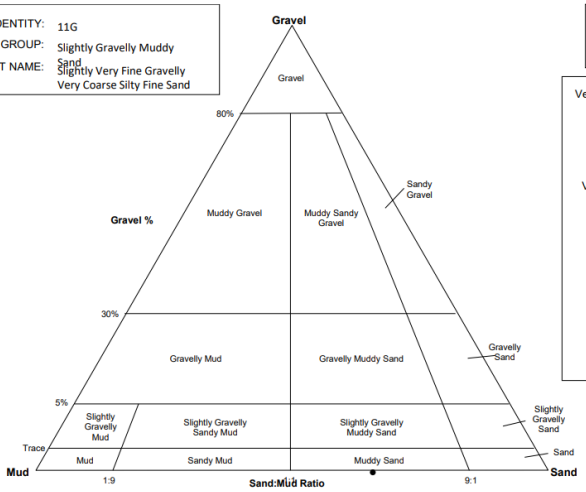

Gravel:	0.0%
Sand:	67.0
Mud:	33.0%

Very Coarse Gravel:	0.0%
Coarse Gravel:	0.0%
Medium Gravel:	0.0%
Fine Gravel:	0.0%
Very Fine Gravel:	0.0%
Very Coarse Sand:	0.1%
Coarse Sand:	2.9%
Medium Sand:	19.6
Fine Sand:	34.3
Very Fine Sand:	10.2
Very Coarse Silt:	3.6%
Coarse Silt:	7.5%
Medium Silt:	9.0%
Fine Silt:	5.1%
Very Fine Silt:	1.5%
Clay:	0.2%

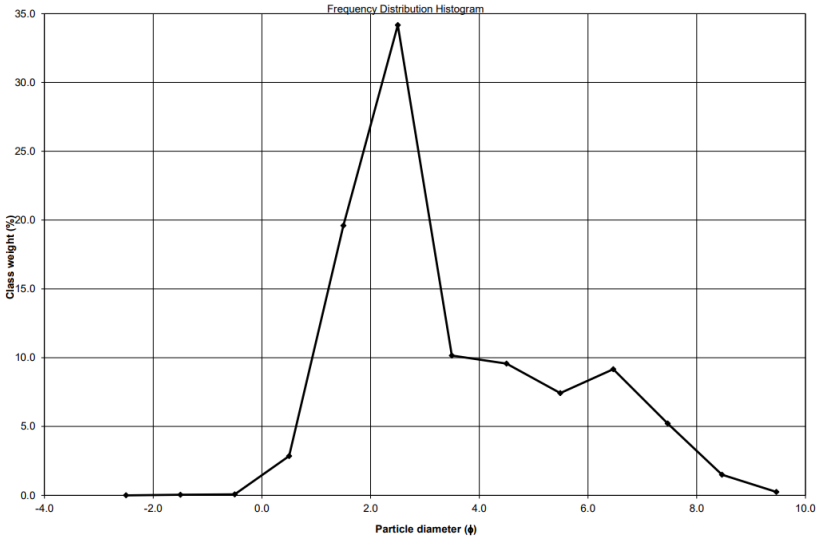

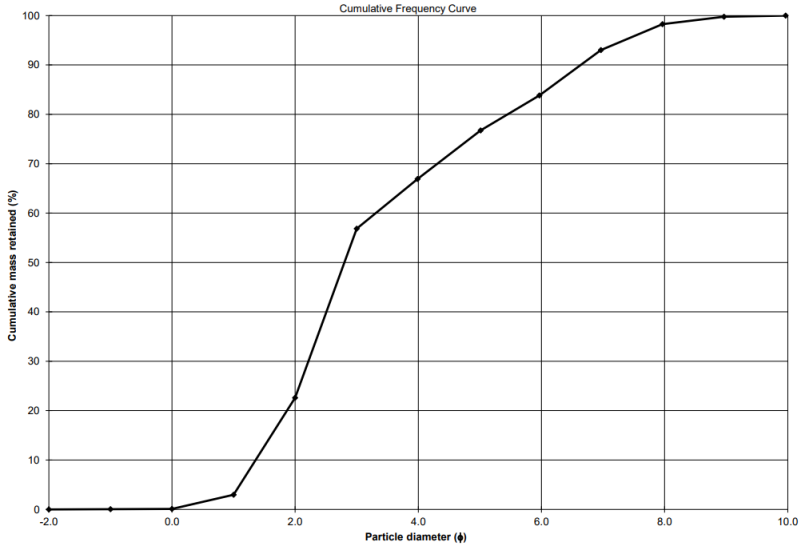

BA-1

SAMPLE STATISTICS

SIEVING ERROR: 0.1%

SAMPLE IDENTITY: **1A**

ANALYST & DATE: J Fleming, 02/05/2024

SAMPLE TYPE: Bimodal, Very Poorly Sorted

TEXTURAL GROUP: Slightly Gravelly Muddy Sand

SEDIMENT NAME: Slightly Very Fine Gravelly Medium Silty Medium Sand

	µm	ϕ
MODE 1:	375.0	1.500
MODE 2:	12.00	6.466
MODE 3:		
D_{10}:	5.745	-0.243
MEDIAN or D_{50}:	220.7	2.180
D_{90}:	1183.9	7.444
(D_{90} / D_{10}):	206.1	-30.570
(D_{90} - D_{10}):	1178.1	7.687
(D_{75} / D_{25}):	22.17	6.515
(D_{75} - D_{25}):	544.4	4.471

GRAIN SIZE DISTRIBUTION

GRAVEL:	3.5%	COARSE SAND:	15.9%
SAND:	65.2%	MEDIUM SAND:	19.0%
MUD:	31.3%	FINE SAND:	16.4%
		V FINE SAND:	5.3%
V COARSE GRAVEL:	0.0%	V COARSE SILT:	4.9%
COARSE GRAVEL:	0.0%	COARSE SILT:	5.1%
MEDIUM GRAVEL:	0.0%	MEDIUM SILT:	8.0%
FINE GRAVEL:	0.4%	FINE SILT:	7.4%
V FINE GRAVEL:	3.1%	V FINE SILT:	4.8%
V COARSE SAND:	8.6%	CLAY:	1.1%

	METHOD OF MOMENTS			FOLK & WARD METHOD		
	Arithmetic µm	Geometric µm	Logarithmic ϕ	Geometric µm	Logarithmic ϕ	Description
MEAN ($\bar{x}$):	476.4	129.5	2.948	122.5	3.030	Very Fine Sand
SORTING (σ):	709.8	7.187	2.845	7.836	2.970	Very Poorly Sorted
SKEWNESS (Sk):	3.314	-0.568	0.568	-0.365	0.365	Very Fine Skewed
KURTOSIS (K):	19.05	2.240	2.240	0.826	0.826	Platykurtic

GRAIN SIZE DISTRIBUTION

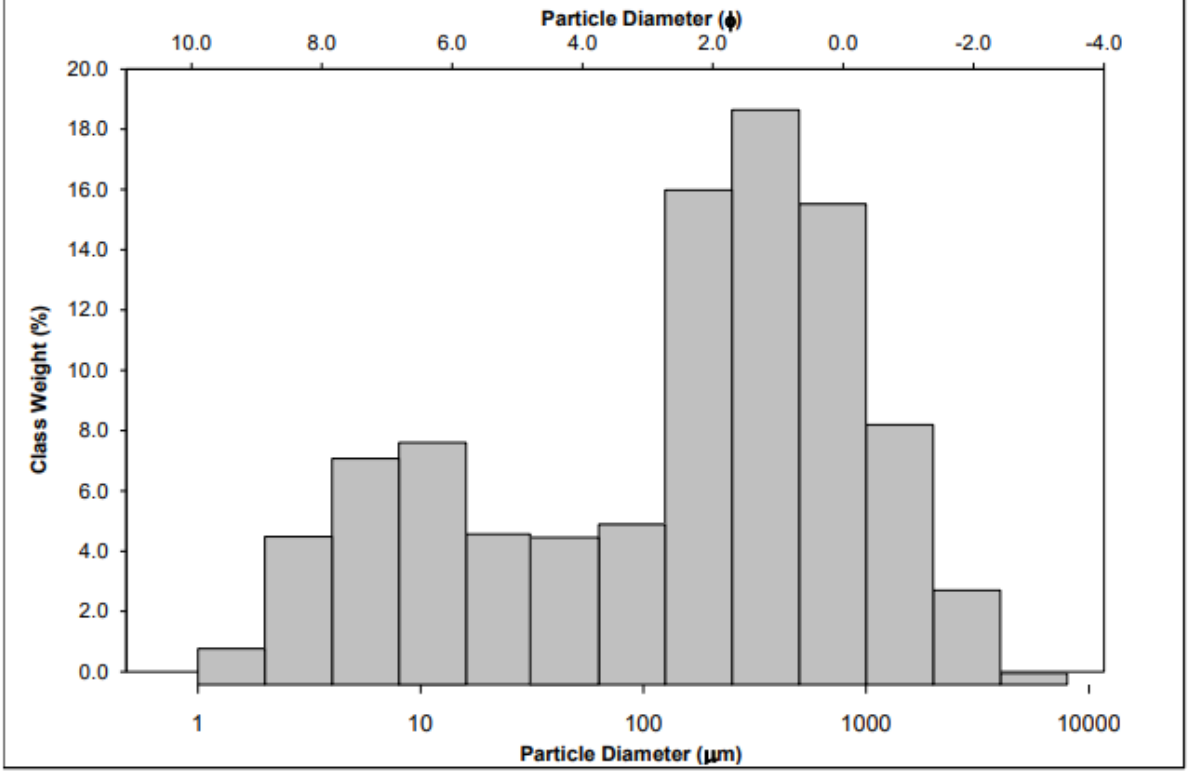

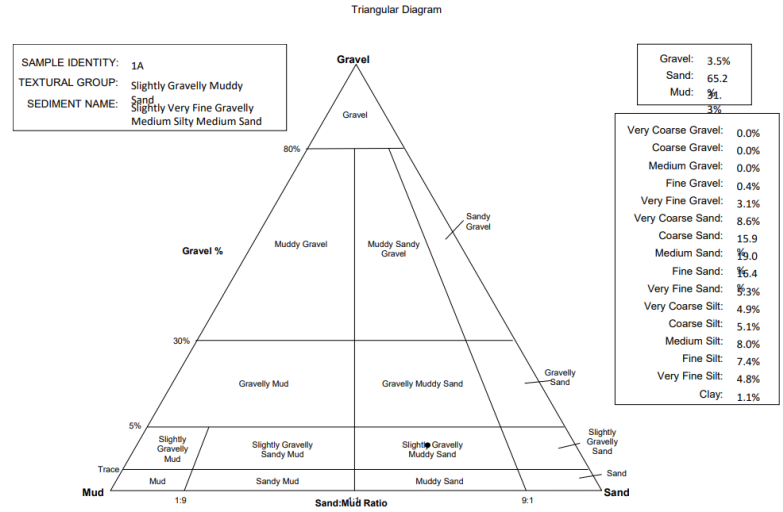
Triangular Diagram
SAMPLE IDENTITY: 1A
TEXTURAL GROUP: Slightly Gravelly Muddy Sand
SEDIMENT NAME: Slightly Very Fine Gravelly Medium Silty Medium Sand
Gravel: 3.5%
Sand: 65.2
Mud: 31.3%
Very Coarse Gravel: 0.0%
Coarse Gravel: 0.0%
Medium Gravel: 0.0%
Fine Gravel: 0.4%
Very Fine Gravel: 3.1%
Very Coarse Sand: 8.6%
Coarse Sand: 15.9
Medium Sand: 19.0
Fine Sand: 15.4
Very Fine Sand: 5.3%
Very Coarse Silt: 4.9%
Coarse Silt: 5.1%
Medium Silt: 8.0%
Fine Silt: 7.4%
Very Fine Silt: 4.8%
Clay: 1.1%
Gravel
80%
30%
5%
Trace
Mud
Sand
Gravel %
Sand:Mud Ratio
1:9
9:1
Gravel
Sandy Gravel
Muddy Gravel
Muddy Sandy Gravel
Gravelly Sand
Gravelly Mud
Gravelly Muddy Sand
Slightly Gravelly Mud
Slightly Gravelly Sandy Mud
Slightly Gravelly Muddy Sand
Slightly Gravelly Sand
Sand
Mud
Sandy Mud
Muddy Sand

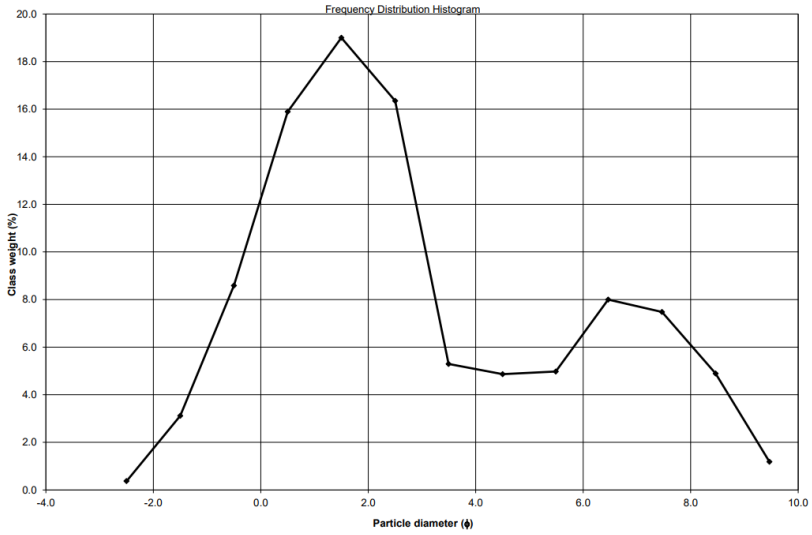
Frequency Distribution Histogram
Class weight (%)
Particle diameter (ϕ)
20.0
18.0
16.0
14.0
12.0
10.0
8.0
6.0
4.0
2.0
0.0
-4.0
-2.0
0.0
2.0
4.0
6.0
8.0
10.0

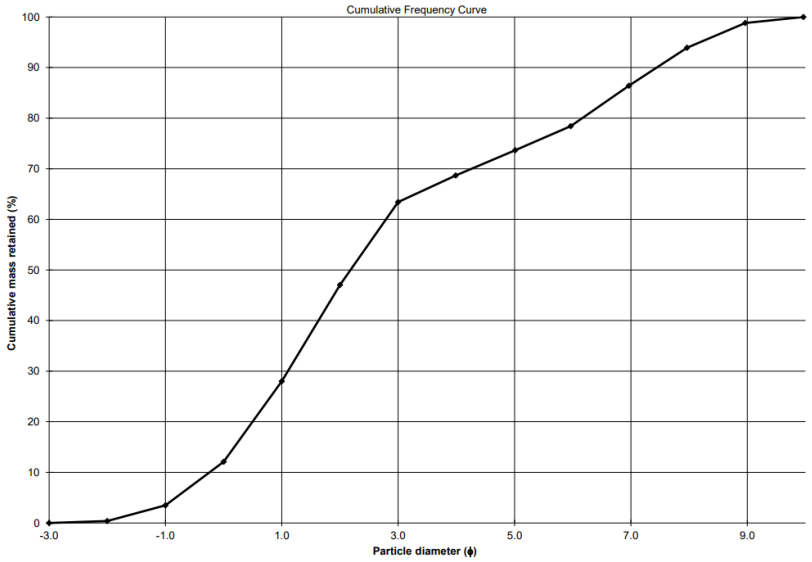
Cumulative Frequency Curve
Cumulative mass retained (%)
Particle diameter (ϕ)
100
90
80
70
60
50
40
30
20
10
0
-3.0
-1.0
1.0
3.0
5.0
7.0
9.0

SAMPLE STATISTICS

SIEVING ERROR: 0.0%

SAMPLE IDENTITY: **6C**

ANALYST & DATE: J Fleming, 02/05/2024

SAMPLE TYPE: Trimodal, Very Poorly Sorted

TEXTURAL GROUP: Gravelly Muddy Sand

SEDIMENT NAME: Fine Gravelly Very Coarse Silty Fine Sand

	µm	ϕ
MODE 1:	187.5	2.500
MODE 2:	47.00	4.500
MODE 3:	12.00	6.466
D_{10}:	10.15	-0.717
MEDIAN or D_{50}:	114.6	3.126
D_{90}:	1644.0	6.622
(D_{90} / D_{10}):	161.9	-9.233
(D_{90} - D_{10}):	1633.9	7.339
(D_{75} / D_{25}):	14.22	3.759
(D_{75} - D_{25}):	355.2	3.830

GRAIN SIZE DISTRIBUTION

GRAVEL:	8.9%	COARSE SAND:	7.3%
SAND:	50.9%	MEDIUM SAND:	12.5%
MUD:	40.2%	FINE SAND:	16.0%
		V FINE SAND:	11.1%
V COARSE GRAVEL:	0.0%	V COARSE SILT:	13.0%
COARSE GRAVEL:	0.0%	COARSE SILT:	10.2%
MEDIUM GRAVEL:	0.0%	MEDIUM SILT:	11.1%
FINE GRAVEL:	5.0%	FINE SILT:	4.9%
V FINE GRAVEL:	3.8%	V FINE SILT:	1.0%
V COARSE SAND:	4.0%	CLAY:	0.1%

	METHOD OF MOMENTS			FOLK & WARD METHOD		
	Arithmetic	Geometric	Logarithmic	Geometric	Logarithmic	Description
	µm	µm	ϕ	µm	ϕ	
MEAN ($\bar{x}$):	469.7	90.72	3.198	107.6	3.216	Very Fine Sand
SORTING (σ):	1065.3	6.631	2.564	7.010	2.809	Very Poorly Sorted
SKEWNESS (Sk):	3.832	-0.035	-0.145	0.035	-0.035	Symmetrical
KURTOSIS (K):	18.51	2.687	2.316	0.984	0.984	Mesokurtic

GRAIN SIZE DISTRIBUTION

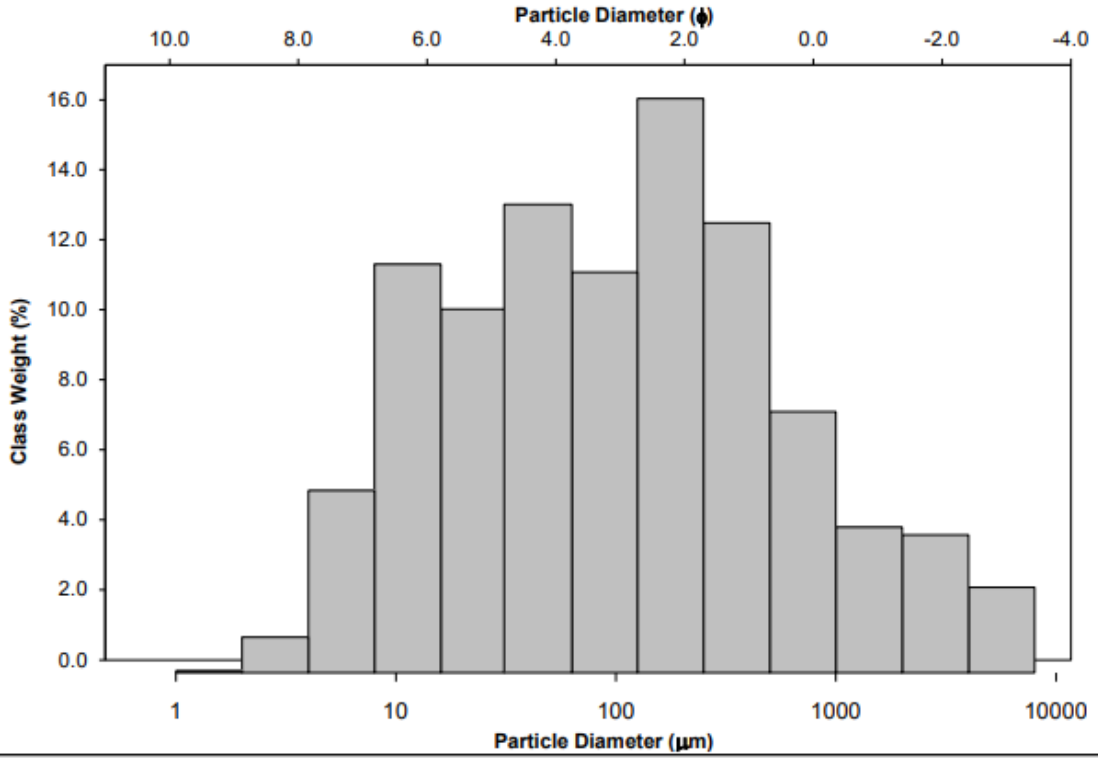

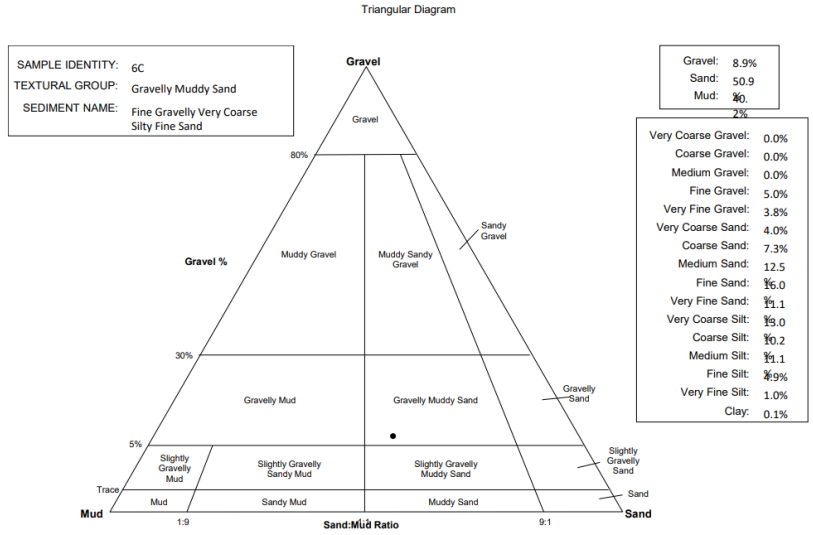
Triangular Diagram
SAMPLE IDENTITY: 6C
TEXTURAL GROUP: Gravelly Muddy Sand
SEDIMENT NAME: Fine Gravelly Very Coarse Silty Fine Sand
Gravel
Gravel
80%
Gravel %
Muddy Gravel
Muddy Sandy Gravel
Sandy Gravel
30%
Gravelly Mud
Gravelly Muddy Sand
Gravelly Sand
5%
Slightly Gravelly Mud
Slightly Gravelly Sandy Mud
Slightly Gravelly Muddy Sand
Slightly Gravelly Sand
Trace
Mud
Sandy Mud
Muddy Sand
Sand
Mud
1:9
Sand:Mud Ratio
9:1
Sand
Gravel: 8.9%
Sand: 50.9
Mud: 40.2%
Very Coarse Gravel: 0.0%
Coarse Gravel: 0.0%
Medium Gravel: 0.0%
Fine Gravel: 5.0%
Very Fine Gravel: 3.8%
Very Coarse Sand: 4.0%
Coarse Sand: 7.3%
Medium Sand: 12.5
Fine Sand: 16.0
Very Fine Sand: 11.1
Very Coarse Silt: 13.0
Coarse Silt: 10.2
Medium Silt: 11.1
Fine Silt: 4.9%
Very Fine Silt: 1.0%
Clay: 0.1%

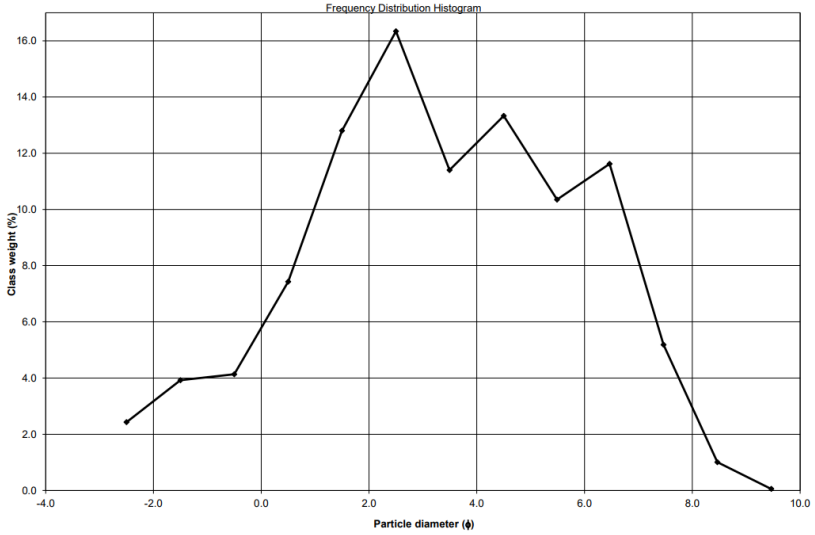
Frequency Distribution Histogram
Class weight (%)
16.0
14.0
12.0
10.0
8.0
6.0
4.0
2.0
0.0
-4.0
-2.0
0.0
2.0
4.0
6.0
8.0
10.0
Particle diameter (ϕ)

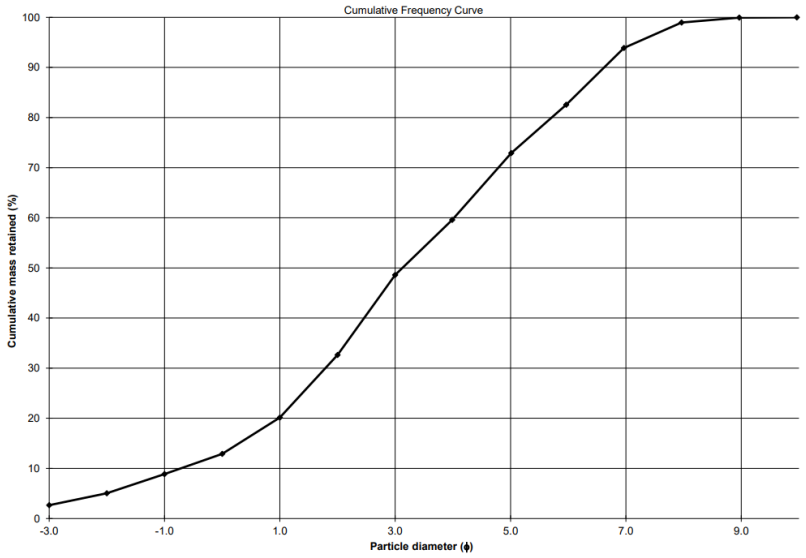
Cumulative Frequency Curve
Cumulative mass retained (%)
100
90
80
70
60
50
40
30
20
10
0
-3.0
-1.0
1.0
3.0
5.0
7.0
9.0
Particle diameter (ϕ)

SAMPLE STATISTICS

SIEVING ERROR: 0.0%

SAMPLE IDENTITY: **7D**

ANALYST & DATE: J Fleming, 02/05/2024

SAMPLE TYPE: Polymodal, Very Poorly Sorted

TEXTURAL GROUP: Gravelly Muddy Sand

SEDIMENT NAME: Very Fine Gravelly Medium Silty Medium Sand

	µm	ϕ
MODE 1:	375.0	1.500
MODE 2:	3000.0	-1.500
MODE 3:	12.00	6.466
D_{10}:	12.04	-1.910
MEDIAN or D_{50}:	371.3	1.429
D_{90}:	3757.5	6.376
(D_{90} / D_{10}):	312.1	-3.339
(D_{90} - D_{10}):	3745.4	8.286
(D_{75} / D_{25}):	27.96	-7.297
(D_{75} - D_{25}):	1440.5	4.805

GRAIN SIZE DISTRIBUTION

GRAVEL:	20.5%	COARSE SAND:	12.6%
SAND:	52.9%	MEDIUM SAND:	14.3%
MUD:	26.7%	FINE SAND:	13.0%
		V FINE SAND:	2.2%
V COARSE GRAVEL:	0.0%	V COARSE SILT:	7.3%
COARSE GRAVEL:	0.0%	COARSE SILT:	6.3%
MEDIUM GRAVEL:	0.0%	MEDIUM SILT:	8.0%
FINE GRAVEL:	9.0%	FINE SILT:	4.1%
V FINE GRAVEL:	11.5%	V FINE SILT:	0.9%
V COARSE SAND:	10.8%	CLAY:	0.1%

	METHOD OF MOMENTS			FOLK & WARD METHOD		
	Arithmetic	Geometric	Logarithmic	Geometric	Logarithmic	Description
	µm	µm	ϕ	µm	ϕ	
MEAN ($\bar{x}$):	1116.0	243.3	1.858	275.5	1.860	Medium Sand
SORTING (σ):	1642.9	8.542	2.911	9.067	3.181	Very Poorly Sorted
SKEWNESS (Sk):	1.923	-0.513	0.430	-0.177	0.177	Fine Skewed
KURTOSIS (K):	5.856	2.426	2.185	0.816	0.816	Platykurtic

GRAIN SIZE DISTRIBUTION

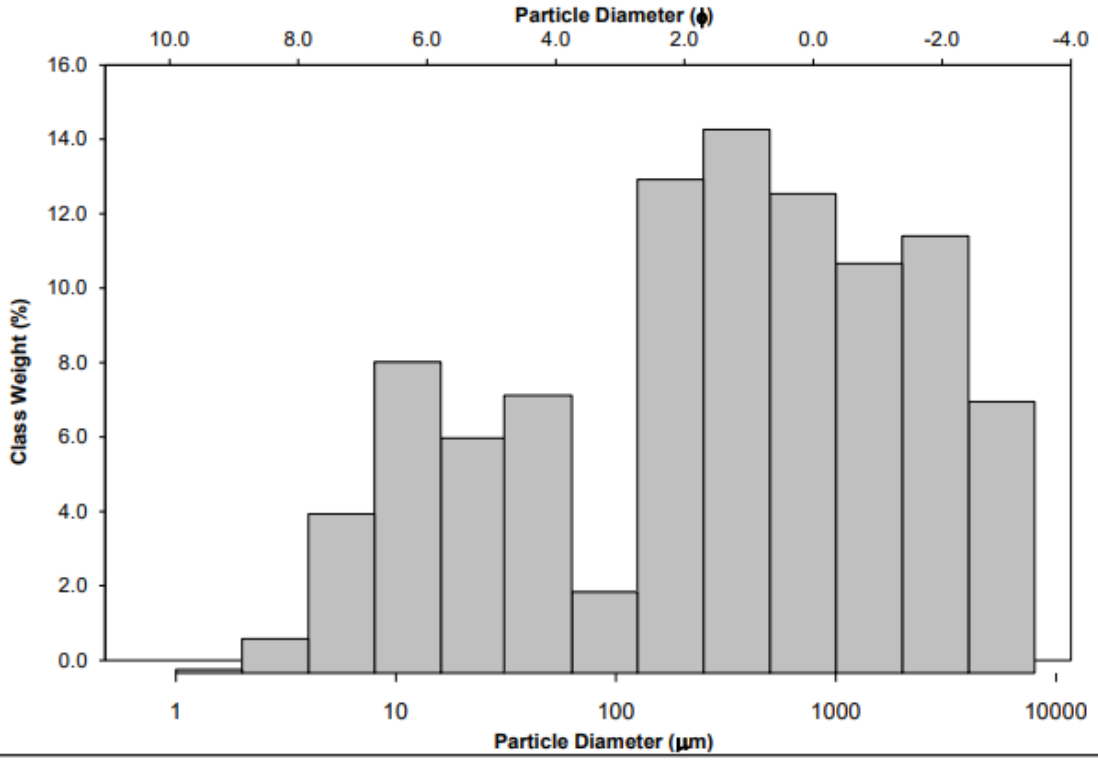

Triangular Diagram

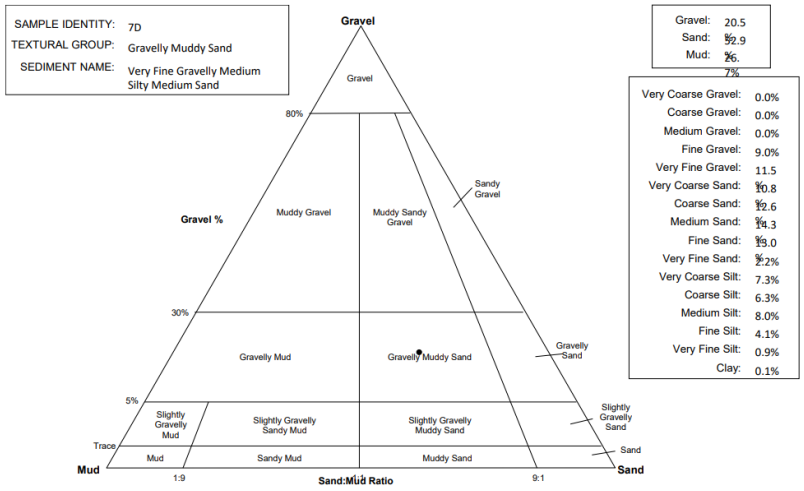

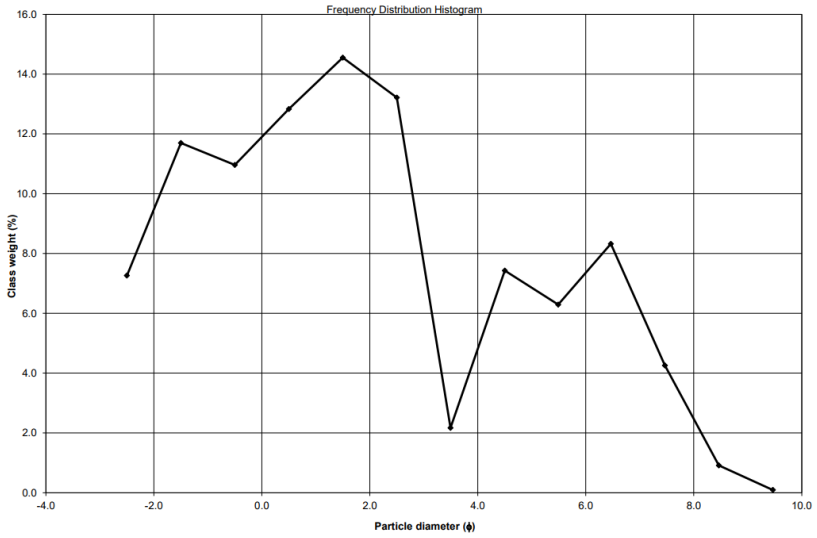

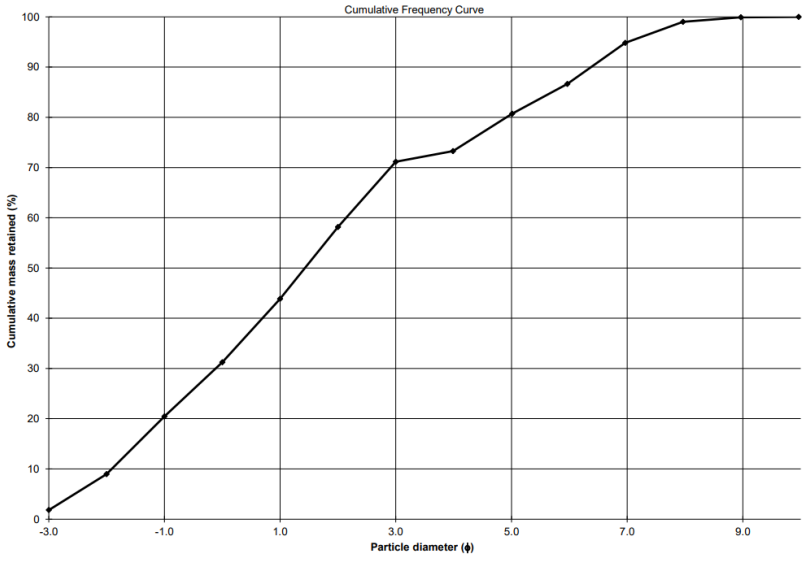

SAMPLE STATISTICS

SIEVING ERROR: 0.0%

SAMPLE IDENTITY: **8E**

ANALYST & DATE: J Fleming, 02/05/2024

SAMPLE TYPE: Bimodal, Very Poorly Sorted

TEXTURAL GROUP: Gravelly Muddy Sand

SEDIMENT NAME: Very Fine Gravelly Very Coarse Silty Fine Sand

	µm	ϕ
MODE 1:	187.5	2.500
MODE 2:	3000.0	-1.500
MODE 3:		
D_{10}:	17.79	-1.442
MEDIAN or D_{50}:	207.9	2.266
D_{90}:	2717.3	5.813
(D_{90} / D_{10}):	152.7	-4.031
(D_{90} - D_{10}):	2699.5	7.255
(D_{75} / D_{25}):	11.43	7.525
(D_{75} - D_{25}):	628.2	3.515

GRAIN SIZE DISTRIBUTION

GRAVEL:	13.7%	COARSE SAND:	7.6%
SAND:	60.7%	MEDIUM SAND:	16.9%
MUD:	25.5%	FINE SAND:	17.5%
		V FINE SAND:	11.6%
V COARSE GRAVEL:	0.0%	V COARSE SILT:	9.8%
COARSE GRAVEL:	0.0%	COARSE SILT:	7.0%
MEDIUM GRAVEL:	0.0%	MEDIUM SILT:	6.0%
FINE GRAVEL:	5.3%	FINE SILT:	2.3%
V FINE GRAVEL:	8.5%	V FINE SILT:	0.4%
V COARSE SAND:	7.2%	CLAY:	0.0%

	METHOD OF MOMENTS			FOLK & WARD METHOD		
	Arithmetic	Geometric	Logarithmic	Geometric	Logarithmic	Description
	µm	µm	ϕ	µm	ϕ	
MEAN ($\bar{x}$):	849.0	208.3	2.263	220.2	2.183	Fine Sand
SORTING (σ):	1474.8	5.894	2.559	6.616	2.726	Very Poorly Sorted
SKEWNESS (Sk):	2.434	-0.017	0.017	0.021	-0.021	Symmetrical
KURTOSIS (K):	8.273	2.380	2.380	1.010	1.010	Mesokurtic

GRAIN SIZE DISTRIBUTION

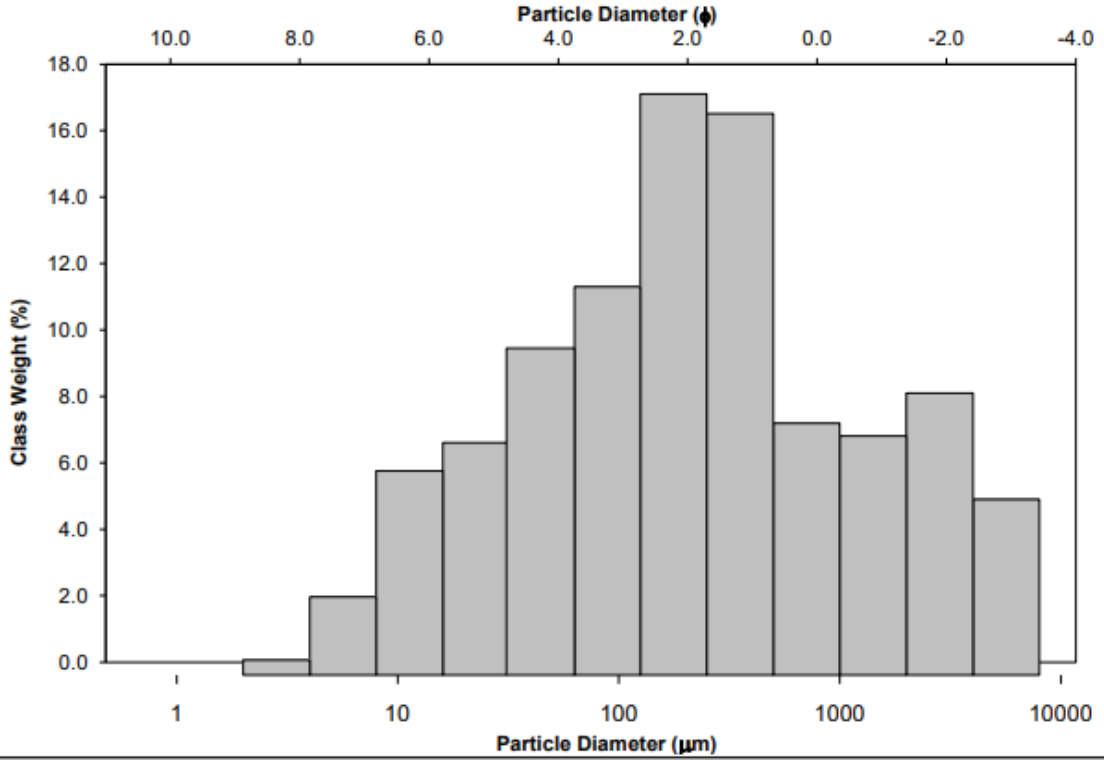

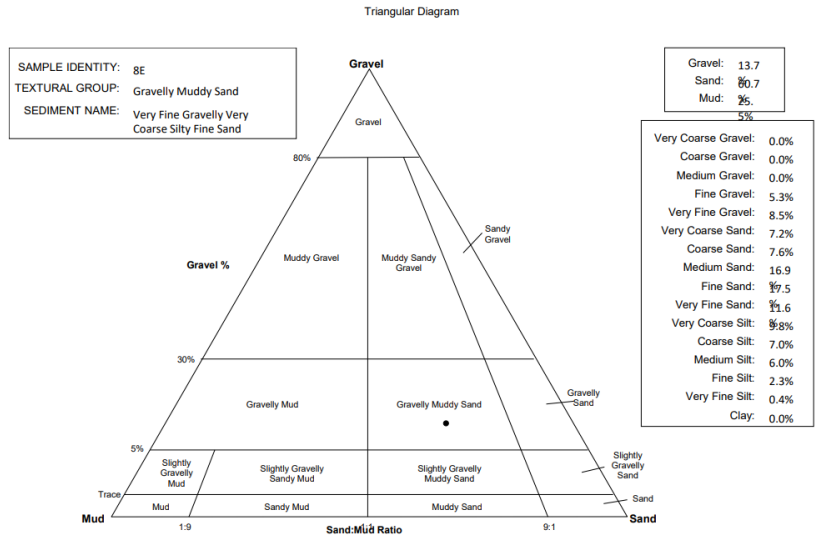
Triangular Diagram
SAMPLE IDENTITY: 8E
TEXTURAL GROUP: Gravelly Muddy Sand
SEDIMENT NAME: Very Fine Gravelly Very Coarse Silty Fine Sand
Gravel: 13.7 %
Sand: 60.7 %
Mud: 25.5 %
Very Coarse Gravel: 0.0%
Coarse Gravel: 0.0%
Medium Gravel: 0.0%
Fine Gravel: 5.3%
Very Fine Gravel: 8.5%
Very Coarse Sand: 7.2%
Coarse Sand: 7.6%
Medium Sand: 16.9%
Fine Sand: 17.5%
Very Fine Sand: 11.6%
Very Coarse Silt: 3.8%
Coarse Silt: 7.0%
Medium Silt: 6.0%
Fine Silt: 2.3%
Very Fine Silt: 0.4%
Clay: 0.0%
Gravel
80%
30%
5%
Trace
Mud
Sand
Gravel %
Muddy Gravel
Muddy Sandy Gravel
Sandy Gravel
Gravelly Mud
Gravelly Muddy Sand
Gravelly Sand
Slightly Gravelly Mud
Slightly Gravelly Sandy Mud
Slightly Gravelly Muddy Sand
Slightly Gravelly Sand
Mud
Sandy Mud
Muddy Sand
Sand
1:9
1:1
9:1
Sand:Mud Ratio

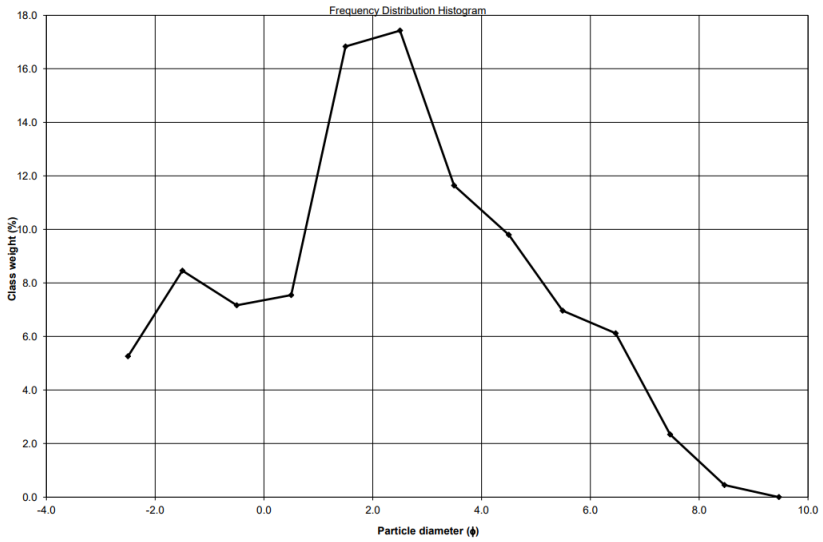
Frequency Distribution Histogram
Class weight (%)
18.0
16.0
14.0
12.0
10.0
8.0
6.0
4.0
2.0
0.0
-4.0
-2.0
0.0
2.0
4.0
6.0
8.0
10.0
Particle diameter (ϕ)

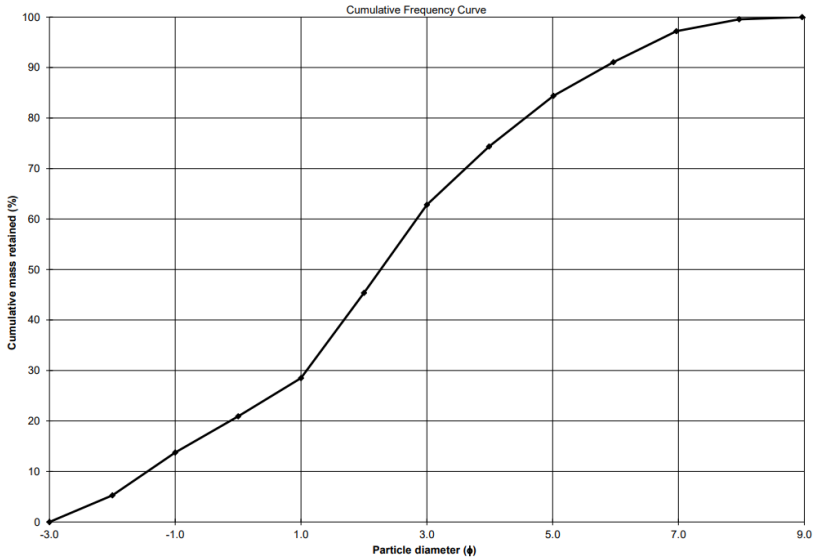
Cumulative Frequency Curve
Cumulative mass retained (%)
100
90
80
70
60
50
40
30
20
10
0
-3.0
-1.0
1.0
3.0
5.0
7.0
9.0
Particle diameter (ϕ)

BAT-2

SAMPLE STATISTICS

SIEVING ERROR: 0.0%

SAMPLE IDENTITY: **5I**

ANALYST & DATE: J Fleming, 02/05/2024

SAMPLE TYPE: Bimodal, Poorly Sorted

TEXTURAL GROUP: Slightly Gravelly Muddy Sand

SEDIMENT NAME: Slightly Very Fine Gravelly Very Coarse Silty Fine Sand

	µm	ϕ
MODE 1:	187.5	2.500
MODE 2:	47.00	4.500
MODE 3:		
D_{10}:	11.39	1.294
MEDIAN or D_{50}:	94.09	3.410
D_{90}:	407.9	6.456
(D_{90} / D_{10}):	35.80	4.990
(D_{90} - D_{10}):	396.5	5.162
(D_{75} / D_{25}):	7.659	2.340
(D_{75} - D_{25}):	190.3	2.937

GRAIN SIZE DISTRIBUTION

GRAVEL:	0.1%	COARSE SAND:	4.8%
SAND:	58.6%	MEDIUM SAND:	14.9%
MUD:	41.3%	FINE SAND:	23.5%
		V FINE SAND:	14.7%
V COARSE GRAVEL:	0.0%	V COARSE SILT:	14.8%
COARSE GRAVEL:	0.0%	COARSE SILT:	11.8%
MEDIUM GRAVEL:	0.0%	MEDIUM SILT:	10.3%
FINE GRAVEL:	0.0%	FINE SILT:	3.8%
V FINE GRAVEL:	0.1%	V FINE SILT:	0.7%
V COARSE SAND:	0.7%	CLAY:	0.0%

	METHOD OF MOMENTS			FOLK & WARD METHOD		
	Arithmetic	Geometric	Logarithmic	Geometric	Logarithmic	Description
	µm	µm	ϕ	µm	ϕ	
MEAN ($\bar{x}$):	174.7	78.75	3.666	78.73	3.667	Very Fine Sand
SORTING (σ):	231.5	3.787	1.921	3.911	1.968	Poorly Sorted
SKEWNESS (Sk):	4.161	-0.275	0.275	-0.173	0.173	Fine Skewed
KURTOSIS (K):	35.65	2.296	2.296	0.846	0.846	Platykurtic

GRAIN SIZE DISTRIBUTION

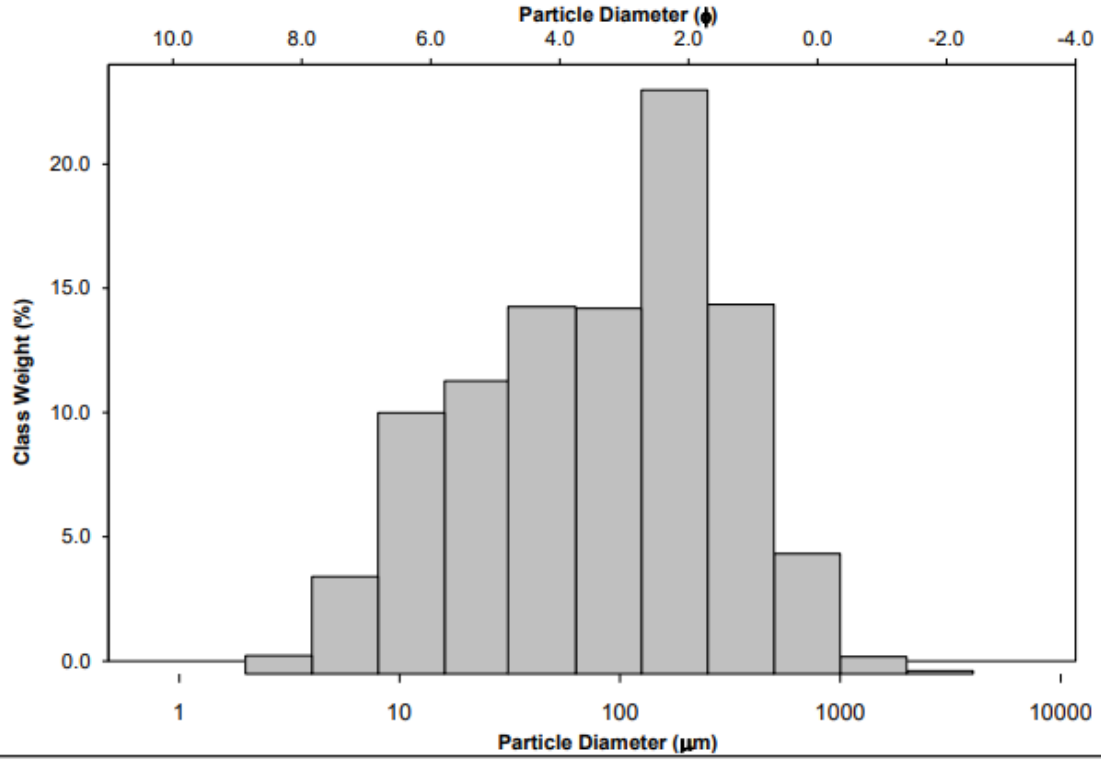

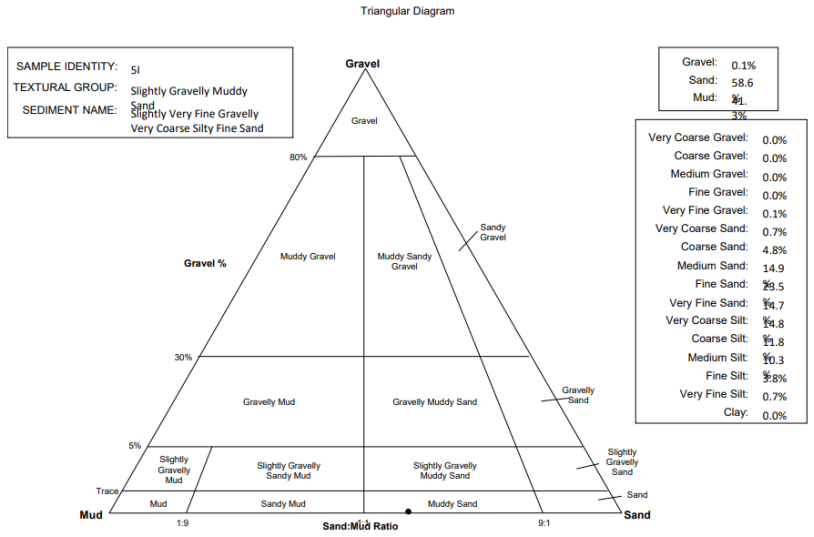
Triangular Diagram
SAMPLE IDENTITY: 5I
TEXTURAL GROUP: Slightly Gravelly Muddy Sand
SEDIMENT NAME: Slightly Very Fine Gravelly Very Coarse Silty Fine Sand
Gravel
Gravel
80%
Gravel %
Muddy Gravel
Muddy Sandy Gravel
Sandy Gravel
30%
Gravelly Mud
Gravelly Muddy Sand
Gravelly Sand
5%
Slightly Gravelly Mud
Slightly Gravelly Sandy Mud
Slightly Gravelly Muddy Sand
Slightly Gravelly Sand
Trace
Mud
Mud
Sandy Mud
Muddy Sand
Sand
Sand
1:9
9:1
Sand:Mud Ratio
Gravel: 0.1%
Sand: 58.6
Mud: 41.3%
Very Coarse Gravel: 0.0%
Coarse Gravel: 0.0%
Medium Gravel: 0.0%
Fine Gravel: 0.0%
Very Fine Gravel: 0.1%
Very Coarse Sand: 0.7%
Coarse Sand: 4.8%
Medium Sand: 14.9
Fine Sand: 29.5
Very Fine Sand: 14.7
Very Coarse Silt: 14.8
Coarse Silt: 11.8
Medium Silt: 10.3
Fine Silt: 3.8%
Very Fine Silt: 0.7%
Clay: 0.0%

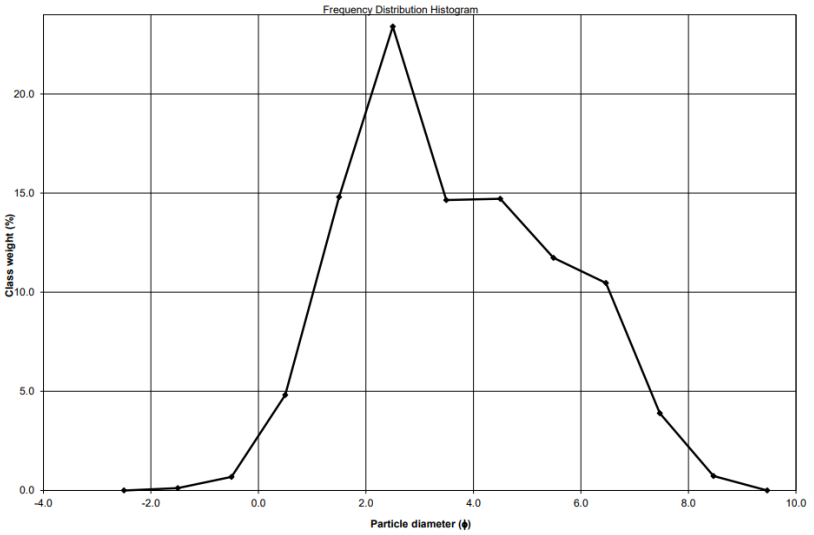
Frequency Distribution Histogram
Class weight (%)
20.0
15.0
10.0
5.0
0.0
-4.0
-2.0
0.0
2.0
4.0
6.0
8.0
10.0
Particle diameter (ϕ)

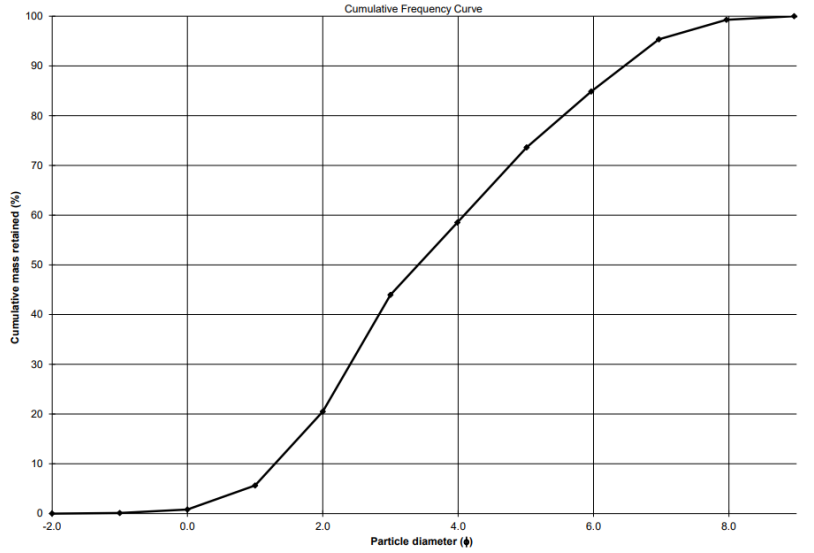
Cumulative Frequency Curve
Cumulative mass retained (%)
100
90
80
70
60
50
40
30
20
10
0
-2.0
0.0
2.0
4.0
6.0
8.0
Particle diameter (ϕ)

SAMPLE STATISTICS

SIEVING ERROR: 0.0%

SAMPLE IDENTITY: **9G**

ANALYST & DATE: J Fleming, 02/05/2024

SAMPLE TYPE: Unimodal, Poorly Sorted

TEXTURAL GROUP: Slightly Gravelly Muddy Sand

SEDIMENT NAME: Slightly Very Fine Gravelly Very Coarse Silty Fine Sand

	µm	ϕ
MODE 1:	187.5	2.500
MODE 2:		
MODE 3:		
D_{10}:	16.72	1.494
MEDIAN or D_{50}:	117.8	3.086
D_{90}:	355.0	5.902
(D_{90} / D_{10}):	21.23	3.950
(D_{90} - D_{10}):	338.2	4.408
(D_{75} / D_{25}):	4.833	1.997
(D_{75} - D_{25}):	163.3	2.273

GRAIN SIZE DISTRIBUTION

GRAVEL:	0.1%	COARSE SAND:	3.3%
SAND:	66.8%	MEDIUM SAND:	11.7%
MUD:	33.2%	FINE SAND:	32.5%
		V FINE SAND:	18.4%
V COARSE GRAVEL:	0.0%	V COARSE SILT:	14.8%
COARSE GRAVEL:	0.0%	COARSE SILT:	9.2%
MEDIUM GRAVEL:	0.0%	MEDIUM SILT:	6.5%
FINE GRAVEL:	0.0%	FINE SILT:	2.3%
V FINE GRAVEL:	0.1%	V FINE SILT:	0.4%
V COARSE SAND:	0.9%	CLAY:	0.0%

	METHOD OF MOMENTS			FOLK & WARD METHOD		
	Arithmetic	Geometric	Logarithmic	Geometric	Logarithmic	Description
	µm	µm	ϕ	µm	ϕ	
MEAN ($\bar{x}$):	171.8	92.09	3.441	91.71	3.447	Very Fine Sand
SORTING (σ):	211.0	3.190	1.673	3.150	1.655	Poorly Sorted
SKEWNESS (Sk):	4.434	-0.485	0.485	-0.304	0.304	Very Fine Skewed
KURTOSIS (K):	36.87	2.947	2.947	1.003	1.003	Mesokurtic

GRAIN SIZE DISTRIBUTION

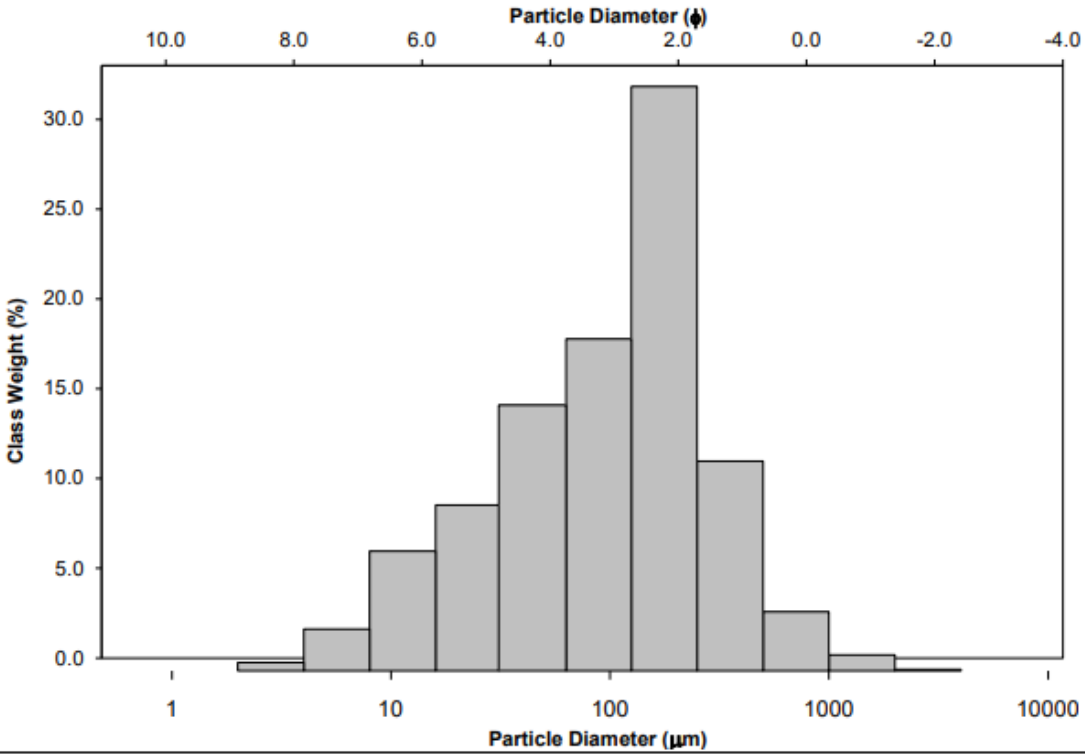

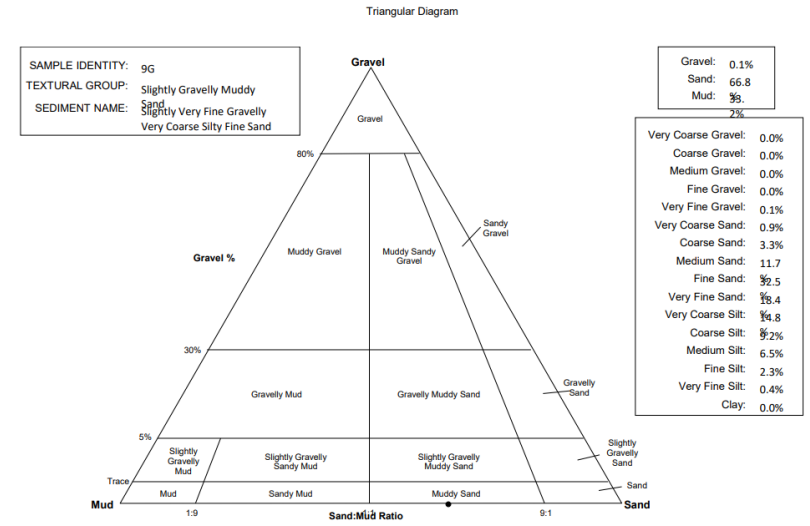
Triangular Diagram
SAMPLE IDENTITY: 9G
TEXTURAL GROUP: Slightly Gravelly Muddy Sand
SEDIMENT NAME: Slightly Very Fine Gravelly Very Coarse Silty Fine Sand
Gravel: 0.1%
Sand: 66.8
Mud: 33.2%
Very Coarse Gravel: 0.0%
Coarse Gravel: 0.0%
Medium Gravel: 0.0%
Fine Gravel: 0.0%
Very Fine Gravel: 0.1%
Very Coarse Sand: 0.9%
Coarse Sand: 3.3%
Medium Sand: 11.7
Fine Sand: 32.5
Very Fine Sand: 18.4
Very Coarse Silt: 14.8
Coarse Silt: 9.2%
Medium Silt: 6.5%
Fine Silt: 2.3%
Very Fine Silt: 0.4%
Clay: 0.0%
Gravel
80%
Gravel %
30%
5%
Trace
Mud
Sand
Muddy Gravel
Muddy Sandy Gravel
Sandy Gravel
Gravelly Mud
Gravelly Muddy Sand
Gravelly Sand
Slightly Gravelly Mud
Slightly Gravelly Sandy Mud
Slightly Gravelly Muddy Sand
Slightly Gravelly Sand
Mud
Sandy Mud
Muddy Sand
Sand
1:9
Sand:Mud Ratio
9:1

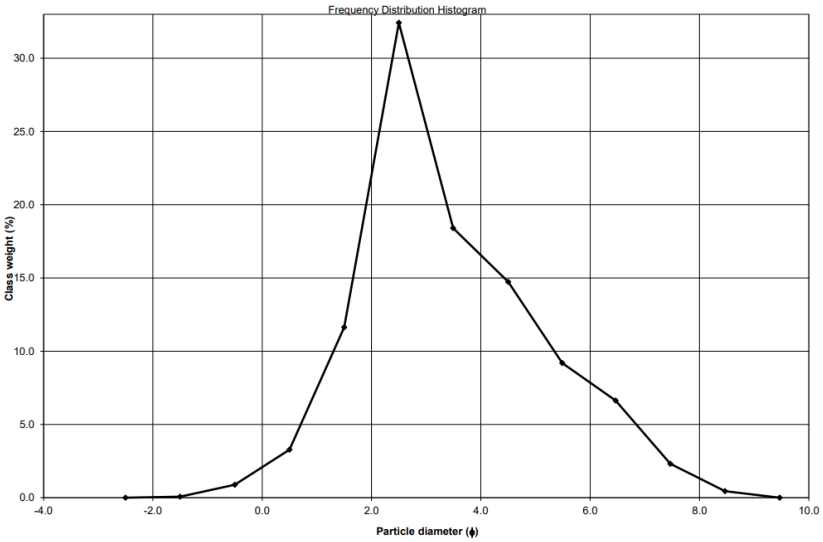
Frequency Distribution Histogram
Class weight (%)
30.0
25.0
20.0
15.0
10.0
5.0
0.0
-4.0
-2.0
0.0
2.0
4.0
6.0
8.0
10.0
Particle diameter (ϕ)

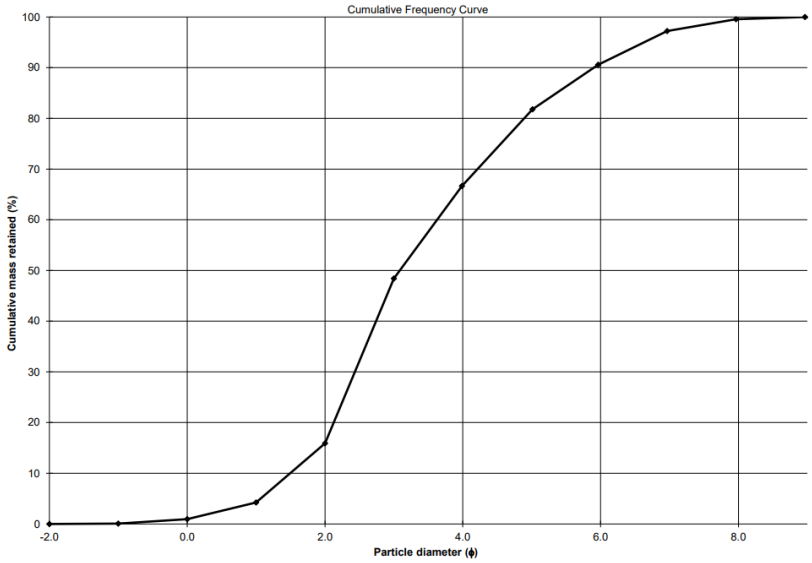
Cumulative Frequency Curve
Cumulative mass retained (%)
100
90
80
70
60
50
40
30
20
10
0
-2.0
0.0
2.0
4.0
6.0
8.0
Particle diameter (ϕ)

SAMPLE STATISTICS

SIEVING ERROR: 0.0%

SAMPLE IDENTITY: **12H**

ANALYST & DATE: J Fleming, 02/05/2024

SAMPLE TYPE: Bimodal, Poorly Sorted

TEXTURAL GROUP: Muddy Sand

SEDIMENT NAME: Very Coarse Silty Fine Sand

	µm	ϕ
MODE 1:	187.5	2.500
MODE 2:	47.00	4.500
MODE 3:		
D_{10}:	12.44	1.614
MEDIAN or D_{50}:	97.20	3.363
D_{90}:	326.7	6.329
(D_{90} / D_{10}):	26.26	3.921
(D_{90} - D_{10}):	314.3	4.715
(D_{75} / D_{25}):	6.869	2.196
(D_{75} - D_{25}):	170.6	2.780

GRAIN SIZE DISTRIBUTION

GRAVEL:	0.0%	COARSE SAND:	1.6%
SAND:	58.2%	MEDIUM SAND:	13.6%
MUD:	41.8%	FINE SAND:	30.1%
		V FINE SAND:	12.9%
V COARSE GRAVEL:	0.0%	V COARSE SILT:	15.4%
COARSE GRAVEL:	0.0%	COARSE SILT:	13.2%
MEDIUM GRAVEL:	0.0%	MEDIUM SILT:	9.6%
FINE GRAVEL:	0.0%	FINE SILT:	3.1%
V FINE GRAVEL:	0.0%	V FINE SILT:	0.6%
V COARSE SAND:	0.1%	CLAY:	0.0%

	METHOD OF MOMENTS			FOLK & WARD METHOD		
	Arithmetic	Geometric	Logarithmic	Geometric	Logarithmic	Description
	µm	µm	ϕ	µm	ϕ	
MEAN ($\bar{x}$):	144.0	75.31	3.731	75.71	3.723	Very Fine Sand
SORTING (σ):	144.8	3.394	1.763	3.450	1.787	Poorly Sorted
SKEWNESS (Sk):	2.038	-0.433	0.433	-0.265	0.265	Fine Skewed
KURTOSIS (K):	11.00	2.261	2.261	0.825	0.825	Platykurtic

GRAIN SIZE DISTRIBUTION

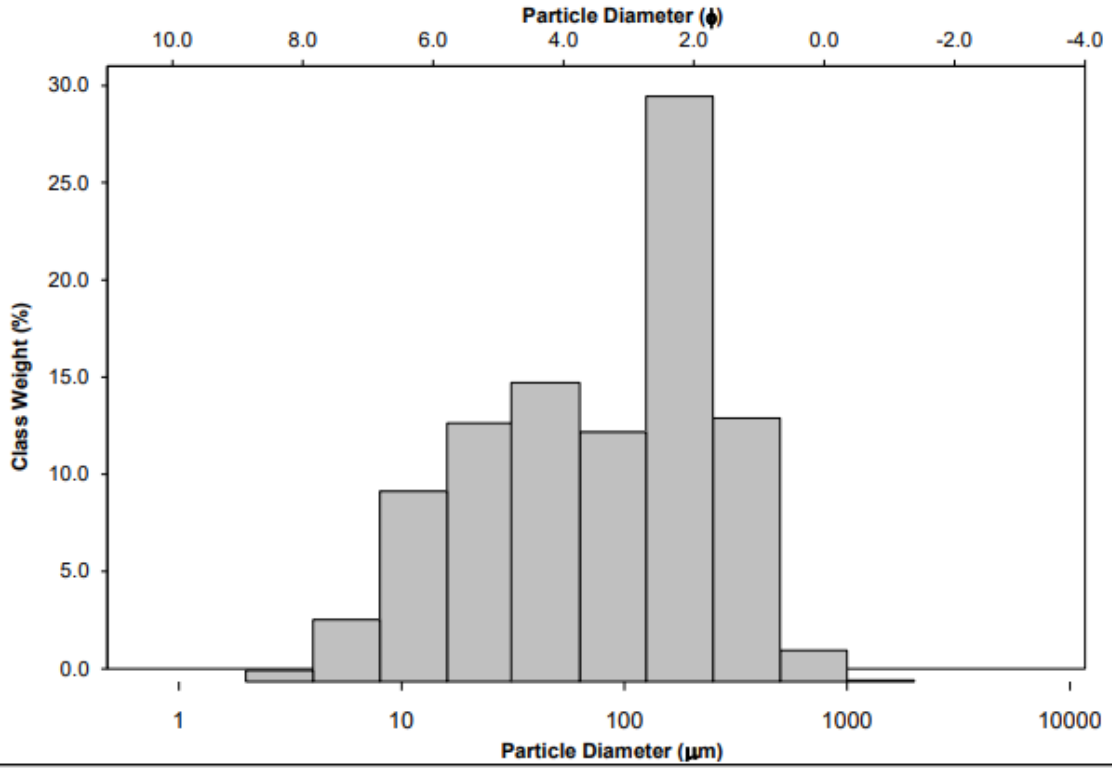

Triangular Diagram

SAMPLE IDENTITY: 12H
TEXTURAL GROUP: Muddy Sand
SEDIMENT NAME: Very Coarse Silty Fine Sand

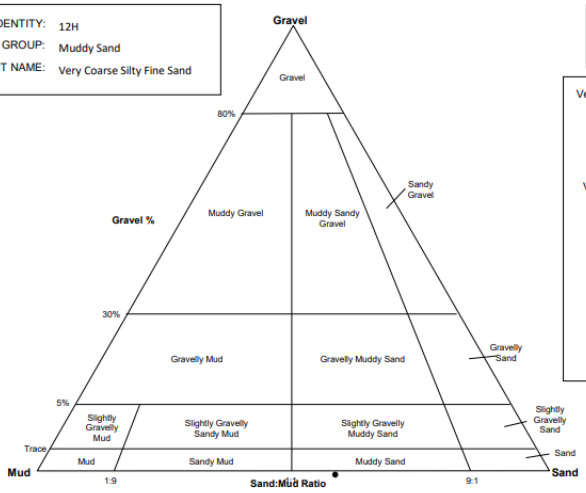

Gravel:	0.0%
Sand:	58.2
Mud:	41.8%

Very Coarse Gravel:	0.0%
Coarse Gravel:	0.0%
Medium Gravel:	0.0%
Fine Gravel:	0.0%
Very Fine Gravel:	0.0%
Very Coarse Sand:	0.1%
Coarse Sand:	1.6%
Medium Sand:	13.6
Fine Sand:	30.1
Very Fine Sand:	12.9
Very Coarse Silt:	15.4
Coarse Silt:	13.2
Medium Silt:	9.6%
Fine Silt:	3.1%
Very Fine Silt:	0.6%
Clay:	0.0%

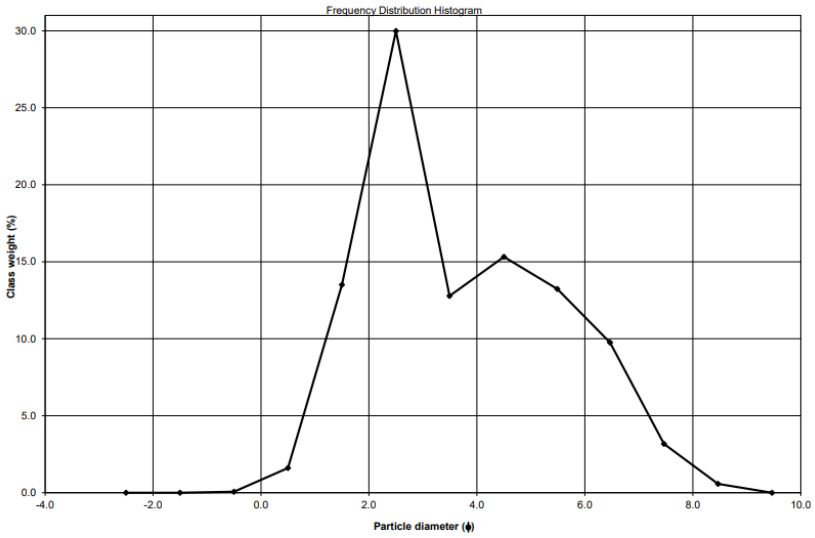

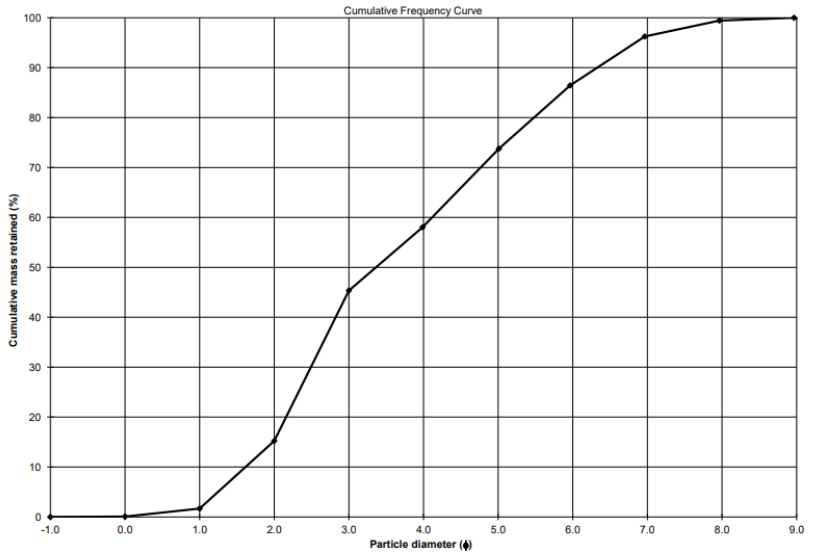

SAMPLE STATISTICS

SIEVING ERROR: 0.0%

SAMPLE IDENTITY: **13J**

ANALYST & DATE: J Fleming, 02/05/2024

SAMPLE TYPE: Unimodal, Poorly Sorted

TEXTURAL GROUP: Slightly Gravelly Muddy Sand

SEDIMENT NAME: Slightly Very Fine Gravelly Very Coarse Silty Fine Sand

	µm	ϕ
MODE 1:	187.5	2.500
MODE 2:		
MODE 3:		
D_{10}:	22.62	0.581
MEDIAN or D_{50}:	137.5	2.863
D_{90}:	668.4	5.466
(D_{90} / D_{10}):	29.55	9.404
(D_{90} - D_{10}):	645.8	4.885
(D_{75} / D_{25}):	5.298	2.398
(D_{75} - D_{25}):	246.1	2.406

GRAIN SIZE DISTRIBUTION

GRAVEL: 0.7%	COARSE SAND: 9.9%
SAND: 72.6%	MEDIUM SAND: 15.0%
MUD: 26.7%	FINE SAND: 24.1%
	V FINE SAND: 20.0%
V COARSE GRAVEL: 0.0%	V COARSE SILT: 13.6%
COARSE GRAVEL: 0.0%	COARSE SILT: 6.5%
MEDIUM GRAVEL: 0.0%	MEDIUM SILT: 4.5%
FINE GRAVEL: 0.0%	FINE SILT: 1.7%
V FINE GRAVEL: 0.7%	V FINE SILT: 0.4%
V COARSE SAND: 3.5%	CLAY: 0.0%

	METHOD OF MOMENTS			FOLK & WARD METHOD		
	Arithmetic	Geometric	Logarithmic	Geometric	Logarithmic	Description
	µm	µm	ϕ	µm	ϕ	
MEAN ($\bar{x}$):	277.2	127.6	2.971	131.7	2.924	Fine Sand
SORTING (σ):	390.4	3.559	1.831	3.645	1.866	Poorly Sorted
SKEWNESS (Sk):	3.511	-0.261	0.261	-0.081	0.081	Symmetrical
KURTOSIS (K):	19.95	2.934	2.934	1.068	1.068	Mesokurtic

GRAIN SIZE DISTRIBUTION

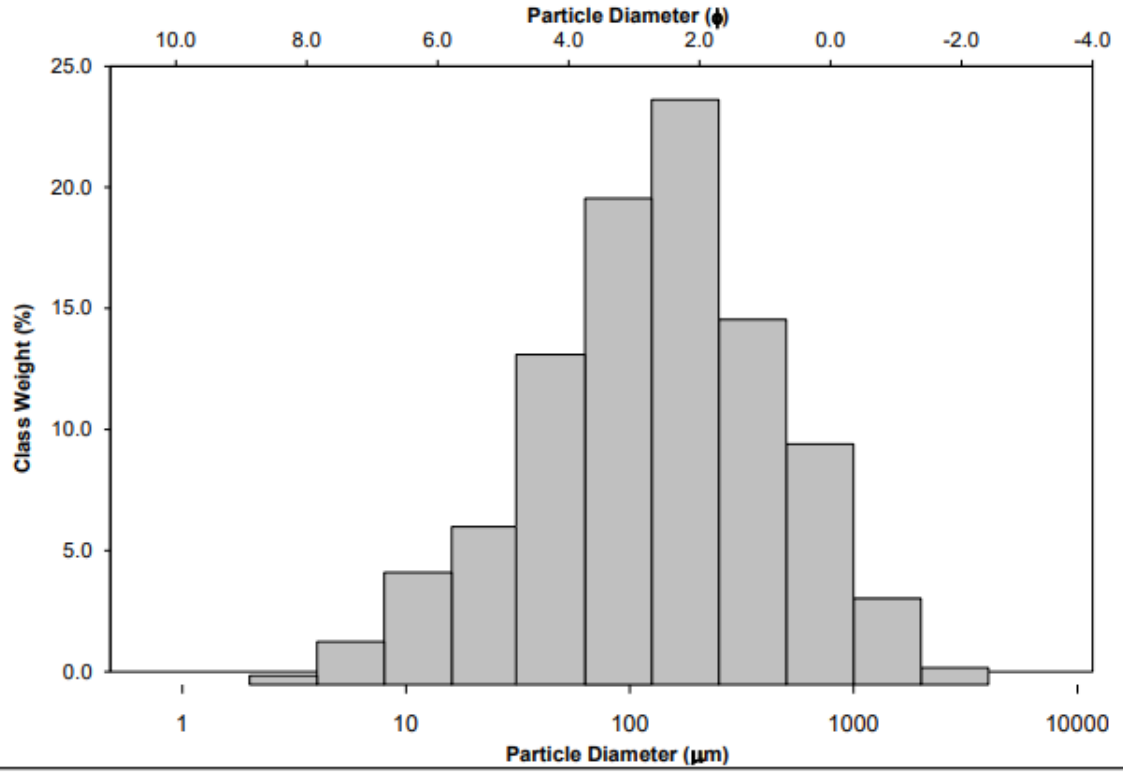

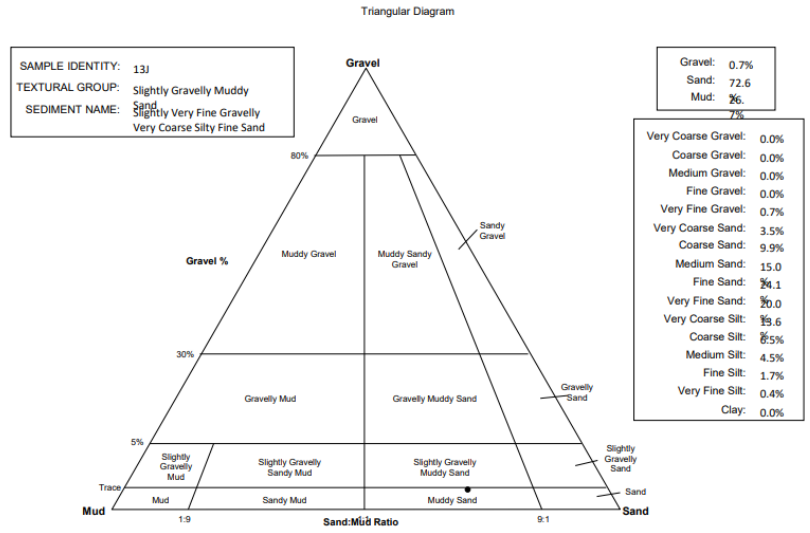
Triangular Diagram
SAMPLE IDENTITY: 13J
TEXTURAL GROUP: Slightly Gravelly Muddy Sand
SEDIMENT NAME: Slightly Very Fine Gravelly Very Coarse Silty Fine Sand
Gravel
Gravel
80%
Gravel %
Muddy Gravel
Muddy Sandy Gravel
Sandy Gravel
30%
Gravelly Mud
Gravelly Muddy Sand
Gravelly Sand
5%
Slightly Gravelly Mud
Slightly Gravelly Sandy Mud
Slightly Gravelly Muddy Sand
Slightly Gravelly Sand
Trace
Mud
Mud
Sandy Mud
Muddy Sand
Sand
Sand
1:9
9:1
Sand:Mud Ratio
Gravel: 0.7%
Sand: 72.6
Very Coarse Gravel: 0.0%
Coarse Gravel: 0.0%
Medium Gravel: 0.0%
Fine Gravel: 0.0%
Very Fine Gravel: 0.7%
Very Coarse Sand: 3.5%
Coarse Sand: 9.9%
Medium Sand: 15.0
Fine Sand: 24.1
Very Fine Sand: 20.0
Very Coarse Silt: 13.6
Coarse Silt: 6.5%
Medium Silt: 4.5%
Fine Silt: 1.7%
Very Fine Silt: 0.4%
Clay: 0.0%

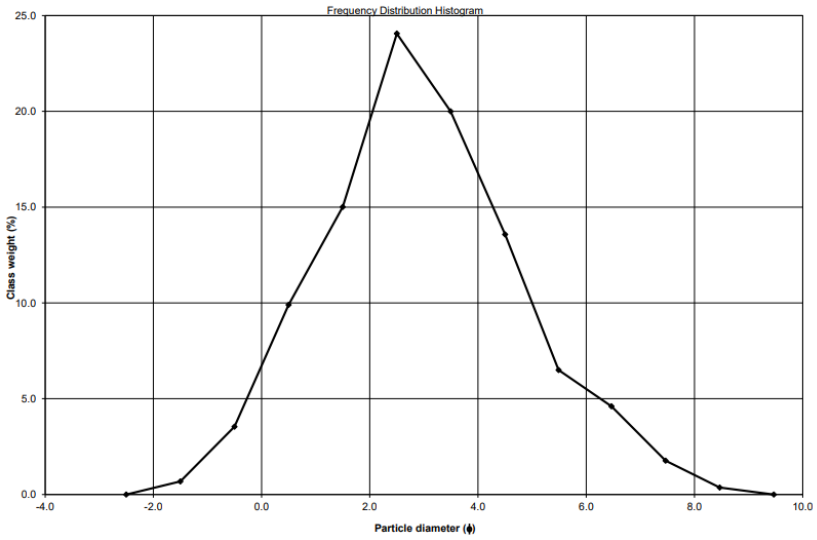
Frequency Distribution Histogram
Class weight (%)
25.0
20.0
15.0
10.0
5.0
0.0
-4.0
-2.0
0.0
2.0
4.0
6.0
8.0
10.0
Particle diameter (ϕ)

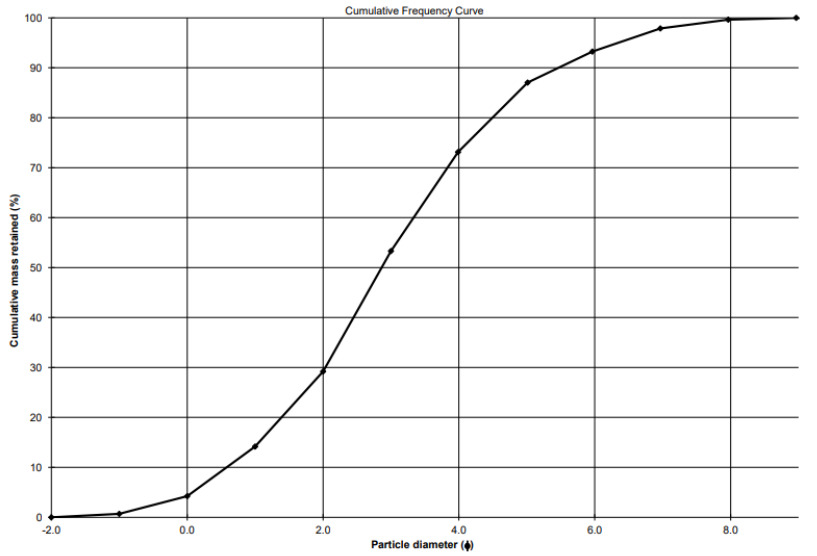
Cumulative Frequency Curve
Cumulative mass retained (%)
100
90
80
70
60
50
40
30
20
10
0
-2.0
0.0
2.0
4.0
6.0
8.0
Particle diameter (ϕ)

SAMPLE STATISTICS

SIEVING ERROR: 0.0%

SAMPLE IDENTITY: **14K**

ANALYST & DATE: J Fleming, 02/05/2024

SAMPLE TYPE: Unimodal, Poorly Sorted

TEXTURAL GROUP: Slightly Gravelly Muddy Sand

SEDIMENT NAME: Slightly Very Fine Gravelly Very Coarse Silty Very Fine Sand

	µm	ϕ
MODE 1:	94.00	3.494
MODE 2:		
MODE 3:		
D_{10}:	22.82	1.727
MEDIAN or D_{50}:	94.40	3.405
D_{90}:	302.1	5.453
(D_{90} / D_{10}):	13.24	3.158
(D_{90} - D_{10}):	279.3	3.727
(D_{75} / D_{25}):	3.617	1.736
(D_{75} - D_{25}):	126.2	1.855

GRAIN SIZE DISTRIBUTION

GRAVEL: 2.6%	COARSE SAND: 1.4%
SAND: 65.5%	MEDIUM SAND: 5.2%
MUD: 31.9%	FINE SAND: 26.1%
	V FINE SAND: 30.6%
V COARSE GRAVEL: 0.0%	V COARSE SILT: 18.4%
COARSE GRAVEL: 0.0%	COARSE SILT: 7.5%
MEDIUM GRAVEL: 0.0%	MEDIUM SILT: 4.3%
FINE GRAVEL: 0.0%	FINE SILT: 1.5%
V FINE GRAVEL: 2.6%	V FINE SILT: 0.2%
V COARSE SAND: 2.3%	CLAY: 0.0%

	METHOD OF MOMENTS			FOLK & WARD METHOD		
	Arithmetic µm	Geometric µm	Logarithmic ϕ	Geometric µm	Logarithmic ϕ	Description
MEAN ($\bar{x}$):	230.4	94.49	3.404	89.53	3.481	Very Fine Sand
SORTING (σ):	509.2	3.155	1.658	3.035	1.602	Poorly Sorted
SKEWNESS (Sk):	4.528	0.402	-0.402	-0.004	0.004	Symmetrical
KURTOSIS (K):	23.67	4.396	4.396	1.356	1.356	Leptokurtic

GRAIN SIZE DISTRIBUTION

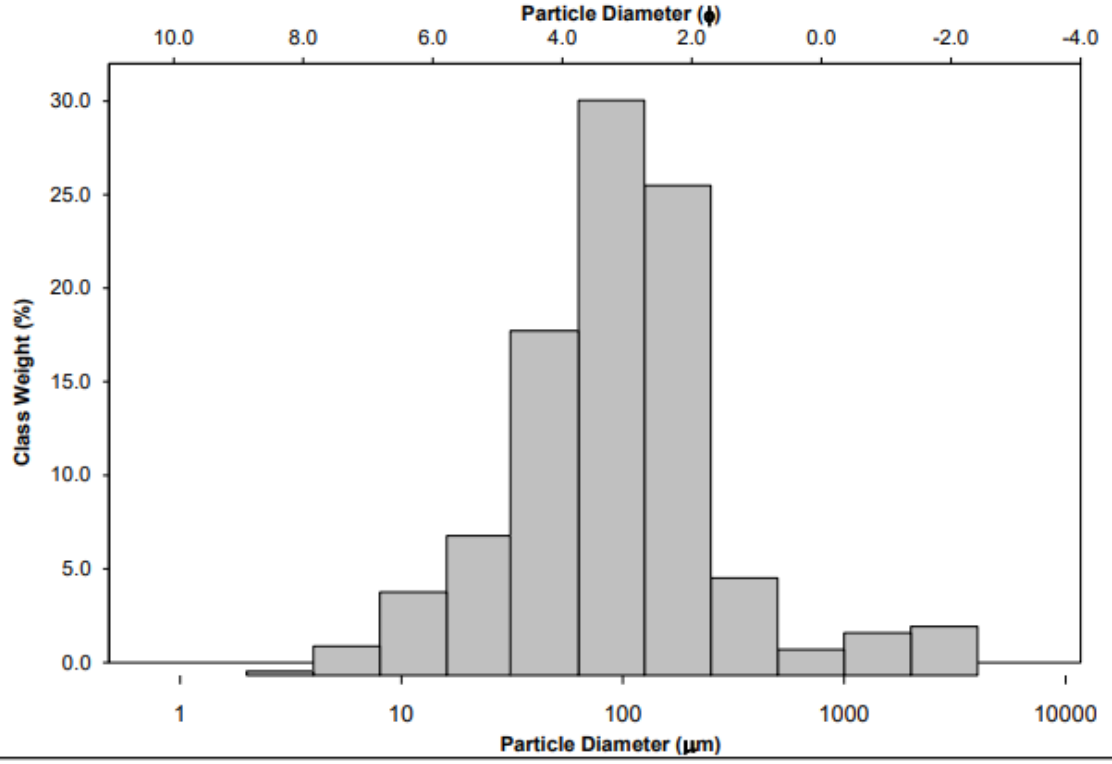

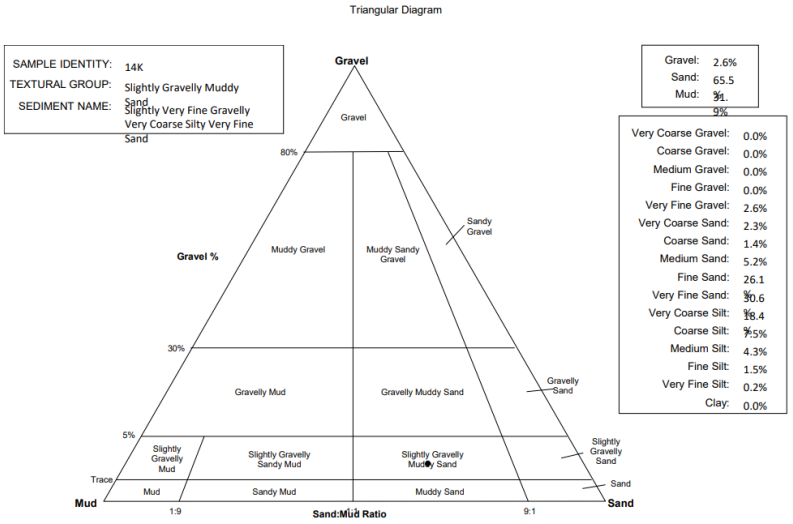
Triangular Diagram
SAMPLE IDENTITY: 14K
TEXTURAL GROUP: Slightly Gravelly Muddy Sand
SEDIMENT NAME: Slightly Very Fine Gravelly Very Coarse Silty Very Fine Sand
Gravel: 2.6%
Sand: 65.5
Mud: 31.9%
Very Coarse Gravel: 0.0%
Coarse Gravel: 0.0%
Medium Gravel: 0.0%
Fine Gravel: 0.0%
Very Fine Gravel: 2.6%
Very Coarse Sand: 2.3%
Coarse Sand: 1.4%
Medium Sand: 5.2%
Fine Sand: 26.1
Very Fine Sand: 30.6
Very Coarse Silt: 18.4
Coarse Silt: 7.5%
Medium Silt: 4.3%
Fine Silt: 1.5%
Very Fine Silt: 0.2%
Clay: 0.0%
Gravel
Gravel
80%
Gravel %
Muddy Gravel
Muddy Sandy Gravel
Sandy Gravel
30%
Gravelly Mud
Gravelly Muddy Sand
Gravelly Sand
5%
Slightly Gravelly Mud
Slightly Gravelly Sandy Mud
Slightly Gravelly Muddy Sand
Slightly Gravelly Sand
Trace
Mud
Sandy Mud
Muddy Sand
Sand
Mud
1:9
Sand:Mud Ratio
9:1
Sand

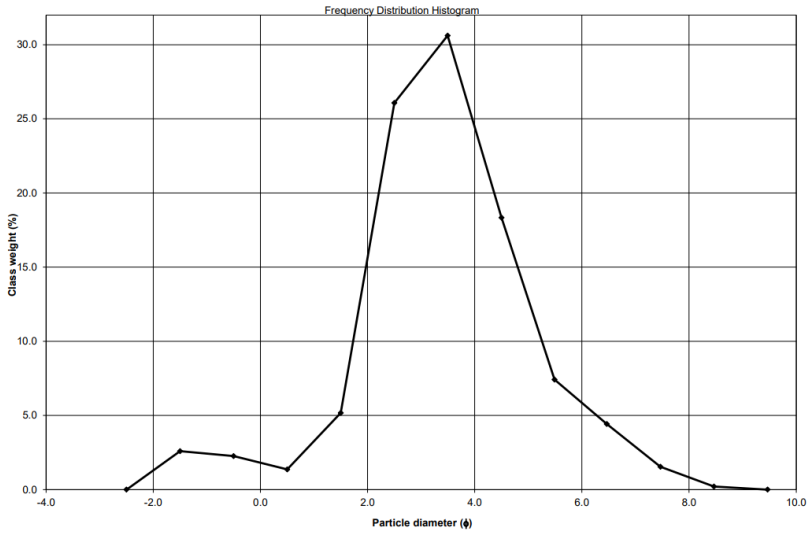
Frequency Distribution Histogram
Class weight (%)
30.0
25.0
20.0
15.0
10.0
5.0
0.0
-4.0
-2.0
0.0
2.0
4.0
6.0
8.0
10.0
Particle diameter (ϕ)

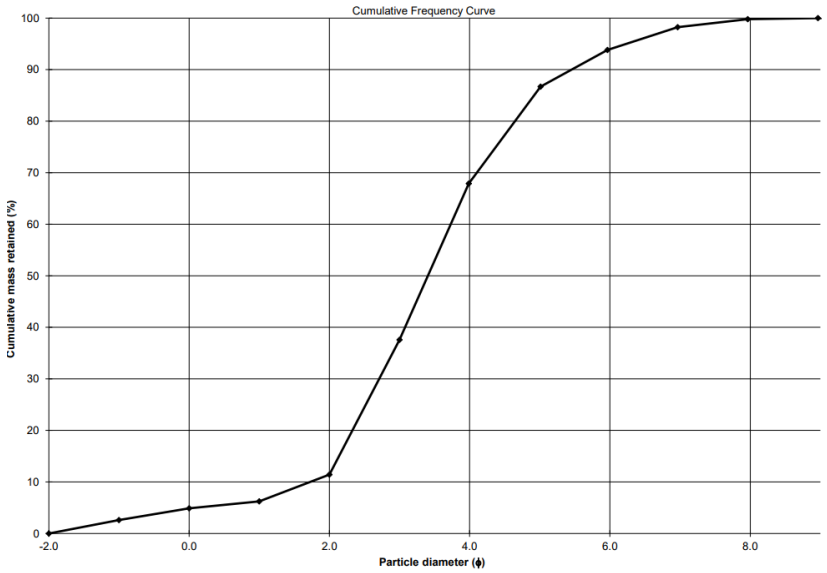
Cumulative Frequency Curve
Cumulative mass retained (%)
100
90
80
70
60
50
40
30
20
10
0
-2.0
0.0
2.0
4.0
6.0
8.0
Particle diameter (ϕ)

SAMPLE STATISTICS

SIEVING ERROR: 0.0%

SAMPLE IDENTITY: **15L**

ANALYST & DATE: J Fleming, 02/05/2024

SAMPLE TYPE: Unimodal, Poorly Sorted

TEXTURAL GROUP: Muddy Sand

SEDIMENT NAME: Very Coarse Silty Fine Sand

	µm	ϕ
MODE 1:	187.5	2.500
MODE 2:		
MODE 3:		
D_{10}:	20.32	2.079
MEDIAN or D_{50}:	92.94	3.428
D_{90}:	236.7	5.621
(D_{90} / D_{10}):	11.65	2.704
(D_{90} - D_{10}):	216.4	3.542
(D_{75} / D_{25}):	3.730	1.737
(D_{75} - D_{25}):	122.6	1.899

GRAIN SIZE DISTRIBUTION

GRAVEL:	0.0%	COARSE SAND:	0.9%
SAND:	66.3%	MEDIUM SAND:	6.3%
MUD:	33.7%	FINE SAND:	30.1%
		V FINE SAND:	28.6%
V COARSE GRAVEL:	0.0%	V COARSE SILT:	18.2%
COARSE GRAVEL:	0.0%	COARSE SILT:	8.6%
MEDIUM GRAVEL:	0.0%	MEDIUM SILT:	5.0%
FINE GRAVEL:	0.0%	FINE SILT:	1.6%
V FINE GRAVEL:	0.0%	V FINE SILT:	0.2%
V COARSE SAND:	0.4%	CLAY:	0.0%

	METHOD OF MOMENTS			FOLK & WARD METHOD		
	Arithmetic	Geometric	Logarithmic	Geometric	Logarithmic	Description
	µm	µm	ϕ	µm	ϕ	
MEAN ($\bar{x}$):	131.2	82.05	3.607	84.86	3.559	Very Fine Sand
SORTING (σ):	140.2	2.649	1.405	2.634	1.397	Poorly Sorted
SKEWNESS (Sk):	4.845	-0.559	0.559	-0.187	0.187	Fine Skewed
KURTOSIS (K):	41.52	3.424	3.424	1.032	1.032	Mesokurtic

GRAIN SIZE DISTRIBUTION

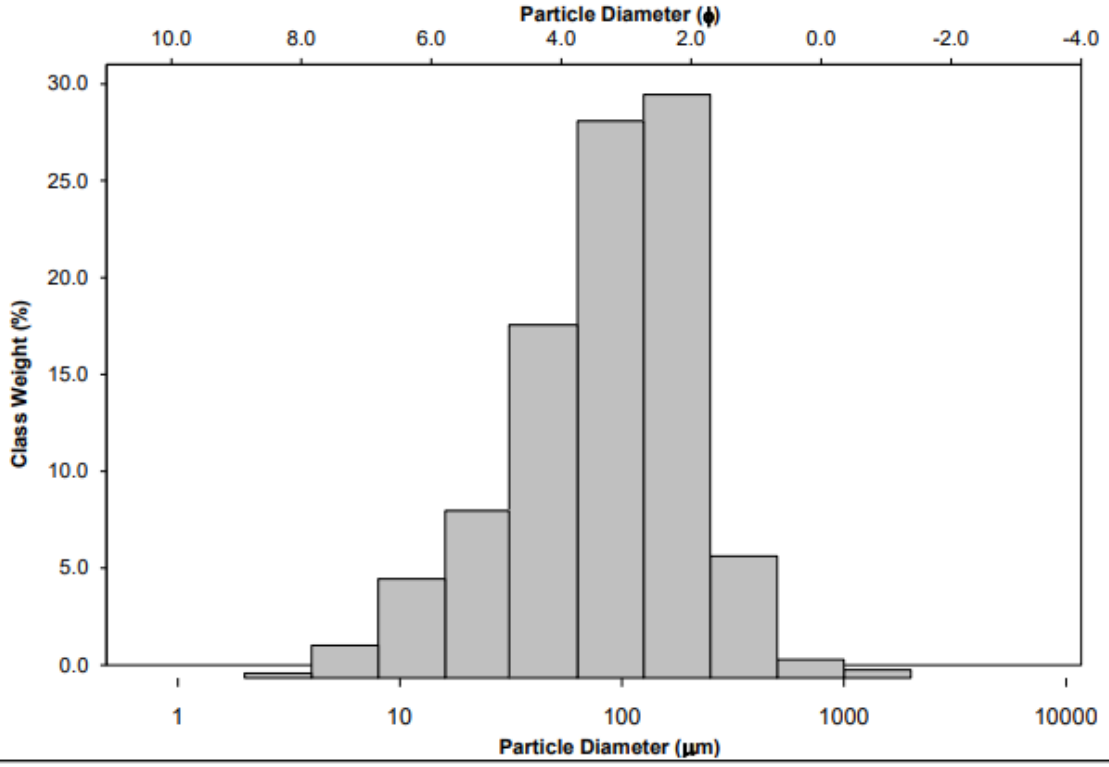

Triangular Diagram

SAMPLE IDENTITY: 15L
TEXTURAL GROUP: Muddy Sand
SEDIMENT NAME: Very Coarse Silty Fine Sand

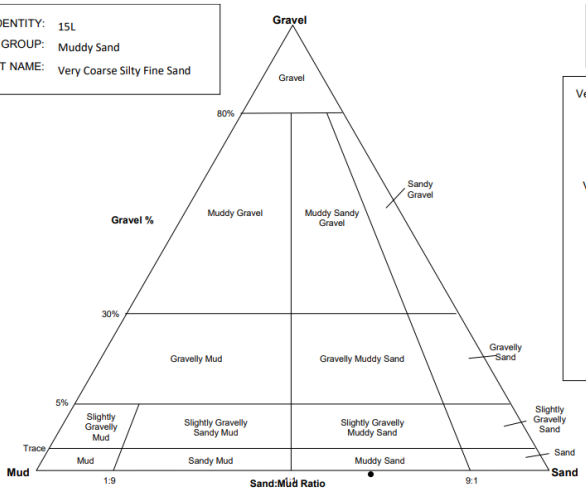

Gravel:	0.0%
Sand:	66.3
Mud:	33.7%

Very Coarse Gravel:	0.0%
Coarse Gravel:	0.0%
Medium Gravel:	0.0%
Fine Gravel:	0.0%
Very Fine Gravel:	0.0%
Very Coarse Sand:	0.4%
Coarse Sand:	0.9%
Medium Sand:	6.3%
Fine Sand:	30.1
Very Fine Sand:	28.6
Very Coarse Silt:	18.2
Coarse Silt:	8.6%
Medium Silt:	5.0%
Fine Silt:	1.6%
Very Fine Silt:	0.2%
Clay:	0.0%

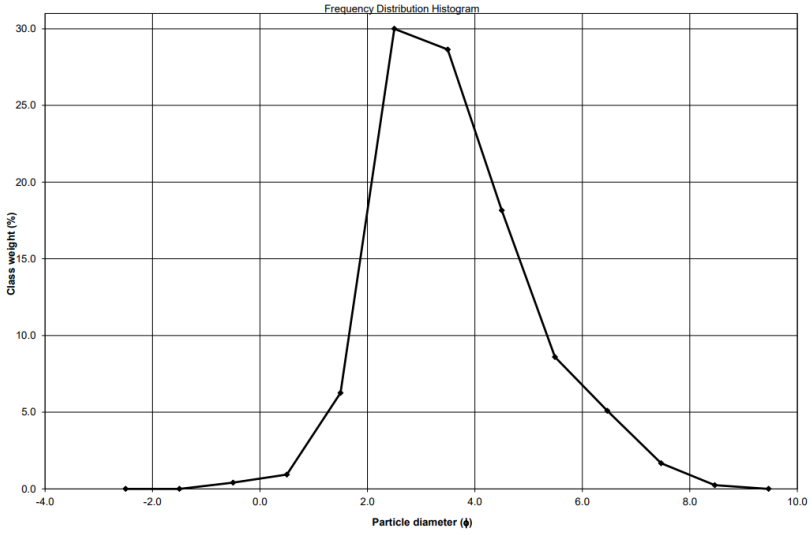

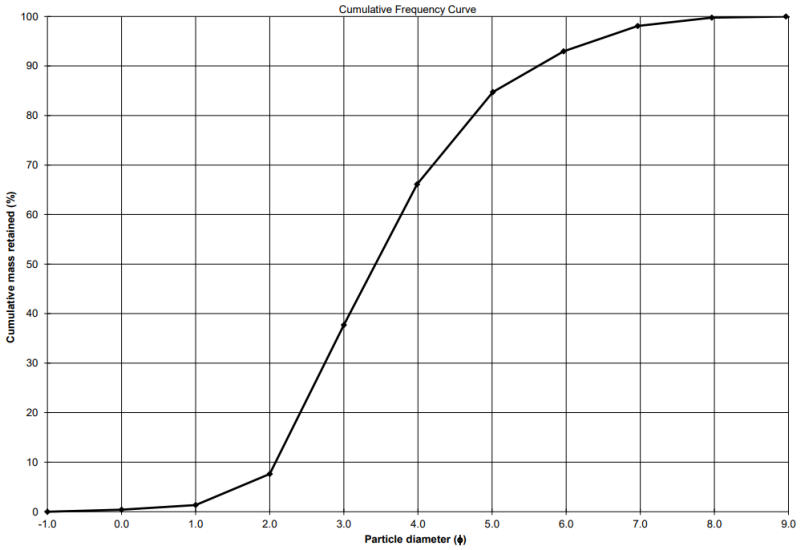

BAT-1

SAMPLE STATISTICS

SIEVING ERROR: 0.0%

SAMPLE IDENTITY: **4G**

ANALYST & DATE: J Fleming, 02/05/2024

SAMPLE TYPE: Bimodal, Very Poorly Sorted

TEXTURAL GROUP: Muddy Sand

SEDIMENT NAME: Coarse Silty Fine Sand

	µm	ϕ
MODE 1:	187.5	2.500
MODE 2:	23.50	5.489
MODE 3:		
D_{10}:	12.34	1.069
MEDIAN or D_{50}:	166.2	2.589
D_{90}:	476.6	6.340
(D_{90} / D_{10}):	38.61	5.930
(D_{90} - D_{10}):	464.2	5.271
(D_{75} / D_{25}):	8.181	2.789
(D_{75} - D_{25}):	271.2	3.032

GRAIN SIZE DISTRIBUTION

GRAVEL:	0.0%	COARSE SAND:	7.8%
SAND:	69.1%	MEDIUM SAND:	24.0%
MUD:	30.9%	FINE SAND:	30.0%
		V FINE SAND:	6.7%
V COARSE GRAVEL:	0.0%	V COARSE SILT:	8.1%
COARSE GRAVEL:	0.0%	COARSE SILT:	9.6%
MEDIUM GRAVEL:	0.0%	MEDIUM SILT:	9.3%
FINE GRAVEL:	0.0%	FINE SILT:	3.3%
V FINE GRAVEL:	0.0%	V FINE SILT:	0.6%
V COARSE SAND:	0.5%	CLAY:	0.0%

	METHOD OF MOMENTS			FOLK & WARD METHOD		
	Arithmetic µm	Geometric µm	Logarithmic ϕ	Geometric µm	Logarithmic ϕ	Description
MEAN ($\bar{x}$):	226.2	110.4	3.179	108.4	3.206	Very Fine Sand
SORTING (σ):	222.0	3.950	1.982	4.145	2.051	Very Poorly Sorted
SKEWNESS (Sk):	1.789	-0.697	0.697	-0.391	0.391	Very Fine Skewed
KURTOSIS (K):	8.109	2.462	2.462	0.851	0.851	Platykurtic

GRAIN SIZE DISTRIBUTION

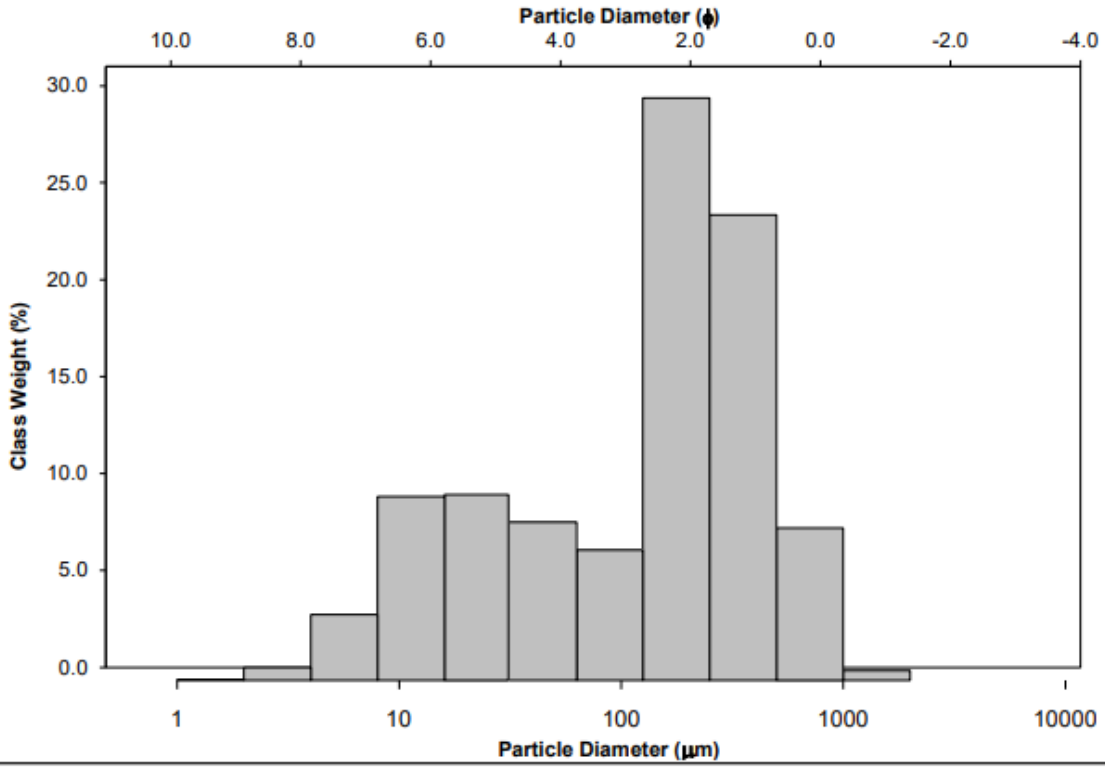

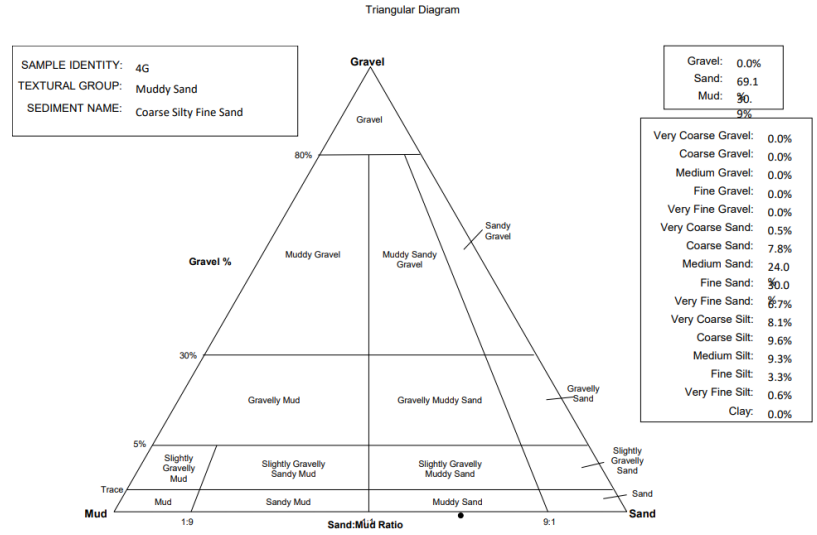
Triangular Diagram
SAMPLE IDENTITY: 4G
TEXTURAL GROUP: Muddy Sand
SEDIMENT NAME: Coarse Silty Fine Sand
Gravel: 0.0%
Sand: 69.1%
Mud: 30.9%
Very Coarse Gravel: 0.0%
Coarse Gravel: 0.0%
Medium Gravel: 0.0%
Fine Gravel: 0.0%
Very Fine Gravel: 0.0%
Very Coarse Sand: 0.5%
Coarse Sand: 7.8%
Medium Sand: 24.0%
Fine Sand: 30.0%
Very Fine Sand: 6.7%
Very Coarse Silt: 8.1%
Coarse Silt: 9.6%
Medium Silt: 9.3%
Fine Silt: 3.3%
Very Fine Silt: 0.6%
Clay: 0.0%
Gravel
Gravel
80%
Gravel %
Muddy Gravel
Muddy Sandy Gravel
Sandy Gravel
30%
Gravelly Mud
Gravelly Muddy Sand
Gravelly Sand
5%
Slightly Gravelly Mud
Slightly Gravelly Sandy Mud
Slightly Gravelly Muddy Sand
Slightly Gravelly Sand
Trace
Mud
Sandy Mud
Muddy Sand
Sand
Mud
1:9
Sand:Mud Ratio
9:1
Sand

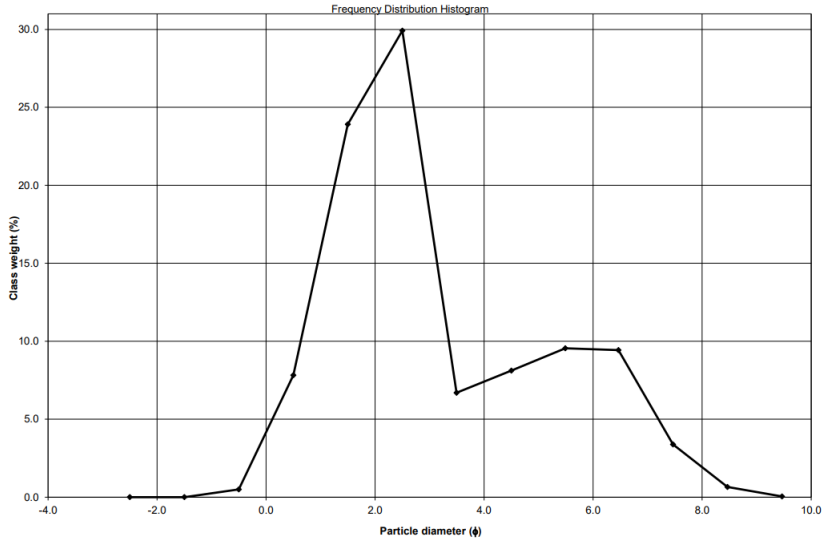
Frequency Distribution Histogram
Class weight (%)
30.0
25.0
20.0
15.0
10.0
5.0
0.0
-4.0
-2.0
0.0
2.0
4.0
6.0
8.0
10.0
Particle diameter (ϕ)

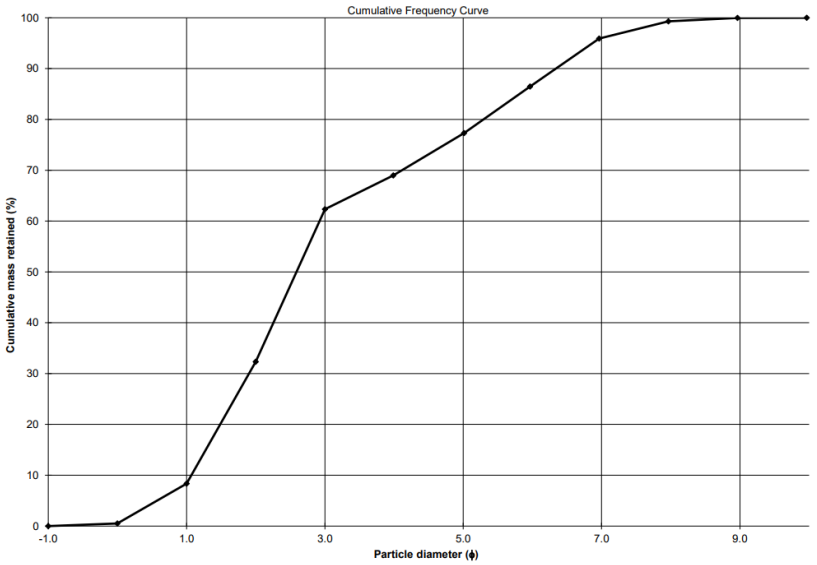
Cumulative Frequency Curve
Cumulative mass retained (%)
100
90
80
70
60
50
40
30
20
10
0
-1.0
1.0
3.0
5.0
7.0
9.0
Particle diameter (ϕ)

SAMPLE STATISTICS

SIEVING ERROR: 0.0%

SAMPLE IDENTITY: **10D**

ANALYST & DATE: J Fleming, 02/05/2024

SAMPLE TYPE: Unimodal, Poorly Sorted

TEXTURAL GROUP: Muddy Sand

SEDIMENT NAME: Very Coarse Silty Fine Sand

	µm	ϕ
MODE 1:	187.5	2.500
MODE 2:		
MODE 3:		
D_{10}:	21.07	1.489
MEDIAN or D_{50}:	106.1	3.236
D_{90}:	356.2	5.569
(D_{90} / D_{10}):	16.90	3.739
(D_{90} - D_{10}):	335.1	4.079
(D_{75} / D_{25}):	4.461	1.930
(D_{75} - D_{25}):	155.4	2.157

GRAIN SIZE DISTRIBUTION

GRAVEL:	0.0%	COARSE SAND:	3.8%
SAND:	66.4%	MEDIUM SAND:	11.0%
MUD:	33.6%	FINE SAND:	29.3%
		V FINE SAND:	21.5%
V COARSE GRAVEL:	0.0%	V COARSE SILT:	18.0%
COARSE GRAVEL:	0.0%	COARSE SILT:	9.6%
MEDIUM GRAVEL:	0.0%	MEDIUM SILT:	4.6%
FINE GRAVEL:	0.0%	FINE SILT:	1.3%
V FINE GRAVEL:	0.0%	V FINE SILT:	0.2%
V COARSE SAND:	0.8%	CLAY:	0.0%

	METHOD OF MOMENTS			FOLK & WARD METHOD		
	Arithmetic	Geometric	Logarithmic	Geometric	Logarithmic	Description
	µm	µm	ϕ	µm	ϕ	
MEAN ($\bar{x}$):	168.5	94.37	3.406	94.17	3.409	Very Fine Sand
SORTING (σ):	199.2	2.929	1.550	2.879	1.526	Poorly Sorted
SKEWNESS (Sk):	3.424	-0.294	0.294	-0.162	0.162	Fine Skewed
KURTOSIS (K):	19.54	2.937	2.937	0.984	0.984	Mesokurtic

GRAIN SIZE DISTRIBUTION

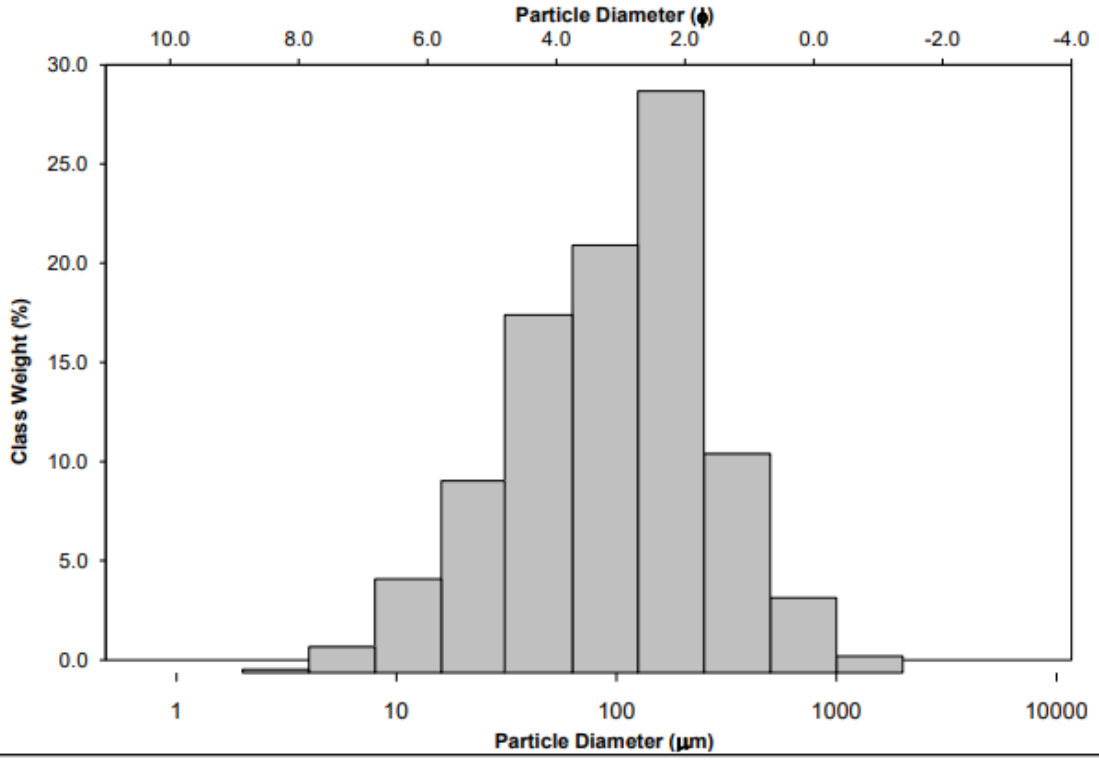

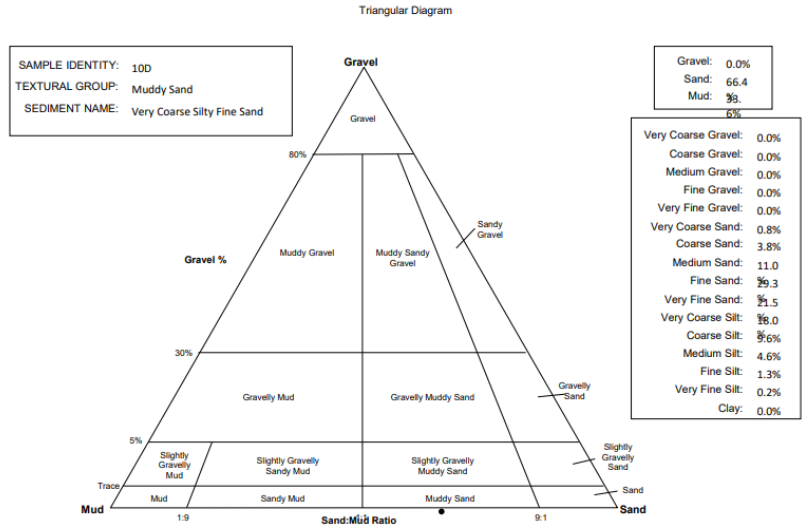
Triangular Diagram
SAMPLE IDENTITY: 10D
TEXTURAL GROUP: Muddy Sand
SEDIMENT NAME: Very Coarse Silty Fine Sand
Gravel: 0.0%
Sand: 66.4
Mud: 33.6%
Very Coarse Gravel: 0.0%
Coarse Gravel: 0.0%
Medium Gravel: 0.0%
Fine Gravel: 0.0%
Very Fine Gravel: 0.0%
Very Coarse Sand: 0.8%
Coarse Sand: 3.8%
Medium Sand: 11.0
Fine Sand: 29.3
Very Fine Sand: 21.5
Very Coarse Silt: 18.0
Coarse Silt: 9.6%
Medium Silt: 4.6%
Fine Silt: 1.3%
Very Fine Silt: 0.2%
Clay: 0.0%
Gravel
80%
30%
5%
Trace
Gravel %
Muddy Gravel
Muddy Sandy Gravel
Sandy Gravel
Gravelly Mud
Gravelly Muddy Sand
Gravelly Sand
Slightly Gravelly Mud
Slightly Gravelly Sandy Mud
Slightly Gravelly Muddy Sand
Slightly Gravelly Sand
Mud
Sandy Mud
Muddy Sand
Sand
Mud
1:9
Sand:Mud Ratio
9:1
Sand

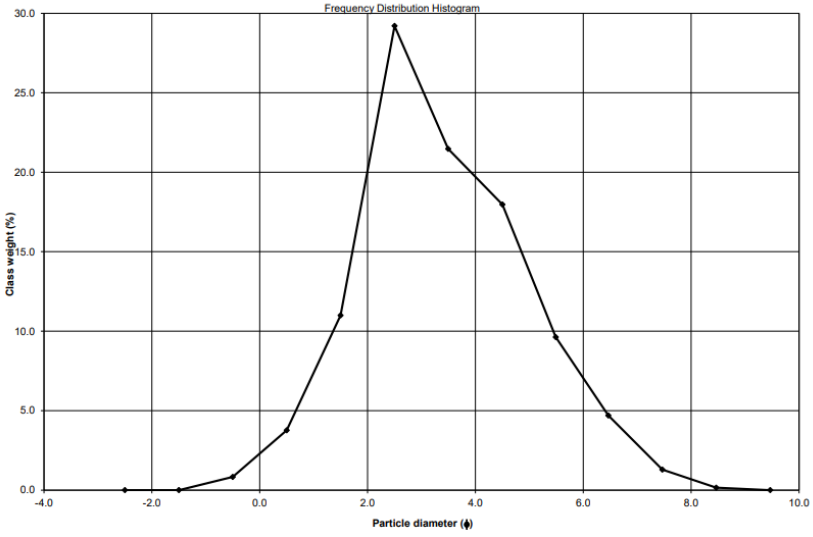
Frequency Distribution Histogram
Class weight (%)
30.0
25.0
20.0
15.0
10.0
5.0
0.0
-4.0
-2.0
0.0
2.0
4.0
6.0
8.0
10.0
Particle diameter (ϕ)

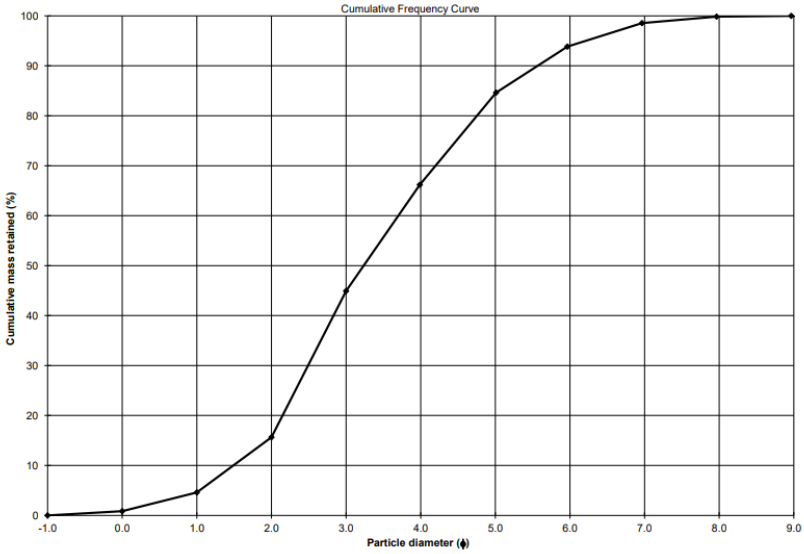
Cumulative Frequency Curve
Cumulative mass retained (%)
100
90
80
70
60
50
40
30
20
10
0
-1.0
0.0
1.0
2.0
3.0
4.0
5.0
6.0
7.0
8.0
9.0
Particle diameter (ϕ)

SAMPLE STATISTICS

SIEVING ERROR: 0.0%

SAMPLE IDENTITY: **16D**

ANALYST & DATE: J Fleming, 02/05/2024

SAMPLE TYPE: Bimodal, Poorly Sorted

TEXTURAL GROUP: Slightly Gravelly Muddy Sand

SEDIMENT NAME: Slightly Very Fine Gravelly Very Coarse Silty Fine Sand

	µm	ϕ
MODE 1:	187.5	2.500
MODE 2:	47.00	4.500
MODE 3:		
D_{10}:	17.05	1.387
MEDIAN or D_{50}:	122.4	3.030
D_{90}:	382.3	5.874
(D_{90} / D_{10}):	22.42	4.234
(D_{90} - D_{10}):	365.2	4.486
(D_{75} / D_{25}):	5.531	2.112
(D_{75} - D_{25}):	176.0	2.467

GRAIN SIZE DISTRIBUTION

GRAVEL:	0.0%	COARSE SAND:	4.0%
SAND:	64.3%	MEDIUM SAND:	13.3%
MUD:	35.7%	FINE SAND:	31.4%
		V FINE SAND:	14.8%
V COARSE GRAVEL:	0.0%	V COARSE SILT:	15.6%
COARSE GRAVEL:	0.0%	COARSE SILT:	11.4%
MEDIUM GRAVEL:	0.0%	MEDIUM SILT:	6.6%
FINE GRAVEL:	0.0%	FINE SILT:	1.8%
V FINE GRAVEL:	0.0%	V FINE SILT:	0.3%
V COARSE SAND:	0.8%	CLAY:	0.0%

	METHOD OF MOMENTS			FOLK & WARD METHOD		
	Arithmetic	Geometric	Logarithmic	Geometric	Logarithmic	Description
	µm	µm	ϕ	µm	ϕ	
MEAN ($\bar{x}$):	176.9	92.62	3.433	94.25	3.407	Very Fine Sand
SORTING (σ):	211.2	3.255	1.703	3.289	1.717	Poorly Sorted
SKEWNESS (Sk):	3.732	-0.381	0.381	-0.296	0.296	Fine Skewed
KURTOSIS (K):	27.59	2.617	2.617	0.920	0.920	Mesokurtic

GRAIN SIZE DISTRIBUTION

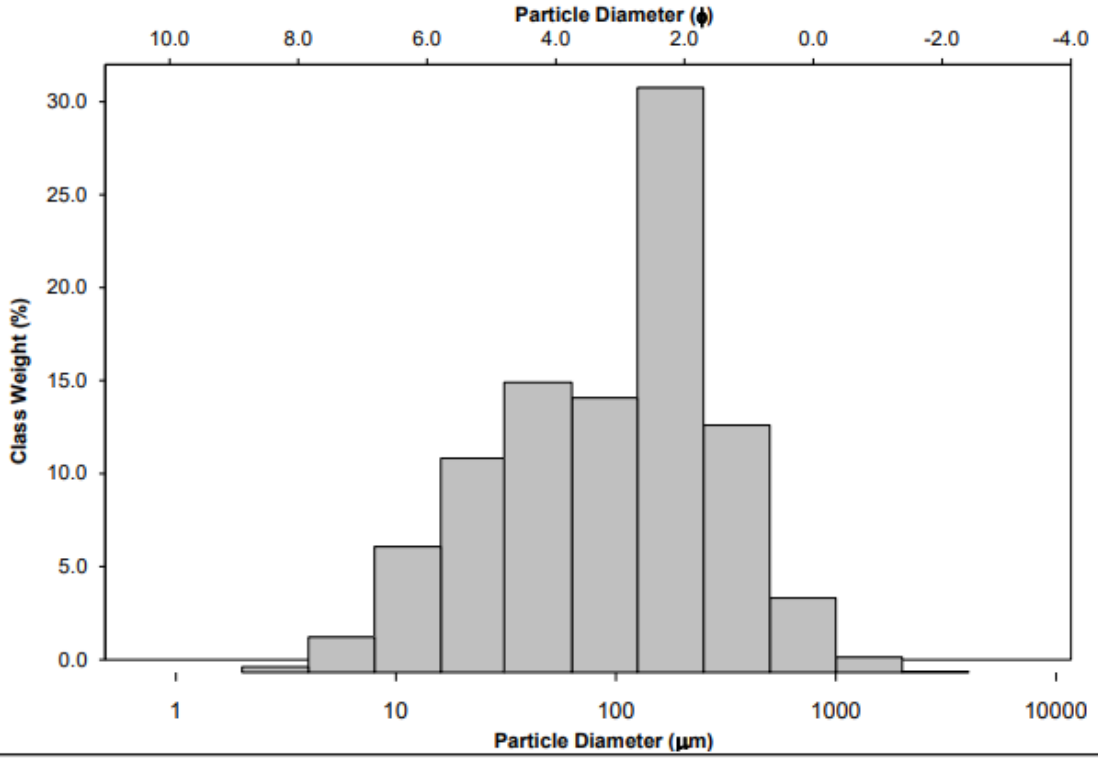

Triangular Diagram

SAMPLE IDENTITY: 16D
TEXTURAL GROUP: Slightly Gravelly Muddy Sand
SEDIMENT NAME: Slightly Very Fine Gravelly Very Coarse Silty Fine Sand

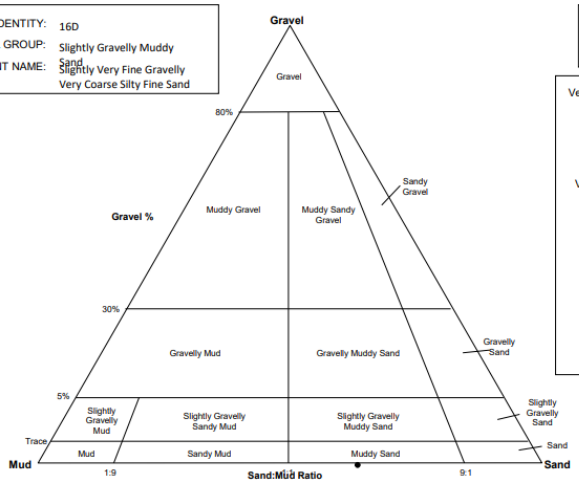

Gravel:	0.0%
Sand:	64.3
Mud:	35.7%

Very Coarse Gravel:	0.0%
Coarse Gravel:	0.0%
Medium Gravel:	0.0%
Fine Gravel:	0.0%
Very Fine Gravel:	0.0%
Very Coarse Sand:	0.8%
Coarse Sand:	4.0%
Medium Sand:	13.3
Fine Sand:	31.4
Very Fine Sand:	14.8
Very Coarse Silt:	15.6
Coarse Silt:	11.4
Medium Silt:	6.6%
Fine Silt:	1.8%
Very Fine Silt:	0.3%
Clay:	0.0%

Frequency Distribution Histogram

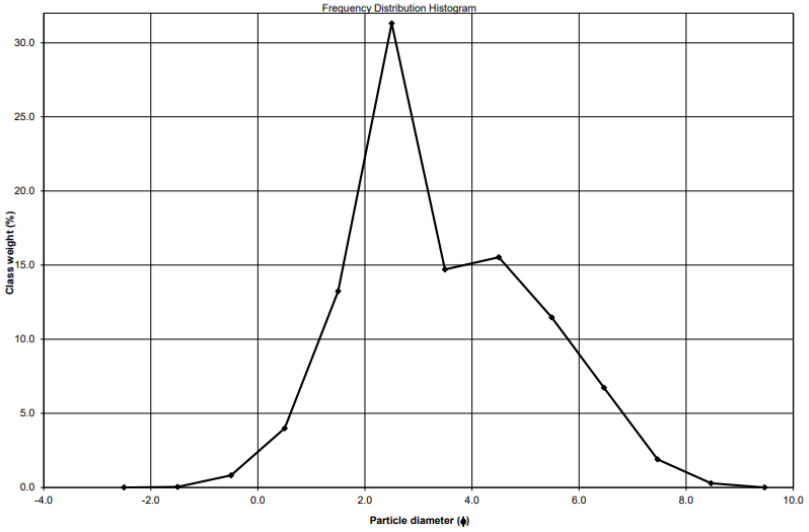

Cumulative Frequency Curve

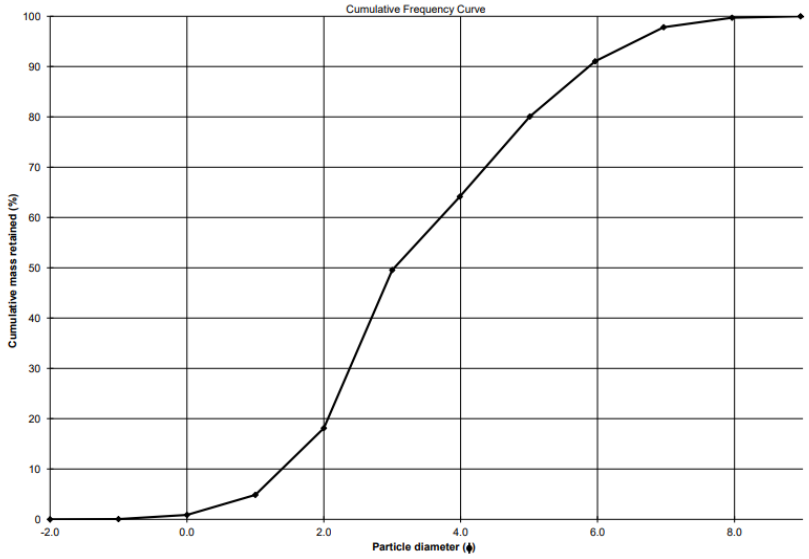

SAMPLE STATISTICS

SIEVING ERROR: 0.0%

SAMPLE IDENTITY: **17K**

ANALYST & DATE: J Fleming, 02/05/2024

SAMPLE TYPE: Bimodal, Poorly Sorted

TEXTURAL GROUP: Slightly Gravelly Muddy Sand

SEDIMENT NAME: Slightly Very Fine Gravelly Medium Silty Fine Sand

	µm	ϕ
MODE 1:	187.5	2.500
MODE 2:	12.00	6.466
MODE 3:		
D_{10}:	10.80	1.319
MEDIAN or D_{50}:	138.7	2.850
D_{90}:	400.9	6.533
(D_{90} / D_{10}):	37.14	4.955
(D_{90} - D_{10}):	390.1	5.215
(D_{75} / D_{25}):	7.057	2.321
(D_{75} - D_{25}):	195.6	2.819

GRAIN SIZE DISTRIBUTION

GRAVEL:	0.7%	COARSE SAND:	3.4%
SAND:	65.0%	MEDIUM SAND:	15.2%
MUD:	34.3%	FINE SAND:	34.9%
		V FINE SAND:	10.5%
V COARSE GRAVEL:	0.0%	V COARSE SILT:	9.7%
COARSE GRAVEL:	0.0%	COARSE SILT:	9.0%
MEDIUM GRAVEL:	0.0%	MEDIUM SILT:	10.1%
FINE GRAVEL:	0.3%	FINE SILT:	4.4%
V FINE GRAVEL:	0.4%	V FINE SILT:	0.9%
V COARSE SAND:	1.0%	CLAY:	0.1%

	METHOD OF MOMENTS			FOLK & WARD METHOD		
	Arithmetic	Geometric	Logarithmic	Geometric	Logarithmic	Description
	µm	µm	ϕ	µm	ϕ	
MEAN ($\bar{x}$):	210.2	90.15	3.471	88.11	3.504	Very Fine Sand
SORTING (σ):	405.7	3.964	1.987	3.967	1.988	Poorly Sorted
SKEWNESS (Sk):	9.189	-0.468	0.468	-0.422	0.422	Very Fine Skewed
KURTOSIS (K):	116.0	2.689	2.689	0.891	0.891	Platykurtic

GRAIN SIZE DISTRIBUTION

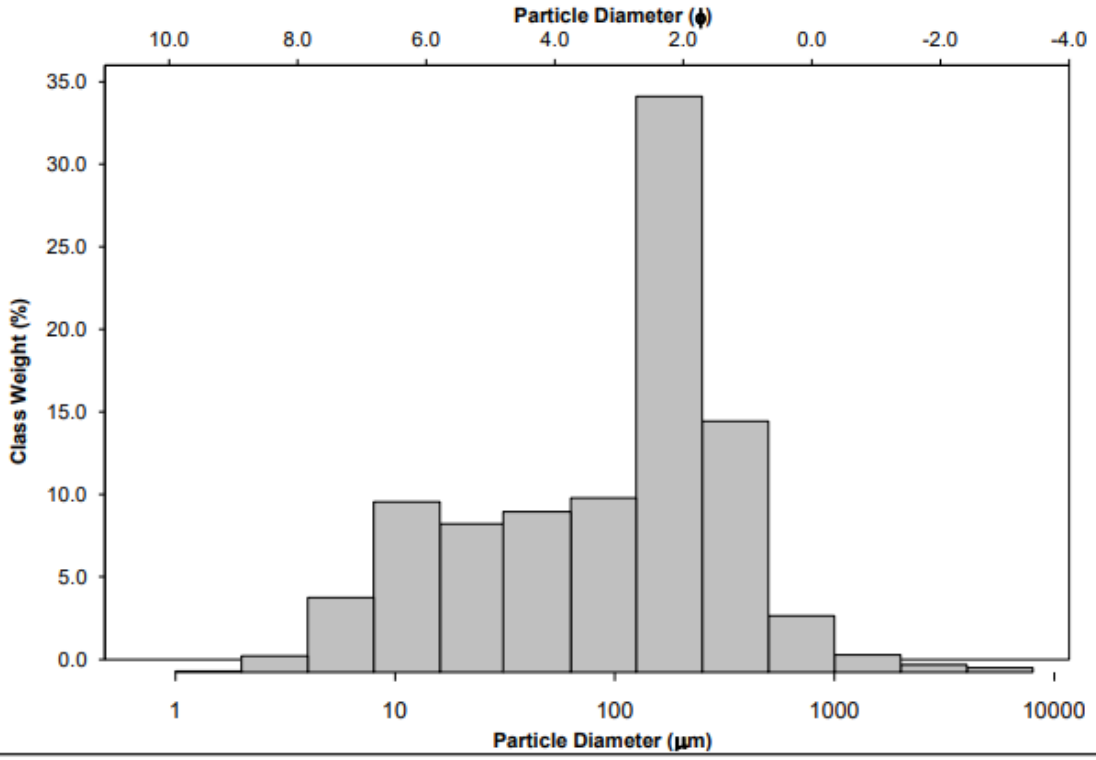

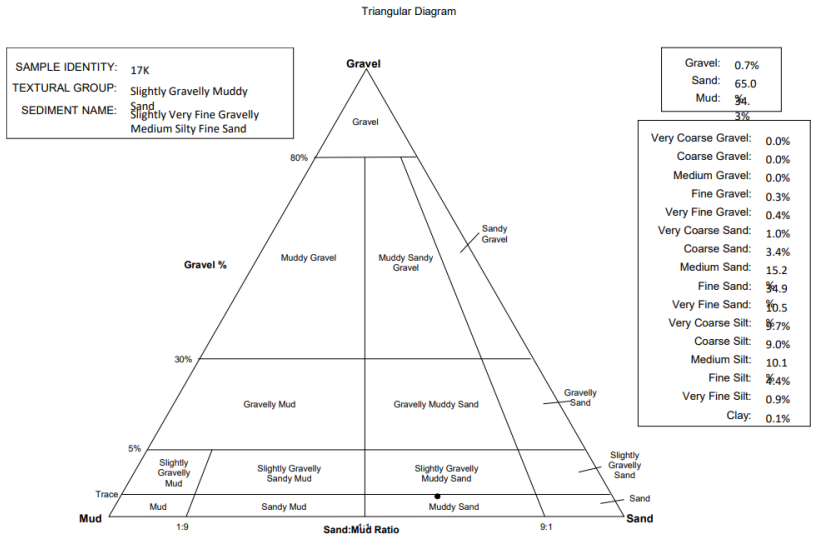
Triangular Diagram
SAMPLE IDENTITY: 17K
TEXTURAL GROUP: Slightly Gravelly Muddy Sand
SEDIMENT NAME: Slightly Very Fine Gravelly Medium Silty Fine Sand
Gravel: 0.7%
Sand: 65.0
Mud: 34.3%
Very Coarse Gravel: 0.0%
Coarse Gravel: 0.0%
Medium Gravel: 0.0%
Fine Gravel: 0.3%
Very Fine Gravel: 0.4%
Very Coarse Sand: 1.0%
Coarse Sand: 3.4%
Medium Sand: 15.2
Fine Sand: 34.9
Very Fine Sand: 10.5
Very Coarse Silt: 9.7%
Coarse Silt: 9.0%
Medium Silt: 10.1
Fine Silt: 6.4%
Very Fine Silt: 0.9%
Clay: 0.1%
Gravel
80%
30%
5%
Trace
Mud
Gravel %
Muddy Gravel
Muddy Sandy Gravel
Sandy Gravel
Gravelly Mud
Gravelly Muddy Sand
Gravelly Sand
Slightly Gravelly Mud
Slightly Gravelly Sandy Mud
Slightly Gravelly Muddy Sand
Slightly Gravelly Sand
Mud
Sandy Mud
Muddy Sand
Sand
1:9
9:1
Sand:Mud Ratio
Sand

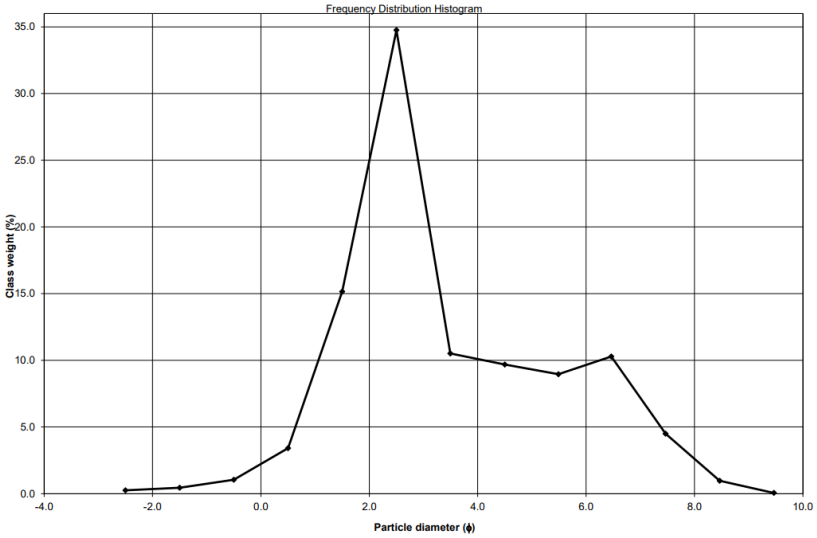
Frequency Distribution Histogram
Class weight (%)
35.0
30.0
25.0
20.0
15.0
10.0
5.0
0.0
-4.0
-2.0
0.0
2.0
4.0
6.0
8.0
10.0
Particle diameter (ϕ)

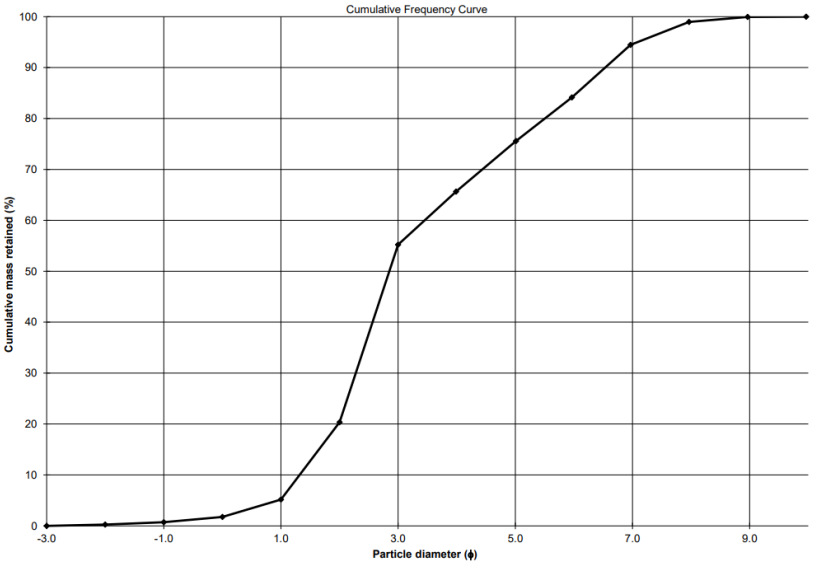
Cumulative Frequency Curve
Cumulative mass retained (%)
100
90
80
70
60
50
40
30
20
10
0
-3.0
-1.0
1.0
3.0
5.0
7.0
9.0
Particle diameter (ϕ)

OL-2

SAMPLE STATISTICS

SIEVING ERROR: 0.0%

SAMPLE IDENTITY: **18D**

ANALYST & DATE: J Fleming, 02/05/2024

SAMPLE TYPE: Bimodal, Very Poorly Sorted

TEXTURAL GROUP: Gravelly Muddy Sand

SEDIMENT NAME: Very Fine Gravelly Very Coarse Silty Coarse Sand

	µm	ϕ
MODE 1:	750.0	0.500
MODE 2:	47.00	4.500
MODE 3:		
D_{10}:	18.42	-0.585
MEDIAN or D_{50}:	364.6	1.456
D_{90}:	1499.8	5.763
(D_{90} / D_{10}):	81.43	-9.854
(D_{90} - D_{10}):	1481.4	6.348
(D_{75} / D_{25}):	9.845	10.32
(D_{75} - D_{25}):	702.9	3.299

GRAIN SIZE DISTRIBUTION

GRAVEL:	6.0%	COARSE SAND:	26.4%
SAND:	71.2%	MEDIUM SAND:	17.4%
MUD:	22.8%	FINE SAND:	11.4%
		V FINE SAND:	6.3%
V COARSE GRAVEL:	0.0%	V COARSE SILT:	7.5%
COARSE GRAVEL:	0.0%	COARSE SILT:	6.9%
MEDIUM GRAVEL:	0.0%	MEDIUM SILT:	5.8%
FINE GRAVEL:	2.6%	FINE SILT:	2.1%
V FINE GRAVEL:	3.4%	V FINE SILT:	0.5%
V COARSE SAND:	9.7%	CLAY:	0.0%

	METHOD OF MOMENTS			FOLK & WARD METHOD		
	Arithmetic	Geometric	Logarithmic	Geometric	Logarithmic	Description
	µm	µm	ϕ	µm	ϕ	
MEAN ($\bar{x}$):	698.8	245.2	2.028	229.5	2.124	Fine Sand
SORTING (σ):	1069.5	5.213	2.382	5.327	2.413	Very Poorly Sorted
SKEWNESS (Sk):	3.442	-0.571	0.571	-0.356	0.356	Very Fine Skewed
KURTOSIS (K):	16.41	2.642	2.642	0.977	0.977	Mesokurtic

GRAIN SIZE DISTRIBUTION

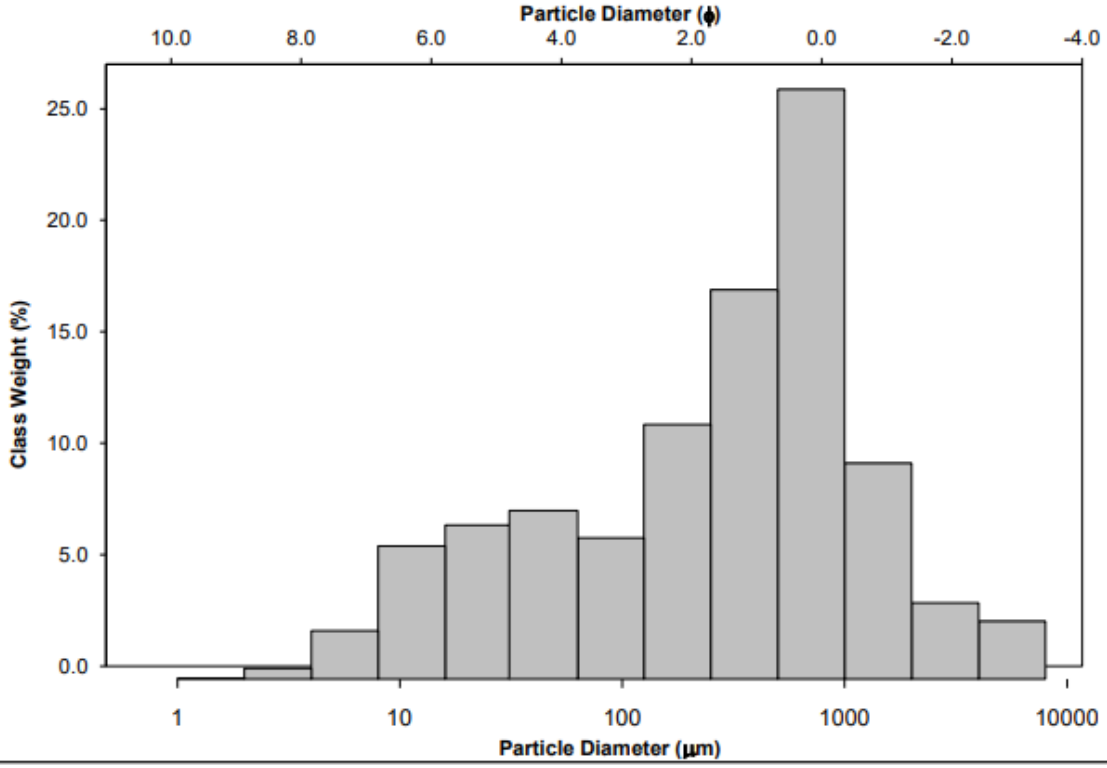

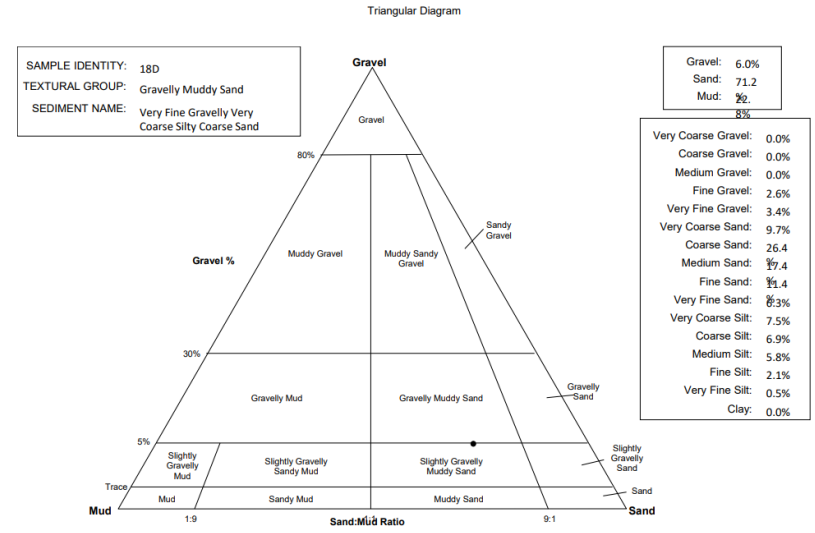
Triangular Diagram
SAMPLE IDENTITY: 18D
TEXTURAL GROUP: Gravelly Muddy Sand
SEDIMENT NAME: Very Fine Gravelly Very Coarse Silty Coarse Sand
Gravel
Gravel
80%
Sandy Gravel
Gravel %
Muddy Gravel
Muddy Sandy Gravel
30%
Gravelly Mud
Gravelly Muddy Sand
Gravelly Sand
5%
Slightly Gravelly Mud
Slightly Gravelly Sandy Mud
Slightly Gravelly Muddy Sand
Slightly Gravelly Sand
Trace
Mud
Sandy Mud
Muddy Sand
Sand
Mud
Sand
1:9
Sand:Mud Ratio
9:1
Gravel: 6.0%
Sand: 71.2
Mud: 22.8%
Very Coarse Gravel: 0.0%
Coarse Gravel: 0.0%
Medium Gravel: 0.0%
Fine Gravel: 2.6%
Very Fine Gravel: 3.4%
Very Coarse Sand: 9.7%
Coarse Sand: 26.4
Medium Sand: 17.4
Fine Sand: 11.4
Very Fine Sand: 6.3%
Very Coarse Silt: 7.5%
Coarse Silt: 6.9%
Medium Silt: 5.8%
Fine Silt: 2.1%
Very Fine Silt: 0.5%
Clay: 0.0%

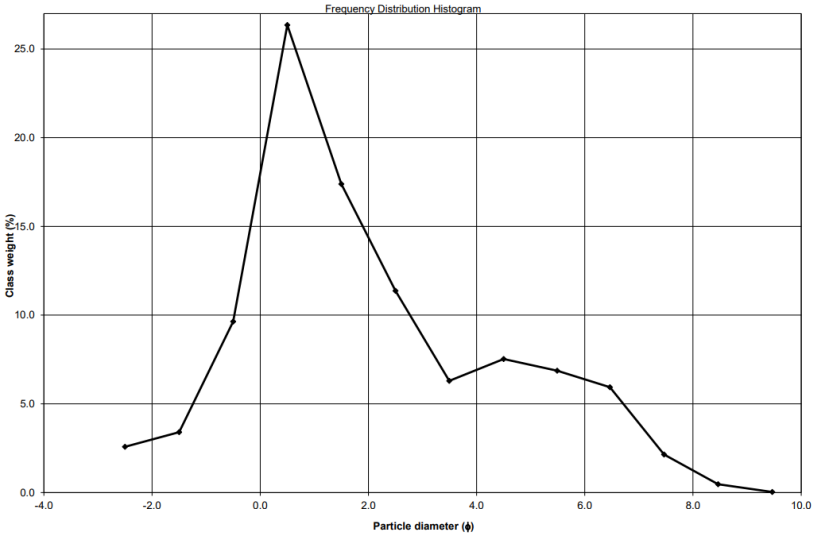
Frequency Distribution Histogram
Class weight (%)
25.0
20.0
15.0
10.0
5.0
0.0
-4.0
-2.0
0.0
2.0
4.0
6.0
8.0
10.0
Particle diameter (ϕ)

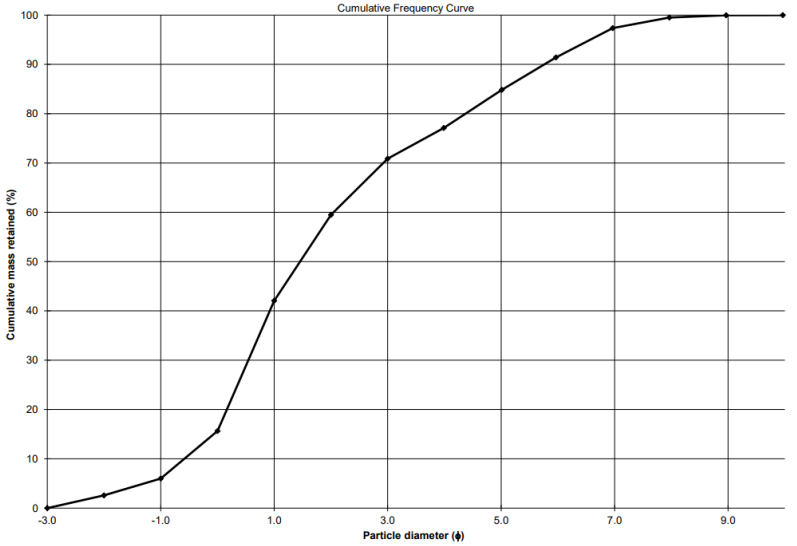
Cumulative Frequency Curve
Cumulative mass retained (%)
100
90
80
70
60
50
40
30
20
10
0
-3.0
-1.0
1.0
3.0
5.0
7.0
9.0
Particle diameter (ϕ)

OL-1

SAMPLE STATISTICS

SIEVING ERROR: 0.0%

SAMPLE IDENTITY: **21C**

ANALYST & DATE: J Fleming, 02/05/2024

SAMPLE TYPE: Unimodal, Moderately Sorted

TEXTURAL GROUP: Gravel

SEDIMENT NAME: Fine Gravel

	µm	ϕ
MODE 1:	6000.0	-2.500
MODE 2:		
MODE 3:		
D_{10}:	136.7	-9.981
MEDIAN or D_{50}:	7855.8	-2.974
D_{90}:	1010417.5	2.871
(D_{90} / D_{10}):	7389.4	-0.288
(D_{90} - D_{10}):	1010280.8	12.85
(D_{75} / D_{25}):	0.742	1.284
(D_{75} - D_{25}):	-999.907	-0.431

GRAIN SIZE DISTRIBUTION

GRAVEL:	83.0%	COARSE SAND:	0.9%
SAND:	9.3%	MEDIUM SAND:	1.5%
MUD:	7.7%	FINE SAND:	2.2%
		V FINE SAND:	2.0%
V COARSE GRAVEL:	0.0%	V COARSE SILT:	2.1%
COARSE GRAVEL:	0.0%	COARSE SILT:	1.8%
MEDIUM GRAVEL:	0.0%	MEDIUM SILT:	2.3%
FINE GRAVEL:	74.6%	FINE SILT:	1.2%
V FINE GRAVEL:	8.4%	V FINE SILT:	0.2%
V COARSE SAND:	2.7%	CLAY:	0.0%

	METHOD OF MOMENTS			FOLK & WARD METHOD		
	Arithmetic	Geometric	Logarithmic	Geometric	Logarithmic	Description
	µm	µm	ϕ	µm	ϕ	
MEAN ($\bar{x}$):	1828.5	37.07	-0.163	2881.9	-1.527	Very Fine Gravel
SORTING (σ):	2564.3	48.60	2.227	1.911	0.934	Moderately Sorted
SKEWNESS (Sk):	0.874	0.296	1.556	-7.388	7.388	Very Fine Skewed
KURTOSIS (K):	1.929	1.237	5.722	-5.326	-5.326	Very Platykurtic

GRAIN SIZE DISTRIBUTION

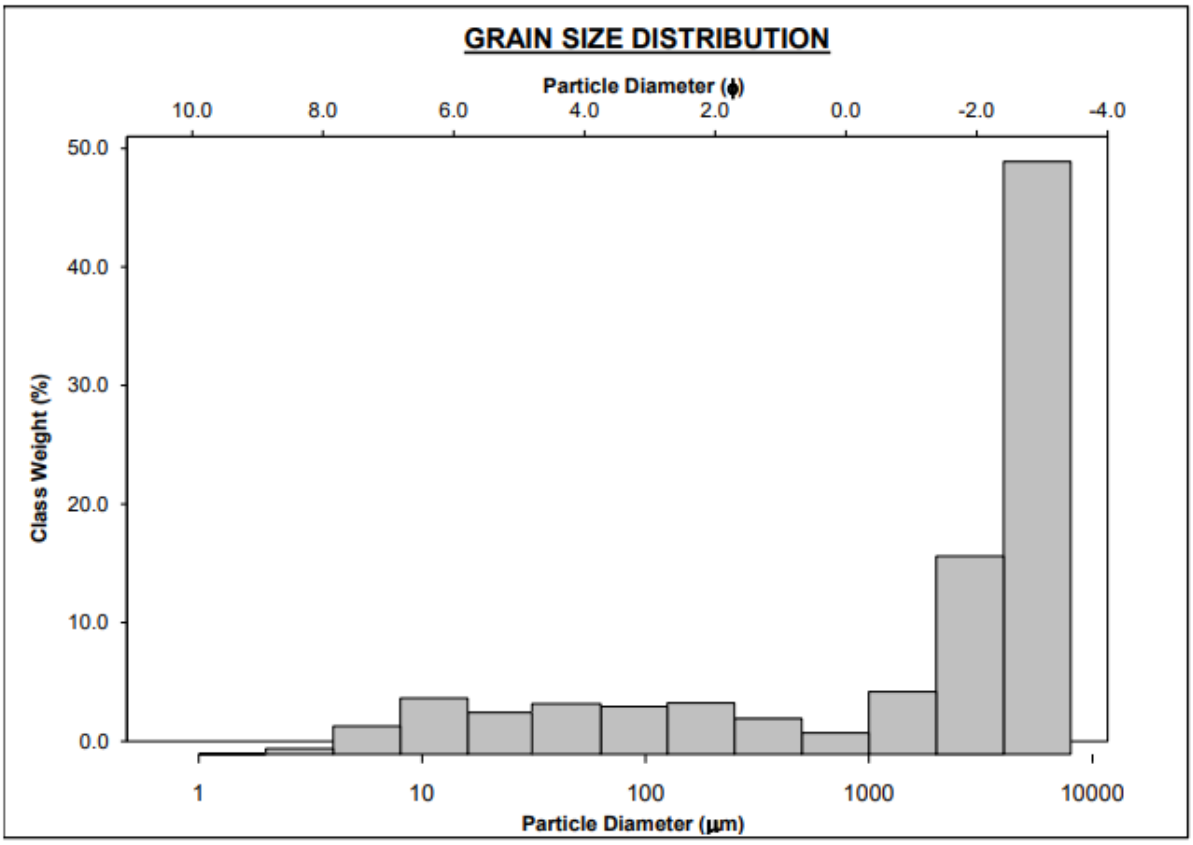

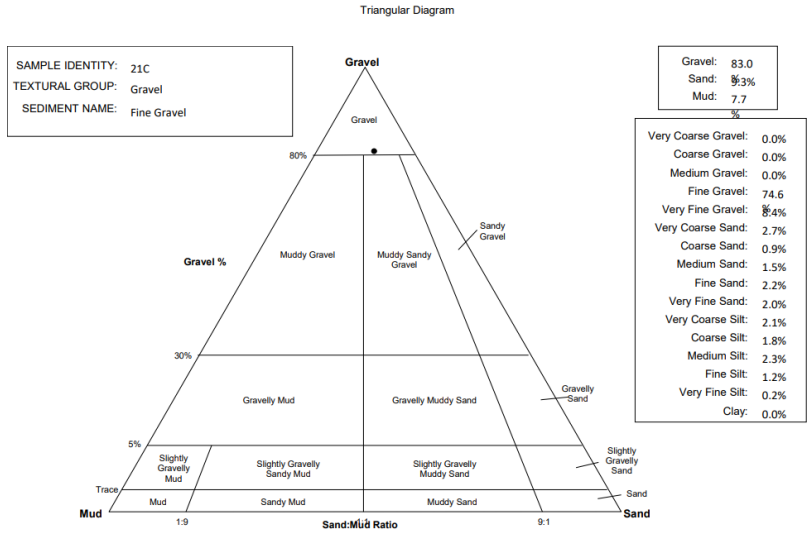
Triangular Diagram
SAMPLE IDENTITY: 21C
TEXTURAL GROUP: Gravel
SEDIMENT NAME: Fine Gravel
Gravel: 83.0 %
Sand: 9.3 %
Mud: 7.7 %
Very Coarse Gravel: 0.0%
Coarse Gravel: 0.0%
Medium Gravel: 0.0%
Fine Gravel: 74.6
Very Fine Gravel: 8.4%
Very Coarse Sand: 2.7%
Coarse Sand: 0.9%
Medium Sand: 1.5%
Fine Sand: 2.2%
Very Fine Sand: 2.0%
Very Coarse Silt: 2.1%
Coarse Silt: 1.8%
Medium Silt: 2.3%
Fine Silt: 1.2%
Very Fine Silt: 0.2%
Clay: 0.0%
Gravel
Gravel
80%
Gravel %
Muddy Gravel
Muddy Sandy Gravel
Sandy Gravel
30%
Gravelly Mud
Gravelly Muddy Sand
Gravelly Sand
5%
Slightly Gravelly Mud
Slightly Gravelly Sandy Mud
Slightly Gravelly Muddy Sand
Slightly Gravelly Sand
Trace
Mud
Sandy Mud
Muddy Sand
Sand
Mud
1:9
Sand:Mud Ratio
9:1
Sand

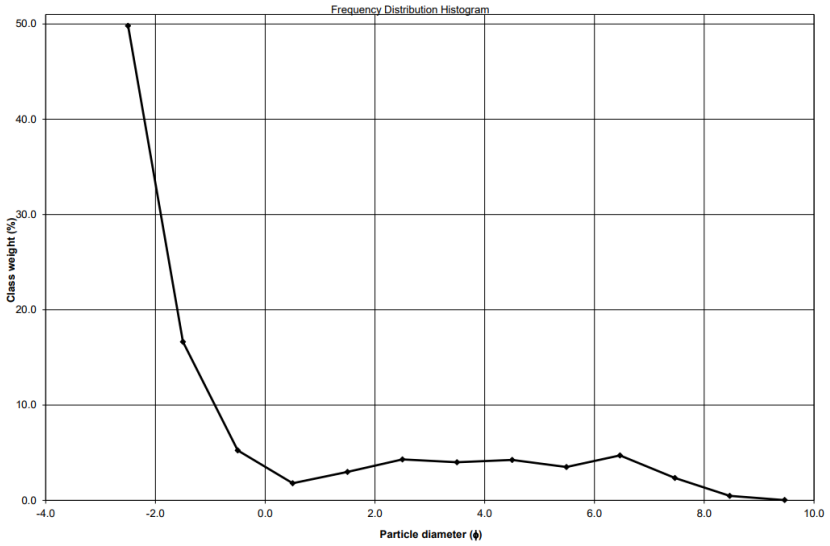
Frequency Distribution Histogram
Class weight (%)
50.0
40.0
30.0
20.0
10.0
0.0
-4.0
-2.0
0.0
2.0
4.0
6.0
8.0
10.0
Particle diameter (ϕ)

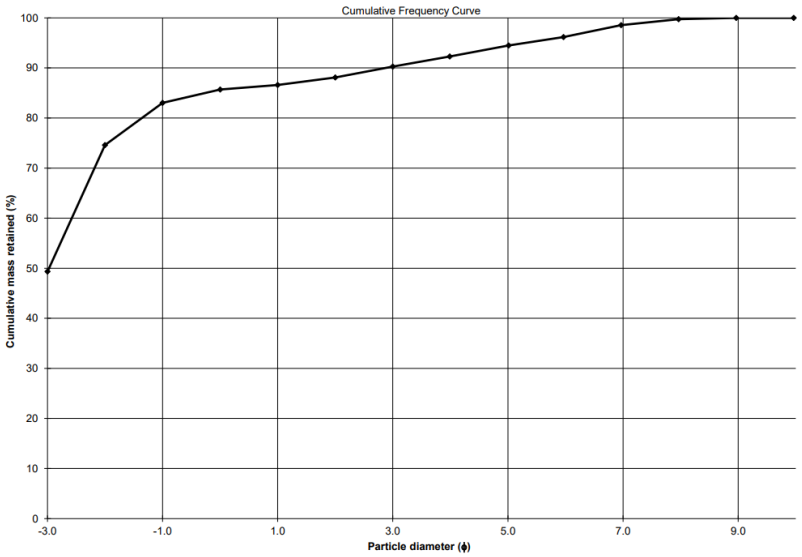
Cumulative Frequency Curve
Cumulative mass retained (%)
100
90
80
70
60
50
40
30
20
10
0
-3.0
-1.0
1.0
3.0
5.0
7.0
9.0
Particle diameter (ϕ)

SAMPLE STATISTICS

SIEVING ERROR: 0.0%

SAMPLE IDENTITY: **22D**

ANALYST & DATE: J Fleming, 02/05/2024

SAMPLE TYPE: Bimodal, Very Poorly Sorted

TEXTURAL GROUP: Muddy Sandy Gravel

SEDIMENT NAME: Very Coarse Silty Sandy Fine Gravel

	µm	ϕ
MODE 1:	3000.0	-1.500
MODE 2:	47.00	4.500
MODE 3:		
D_{10}:	19.80	-2.473
MEDIAN or D_{50}:	648.6	0.625
D_{90}:	5552.7	5.658
(D_{90} / D_{10}):	280.4	-2.288
(D_{90} - D_{10}):	5532.9	8.131
(D_{75} / D_{25}):	36.14	-2.659
(D_{75} - D_{25}):	2591.9	5.175

GRAIN SIZE DISTRIBUTION

GRAVEL:	31.3%	COARSE SAND:	10.8%
SAND:	45.3%	MEDIUM SAND:	8.5%
MUD:	23.4%	FINE SAND:	7.4%
		V FINE SAND:	6.7%
V COARSE GRAVEL:	0.0%	V COARSE SILT:	8.5%
COARSE GRAVEL:	0.0%	COARSE SILT:	7.3%
MEDIUM GRAVEL:	0.0%	MEDIUM SILT:	5.4%
FINE GRAVEL:	16.1%	FINE SILT:	1.8%
V FINE GRAVEL:	15.1%	V FINE SILT:	0.4%
V COARSE SAND:	12.0%	CLAY:	0.0%

	METHOD OF MOMENTS			FOLK & WARD METHOD		
	Arithmetic	Geometric	Logarithmic	Geometric	Logarithmic	Description
	µm	µm	ϕ	µm	ϕ	
MEAN ($\bar{x}$):	1551.4	328.8	1.289	447.4	1.160	Medium Sand
SORTING (σ):	1992.4	9.677	2.914	8.764	3.132	Very Poorly Sorted
SKEWNESS (Sk):	1.308	-0.620	0.452	-0.243	0.243	Fine Skewed
KURTOSIS (K):	3.405	2.542	2.035	0.738	0.738	Platykurtic

GRAIN SIZE DISTRIBUTION

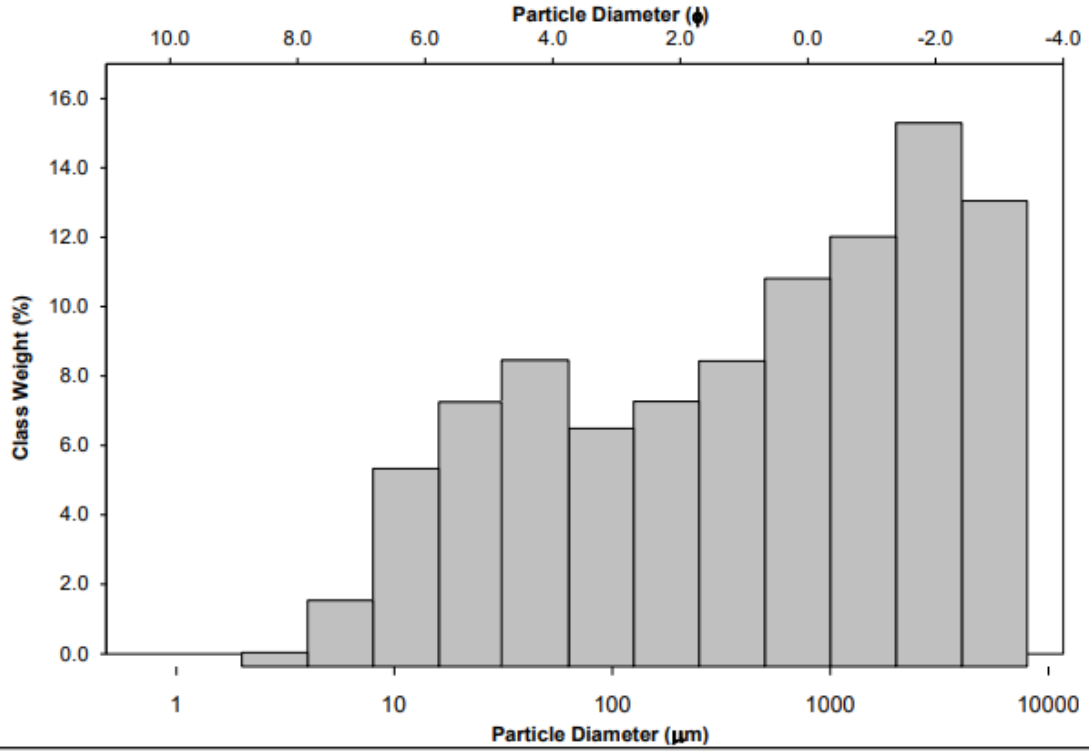

Triangular Diagram

SAMPLE IDENTITY: 22D
TEXTURAL GROUP: Muddy Sandy Gravel
SEDIMENT NAME: Very Coarse Silty Sandy Fine Gravel

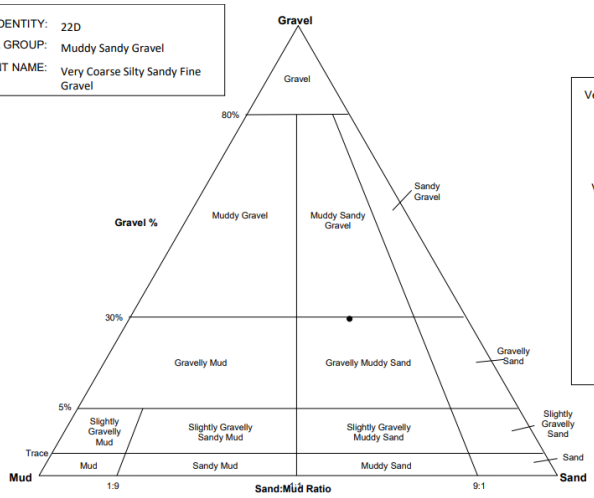

Gravel:	31.3 %
Sand:	45.3 %
Mud:	23.4%

Very Coarse Gravel:	0.0%
Coarse Gravel:	0.0%
Medium Gravel:	0.0%
Fine Gravel:	16.1 %
Very Fine Gravel:	15.1 %
Very Coarse Sand:	12.0 %
Coarse Sand:	10.8 %
Medium Sand:	8.5%
Fine Sand:	7.4%
Very Fine Sand:	6.7%
Very Coarse Silt:	8.5%
Coarse Silt:	7.3%
Medium Silt:	5.4%
Fine Silt:	1.8%
Very Fine Silt:	0.4%
Clay:	0.0%

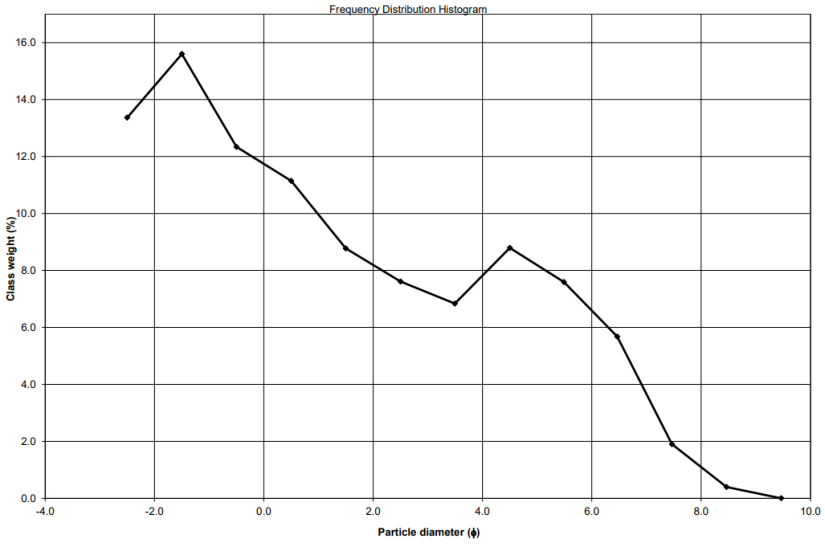

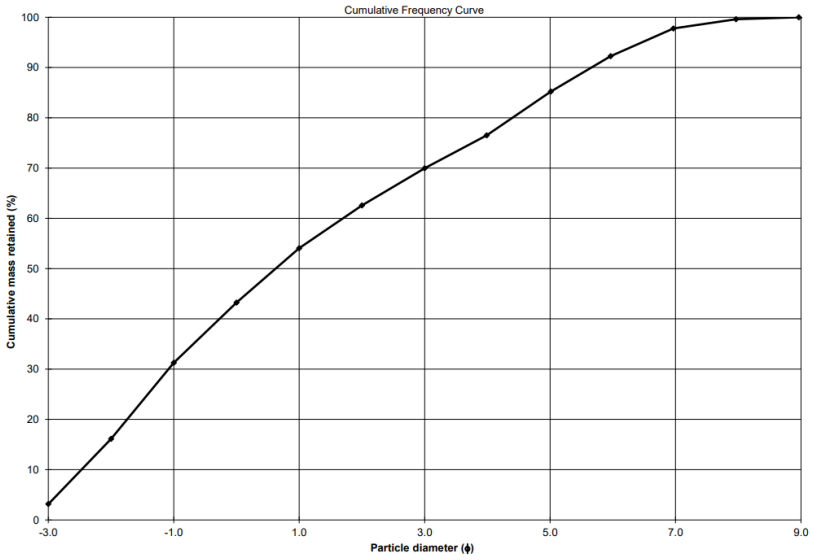

SAMPLE STATISTICS

SIEVING ERROR: 0.0%

SAMPLE IDENTITY: **23E**

ANALYST & DATE: J Fleming, 02/05/2024

SAMPLE TYPE: Trimodal, Very Poorly Sorted

TEXTURAL GROUP: Muddy Sandy Gravel

SEDIMENT NAME: Medium Silty Sandy Fine Gravel

	µm	ϕ
MODE 1:	1500.0	-0.500
MODE 2:	12.00	6.466
MODE 3:	47.00	4.500
D_{10}:	44.37	-3.961
MEDIAN or D_{50}:	1556.1	-0.638
D_{90}:	15569.0	4.494
(D_{90} / D_{10}):	350.9	-1.135
(D_{90} - D_{10}):	15524.6	8.455
(D_{75} / D_{25}):	10.82	-0.396
(D_{75} - D_{25}):	4996.2	3.436

GRAIN SIZE DISTRIBUTION

GRAVEL:	43.9%	COARSE SAND:	14.6%
SAND:	44.5%	MEDIUM SAND:	5.8%
MUD:	11.6%	FINE SAND:	4.4%
		V FINE SAND:	2.8%
V COARSE GRAVEL:	0.0%	V COARSE SILT:	3.3%
COARSE GRAVEL:	0.0%	COARSE SILT:	3.0%
MEDIUM GRAVEL:	0.0%	MEDIUM SILT:	3.6%
FINE GRAVEL:	30.8%	FINE SILT:	1.5%
V FINE GRAVEL:	13.1%	V FINE SILT:	0.3%
V COARSE SAND:	16.8%	CLAY:	0.0%

	METHOD OF MOMENTS			FOLK & WARD METHOD		
	Arithmetic	Geometric	Logarithmic	Geometric	Logarithmic	Description
	µm	µm	ϕ	µm	ϕ	
MEAN ($\bar{x}$):	1548.4	208.2	0.452	1156.5	-0.210	Very Coarse Sand
SORTING (σ):	1949.8	20.44	2.412	5.167	2.369	Very Poorly Sorted
SKEWNESS (Sk):	1.362	-0.787	1.235	-0.594	0.594	Very Fine Skewed
KURTOSIS (K):	3.621	2.152	4.084	0.824	0.824	Platykurtic

GRAIN SIZE DISTRIBUTION

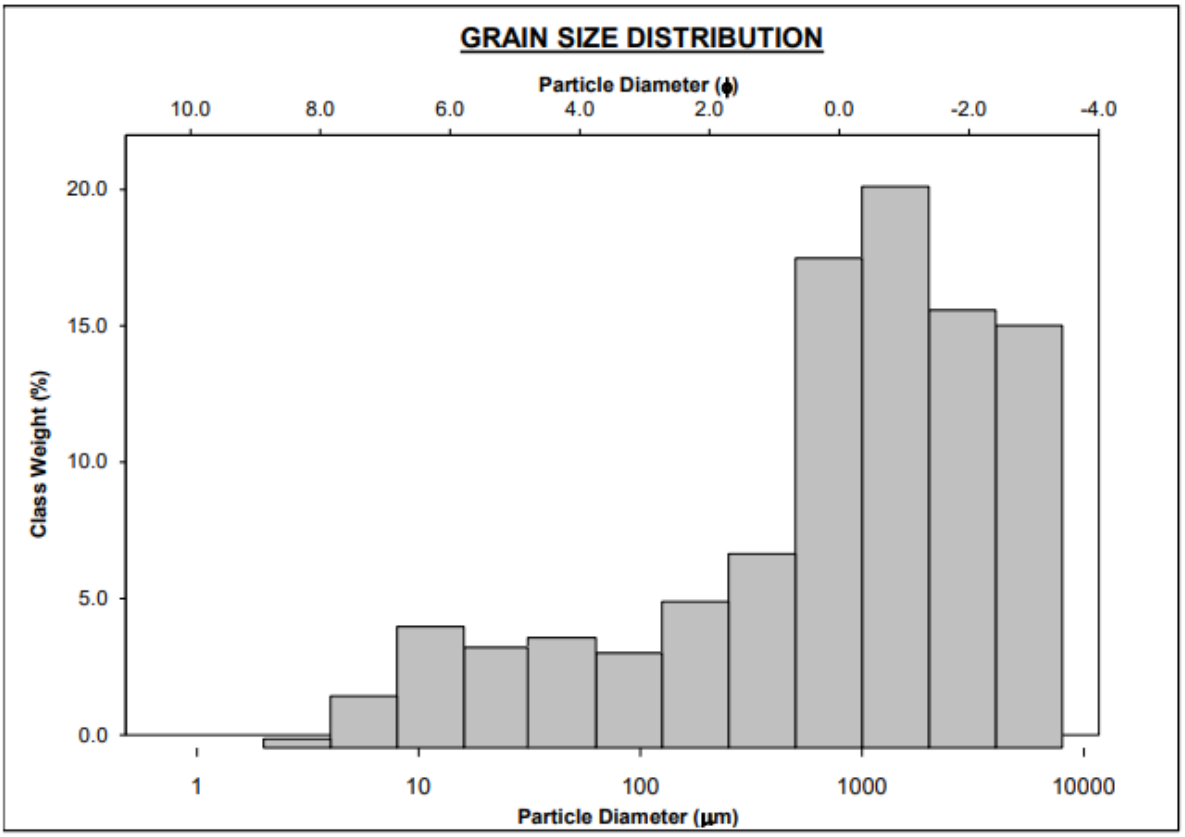

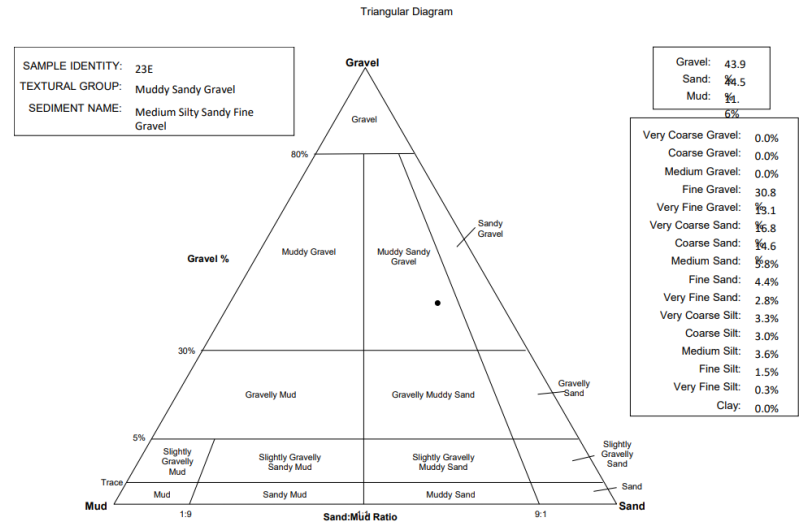
Triangular Diagram
SAMPLE IDENTITY: 23E
TEXTURAL GROUP: Muddy Sandy Gravel
SEDIMENT NAME: Medium Silty Sandy Fine Gravel
Gravel: 43.9 %
Sand: 44.5 %
Mud: 11.6%
Very Coarse Gravel: 0.0%
Coarse Gravel: 0.0%
Medium Gravel: 0.0%
Fine Gravel: 30.8 %
Very Fine Gravel: 13.1 %
Very Coarse Sand: 16.8 %
Coarse Sand: 14.6 %
Medium Sand: 5.8%
Fine Sand: 4.4%
Very Fine Sand: 2.8%
Very Coarse Silt: 3.3%
Coarse Silt: 3.0%
Medium Silt: 3.6%
Fine Silt: 1.5%
Very Fine Silt: 0.3%
Clay: 0.0%
Gravel
Gravel
80%
Gravel %
Muddy Gravel
Muddy Sandy Gravel
Sandy Gravel
30%
Gravelly Mud
Gravelly Muddy Sand
Gravelly Sand
5%
Slightly Gravelly Mud
Slightly Gravelly Sandy Mud
Slightly Gravelly Muddy Sand
Slightly Gravelly Sand
Trace
Mud
Sandy Mud
Muddy Sand
Sand
Mud
Sand
1:9
9:1
Sand:Mud Ratio

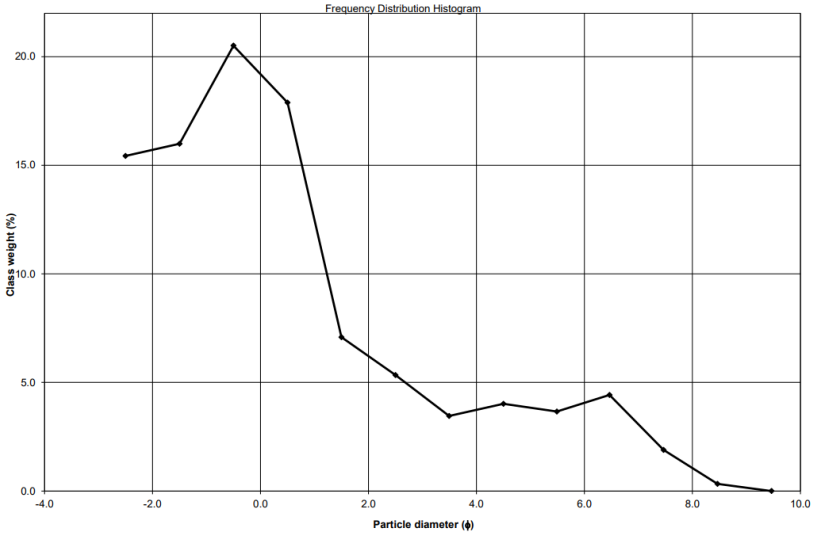
Frequency Distribution Histogram
Class weight (%)
20.0
15.0
10.0
5.0
0.0
-4.0
-2.0
0.0
2.0
4.0
6.0
8.0
10.0
Particle diameter (ϕ)

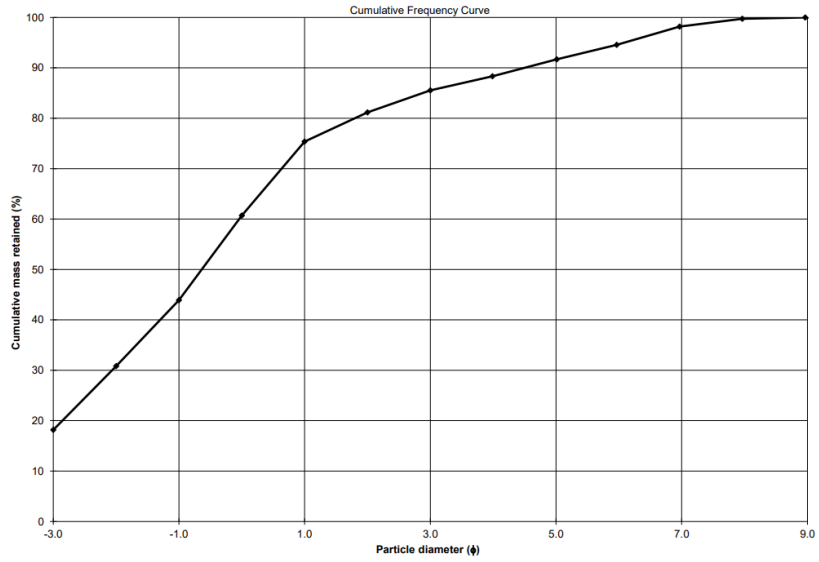
Cumulative Frequency Curve
Cumulative mass retained (%)
100
90
80
70
60
50
40
30
20
10
0
-3.0
-1.0
1.0
3.0
5.0
7.0
9.0
Particle diameter (ϕ)

OL-3

SAMPLE STATISTICS

SIEVING ERROR: 0.0%

SAMPLE IDENTITY: **25D**

ANALYST & DATE: J Fleming, 02/05/2024

SAMPLE TYPE: Trimodal, Very Poorly Sorted

TEXTURAL GROUP: Muddy Sandy Gravel

SEDIMENT NAME: Very Coarse Silty Sandy Fine Gravel

	µm	ϕ
MODE 1:	187.5	2.500
MODE 2:	6000.0	-2.500
MODE 3:	47.00	4.500
D_{10}:	27.65	-11.533
MEDIAN or D_{50}:	7759.7	-2.956
D_{90}:	2963778.5	5.177
(D_{90} / D_{10}):	107205.2	-0.449
(D_{90} - D_{10}):	2963750.9	16.71
(D_{75} / D_{25}):	15.79	-1.694
(D_{75} - D_{25}):	2609.3	3.981

GRAIN SIZE DISTRIBUTION

GRAVEL:	57.3%	COARSE SAND:	4.4%
SAND:	26.9%	MEDIUM SAND:	7.0%
MUD:	15.8%	FINE SAND:	9.3%
		V FINE SAND:	4.6%
V COARSE GRAVEL:	0.0%	V COARSE SILT:	5.0%
COARSE GRAVEL:	0.0%	COARSE SILT:	4.5%
MEDIUM GRAVEL:	0.0%	MEDIUM SILT:	4.3%
FINE GRAVEL:	55.8%	FINE SILT:	1.6%
V FINE GRAVEL:	1.5%	V FINE SILT:	0.3%
V COARSE SAND:	1.6%	CLAY:	0.0%

	METHOD OF MOMENTS			FOLK & WARD METHOD		
	Arithmetic	Geometric	Logarithmic	Geometric	Logarithmic	Description
	µm	µm	ϕ	µm	ϕ	
MEAN ($\bar{x}$):	458.7	12.48	1.267	989.2	0.016	Coarse Sand
SORTING (σ):	1352.0	18.06	2.327	4.665	2.222	Very Poorly Sorted
SKEWNESS (Sk):	3.578	0.628	1.030	-1.814	1.814	Very Fine Skewed
KURTOSIS (K):	14.53	1.975	3.403	0.678	0.678	Platykurtic

GRAIN SIZE DISTRIBUTION

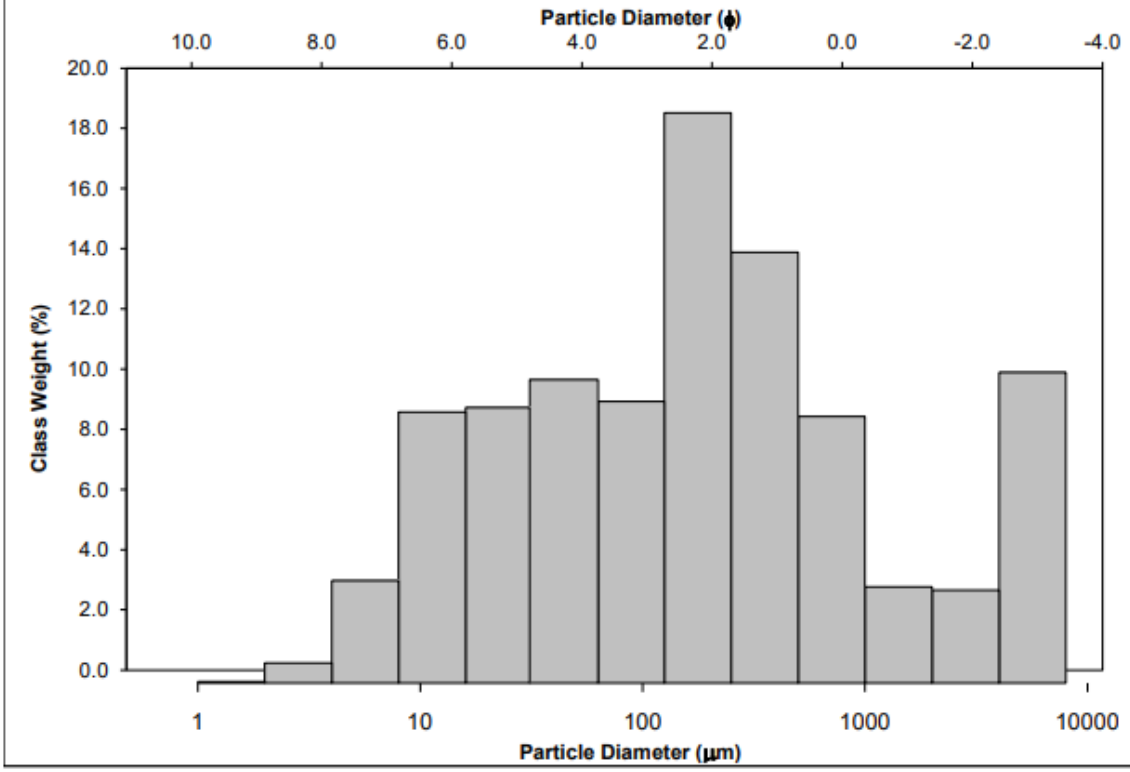

Triangular Diagram

SAMPLE IDENTITY:	25D
TEXTURAL GROUP:	Muddy Sandy Gravel
SEDIMENT NAME:	Very Coarse Silty Sandy Fine Gravel

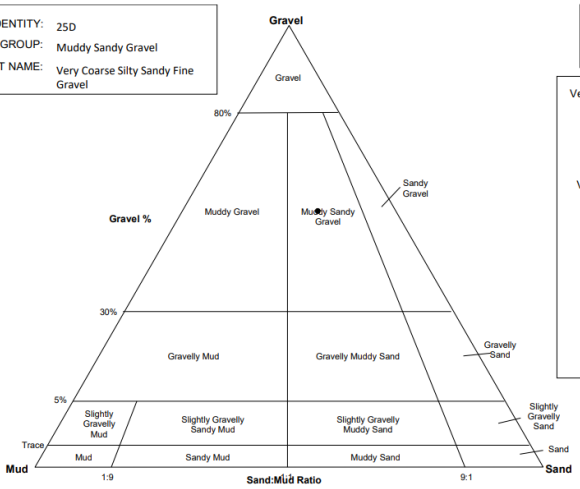

Gravel:	57.3
Sand:	26.9
Mud:	15.8%

Very Coarse Gravel:	0.0%
Coarse Gravel:	0.0%
Medium Gravel:	0.0%
Fine Gravel:	55.8
Very Fine Gravel:	1.5%
Very Coarse Sand:	1.6%
Coarse Sand:	4.4%
Medium Sand:	7.0%
Fine Sand:	9.3%
Very Fine Sand:	4.6%
Very Coarse Silt:	5.0%
Coarse Silt:	4.5%
Medium Silt:	4.3%
Fine Silt:	1.6%
Very Fine Silt:	0.3%
Clay:	0.0%

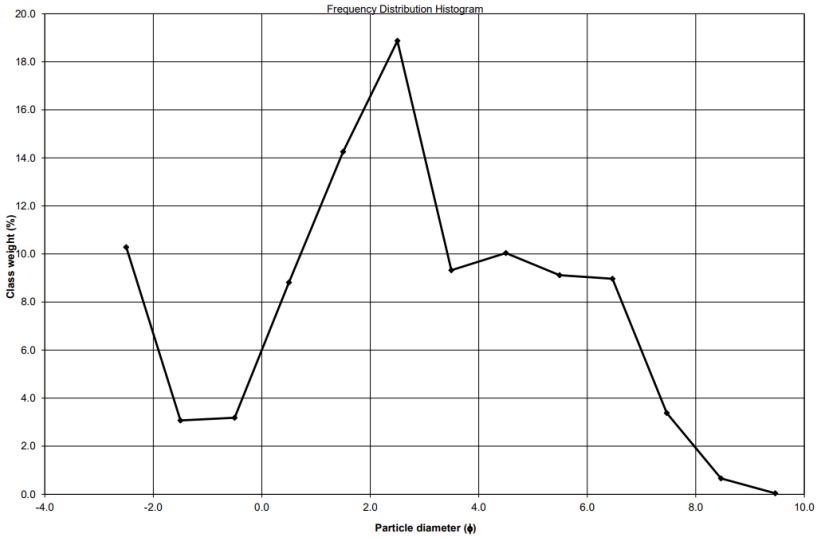

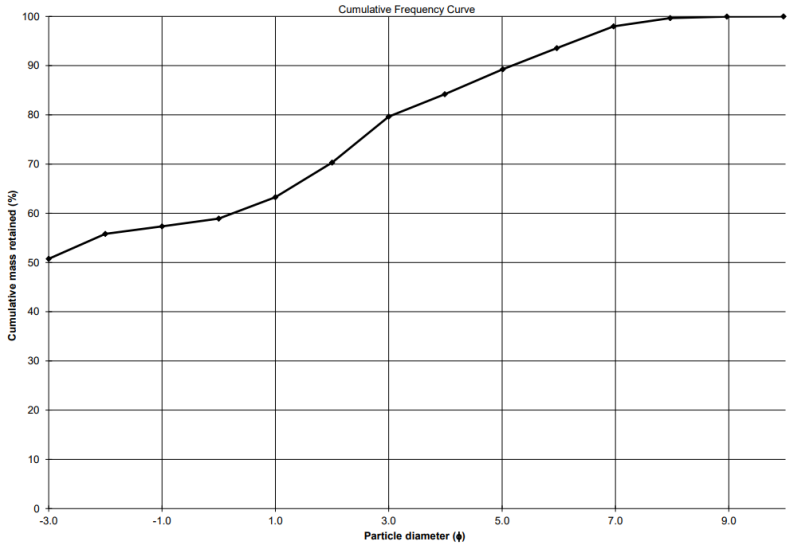

SAMPLE STATISTICS

SIEVING ERROR: 0.0%

SAMPLE IDENTITY: **26E**

ANALYST & DATE: J Fleming, 02/05/2024

SAMPLE TYPE: Trimodal, Very Poorly Sorted

TEXTURAL GROUP: Muddy Sandy Gravel

SEDIMENT NAME: Very Coarse Silty Sandy Fine Gravel

	µm	ϕ
MODE 1:	187.5	2.500
MODE 2:	6000.0	-2.500
MODE 3:	12.00	6.466
D_{10}:	22.87	-4.359
MEDIAN or D_{50}:	369.8	1.435
D_{90}:	20524.7	5.450
(D_{90} / D_{10}):	897.3	-1.250
(D_{90} - D_{10}):	20501.8	9.809
(D_{75} / D_{25}):	70.31	-1.256
(D_{75} - D_{25}):	6493.9	6.136

GRAIN SIZE DISTRIBUTION

GRAVEL:	39.4%	COARSE SAND:	3.8%
SAND:	41.2%	MEDIUM SAND:	10.6%
MUD:	19.5%	FINE SAND:	15.0%
		V FINE SAND:	9.5%
V COARSE GRAVEL:	0.0%	V COARSE SILT:	7.4%
COARSE GRAVEL:	0.0%	COARSE SILT:	4.5%
MEDIUM GRAVEL:	0.0%	MEDIUM SILT:	4.9%
FINE GRAVEL:	35.7%	FINE SILT:	2.2%
V FINE GRAVEL:	3.7%	V FINE SILT:	0.4%
V COARSE SAND:	2.2%	CLAY:	0.0%

	METHOD OF MOMENTS			FOLK & WARD METHOD		
	Arithmetic	Geometric	Logarithmic	Geometric	Logarithmic	Description
	µm	µm	ϕ	µm	ϕ	
MEAN ($\bar{x}$):	1145.6	80.94	1.551	435.4	1.200	Medium Sand
SORTING (σ):	2112.0	17.99	2.728	6.908	2.788	Very Poorly Sorted
SKEWNESS (Sk):	1.736	-0.183	0.273	-0.150	0.150	Fine Skewed
KURTOSIS (K):	4.218	1.968	2.338	0.483	0.483	Very Platykurtic

GRAIN SIZE DISTRIBUTION

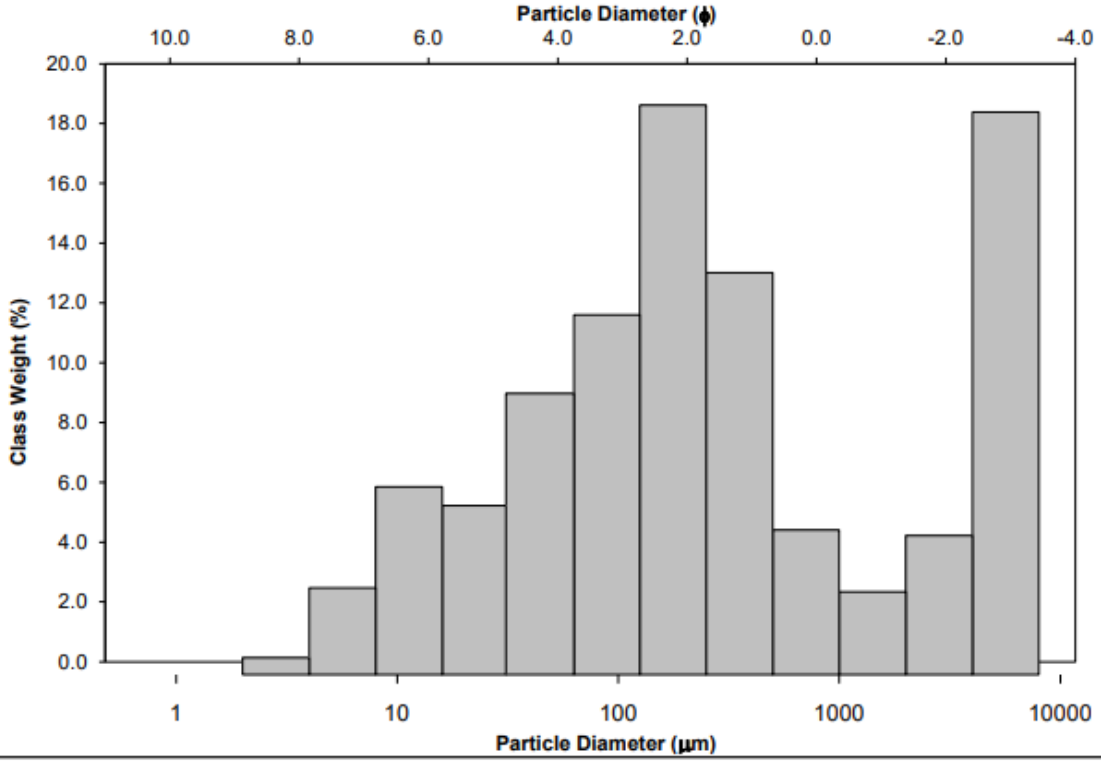

Triangular Diagram

SAMPLE IDENTITY:	26E
TEXTURAL GROUP:	Muddy Sandy Gravel
SEDIMENT NAME:	Very Coarse Silty Sandy Fine Gravel

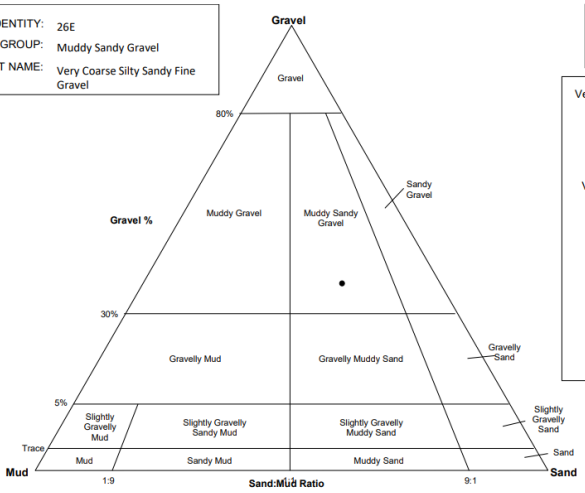

Gravel:	39.4 %
Sand:	41.2 %
Mud:	19.5%

Very Coarse Gravel:	0.0%
Coarse Gravel:	0.0%
Medium Gravel:	0.0%
Fine Gravel:	35.7 %
Very Fine Gravel:	3.7%
Very Coarse Sand:	2.2%
Coarse Sand:	3.8%
Medium Sand:	10.6 %
Fine Sand:	15.0 %
Very Fine Sand:	9.5%
Very Coarse Silt:	7.4%
Coarse Silt:	4.5%
Medium Silt:	4.9%
Fine Silt:	2.2%
Very Fine Silt:	0.4%
Clay:	0.0%

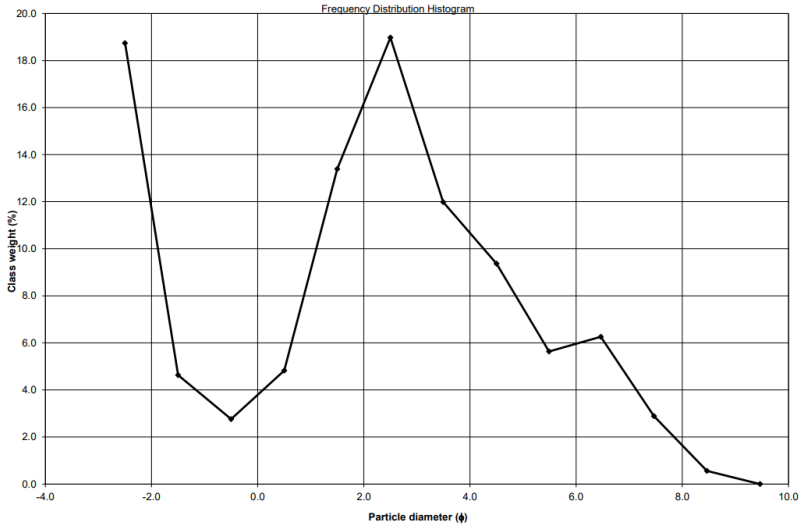

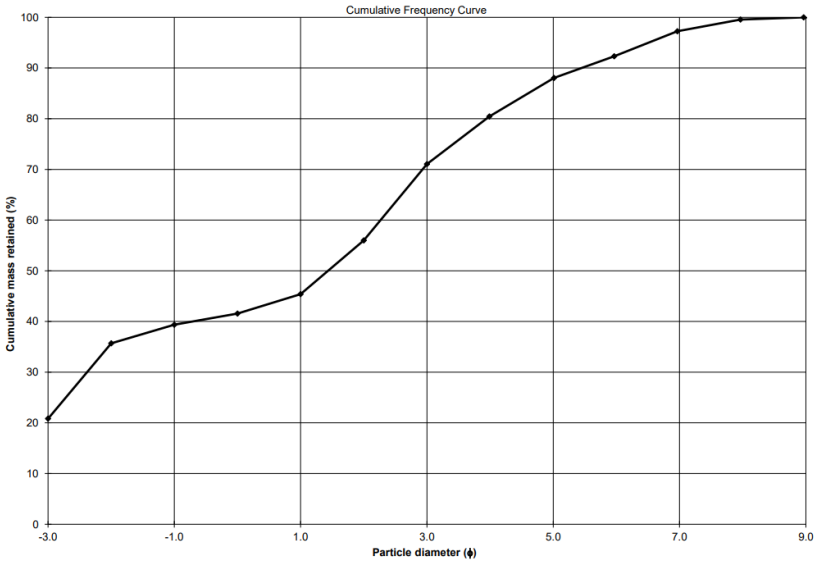

Other Data

SAMPLE STATISTICS

SIEVING ERROR: 0.0%

SAMPLE IDENTITY: **19H**

ANALYST & DATE: J Fleming, 02/05/2024

SAMPLE TYPE: Unimodal, Poorly Sorted

TEXTURAL GROUP: Muddy Sandy Gravel

SEDIMENT NAME: Very Coarse Silty Sandy Fine Gravel

	µm	ϕ
MODE 1:	3000.0	-1.500
MODE 2:		
MODE 3:		
D_{10}:	560.2	-3.212
MEDIAN or D_{50}:	3256.0	-1.703
D_{90}:	9269.2	0.836
(D_{90} / D_{10}):	16.55	-0.260
(D_{90} - D_{10}):	8709.0	4.048
(D_{75} / D_{25}):	3.426	0.306
(D_{75} - D_{25}):	4177.9	1.777

GRAIN SIZE DISTRIBUTION

GRAVEL:	71.3%	COARSE SAND:	1.9%
SAND:	22.3%	MEDIUM SAND:	0.3%
MUD:	6.4%	FINE SAND:	0.9%
		V FINE SAND:	2.1%
V COARSE GRAVEL:	0.0%	V COARSE SILT:	2.1%
COARSE GRAVEL:	0.0%	COARSE SILT:	1.5%
MEDIUM GRAVEL:	0.0%	MEDIUM SILT:	1.7%
FINE GRAVEL:	41.0%	FINE SILT:	0.8%
V FINE GRAVEL:	30.3%	V FINE SILT:	0.2%
V COARSE SAND:	17.1%	CLAY:	0.0%

	METHOD OF MOMENTS			FOLK & WARD METHOD		
	Arithmetic µm	Geometric µm	Logarithmic ϕ	Geometric µm	Logarithmic ϕ	Description
MEAN ($\bar{x}$):	2898.3	722.5	-0.773	3056.6	-1.612	Very Fine Gravel
SORTING (σ):	2235.1	17.75	2.112	2.915	1.543	Poorly Sorted
SKEWNESS (Sk):	0.234	-1.518	2.149	-0.637	0.637	Very Fine Skewed
KURTOSIS (K):	1.704	3.741	7.648	1.353	1.353	Leptokurtic

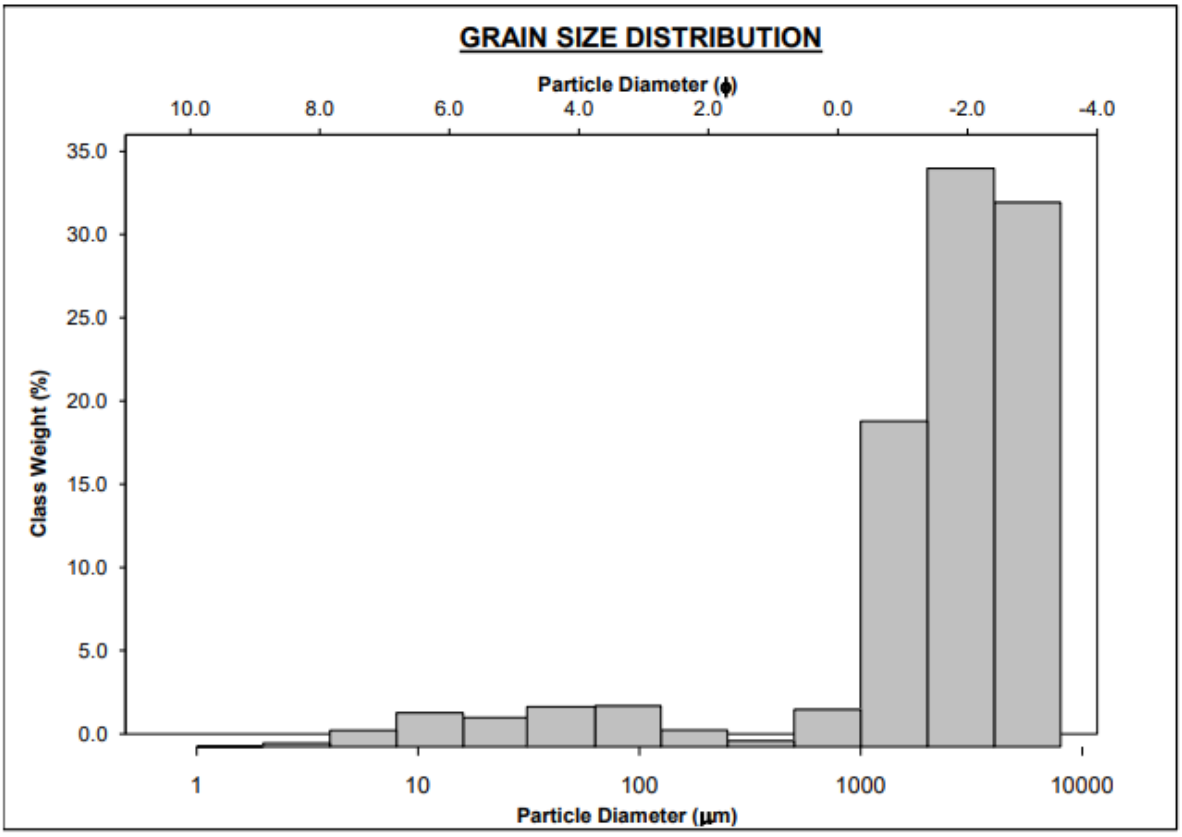

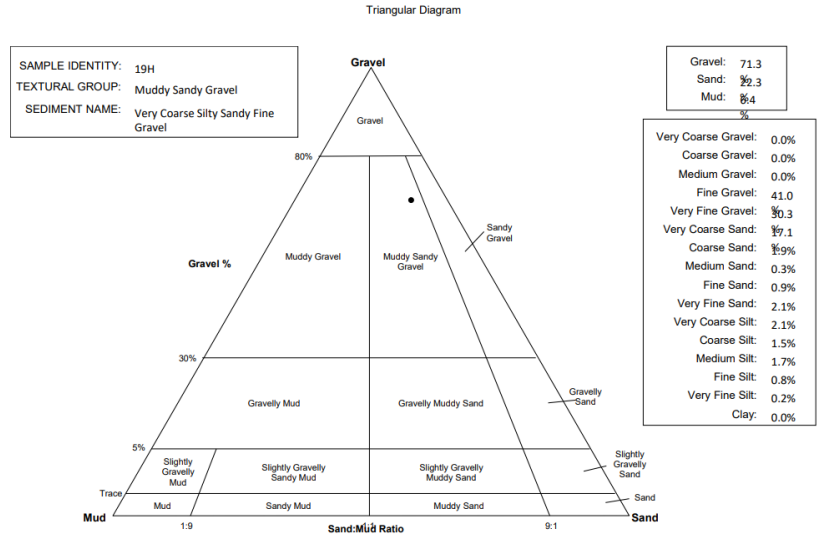
Triangular Diagram
SAMPLE IDENTITY: 19H
TEXTURAL GROUP: Muddy Sandy Gravel
SEDIMENT NAME: Very Coarse Silty Sandy Fine Gravel
Gravel
Gravel
80%
Sandy Gravel
Gravel %
Muddy Gravel
Muddy Sandy Gravel
30%
Gravelly Mud
Gravelly Muddy Sand
Gravelly Sand
5%
Slightly Gravelly Mud
Slightly Gravelly Sandy Mud
Slightly Gravelly Muddy Sand
Slightly Gravelly Sand
Trace
Mud
Sandy Mud
Muddy Sand
Sand
Mud
1:9
Sand:Mud Ratio
9:1
Sand
Gravel: 71.3 %
Sand: 22.3 %
Mud: 6.4 %
Very Coarse Gravel: 0.0%
Coarse Gravel: 0.0%
Medium Gravel: 0.0%
Fine Gravel: 41.0
Very Fine Gravel: 30.3
Very Coarse Sand: 17.1
Coarse Sand: 1.9%
Medium Sand: 0.3%
Fine Sand: 0.9%
Very Fine Sand: 2.1%
Very Coarse Silt: 2.1%
Coarse Silt: 1.5%
Medium Silt: 1.7%
Fine Silt: 0.8%
Very Fine Silt: 0.2%
Clay: 0.0%

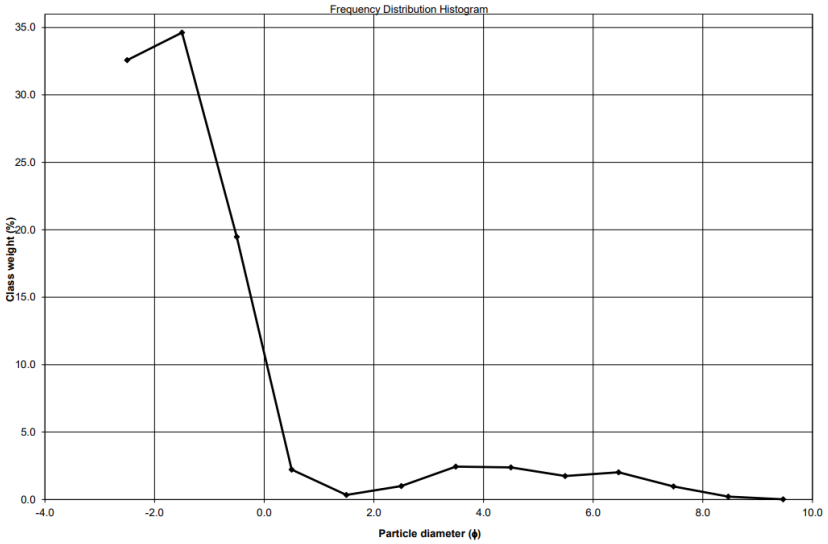
Frequency Distribution Histogram
Class weight (%)
35.0
30.0
25.0
20.0
15.0
10.0
5.0
0.0
-4.0
-2.0
0.0
2.0
4.0
6.0
8.0
10.0
Particle diameter (ϕ)

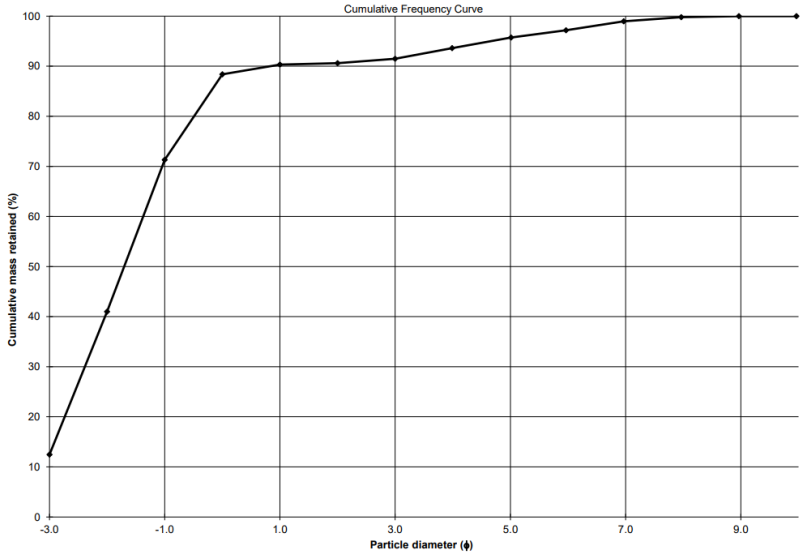
Cumulative Frequency Curve
Cumulative mass retained (%)
100
90
80
70
60
50
40
30
20
10
0
-3.0
-1.0
1.0
3.0
5.0
7.0
9.0
Particle diameter (ϕ)

SAMPLE STATISTICS

SIEVING ERROR: 0.0%

SAMPLE IDENTITY: **20B**

ANALYST & DATE: J Fleming, 02/05/2024

SAMPLE TYPE: Bimodal, Very Poorly Sorted

TEXTURAL GROUP: Muddy Sandy Gravel

SEDIMENT NAME: Very Coarse Silty Sandy Fine Gravel

	µm	ϕ
MODE 1:	94.00	3.494
MODE 2:	6000.0	-2.500
MODE 3:		
D_{10}:	34.19	-6.986
MEDIAN or D_{50}:	785.9	0.348
D_{90}:	126783.3	4.870
(D_{90} / D_{10}):	3708.4	-0.697
(D_{90} - D_{10}):	126749.1	11.86
(D_{75} / D_{25}):	44.31	-1.633
(D_{75} - D_{25}):	4125.6	5.469

GRAIN SIZE DISTRIBUTION

GRAVEL:	45.8%	COARSE SAND:	3.3%
SAND:	36.9%	MEDIUM SAND:	5.4%
MUD:	17.3%	FINE SAND:	12.5%
		V FINE SAND:	12.7%
V COARSE GRAVEL:	0.0%	V COARSE SILT:	8.4%
COARSE GRAVEL:	0.0%	COARSE SILT:	3.8%
MEDIUM GRAVEL:	0.0%	MEDIUM SILT:	3.3%
FINE GRAVEL:	42.1%	FINE SILT:	1.5%
V FINE GRAVEL:	3.7%	V FINE SILT:	0.3%
V COARSE SAND:	3.1%	CLAY:	0.0%

	METHOD OF MOMENTS			FOLK & WARD METHOD		
	Arithmetic	Geometric	Logarithmic	Geometric	Logarithmic	Description
	µm	µm	ϕ	µm	ϕ	
MEAN ($\bar{x}$):	602.2	27.80	1.571	480.2	1.058	Medium Sand
SORTING (σ):	1493.3	17.96	2.399	5.089	2.347	Very Poorly Sorted
SKEWNESS (Sk):	2.952	0.171	0.480	-0.576	0.576	Very Fine Skewed
KURTOSIS (K):	10.51	1.781	2.544	0.483	0.483	Very Platykurtic

GRAIN SIZE DISTRIBUTION

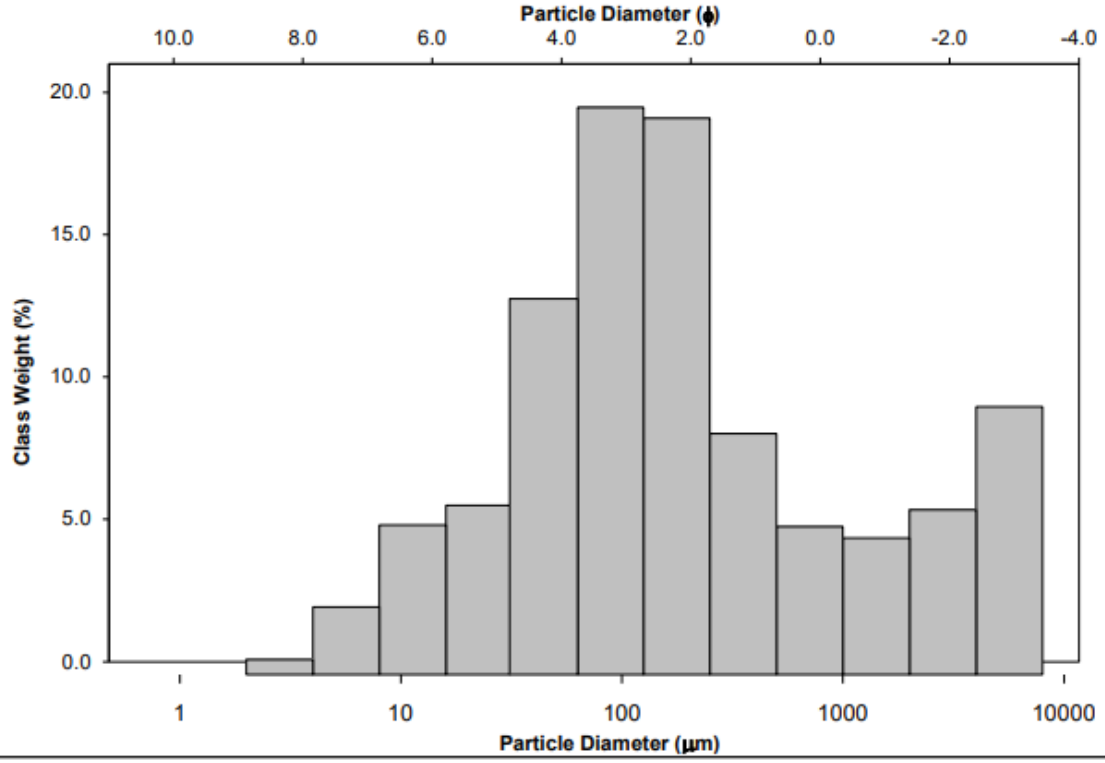

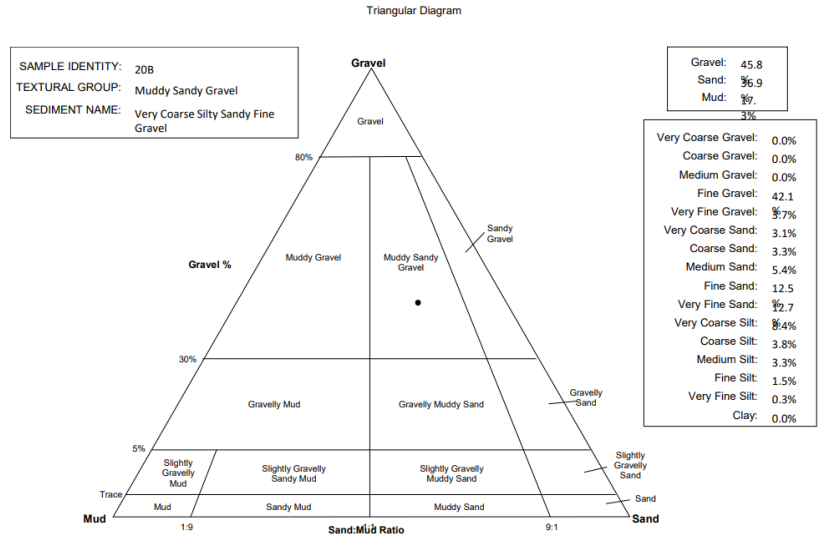
Triangular Diagram
SAMPLE IDENTITY: 20B
TEXTURAL GROUP: Muddy Sandy Gravel
SEDIMENT NAME: Very Coarse Silty Sandy Fine Gravel
Gravel: 45.8%
Sand: 36.9%
Mud: 17.3%
Very Coarse Gravel: 0.0%
Coarse Gravel: 0.0%
Medium Gravel: 0.0%
Fine Gravel: 42.1%
Very Fine Gravel: 3.7%
Very Coarse Sand: 3.1%
Coarse Sand: 3.3%
Medium Sand: 5.4%
Fine Sand: 12.5%
Very Fine Sand: 12.7%
Very Coarse Silt: 8.4%
Coarse Silt: 3.8%
Medium Silt: 3.3%
Fine Silt: 1.5%
Very Fine Silt: 0.3%
Clay: 0.0%
Gravel
80%
30%
5%
Trace
Mud
Gravel %
Muddy Gravel
Muddy Sandy Gravel
Sandy Gravel
Gravelly Mud
Gravelly Muddy Sand
Gravelly Sand
Slightly Gravelly Mud
Slightly Gravelly Sandy Mud
Slightly Gravelly Muddy Sand
Slightly Gravelly Sand
Sand
Mud
Sandy Mud
Muddy Sand
1:9
9:1
Sand:Mud Ratio
Sand

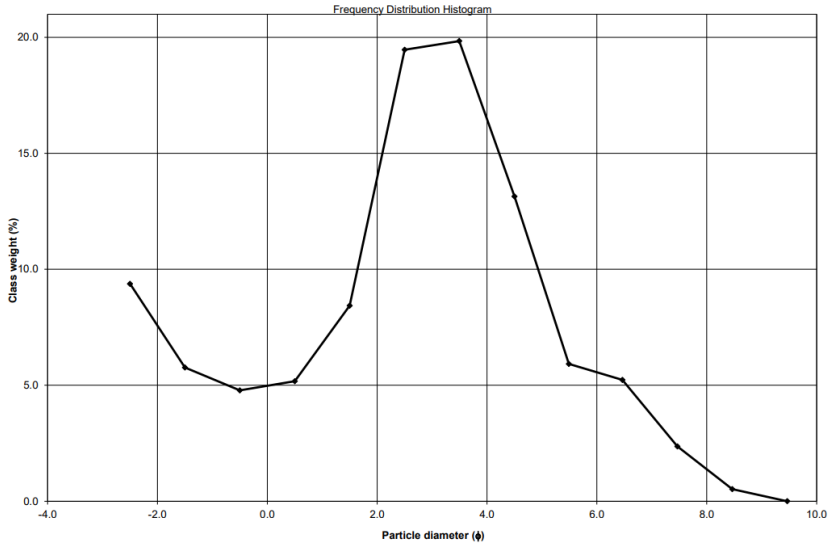
Frequency Distribution Histogram
Class weight (%)
20.0
15.0
10.0
5.0
0.0
-4.0
-2.0
0.0
2.0
4.0
6.0
8.0
10.0
Particle diameter (ϕ)

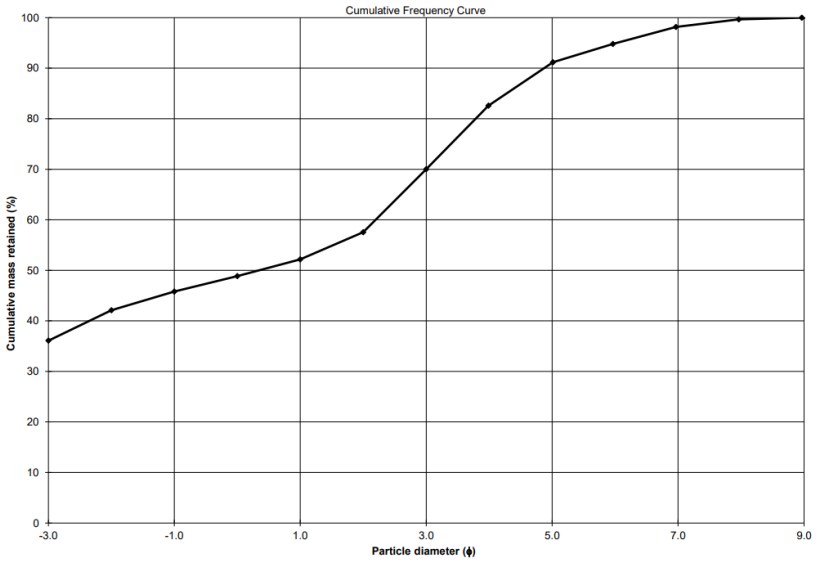
Cumulative Frequency Curve
Cumulative mass retained (%)
100
90
80
70
60
50
40
30
20
10
0
-3.0
-1.0
1.0
3.0
5.0
7.0
9.0
Particle diameter (ϕ)

SAMPLE STATISTICS

SIEVING ERROR: 0.0%

SAMPLE IDENTITY: **24F**

ANALYST & DATE: J Fleming, 02/05/2024

SAMPLE TYPE: Bimodal, Very Poorly Sorted

TEXTURAL GROUP: Gravelly Muddy Sand

SEDIMENT NAME: Very Fine Gravelly Very Coarse Silty Fine Sand

	µm	ϕ
MODE 1:	187.5	2.500
MODE 2:	1500.0	-0.500
MODE 3:		
D_{10}:	14.50	-1.205
MEDIAN or D_{50}:	161.2	2.633
D_{90}:	2305.7	6.108
(D_{90} / D_{10}):	159.0	-5.068
(D_{90} - D_{10}):	2291.2	7.313
(D_{75} / D_{25}):	18.36	18.54
(D_{75} - D_{25}):	801.0	4.199

GRAIN SIZE DISTRIBUTION

GRAVEL:	11.6%	COARSE SAND:	6.5%
SAND:	58.9%	MEDIUM SAND:	8.2%
MUD:	29.6%	FINE SAND:	18.7%
		V FINE SAND:	13.6%
V COARSE GRAVEL:	0.0%	V COARSE SILT:	10.4%
COARSE GRAVEL:	0.0%	COARSE SILT:	8.4%
MEDIUM GRAVEL:	0.0%	MEDIUM SILT:	7.3%
FINE GRAVEL:	3.9%	FINE SILT:	2.8%
V FINE GRAVEL:	7.7%	V FINE SILT:	0.6%
V COARSE SAND:	11.9%	CLAY:	0.0%

	METHOD OF MOMENTS			FOLK & WARD METHOD		
	Arithmetic	Geometric	Logarithmic	Geometric	Logarithmic	Description
	µm	µm	ϕ	µm	ϕ	
MEAN ($\bar{x}$):	776.3	177.2	2.497	181.7	2.460	Fine Sand
SORTING (σ):	1343.2	6.273	2.649	7.003	2.808	Very Poorly Sorted
SKEWNESS (Sk):	2.550	0.038	-0.038	0.063	-0.063	Symmetrical
KURTOSIS (K):	9.457	2.189	2.189	0.842	0.842	Platykurtic

GRAIN SIZE DISTRIBUTION

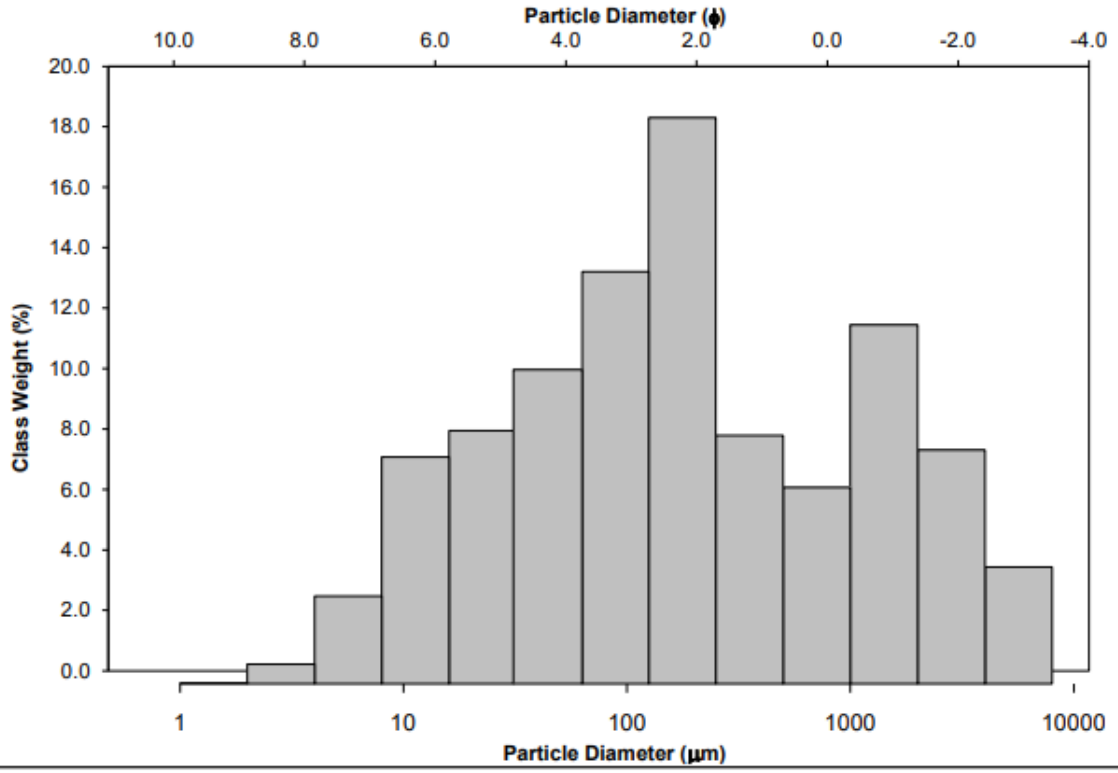

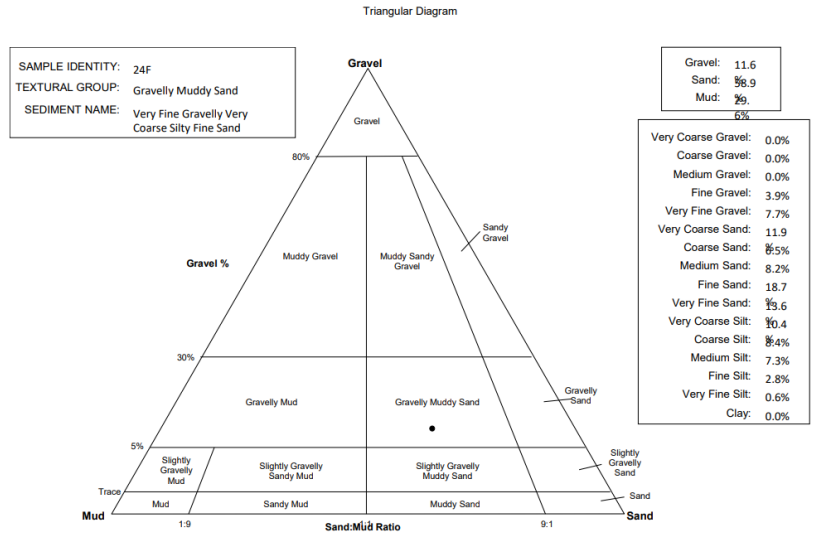
Triangular Diagram
SAMPLE IDENTITY: 24F
TEXTURAL GROUP: Gravelly Muddy Sand
SEDIMENT NAME: Very Fine Gravelly Very Coarse Silty Fine Sand
Gravel: 11.6
Sand: 58.9
Mud: 29.6%
Very Coarse Gravel: 0.0%
Coarse Gravel: 0.0%
Medium Gravel: 0.0%
Fine Gravel: 3.9%
Very Fine Gravel: 7.7%
Very Coarse Sand: 11.9
Coarse Sand: 6.5%
Medium Sand: 8.2%
Fine Sand: 18.7
Very Fine Sand: 13.6
Very Coarse Silt: 10.4
Coarse Silt: 8.4%
Medium Silt: 7.3%
Fine Silt: 2.8%
Very Fine Silt: 0.6%
Clay: 0.0%
Gravel
Gravel
80%
Gravel %
Muddy Gravel
Muddy Sandy Gravel
Sandy Gravel
30%
Gravelly Mud
Gravelly Muddy Sand
Gravelly Sand
5%
Slightly Gravelly Mud
Slightly Gravelly Sandy Mud
Slightly Gravelly Muddy Sand
Slightly Gravelly Sand
Trace
Mud
Sandy Mud
Muddy Sand
Sand
Mud
1:9
Sand:Mud Ratio
9:1
Sand

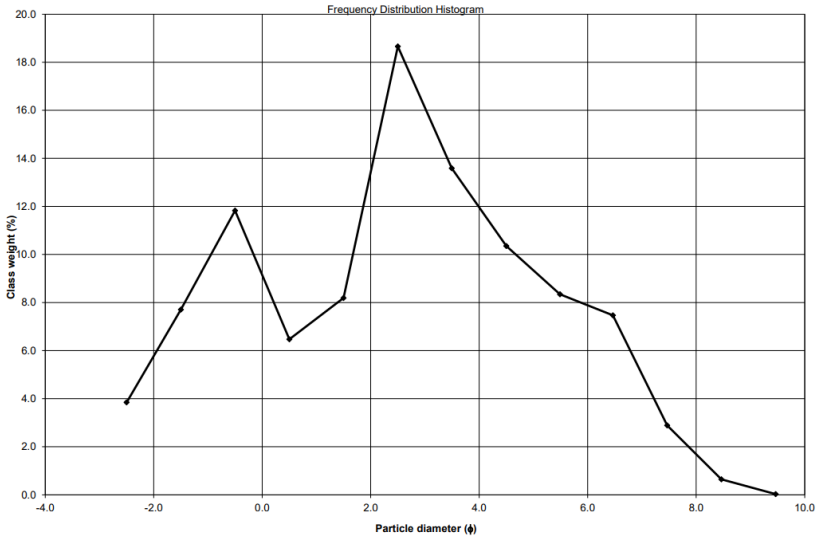
Frequency Distribution Histogram
Class weight (%)
20.0
18.0
16.0
14.0
12.0
10.0
8.0
6.0
4.0
2.0
0.0
-4.0
-2.0
0.0
2.0
4.0
6.0
8.0
10.0
Particle diameter (ϕ)

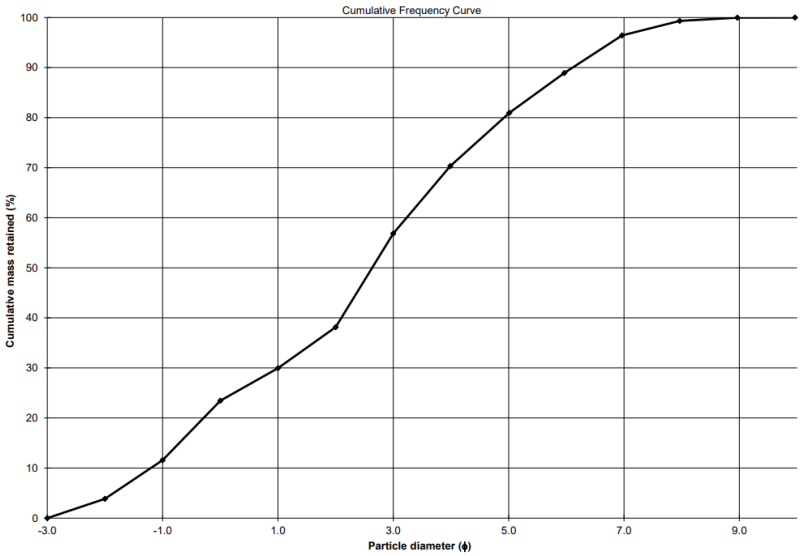
Cumulative Frequency Curve
Cumulative mass retained (%)
100
90
80
70
60
50
40
30
20
10
0
-3.0
-1.0
1.0
3.0
5.0
7.0
9.0
Particle diameter (ϕ)